University of Southampton

Faculty of Engineering, Science and Mathematics

School of Chemistry

Mechanistic Aspects of Thiamine Biosynthesis in *Escherichia coli*

By

Martin R. Challand

Thesis for the degree of Doctor of Philosophy

December 2010

Declaration

I, Martin Challand, declare that this thesis entitled "Mechanistic Aspects of Thiamine Biosynthesis in *Escherichia coli*" and the work presented within are both my own, and have been generated by me as the result of my own original research. I confirm that:

- This work was done wholly or mainly while in candidature for a research degree at this University;

- Where any part of this thesis has previously been submitted for a degree or any other qualification at this University or any other institution, this has been clearly stated;

- Where I have consulted the published work of others, this is always clearly attributed;

- Where I have quoted from the work of others, the source is always given. With the exception of such quotations, this thesis is entirely my own work;

- I have acknowledged all main sources of help;

- Where the thesis is based on work done by myself jointly with others, I have made clear exactly what was done by others and what I have contributed myself;

- Parts of this work have been published as:

  Kriek M., Martins F., Challand M. R., Croft A. and Roach P. L., Thiamine Biosynthesis in Escerichia coli: Identification of the Intermediate and By-product Derived from Tyrosine, *Angew. Chem. Int. ed. Eng.*, **2007**, *46*, 9223

  Challand M. R., Ziegert T., Douglas P., Wood R. J., Kriek M., Shaw N. M. And Roach P. L., Product Inhibition in the Radical S-Adenosylmethionine Family, *FEBS Lett.*, **2009**, *583*, 1358

  Challand M. R., Martins F. T. and Roach P. L., Catalytic Activity of the Anaerobic Tyrosine Lyase Required for Thiamine Biosynthesis in *Escherichia coli*, *J. Biol. Chem*., **2010**, *285*, 5240

Signed: **Date:**

UNIVERSITY OF SOUTHAMPTON

ABSTRACT

FACULTY OF ENGINEERING, SCIENCE AND MATHEMATICS
SCHOOL OF CHEMISTRY

Doctor of Philosophy

MECHANISTIC ASPECT OF THIAMINE BIOSYNTHESIS IN ESCHERICHIA COLI

by Martin R. Challand

The biosynthesis of the vitamin thiamine is laden with interesting chemistry. In anaerobic bacteria (such as *Escherichia coli*) a reactive intermediate, dehydroglycine, required for the biosynthesis of the thiazole moiety is derived from cleavage of the Cα—Cβ bond of tyrosine in a reaction catalysed by the radical S-adenosyl-L-methionine (SAM) enzyme, tyrosine lyase (ThiH). The aromatic by-product of this reaction *in vivo* was unequivocally characterised as *p*-cresol, a result which supported previous *in vitro* observations. Development of a reproducible activity assay for ThiH activity initiated detailed studies on the kinetics. ThiH, isolated either in a complex with thiazole synthase (ThiG), or as a monomer displayed pre-steady state burst phase kinetics. The SAM cleavage products (5'-deoxyadenosine (DOA) and methionine) were identified as inhibitors of ThiH activity and this inhibition could be alleviated by addition of 5'-methylthioadenosine / S-adenosylhomocysteine nucleosidase (MTAN), which catalysed rapid hydrolysis of DOA to adenine and 5'-deoxyribose. The addition of MTAN increased the activity of the ThiGH complex but drastically increased the amount of observed uncoupled cleavage of SAM. The *in vitro* products of tyrosine cleavage (glyoxylate and ammonium ions) were also identified as inhibitors of the ThiH mediated tyrosine cleavage reaction. However, reductive cleavage of SAM continued in an uncoupled manner. Experiments with tyrosine analogues showed that 4-hydroxyphenylpropionic acid compounds could support uncoupled SAM cleavage, but the Cα—Cβ bond cleavage reaction was dependent on a correctly orientated α-amino functional group. A mechanistic model was constructed, based on the available experimental data, which explained the observed product inhibition, uncoupled turnover and complex formation between ThiH and ThiG. The model proposes that ThiH controls the tyrosine cleavage reaction in order to co-ordinate the generation of the intermediate,

dehydroglycine, with its utilisation in the thiazole forming cylisation reaction, catalysed by ThiG.

Table of Contents

Acknowledgements

I am indebted to a many people who made the work presented in this thesis possible.

I would like to thank Anna Croft for the modelling of the reaction thermodynamics and tyrosine radical intermediate and the numerous helpful emails in interpreting the data. I thank Julie Herniman and John Langley for running GCMS experiments and for assistance interpreting the data.

A large part of the experiments and ideas described herein were the result of countless conversations and I would like to begin by thanking my supervisor, Peter Roach. Not only for being at the other end of many of the aforementioned conversations and always remaining enthusiastic, but also for creating a very open atmosphere within the research group which allowed for the discussion of ideas on a regular basis. Also, for his good humour and expert advise in proof reading and correcting the early drafts of this thesis. I would also especially like to thank Filipa Martins for tirelessly training me in the use of laboratory equipment and also helping me in getting to grips all aspects with this project at an early stage. I would also like to thank Rob Wood, who always gave his time generously and whose experience was of great value in designing, understanding and interpreting many experiments. I would also like to thank Jenny McKelvie for helpful discussions about enzyme kinetics and inhibition and Sam Birtwell for assistance in treatment of experimental errors.

Also thanks to other fellow Roach group members (past and present): Rohan Ranasinghe, Graham Broder, Paul Douglas, Penny Bryant, Marco Kriek, Jenny Harmer, Laura Batton,

Rebecca Driesener, Michael Maynard-Smith and Joseph She for making my experience in the group both productive and enjoyable.

I would now especially like to thank my friends: Rohan, Graham, Sam, AD, Wendy, Stephen and Claire for lunchtime banter, extended tea breaks, Drummond drinking, pool playing and Lennon's shapes; Chappers and Irish for being top notch housemates and all the tasty dinners they have prepared and finally my parents for all their support.

List of Abbreviations

AcOH	acetic acid
AIR	5-aminoimidazole ribotide
AnRNR	anaerobic ribonucleotide reductase
anSME	anaerobic Sulfatase Maturating Enzyme
ATP	adenosine triphosphate
BDE	bond dissociation energy
BioB	biotin synthase
B. subtilis	*Bacillus subtilis*
C. difficile	*clostridium difficile*
DCM	dichloromethane
DOA	5'-deoxyadenosine
DTT	dithiothrietol
DXP	1-deoxy-D-xylulose-5-phosphate
Dxs	1-deoxy-D-xylulose-5-phosphate synthase
E. coli	*Escherichia coli*
EPR	electron paramagnetic resonance
ENDOR	electron nuclear double resonance
FAD	flavin adenine dinucleotide

FldA	flavodoxin
FMN	flavin mononucluotide
FPLC	fast protein liquid chromatography
Fpr	flavoprotein: NADPH oxidoreductase
GCMS	gas chromatography mass spectrometary
HMP	4-amino-5-hydroxymethyl-2-methyl pyrimidine
HPLC	high Pressure Liquid Chromatography
4-HPHPA	4-hydroxyphenyl—hydroxypropionic acid
4-HPPA	4-hydroxypropionic acid
Isc	iron sulfur cluster
IPNS	isopenicillin-N synthase
KIE	kinetic isotope effect
LAM	lysine 2,3-aminomutase
LCMS	liquid chromatography mass spectrometary
MeCN	acetonitrile
MeOH	methanol
MOPS	3-(N-morpholino)propanesulfonic acid
MTA	5’-methylthioadenosine
MTAN	5’-methylthioadenosine / S-adenosylhomocysteine nucleosidase
MWCO	molecular weight cut off

m/z	mass to charge ratio
OD_{600}	optical density at 600 nm
NADPH	nicotinamide adenine dinucleotide-phosphate reductase
PFL	pyruvate formate lyase
PFL-AE	pyruvate formate lyase activating enzyme
RNR	ribonucleotide reductase
SAM	S-adenosyl-L-methionine
SDS-PAGE	sodium dodecyl sulfate polyacrylamide gel electrophoresis
TIM	trioesphosphate isomerase
ThiC	HMP synthase
ThiD	HMP kinase
ThiE	thiamine synthase
ThiG	thiazole synthase
ThiH	tyrosine lyase
ThiO	glycine oxidase
TPP	thiamine pyrophosphate
TLC	thin Layer Chromatography
UV	ultraviolet
UV-vis	ultraviolet-visible
XAS	X-ray absorption spectroscopy

2YT Medium	2 x Bacto Tryptone / yeast extract medium

Notations

In this report, gene names are quoted in italics with no capitalization of the first letter, eg. *thiH.* Gene products are named in normal type, with first letter capitalized, eg. ThiH.

The term enzyme is used to describe a biological catalyst that displays more than one turnover either *in vitro* or *in vivo.*

1 Introduction

1.1 *Radical Chemistry in Biology*

1.1.1. Introduction to Radical Chemistry

A free radical is "any species capable of independent existence that contains one or more unpaired electrons"[1]. The unpaired electron occupies a molecular orbital by itself and can arise by loss or gain of an electron (i.e. by oxidation or reduction of a species) or by homolytic fission of a covalent bond (bond dissociation). Unpaired electrons are observed to exist on transition metals or on an organic molecule[1, 2].

Free radicals are generally very reactive due to the presence of the unpaired electron. As such they are more often very short lived species and typically have half lives of less than 10^{-3} s. Their lifetime can be controlled either by thermodynamic or kinetic factors. Kinetic stability is mostly governed by steric constraints, such as crowding around the radical centre can prevent it reacting with another molecule and this increases the half life of the radical. Thermodynamic stability is related to the enthalpy of dissociation of a bond (Scheme 1.1).

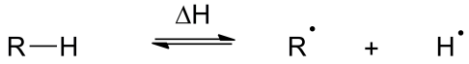

Scheme 1.1. Enthalpy of dissociation of a bond.

This is termed bond dissociation energy (BDE). The BDE is related to the stability of the resultant radical species which is dependent on both the nature of the atom on which the unpaired electron is centred and the delocalisation of the unpaired electron. The BDE's (R—H)

of some organic molecules are shown in Table 1.1. The factors which contribute to the thermodynamic stability of radicals are:

Hyperconjugation – which affects the order of alkyl radical stability: teritiary > secondary > primary > methyl (see examples 1 – 4 in Table 1.1).

Hybridisation – planar radicals are more stabilised as the unpaired electron can purely occupy a p orbital (see examples 5 – 7 in Table 1.1, which have a higher BDE's due to the hybridisation of the radical).

Mesomerisation – leads to stabilisation of a radical by resonance, such as in an allylic, benzylic or phenolic radical (see examples 8 – 11 in Table 1.1).

Captodative effect – leads to stabilisation of an unpaired electron by an adjacent electron donating and an electron withdrawing group. The captodative effect is a common mechanism for the stabilisation of radicals in biology. For example glycyl radicals (see example 13 in Table 1.1) which form on a peptide backbone are stabilised by the captodative effect (see Figure 1.1)[3].

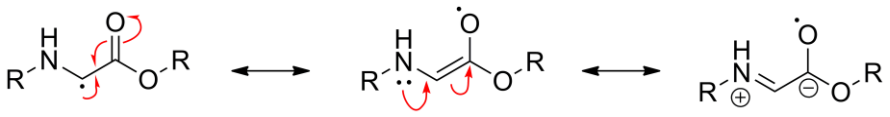

Figure 1.1. Stabilisation of a glycyl radical by the captodative effect.

Example	R—H	BDE / kJmol^{-1}
1		439
2		422
3	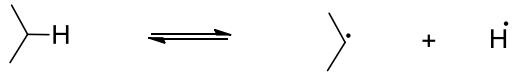	414
4	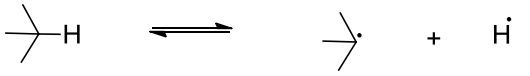	397
5		443
6		435
7	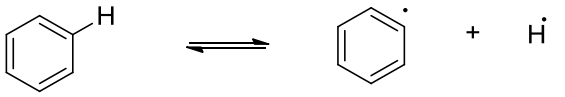	464
8		359
9	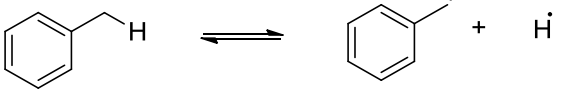	355
10	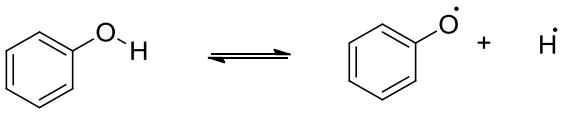	364
11	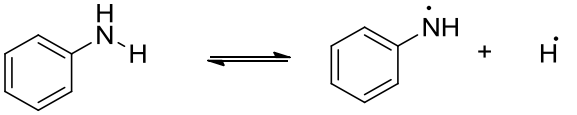	368
12	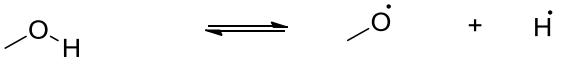	435
13	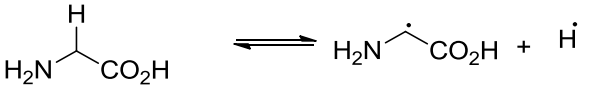	318

Table 1.1 Selected examples of BDE's for some organic radicals[3]

1.1.2. Utilisation of Reactive Radicals in Biology

In biological systems, free radicals are often considered to be harmful due to their high reactivity. Their uncontrolled generation, for example through oxidative stress or photolysis, can initiate harmful chain reactions. A healthy diet includes antioxidants such as vitamin C and vitamin E which quench potentially harmful radical species[1]. However, this thesis probes an example of a biological process which harnesses the reactivity of free radicals to its advantage. More specifically, the discussion focuses on the mechanism by which radical chemistry is utilised to overcome challenging biological transformations. Radical reactions in organic chemistry usually occur in the gas phase or in relatively inert solvents[2]. An environment where radical chemistry is prevalent is in the upper atmosphere, where the low concentration of molecules prolongs the lifetime of reactive free radicals. In biological systems reactions occur in an aqueous environment and there is a multitude of other molecules at a relatively high concentration which could induce side reactions. Radical mediated biotransformations are usually enzyme catalysed and so take place in a proteinaceous active site. A major challenge for biological systems that intend to exploit the reactivity of radical intermediates to its advantage is the control of generation and subsequent reaction of reactive radicals.

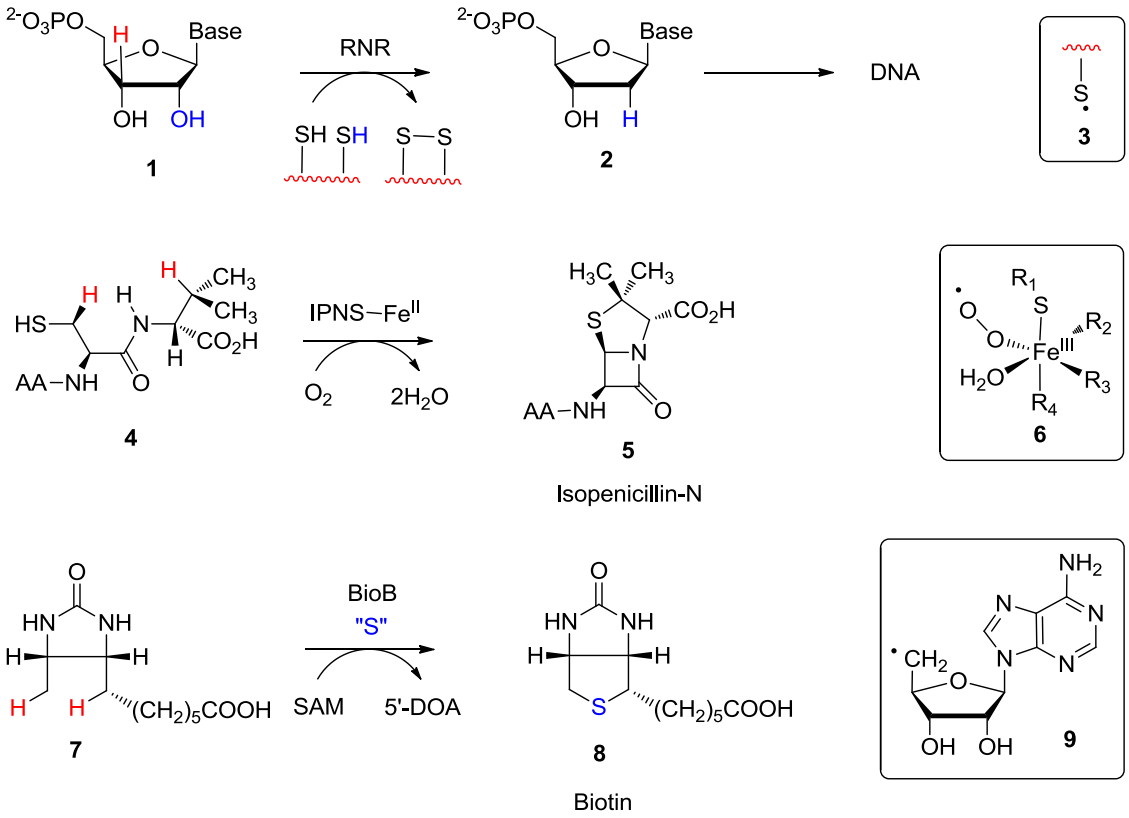

Scheme 1.2 Examples of radical mediated transformations in biology. The radical species that are generated in the active site are shown in boxes. These intermediates initiate the biotransformations by abstracting hydrogen atoms shown in red.

Three examples demonstrating the diversity of radical initiated biotransformations are shown in Scheme 1.2. Ribonucleotide reductases (RNR's) function to reduce ribonuleotides to deoxyribonucleotides, which provides the only source of these building blocks of deoxyribonucleic acid (DNA) and therefore, provides a key link in the evolution to life. The reaction catalysed by RNR's is mediated by the generation of a catalytic thiyl radical (**3**) on an active site cysteine residue, which then activates the substrate by abstracting a hydrogen atom (shown in red in Scheme 1.2)[4, 5]. The reduction of ribonucleotides to deoxyribonucleotides is a chemically difficult transformation and there is no precedent for such a reaction in synthetic chemistry. By contrast, in living systems the enzyme catalysed transformation is achieved under very mild conditions, at physiological temperature and pH. The second example shown is

Isopenicillin-N-synthase which catalysis the formation of the bycyclicpenicillin nucleus. β-lactam formation is energetically demanding and is initiated by the iron oxygen radical (**6)** (shown in the box)[6]. The third example is biotin synthase (BioB), which inserts a sulphur atom into dethiobiotin (**7**) in the final step of biotin (**8**) biosynthesis. The two new C—S bonds are formed at unactivated carbons. BioB uses the 5'-deoxyadenosyl radical (**9**) (generated from S-adenosylmethionine (SAM)) to abstract hydrogen atoms from the two carbons, activating them for formation of a new C—S bond[7]. As C—H bonds are common to many biological molecules, control of the reactive free radical is essential to prevent unwanted side reactions. The three examples shown demonstrate the complexity of possible radical mediated reactions and the unusual chemistry involved. All three examples represent a single metabolic step and are catalysed by a single protein. This highlights that the types of catalysis made possible once an enzyme has control of a reactive radical intermediate can be remarkably efficient. For comparison, in the 1950's Sheehan reported the chemical synthesis of penicillin V, which involved several synthetic steps and the β-lactam forming step alone gave ~10% yield[8].

The example studied in this thesis is a biotransformation involved in the biosynthesis of the vitamin, thiamine (vitamin B1), by the bacterium *Escherichia coli* (*E. coli*). The challenge presented to the micro-organism is the generation of an electrophilic (oxidised) intermediate, dehydroglycine (**11**), under anaerobic (reducing) conditions. The precursor to dehydroglycine is tyrosine (**10**) and the enzyme which catalyses the reaction is tyrosine lyase (ThiH) (see Scheme 1.3). ThiH belongs to the rapidly expanding radical *S*-adenosyl-L-methionine (radical SAM) superfamily. Radical SAM enzymes generate a reactive, primary radical and utilise it to initiate chemically demanding transformations. The work presented herein seeks to elucidate the mechanisms by which ThiH controls and utilises reactive radicals to initiate Cα—Cβ bond cleavage of tyrosine.

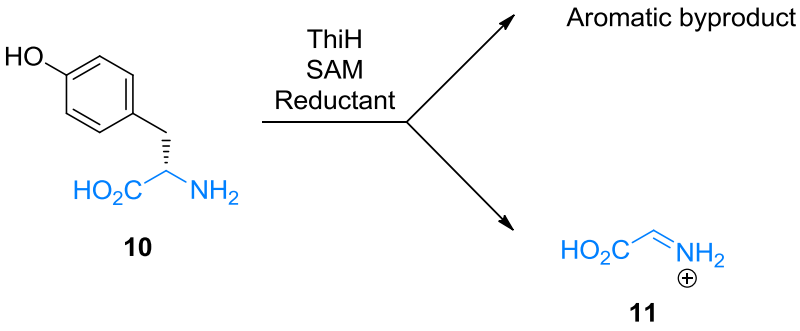

Scheme 1.3. ThiH cleaves the C_{α}—C_{β} of tyrosine to form dehydroglycine.

1.2 ***Radical SAM Enzymes***

1.2.1 *Overview of the Mechanism of Radical SAM Enzymes*

A commonly occurring pathway for the generation of a radical for biological catalysis comes from reduction or oxidation of a transition metal followed by electron transfer to form an organic radical. All radical SAM proteins require the reductive cleavage of SAM to generate the reactive 5'-deoxyadenosyl radical (**9**). As discussed in the previous section, access to highly reactive radical species permits initiation of some truly remarkable biotransformations. The first radical SAM enzyme to be discovered in the 1970's was lysine 2,3-aminomutase (LAM). This enzyme had an absolute requirement for SAM to allow the radical initiated transformation of α-lysine (**12**) to β-lysine (**13**) (see Figure 1.2)[9, 10]. This 1, 2 migration of a functional group is similar to typical examples *S*-adenosylcobalamin (vitamin B_{12}) (**27**) (see Figure 1.3) dependent rearrangements and suggested that SAM was playing the role of the already characterised *S*-adenosylcobalamin coenzyme. Both *S*-adenosylcobalamin dependent enzymes and radical SAM enzymes generate the 5'-deoxyadenosyl radical (**9**) as an intermediate to initiate catalysis and as such the two may be evolutionarily related[10-12]. Upon interaction with a protein *S*-adeosylcobalamin undergoes cleavage of the weak carbon-cobalt bond (BDE ~130 $kJmol^{-1}$) generating cobal(II)amin and a 5'-deoxyadenosyl radical (**9**); however radical SAM enzymes generate this intermediate by cleavage of a carbon-sulfur bond (see Figure 1.3). The BDE of the carbon-sulfur bond in SAM is ~250 $kJmol^{-1}$, therefore fission of this bond is much more energetically demanding and needs to be facilitated by reduction of the sulfonium ion. The mid-point potential for a tri-alkyl sulfonium ion in solution is in the order of -1.8 V[13]. The crux of radical SAM chemistry is the thermodynamically unfavourable reduction of the sulfonium ion as a prelude to carbon sulfur bond homolysis and generation of the reactive radical. Reduction of SAM in radical SAM enzymes is catalysed by a 4Fe-4S cluster.

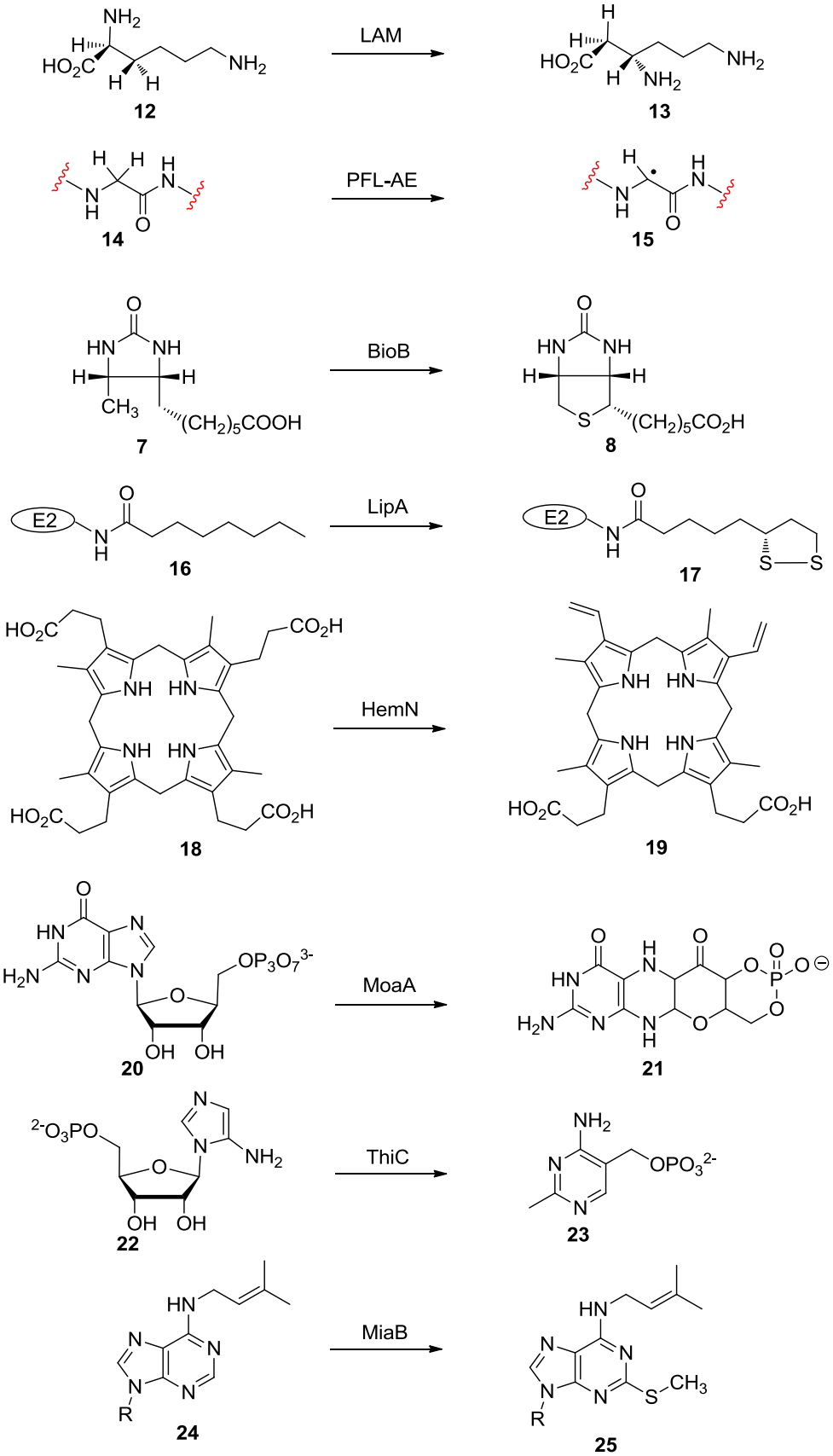

Figure 1.2. Selected examples of transformations catalysed by the radical SAM family.

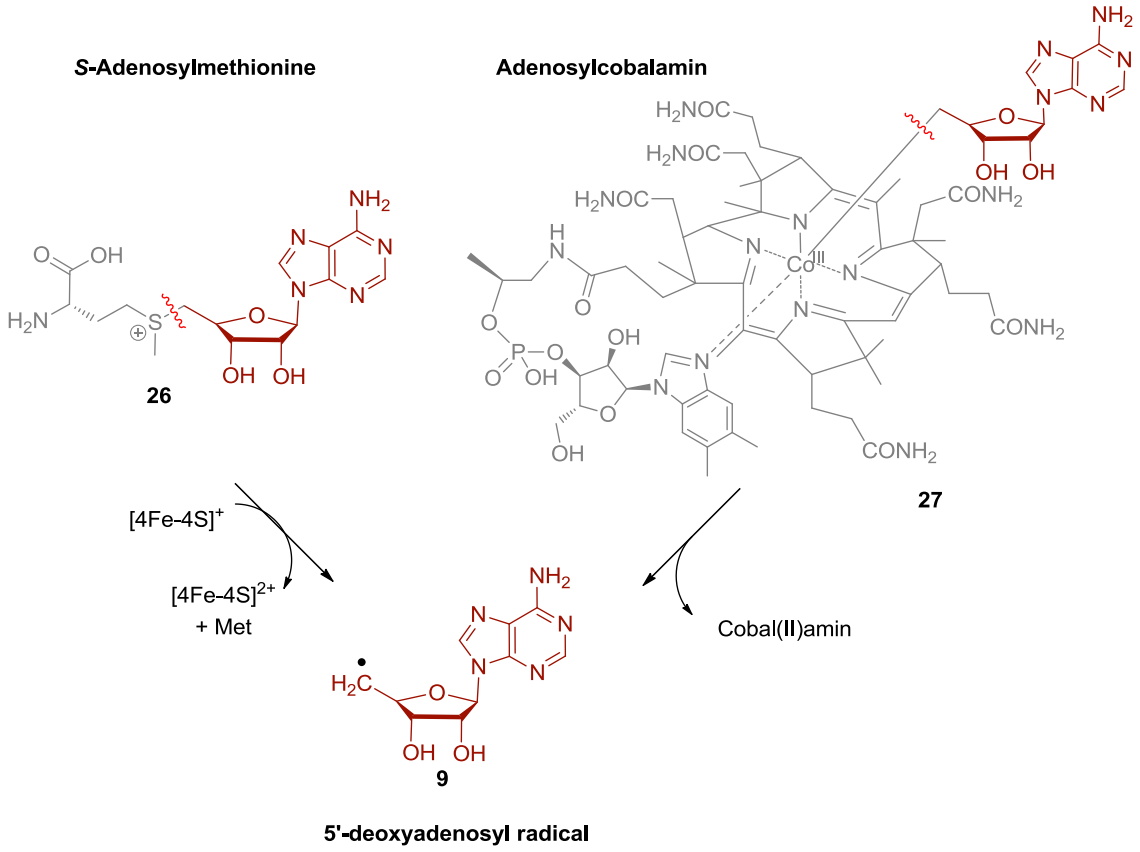

Figure 1.3 Stuructural similarities between S-adenosylmethionine and adenosylcobalamin and the generation of the common 5'deoxyadeosyl radical intermediate.

Iron sulfur clusters are involved in a diverse range of chemical reactions in nature. Their most common function is in redox chemistry, where the iron ions switch between 2+ and 3+ oxidation states. Depending on their environment the redox potential of Fe-S clusters can range from -500 to +300 mV. Some of the known functions of Fe-S clusters include acting as donors and acceptors of electrons, for example in hydrogenases, ferridoxins, mitochondrial and bacterial respiratory complexes I-III and enzyme catalysis[14], which includes radical SAM enzymes. Radical SAM proteins all contain a 4Fe-4S cluster, ligated through three of the iron atoms by three conserved cysteine residues (**28**) (see Scheme 1.4)[15, 16]. Typically these three cysteine residues form part of a conserved CXXXCXXC motif[17], where X is an arbitrary

amino acid. As suggested by their name, radical SAM proteins are also dependent on SAM for activity and the fourth, un-ligated iron co-ordinates to the amino acid functionality of SAM in a bidentate fashion (**29**) (see Scheme 1.4)[18]. The 4Fe-4S cluster can access an overall 2+ or 1+ redox state and functions to receive an electron from an electron donor (such as flavodoxin, ferridoxin or a chemical replacement) and mediate its transfer onto the sulfonium ion of SAM, which causes spontaneous homolysis of the C-S bond. This yields methionine (**33**) and a 5'-deoxyadenosyl radical (**9**)[19, 20]. This primary radical is very reactive and provides the key to all radical SAM catalysed reactions. Subsequent chemical steps are initiated by abstraction of a hydrogen atom from a substrate. In some cases the substrate is another protein, for example in activating enzymes[21].

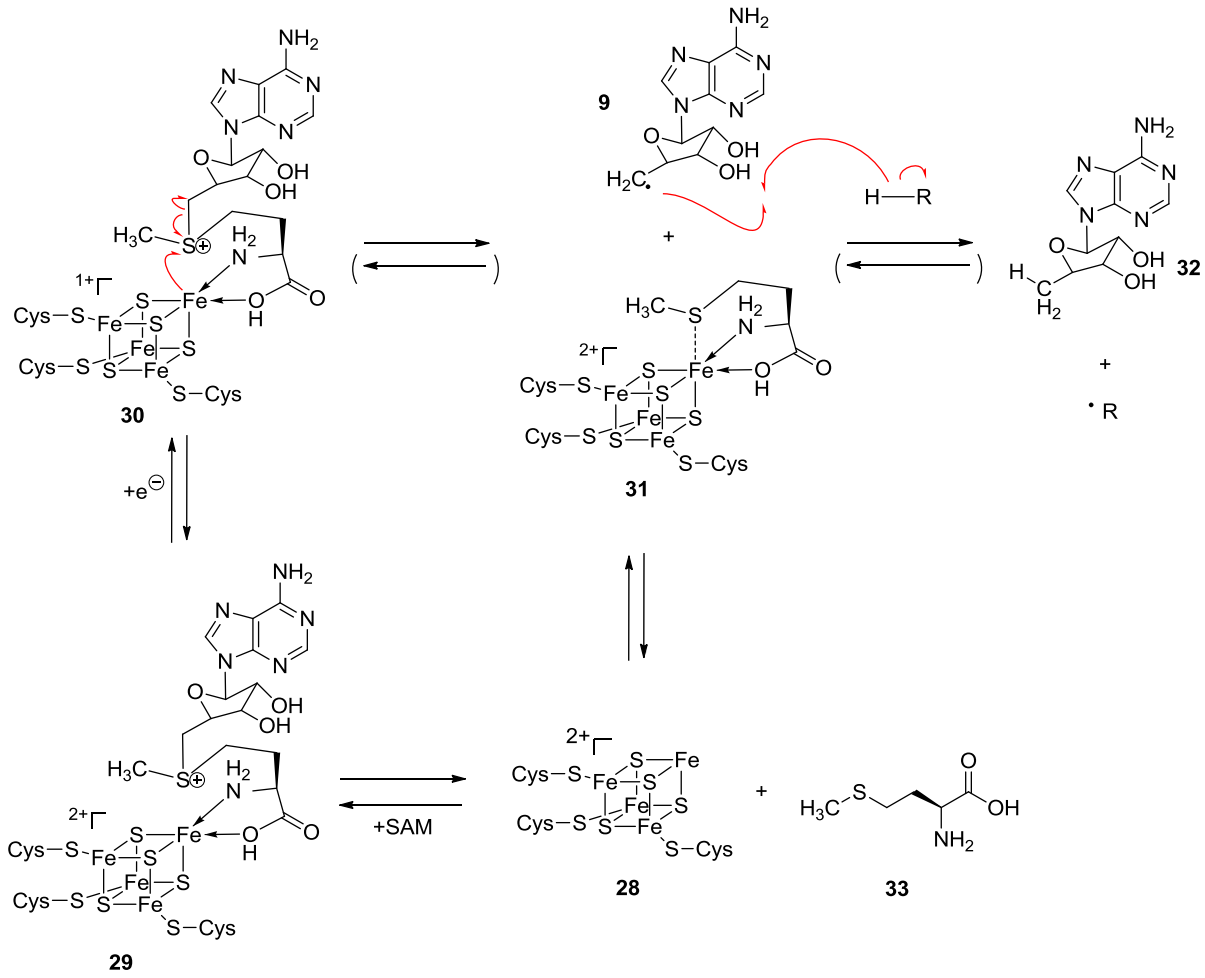

Scheme 1.4 Mechanism of generation of the highly reactive 5'-deoxyadenosyl radical in radical SAM enzymes.

The range of reactions catalysed by members of the radical SAM family is highlighted by the examples shown in Figure 1.2. Many radical SAM enzymes perform essential transformations in the cell, including key steps in vitamin and co-factor biosynthesis. The large activation energies implicit in these chemically demanding transformations result in relatively slow turnover (in the order of 10^{-4} s^{-1}, see Table 1.2), but it seems probable that the priority is successful synthesis of the essential metabolite rather than achieving a high catalytic efficiency. Indeed, some members of the family are constrained to a single turnover *in vitro* (eg BioB and LipA) and achieving catalytic activity in an *in vitro* system can be very difficult[22-25]. The common steps in the mechanism of radical SAM enzymes is shown in Scheme 1.4 and summarised below:

Step 1 – Ligation of SAM to the unique iron of the 4Fe-4S cluster (reversible).

Step 2 – Transfer of an electron to the 4Fe-4S cluster to reduce it to the overall +1 redox state. *In vivo* this is usually accomplished by cellular redox proteins (for example flavodoxin in *E. coli*) (reversible).

Step 3 – Inner sphere electron transfer from the 4Fe-4S cluster to SAM promoted homolysis of the C5-S bond, generating the 5'deoxyadenosyl radical and methionine (this step has been shown to be reversible in some cases).

Step 4 – The 5'-deoxyadenosyl radical abstracts a hydrogen atom from a substrate to generate a substrate radical (this step has been shown to be reversible in some cases).

1.2.2 *Classes of Radical SAM Enzymes*

Radical SAM enzymes can be classified based on their use of the 5'-deoxyadenosyl radical. This can sometimes (such as for LAM) lead to more efficient turnover (see Table 1.2). The three classes are summarised in Scheme 1.5 and discussed in the following paragraphs. There are also several reviews published which address this issue in detail[10, 11, 26, 27].

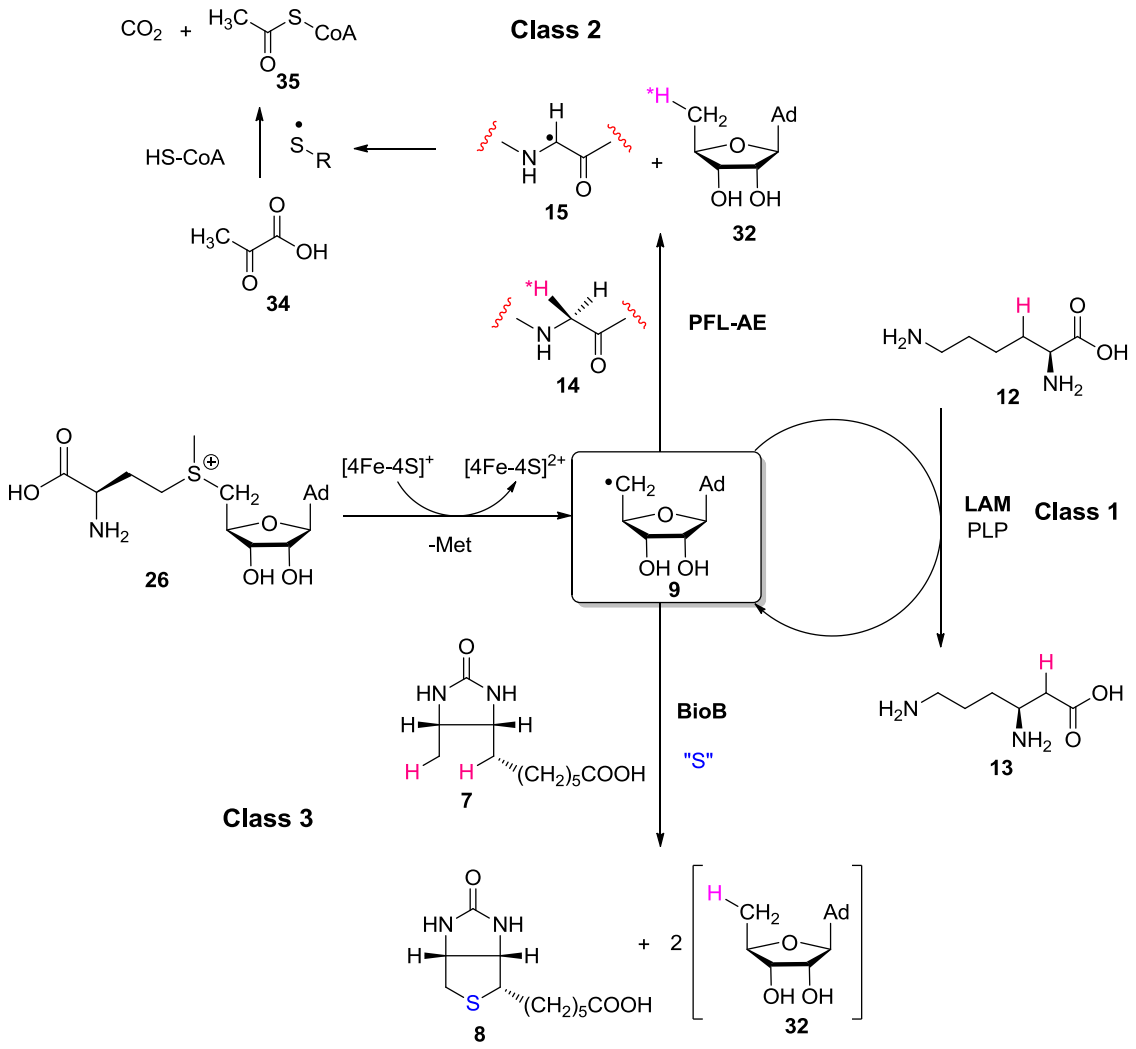

Scheme 1.5 Three classes of radical SAM enzymes shown with a well characterised example of each class.

Class	Protein	Organism	Apparent rate constant (s^{-1})*	T (°C)	Reference
1	KAM	*Clostridium subterminale* SB4	40 s^{-1}	37 °C	[28]
	SPL	*Geobacillus stearothermophilus*	1.4 s^{-1}		[29]
2	PFL AE	*E. coli*	6.41 x10^{-7} s^{-1}	37 °C	[30]
3	BioB	*E. coli*	12 x 10^{-4} s-^{1}	37 °C	[31]
	LipA	*E. coli*	29 x 10^{-4} s^{-1}	37 °C	[32]
	MiaB	*Thermotoga maritima*	10 x 10^{-4} s^{-1}	50 °C	[33]
	AtsB	*K. pneumoniae*	60 x 10-^{4} s^{-1}	37 °C	[34]
	BtrN	*Bacillus circulans*	383 x 10^{-4} s^{-1}	28 °C	[35]

Table 1.2 Rate contants for several members of the radical SAM family.

Class 1 – Enzymes which use SAM as a co-enzyme

Lysine 2,3-aminomutase (LAM)[36, 37] and DNA spore photoproduct lyase[38, 39] are two well characterised examples of enzymes that use SAM as a reversible source of the 5'-deoxyadenosyl radical. The 5'deoxyadensyl radical (**9**) mediates hydrogen transfer and is regenerated during the mechanism. Hence, these two enzymes use SAM as a co-enzyme and it is regenerated in each catalytic cycle. LAM also uses pyridoxal-5-phosphate as a cofactor in the mechanism. (see Scheme 1.6).

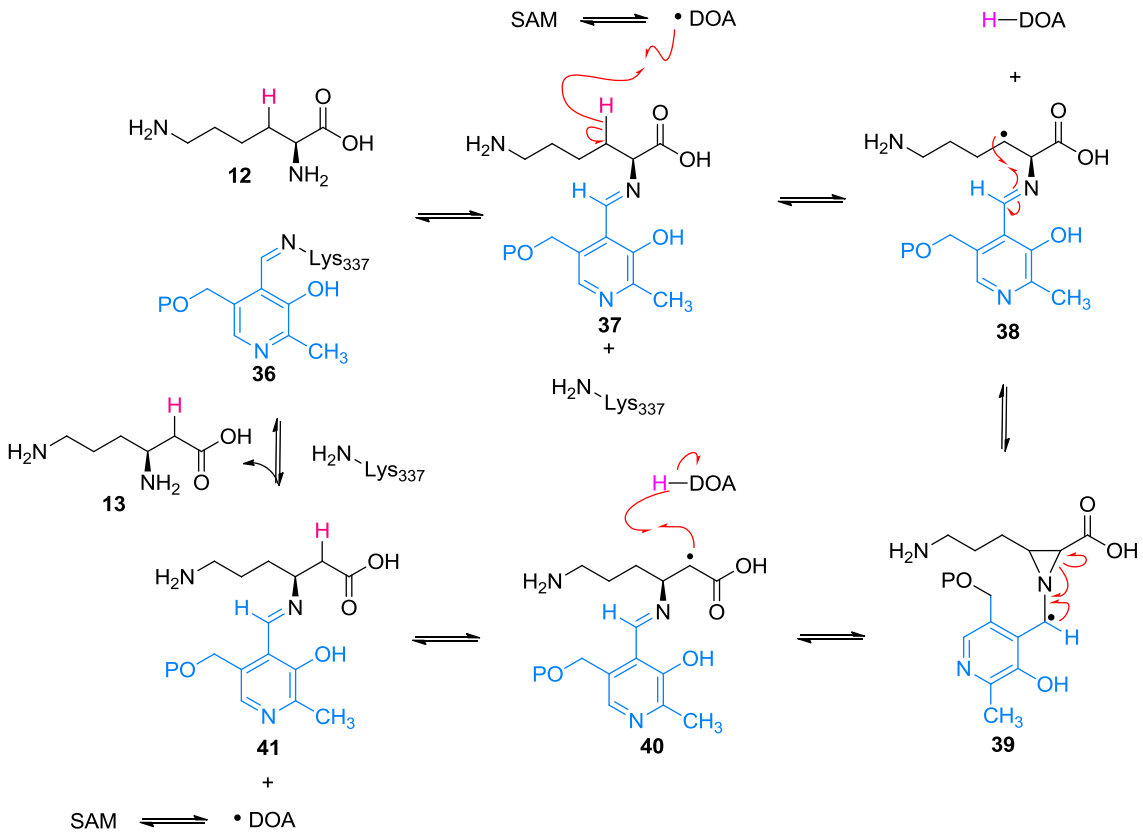

Scheme 1.6 Mechanism of LAM.

Class 2 – Activating enzymes – generating a glycyl radical intermediate

Enzymes of this class consist of two subunits: a catalytic subunit and an activating subunit. The activating subunit (activase) is responsible for generating a catalytic radical and is essential for activity[21]. In anaerobic systems, activase's are often Radical SAM enzymes. These enzymes reductively cleave SAM generating the 5'-deoxyadenosyl radical (**9**). The substrate for these enzymes is the catalytic subunit itself and the 5'-deoxyadenosyl radical abstracts the pro-*S* hydrogen atom of a conserved glycine residue in the peptide backbone of the catalytic subunit. The resulting glycyl radical (**15**) is stabilised by the captodative effect (see Figure 1.1, p2). Radical SAM activating enzymes require a stoichiometric amount of SAM with respect to the number of hydrogen atom abstractions and hence equivalents of glycyl radicals generated. The glycyl radical is transferred to a cysteine residue, generating a thiyl radical. This thiyl radical

interacts with the substrate and is regenerated in quenching the product radical as the final step of the catalytic cycle. Examples of enzymes with a radical SAM activase include: pyruvate formate lyase (PFL)[29] – which was the second member of the radical SAM family discovered in 1984[40], anaerobic ribonucleotide reductase (An-RNR)[41] and 4-hydroxyphenylacetate decarboxylase[42].

Class 3 – Enzymes that use SAM as a co-substrate

Both class 1 and class 3 of radical SAM enzymes involve direct abstraction of a hydrogen atom from the substrate by the 5'-deoxyadenosyl radical. Enzymes in this class use SAM a co-substrate and require a stoichiometric amount of SAM with respect to the number of hydrogen atoms abstracted. Tyrosine lyase (ThiH), the focus of this thesis, falls into this category of radical SAM enzymes. Other examples include: HemN (heme biosynthesis)[43], MoaA (molybdopterin biosynthesis)[44, 45], BtrN (butirosin biosynthesis)[35, 46] and the sulfur transfer proteins: lipoyl synthase (LipA)[23, 32, 47-49] and biotin synthase (BioB)[31, 50-58]. These enzymes have the potential to behave catalytically, under the proviso that there is an adequate quantity of SAM and reductant available. BioB is the most widely studied radical SAM enzyme in this class. The source of sulfur in LipA and BioB has been a source of some debate with the most likely source being a second iron sulfur cluster contained within the protein. As such a single turnover of these proteins results in depletion of the *holo*-protein and limits them to a single turnover *in vitro*. This limitation segregates these two proteins into a subclass that cannot behave catalytically *in vitro*. The generally accepted mechanism proposed by Jarrett and co-workers[31], for biotin formation by BioB is shown in Scheme 1.7. The sulfur is inserted into unreactive C-H bonds, which are activated by hydrogen atom abstraction, forming a substrate radical. LipA is thought to follow an analogous mechanism, with stepwise insertion of two sulfur atoms[23]. The lipoyl and biotin products of LipA and BioB are oxidised in relation to the substrates and therefore SAM can be considered an oxidant in these mechanisms. BioB has been

shown to behave catalytically *in vivo*. This is thought to be as the depleted iron sulfur cluster can be re-formed by the cell's host iron sulfur cluster biosynthesis machinery[14]. Indeed, recently BioB has been shown to form a complex with HscA[59] , a protein which has been shown to act as a chaperone for iron sulfur clusters.

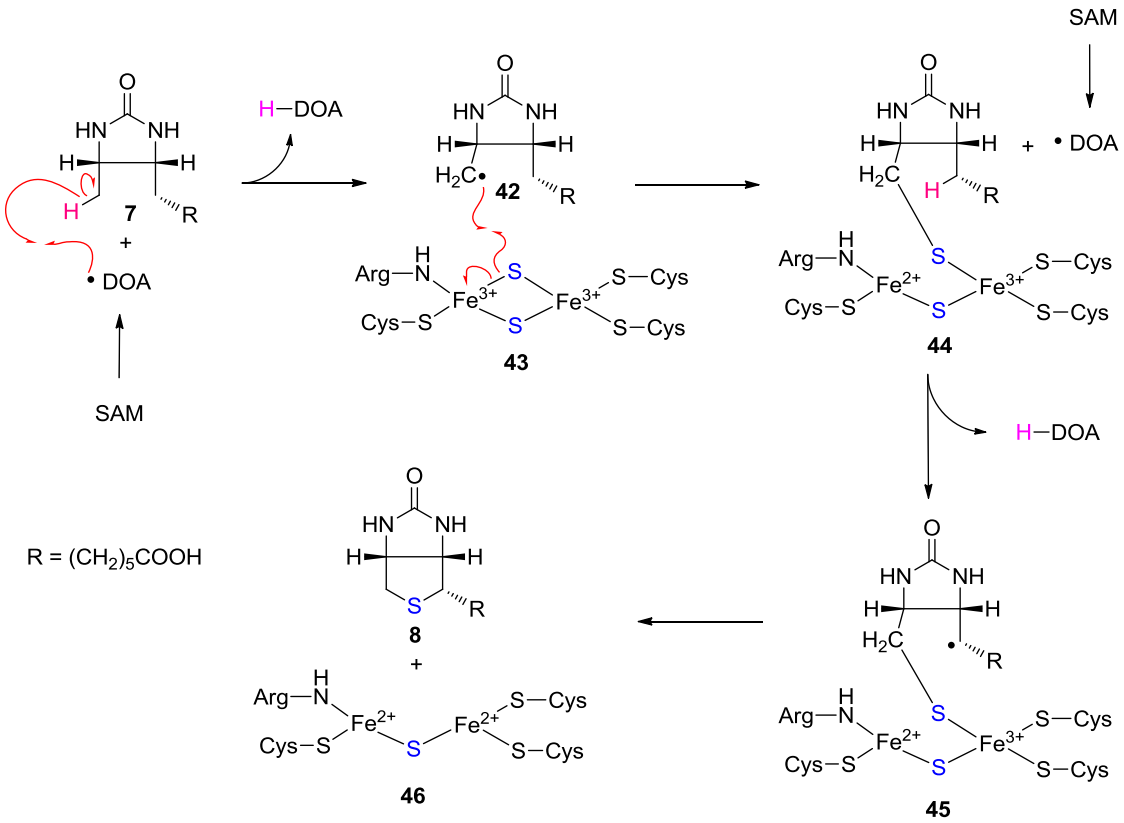

Scheme 1.7 Mechanism for BioB proposed by Taylor *et al.*[31]

LAM utilises SAM as a reversible source of a catalytic 5'deoxyadenosyl radical. It has been proposed from ENDOR, XAS and X-ray structural analysis of LAM[60, 61] that reversible SAM cleavage may be driven by electron transfer from the unique iron atom of the 4Fe-4S cluster to the sulfonium ion of SAM. The resultant hexavalent geometry at the unique iron atom (**31**) (see Figure 1.4) has also been proposed to provide a thermodynamic driving force for reductive cleavage of SAM. ENDOR[18] and Se-XAS experiments[62] on PFL-AE and BioB have lead to

an alternative mechanistic hypothesis for reductive cleavage of SAM in radical SAM enzymes that use the 5'-deoxyadenosyl radical stoichiometrically and have not been shown to reversibly cleave SAM. Instead of ligation to the unique iron atom of the 4Fe-4S cluster after reductive cleavage, the methionyl sulfur atom was found to be associated with a neighbouring sulfide ion in the 4Fe-4S cluster (**47**) (see Figure 1.4), implying that electron transfer was facilitated from the sulfur atom. However, the interpretation of more recent X-ray crystallographic data[63] has suggested that the mechanism for reductive SAM cleavage (shown in Scheme 1.4, p11) is likely to be consistent throughout the radical SAM family. This concept is discussed in more detail in the next sections.

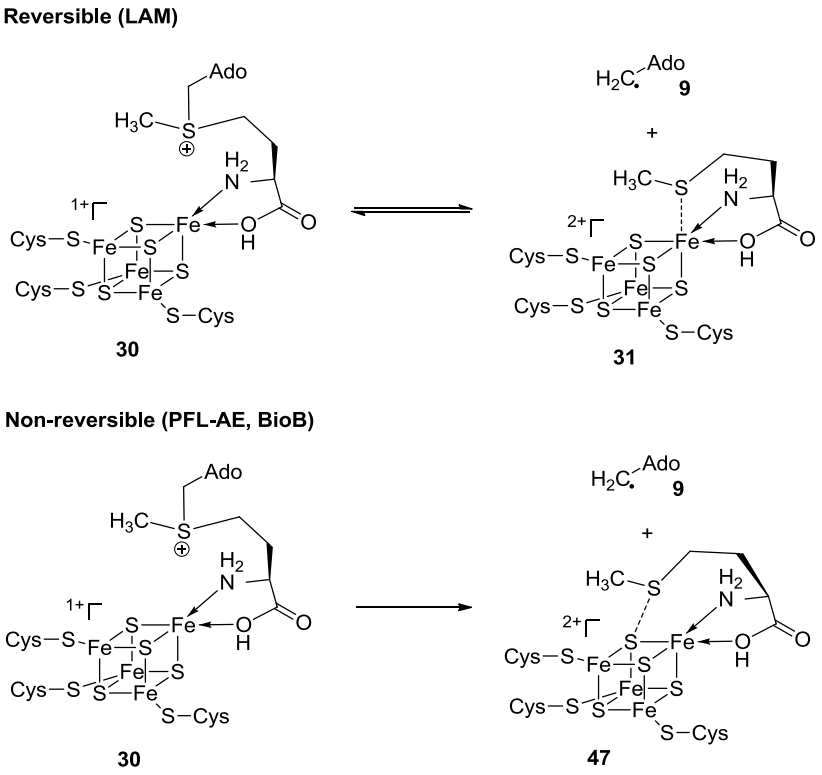

Figure 1.4 Proposed mechanism for SAM interaction with the 4Fe-4S cluster for reductive cleavage in LAM (reversible cleavage) and PFL-AE (non-reversible cleavage).

1.2.3 *X-Ray Structural Studies on Radical SAM Enzymes*

In 2004 Berkovitch et al. reported the X-ray crystal structure of BioB[64] (see Figure 1.5). Along with the X-ray structure of HemN[43], this data provided the initial structural evidence for radical SAM chemistry. The crystal structure confimed that the 4Fe-4S cluster was ligated to the protein backbone through three of its iron atoms by the three cysteines in the conserved "CXXXCXXC" motif and that SAM was ligated to the fourth iron in a bidentate fashion. This supported the mechanistic hypothesis described in section 1.2 that reductive cleavage of SAM was facilitated by electron transfer from the 4Fe-4S cluster. Since the publication of the BioB structure structures of several radical SAM proteins have been reported, including LAM[61], PFL-AE[65], MoaA[66], HemN[43] and HydE[67]. To date all the solved structures have consistently shown similar ligation of the 4Fe-4S cluster to the protein backbone and SAM. In addition all the radical SAM protein structures have shown similar structural folds, all of which form a $(\alpha/\beta)_8$ triosephosphate isomerase (TIM) barrel. The 4Fe-4S cluster binds at one end of the TIM barrel with SAM and other substrate(s) binding along the barrel and sealing off the active site[26]. It is essential that the active site is sealed; in particular so solvated molecules do not infiltrate and interfere with the delicate radical chemistry occurring within. This structural trend in radical SAM proteins is similar to S-adenosylcobalamin dependent enzymes and suggests and evolutionary link between the two[64]. The positioning of the 4Fe-4S cluster binding motif as a loop positioned at the end of the TIM barrel (shown in pink in Figure 1.5) and close to the protein surface suggests the potential that S-adenosylcobalamin dependent enzymes could have replaced the function of this loop with the S-adenosylcobalamin binding subunit and that the TIM barrel is required for chemistry involving the 5'deoxyadenosyl radical.

The positioning of the 4Fe-4S cluster close to the surface is also significant for its assembly and reduction by redox co-factors (such as flavodoxin in *E. coli*). In bacteria the biogenesis of iron sulfur clusters involves cysteine desulfurases and iron sulfur cluster assembly proteins (ISC or

SUF machinery[14]). Thus the region of the protein co-ordinating the 4Fe-4S cluster must be able to involve protein-protein interactions for iron-sulfur cluster assembly and for reduction of the cluster by flavodoxin (in *E. coli*) to initiate the radical SAM chemistry.

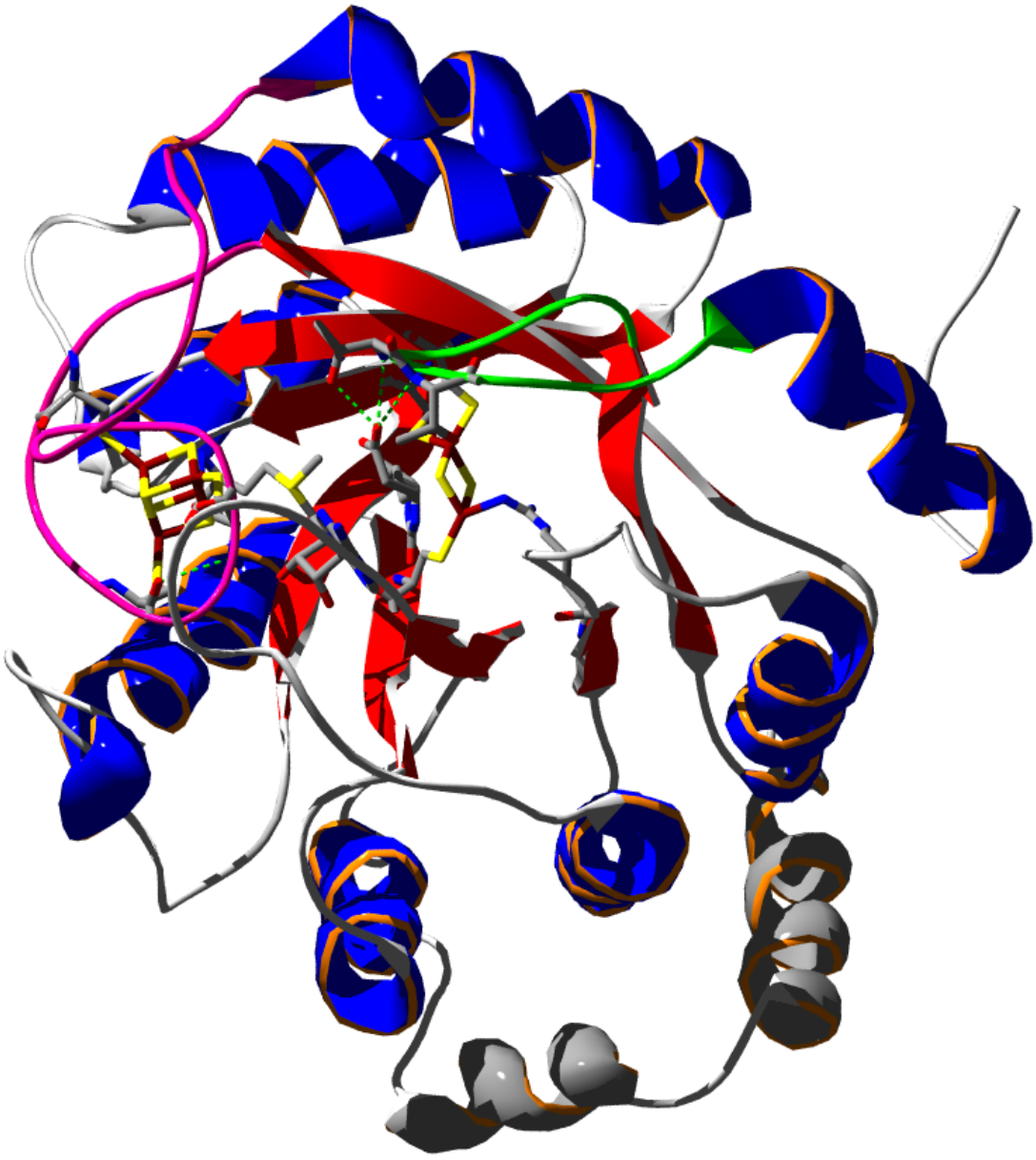

Figure 1.5 X-ray crystal structure of the BioB monomer shown with substrates bound. The α-helices and β-sheets of the $(\alpha/\beta)_8$ TIM barrel are coloured blue and red respectively. Side chains of amino acid residues ligating the iron sulfur clusters are also shown (C = grey; O = red; N = blue; S = yellow). The 4Fe-4S binding loop is coloured pink and the lid loop that binds the carboxylate of dethiobitin is coloured green.

Analysis of sequence alignments of radical SAM proteins in conjunction with the data available from the BioB structure enabled Nicolet *et al.* to identify several important motifs involved in SAM binding[68]. The majority of radical SAM proteins can be identified by the characteristic "CXXXCXXC" motif, which binds the 4Fe-4S cluster. Additionally this motif contains an aromatic amino acid ($X_{(ar)}$ = Y, F of H) at the position just before the third cysteine, i.e. "CXXXCX$X_{(ar)}$C". The function of this aromatic residue is to form π stacking and hydrogen bonding interactions with the adenosyl moiety (see Figure 1.6). In addition two other glycine rich motifs were identified and labelled the "GGE" motif and the "GXIXGXXE" motif (see Figure 1.7). The "GGE" motif binds to the amino group of the methionine on SAM and the "GEIXGXXE" motif interacts with the adenosyl moiety. Other highly conserved residues were identified to be involved in SAM binding including an arginine (R173 in EC BioB), which forms a salt bridge with the carboxylate functional group on SAM and an aspartic acid (D155 in EC BioB), which forms hydrogen bonds with the ribose moiety[68].

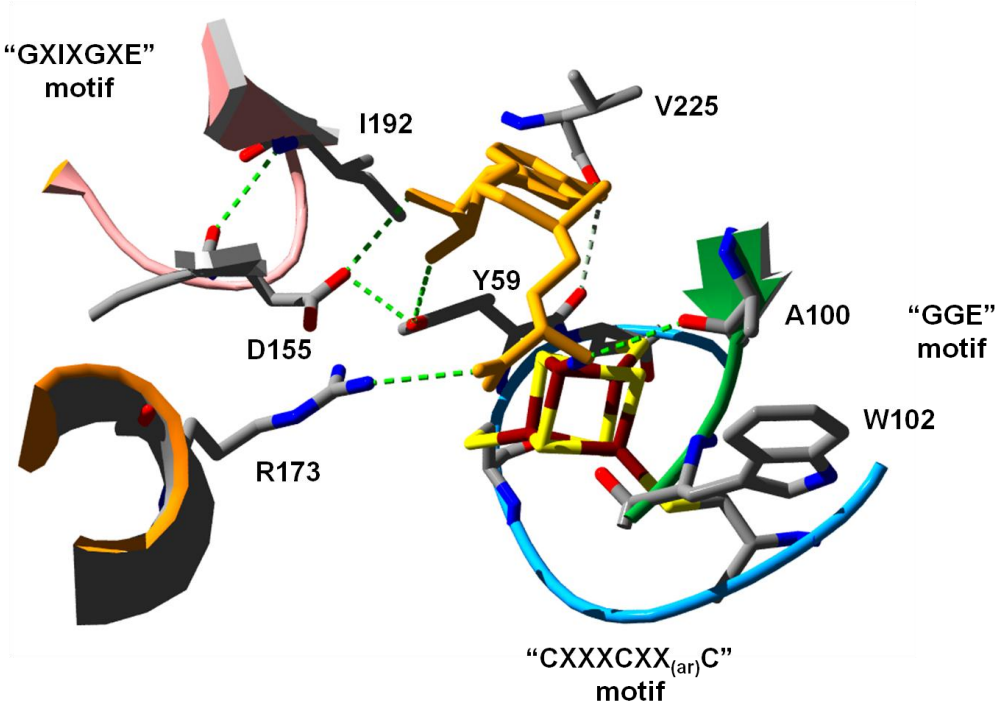

Figure 1.6 Active site of BioB from E. coli showing SAM (orange) co-ordinated to the 4Fe-4S cluster (brown and yellow) and the conserved residues with a role in SAM binding.

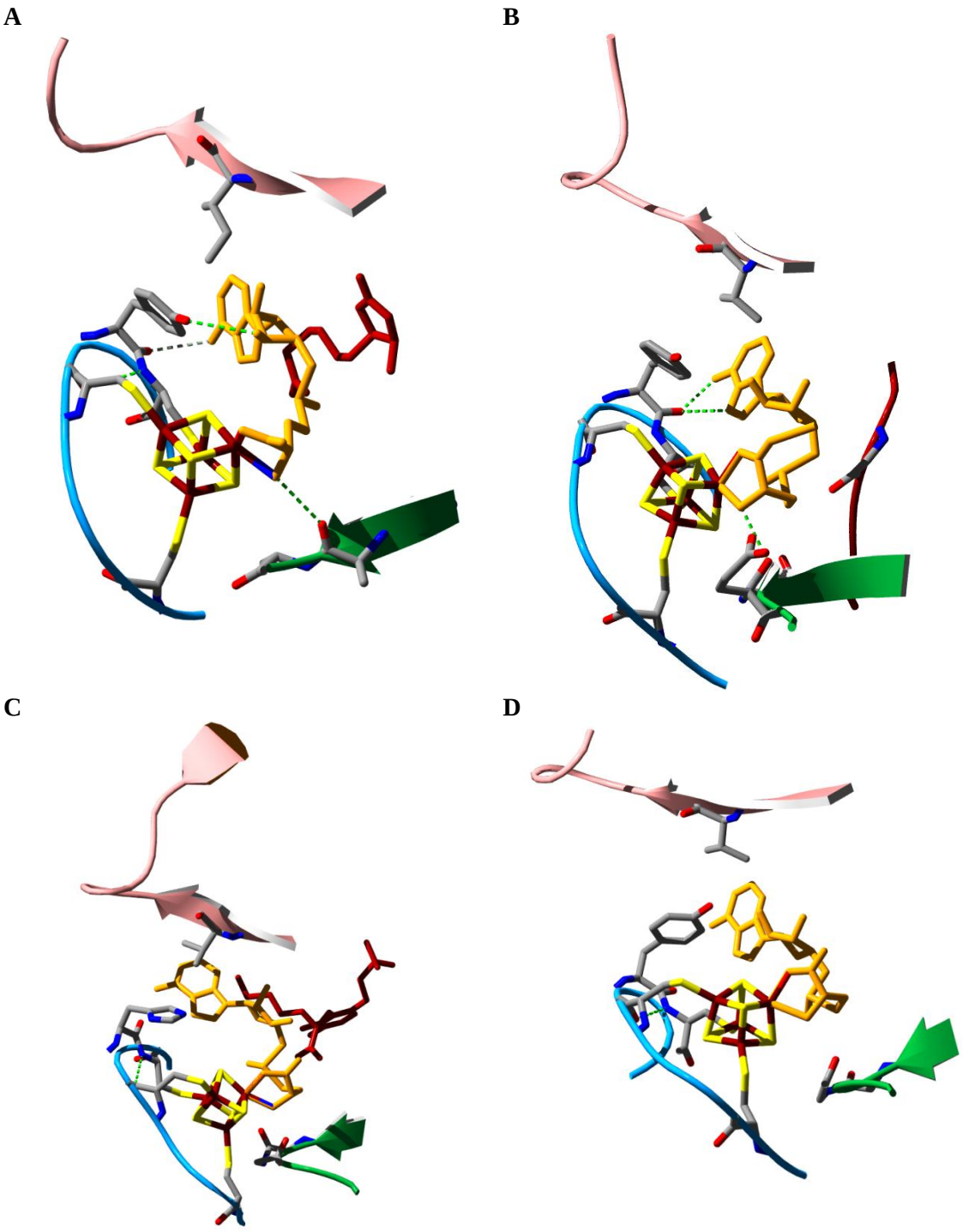

Figure 1.7 Active site region of A) BioB[64], B) PFL-AE[65], C) KAM[61] and D) MoaA[66] showing the conserved 4Fe-4S and SAM binging motifs. Colour scheme is as follows: "CxxxCxx$_{ar}$C" motif is in light blue; "GGE" motif is in green; "GxIxGxxE" motif is in pink; SAM is in orange and substrate (DTB, RVSGYAV heptapeptide or lysine and PLP) in dark red; 4Fe-4S cluster is in brown and yellow; side chains of amino acids are coloured by CPK. (C = grey; O = red; N = blue; S = yellow)

1.2.4 *Mechanisms of Generation and Control of Reactive Radicals*

The high reactivity of radicals is paramount in unlocking the biosynthetic potential for the unusual transformations catalysed by radical SAM enzymes. However, the sensitivity and high reactivity of the chemistry occurring in the active site of these enzymes has potential for unwanted side reactions if it is not suitably controlled. For example, SAM could undergo electrophilic attack on the 4Fe-4S cluster[69, 70], or uncontrolled generation of the 5'deoxyadenosyl radical could result in abstraction of hydrogen atoms from the peptide backbone or other solvated molecules. Therefore, radical SAM enzymes require exquisite control not only over the generations of radicals, but also in directing the reaction towards the desired products.

The X-ray crystal structures[43, 61, 64, 65, 67] have provided a great deal of insight into both the chemical mechanism of radical SAM enzymes and the way in which they control the radical chemistry. The presence of the $(\alpha/\beta)_8$ TIM barrel, which is sealed off by binding of the substrates provides a hydrophobic environment in the active site, preventing the interference of solvent molecules. In addition, the SAM is locked in position, adjacent to the 4Fe-4S cluster by hydrogen bonding, electrostatic, hydrophobic and π stacking interactions with the adenosyl moiety. This holds the sulfonium ion close to the cluster in order to permit inner-sphere electron transfer. In the majority of the solved structures the sulfur atom of SAM is positioned in close proximity (~3 – 4 Å) from the unique iron. The substrate is also orientated so that the 5' carbon of SAM is positioned near to the hydrogen atom that will be abstracted from the substrate. The close proximity of the iron-sulfur cluster and substrates to each other greatly favours radical intermediates reacting with the juxtaposed substrate target, rather than initiating unwanted side reactions. A potential problem for all radical SAM enzymes is the uncontrolled (or uncoupled) generation of the 5'-deoxyadenosyl radical (see Scheme 1.8). If this highly reactive intermediate is formed in the absence of a substrate then it can react with whatever molecules are adjacent. In

the active site, this is likely to involve abstraction of a hydrogen atom from the protein backbone, which risks the cleavage of peptide bonds and destruction of the protein, in addition to the wasteful cleavage of a SAM molecule. Uncoupled turnover has been reported for a number of radical SAM enzymes including: AnRNR-AE, SPL, HydG, HydE, BioB, LipA and HemN[31, 32, 39, 71-73]. The problem of uncoupled turnover with respect to tyrosine lyase is discussed in detail in Chapter 4 of this thesis.

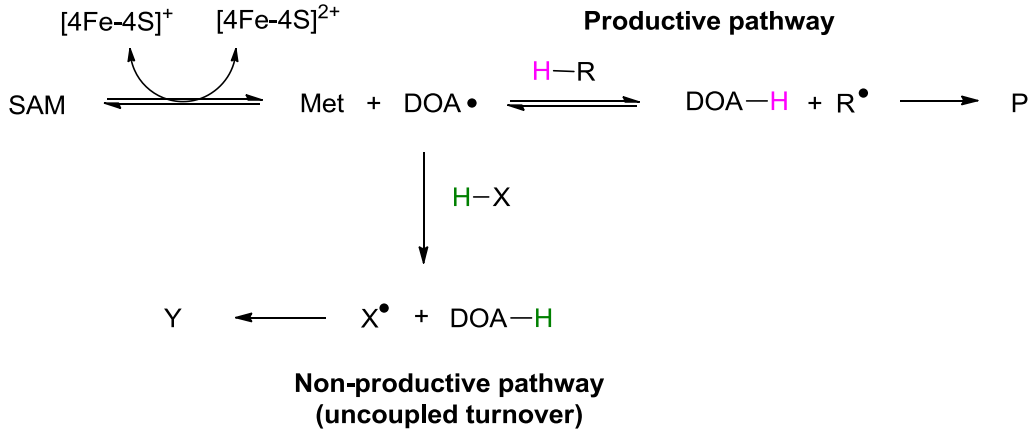

Scheme 1.8 Uncoupled formation of DOA in radical SAM enzymes.

The problem of uncontrolled generation of the 5'-deoxyadenosyl radical intermediate is partly overcome by the energetic demands of reductive cleavage of SAM. The redox potential for reduction of SAM is estimated to be ~ -1800 mV[74], however, a $[4Fe\text{-}4S]^{2+/1+}$ couple is in the order of -450 mV[75]. Therefore, the reduction of SAM by a $[4Fe\text{-}4S]^{1+}$ cluster of a radical SAM enzyme has been measured to be an extremely energetically uphill process (a difference of ~ 1.4 V which corresponds to ~ 130 $kJmol^{-1}$). Hinkley and Frey[75] reported that the mid-point potential for the 4Fe-4S cluster in LAM was raised slightly by the binding of SAM or a SAM analogue. The mid-point potential with SAM as the fourth ligand was found to be ~ 80 mV higher than in the presence of dihydrolipoyl, dithiothreitol (DTT) or cysteinyl ligands. This raise in mid-point potential brings the 4Fe-4S cluster into the range that it can be reduced by physiological reductants, such as ferridoxins or flavodoxin and could suggest the requirement of

substrate binding to tune the redox potential of the 4Fe-4S cluster. This represents one mechanism by which reduction of radical SAM 4Fe-4S clusters is controlled.

Further studies on the mid-point potentials of the 4Fe-4S cluster of LAM by Wang and Frey[74] showed that the energy barrier for reduction of SAM by the cluster could be overcome by binding energy. It was reported that the binding of SAM lowered the energy barrier by 80 $kJmol^{-1}$ and the binding of lysine gave a further 17 $kJmol^{-1}$. Examination of the X-ray crystal structures of radical SAM active sites (Figure 1.5, Figure 1.6 and Figure 1.7) shows the extensive interaction of SAM with surrounding protein residues and also the other substrate(s). These interactions are proposed to fix the substrates in position for the reaction and may explain the lowering of the energy barrier for reductive cleavage by substrate binding. An additional consideration is that upon reductive cleavage the unique iron atom binding the N / O atoms of SAM changes from a pentacoordinate geometry (**30**) to a thermodynamically more favourable hexacoordinate iron atom (**31**) (Scheme 1.4 and Figure 1.4), thus further promoting reductive cleavage of SAM by the 4Fe-4S cluster.

LAM has been shown to use SAM as a co-enzyme and as such cleaves SAM reversibly by electron transfer from the unique iron of the 4Fe-4S cluster. As was discussed and shown in Figure 1.4 the nature of the interaction between SAM and the 4Fe-4S cluster is proposed to differ in radical SAM enzymes that perform non-reversible SAM cleavage and require an equivalent of SAM for each hydrogen atom abstraction. In these cases the sulfonium ion is proposed to interact with the sulfur in the cluster neighbouring the unique iron atom (see Figure 1.4). Recently, however, with the increase in biochemical and structural data available on different examples of the radical SAM family a consensus mechanism for reductive SAM cleavage is emerging. Some of these examples are discussed in the following paragraphs.

The crystal structure of PFL-AE (non-reversible SAM cleavage) has been solved with SAM bound to the cluster in both the presence and absence of a heptapeptide mimic of the glycyl radical domain of the PFL catalytic subunit[65]. In the structure without the heptapeptide the SAM is disordered and not all of the molecule could be resolved in the structure (Figure 1.8 A). In the structure with the heptapeptide bound the SAM was far more ordered and the sulfonium ion of SAM was fixed much closer to the 4Fe-4S cluster (Figure 1.8 B). It can also be noted that the sulfonium occupies a similar position to other radical SAM enzymes, close to the unique iron atom. These two structures further demonstrate how the binding of both substrates position the molecules for radical SAM chemistry and contribute to the lowered energy barrier observed by Wang and Frey.

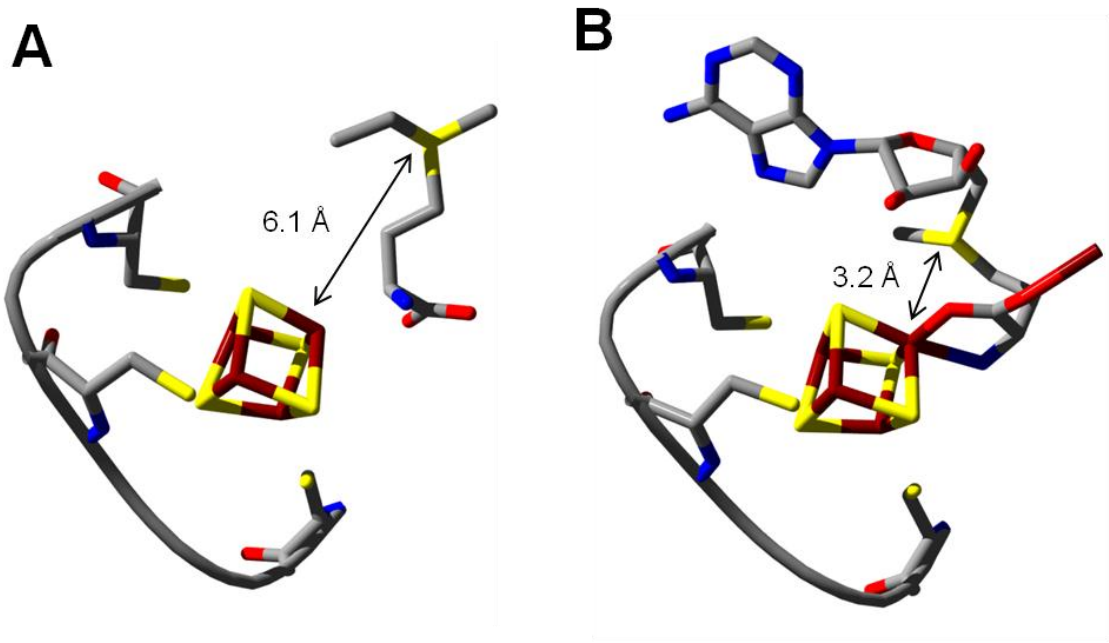

Figure 1.8 X-ray structure of SAM ligation to the 4Fe-4S cluster in the A) absence and B) presence of heptapeptide substrate. In the absence of substrate the SAM is disordered and the adenosyl moiety is not fully resolved.

BtrN is a recently characterised radical SAM enzyme which catalyses the oxidation of 2-deoxy-*scyllo*-inosamine (**48**) as part of the butirosin biosynthetic pathway[35]. This is another example

where SAM is acting as an oxidant[27] (like BioB and LipA discussed earlier). BtrN has been shown to have a stoichiometric requirement of SAM, which would suggest the SAM cleavage is not reversible. The mechanism proposed by Yokoyama *et al.*[35] is shown in Scheme 1.9. Deuterium labelling of the substrate identified the hydrogen atom abstracted by the 5'-deoxyadenosyl radical. When the deuterated substrate was incubated in the assay it was found that some di-deuterated DOA was formed. This indicates that the hydrogen atom abstraction is reversible and the substrate radical can re-abstract a hydrogen atom from DOA-H. The experiments on BtrN with the deuterated substrate showed a very small kinetic isotope effect. The small size of the kinetic isotope effect led the authors to speculate that hydrogen atom abstraction was not the rate determining step. Instead the formation of the ketone was proposed to be rate limiting. Grove *et al.*[46] have demonstrated by Mossbauer spectroscopy that BtrN has a second 4Fe-4S cluster that binds the substrate (**48**) and showed by EPR that it functions as an electron acceptor during catalysis to complete the oxidation. This has led to the postulation of a potential consensus mechanism for enzymes that mediate radical SAM dependent dehydration, such as AtsB[34].

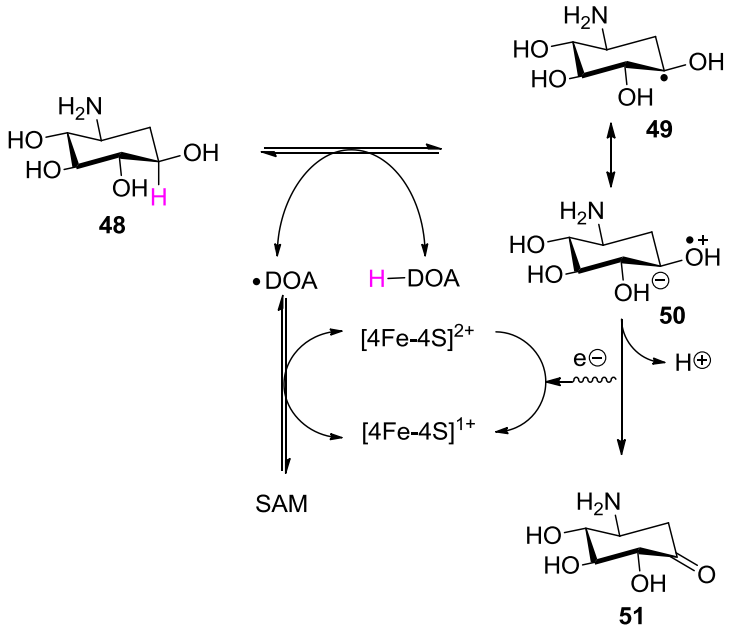

Scheme 1.9 Mechanism for BtrN proposed by Yokayama *et al.*[35]. The proposal that the electron recycles to reduce the 4Fe-4S cluster has not been resolved experimentally.

Similar deuterium labelling experiments have been reported for BioB, where the C9 and C6 positions of dethiobiotin were labelled with deuterium. It was unexpectedly found that both the 9-mercaptodethiobiotin (9-MDTB) intermediate and biotin product contained up to four deuterium atoms[31]. A small amount (2 – 6%) of the deuterium was found to be transferred to different carbons, other than C9 or C6 of 9-MDTB or biotin. This observation was explained by the hydrogen atom abstraction step being reversible and not specific to the C9 or C6 carbons. However, subsequent sulfur insertion only occurs at the C9 or C6 positions, meaning any other substrate radical has the chance to non-specifically re-abstract a hydrogen atom from DOA, thus re-forming the 5'-deoxyadenosyl radical, which in turn could react with methionine and the 4Fe-4S cluster to regenerate SAM. Uncoupled turnover has been reported for BioB (e.g. the ratio of DOA formed to biotin formed is greater than 1), however it is not as a result of non-productive SAM cleavage as no DOA is produced in the absence of dethiobiotin substrate[31]. The excess of DOA produced during *in vitro* BioB assays was instead assigned to the formation of a dethiobiotin derived intermediate.

BioB has been shown to assert additional control to prevent uncoupled SAM cleavage. Ugulava *et al.*[51] demonstrated that the two substrates of BioB bind in a cooperative manner, with the affinity for SAM being greatly increased (by a factor of >20) in the presence of dethiobiotin. As already discussed, SAM interacts with the other substrate in radical SAM enzymes and in the case of BioB, dethiobiotin makes substantial van der Waals contacts with 50% of the surface of SAM. Dethiobiotin also interacts with the protein, including a hydrogen bonding interaction of the carboxylate with two conserved threonine residues (T292 and T293)[64]. These two residues are part of a loop (shown in green in Figure 1.5) that is proposed to close over the active site upon substrate binding, thus further sealing off the TIM barrel for radical SAM chemistry.

HydE is a radical SAM protein which along with HydG and HydF, is involved in the maturation of [FeFe]-hydrogenase cofactors (H clusters)[76-79]. The substrate for HydE is unknown, but it is most likely to be responsible for the biosynthesis of a dithiolate bridge present in the [FeFe]-hydrogenase H cluster. The X-ray crystal structure of HydE has been solved with the SAM and the SAM cleavage products DOA and methionine bound to the active site[63, 67]. In the structure of HydE with SAM bound, the sulfonium ion of SAM was found to reside closest to the unique iron of the 4Fe-4S cluster (Fe_4—Sδ+ = 3.25 Å), similar to other radical SAM enzymes. In the structure with DOA and methionine bound, the position of the adenosine moiety had undergone only very small changes in orientation, whereas the methionine moiety had moved more significantly. The Fe_4—Sδ+ distance was observed to decrease to 2.67 Å[63]. The two structures were used to perform computational experiments on the mechanism of SAM cleavage and model the transition state (the results of these experiments are summarised in Figure 1.9). The calculated activation energy barrier was 54 $kJmol^{-1}$ which was in good agreement with the experimentally determined value of 54.4 $kJmol^{-1}$ for LAM in the absence of substrate or 37.7 $kJmol^{-1}$ in the presence of substrate[74]. In the model of the transition state the Fe_4—Sδ+ had decreased to 2.62 Å and the 5'C—Sδ+ bond had increased to 3.33 Å. The decrease in Fe_4—Sδ+ distance between the SAM bound structure and the DOA and methionine bound structure was attributed to the change in co-ordination environment of the unique iron, having a pseudo-octahedral co-ordination in the products. This accounts for the slightly lower energy of 45.6 $kJmol^{-1}$ estimated for the 5'deoxyadenosyl radical and [4Fe-4S]-methionine intermediates.

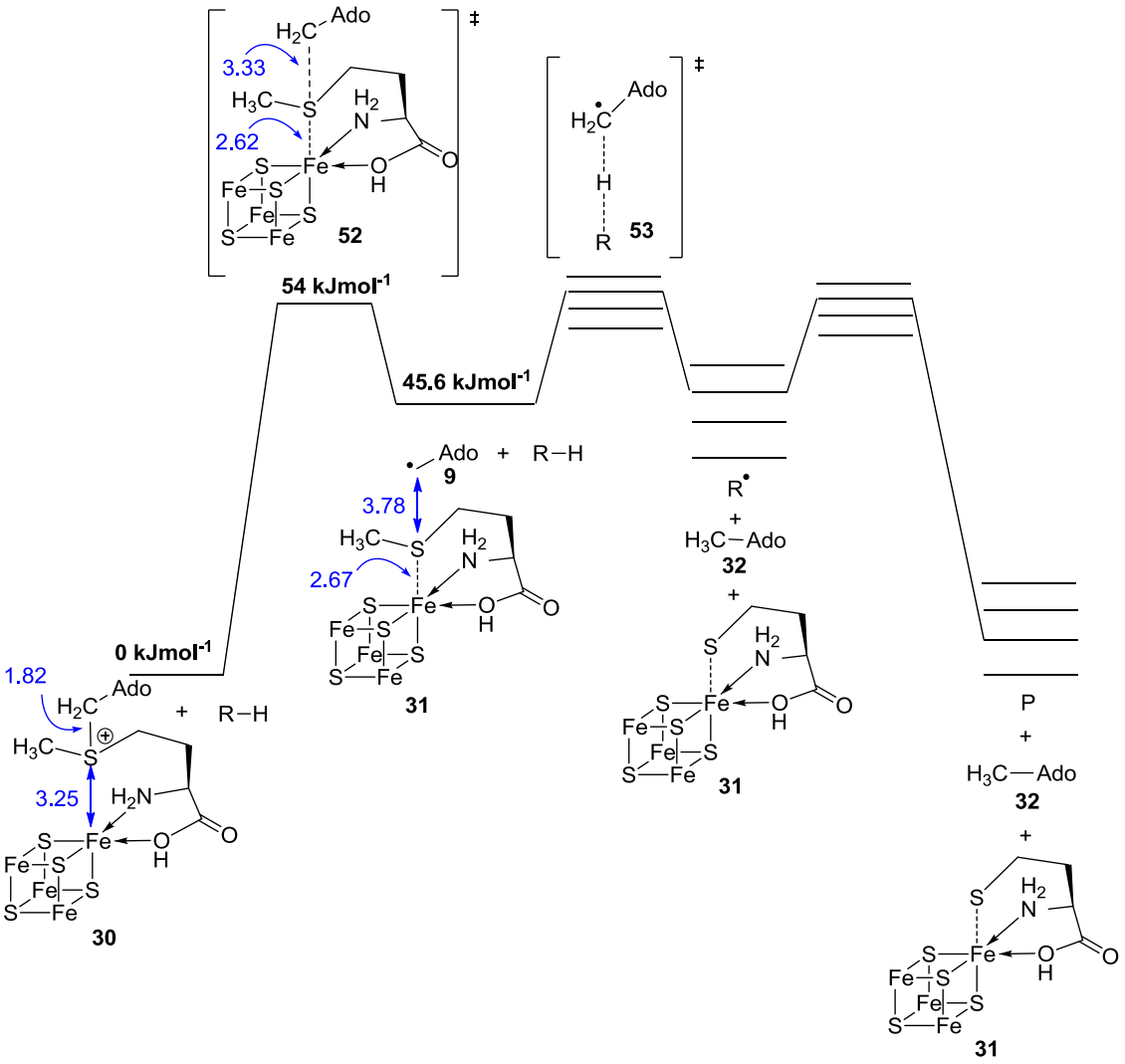

Figure 1.9 Energy profile for reactions catalysed by radical SAM enzymes, showing the distances in Angstroms (shown in blue) and energy levels are as reported by Nicolet *et al.*[63].

The substrate for HydE remains unknown at this stage, therefore, it remains unclear how the presence of a substrate positioned for hydrogen atom abstraction would affect the structure of the transition state (**52**). At the end of their paper Nicolet *et al.*[63] speculate that, based on the geometry of SAM and the 4Fe-4S cluster in available radical SAM crystal structures, the modelled mechanism for reductive cleavage of SAM, with the electron transfer to the sulfonium ion occurring via the unique iron atom, may be common to all members of the radical SAM family. However, this raises an important question about the reversibility of SAM cleavage in

radical SAM enzymes. The reversibility of reductive cleavage of SAM may not depend on the mechanism of electron transfer but may rely on other factors, such as the affinity of the products (DOA and methionine) for the enzyme which may permit the reverse reaction, or the nature of the chemistry being catalysed by the 5'deoxyadenosyl radical.

Radical SAM enzymes can be classified based on their utilisation of the 5'-deoxyadenosyl radical, as discussed in section 1.2.2. All three classes share the mechanistic steps of reductively cleaving SAM through electron transfer from the unique iron of the 4Fe-4S cluster. The variations in subsequent steps, specific to each class (or individual enzyme), including possible variations in rate of reaction (see Table 1.2) could be reflected by differences in the energy levels of subsequent intermediates and transition states and is represented in the energy profile shown in Figure 1.10. LAM utilises the 5'-deoxyadenosyl radical catalytically and as such the system recycles at the high energy levels (see red arrows in Figure 1.10). There is always a reactive radical species (at high energy) at each intermediate during catalysis. BioB on the other hand uses the 5'-deoxyadenosyl radical stoichiometrically with respect to hydrogen atom abstraction steps. The hydrogen atom abstraction generates a radical intermediate which will be similar in energy to the 5'-deoxyadenosyl radical (i.e. a primary or secondary carbon radical – see Scheme 1.7 and Table 1.1). The next step forms a new carbon-sulfur bond (**44** in Scheme 1.7) and the 2Fe-2S cluster acts as an electron acceptor, thus quenching any organic radicals. As such, this is a much more exothermic step, potentially providing the thermodynamic driving force for the reaction (see blue arrow in Figure 1.10). PFL-AE uses the 5'deoxyadenosyl radical stoichiometrically to generate a catalytic radical. The product of PFL-AE is a glycyl radical on the backbone of the PFL catalytic subunit. This radical is stabilised relative to the 5'-deoxyadenosyl radical (see Table 1.1) and does not provide the very large energetic advantage of quenching the radical as proposed for BioB. This may be reflected in the differences in the observed rate constant for the different classes of radical SAM enzyme shown in Table 1.2.

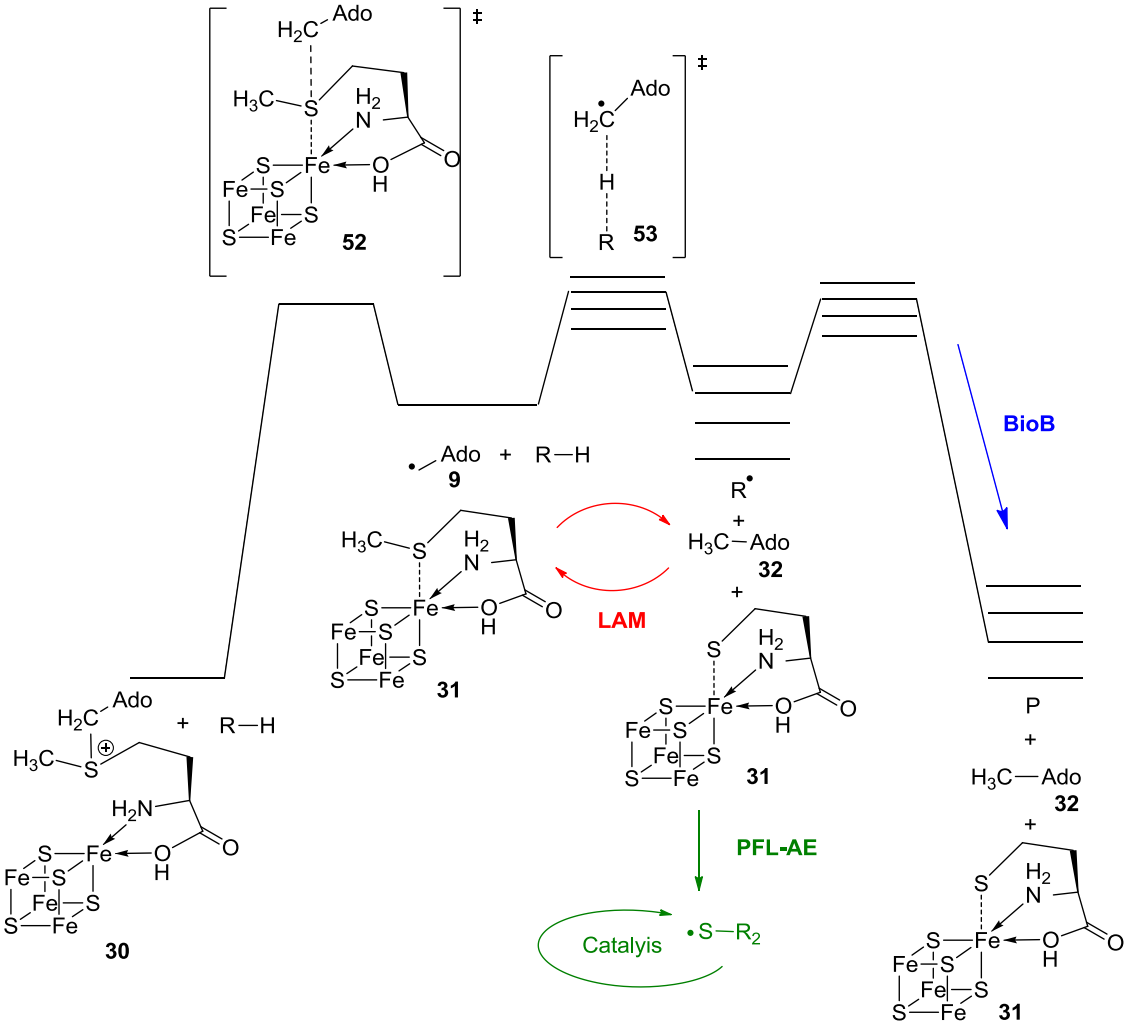

Figure 1.10 Energy profile for reactions catalysed by radical SAM enzymes, showing the variations in the use of the 5'-deoxyadenosyl radical. LAM (shown in red) uses DOA• catalytically, PFL-AE (shown in green) uses stoichiometric DOA• to generate a different catalytic radical and BioB (shown in blue) uses DOA• non-catalytically in the direct generation of a product.

1.2.5 *Variations within the Radical SAM Family*

The radical SAM superfamily was identified in 2001 in a bioinformatics study which noticed the characteristic "CXXXCXXC" motif[17]. This diagnostic motif was reportedly present in >600 proteins sequences and characterised as radical SAM enzymes. It has recently been discovered that variations in the cluster binding motif are possible and radical generation from SAM cleavage by a 4Fe-4S cluster can be achieved in proteins which do not have the "CXXXCXXC" motif. During thiamine biosynthesis, ThiC is the only protein required to convert 5-aminoimidazole ribonucleotide (AIR) into 4-amino-5-hydroxymethyl-2-methylpyrimidine phosphate (HMP-P)[80]. *In vitro* biochemical studies[81, 82] have demonstrated the presence of an oxygen labile [4Fe-4S] cluster and a dependence on SAM and a reductant for activity. Despite these clear indicators of a radical SAM mediated reaction, analysis of the ThiC sequence does not show the presence of the "CXXXCXXC" motif close to the N-terminus. However, a highly conserved "CXXCXXXXC" motif is present near the C-terminus of the enzyme, which has been shown through X-ray structural data to coordinate the 4Fe-4S cluster.

Another variation of the cysteine triad has been observed in HmdB, a protein proposed to function in the maturation of the cofactor for the hydrogen forming methylene-H_4-methanopterin dehydrogenase (HmdA)[83]. The HmdB sequence shows most similarity to a group of radical SAM enzymes (BioB, ThiH, HydE and HydG), but the cluster binding cysteine triad is modified to a "CX_5CX_2C" motif. Studies to probe the biochemical function of HmdB indicate the presence of a [4Fe-4S] cluster capable of binding SAM that upon reduction yields DOA.

A further expansion of the radical SAM family was reported very recently. A novel 4Fe-4S cluster containing protein, termed Dph2, is involved in the post translational modification of a

histidine residue in the biosynthesis of diphthamide[84, 85]. The 4Fe-4S cluster is bound to Dph2 through three conserved cysteine residues; however these do not form the classical "CXXXCXXC" motif. Remarkably, structural analysis of Dph2 has shown that the 4Fe-4S cluster is coordinated by three cysteine residues derived from three different domains (Cys59, Cys163 and Cys287), an arrangement that achieves a similar function to the CX_3CX_2C motif but uses a completely different structural framework. The 4Fe-4S cluster is proposed to interact with SAM in a similar fashion to in classical radical SAM enzymes; however the electron transfer from the 4Fe-4S cluster to the sulfonium ion occurs slightly differently. Rather than homolysis of the 5'C-S bond, generating the 5'deoxyadenosyl radical which forms DOA after abstraction of a hydrogen atom, Zhang *et al.*[85] reported the formation of 5'methylthioadenosine (**54**) (and not DOA) as a by product of Dph2 activity. This implies that Dph2 breaks the S-C bond to the 3-amino-3-carboxy-propyl group and not the 5'C-S bond, thus generating the 3-amino-3-carboxypropyl radical (**55**) which can then functionalize the histidine residue. The X-ray crystal structure of Dph2 reported does not show the enzyme in a complex with SAM. Despite this lack of evidence it is tempting to speculate that SAM would be orientated slightly differently around the 4Fe-4S cluster than in classical radical SAM enzymes. Thus allowing for overlap for the appropriate σ* orbital with the electron donating orbital in the 4Fe-4S cluster.

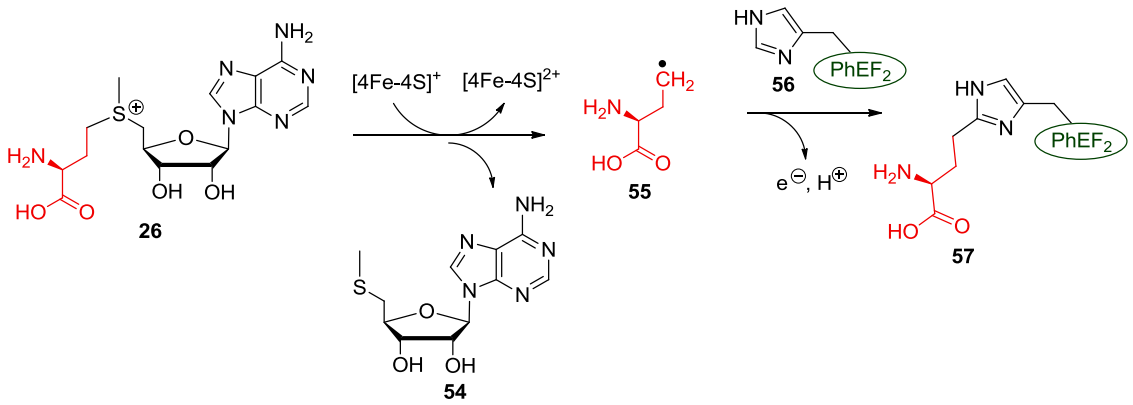

Scheme 1.10 The involvement of Dph2 in generating the 3-amino-3-carboxy-propyl radical towards the biosynthesis of diphthamide.

1.3 *Bacterial Thiamine biosynthesis and Tyrosine Lyase*

1.3.1 *Thiamine and its Biological Function*

Thiamine pyrophosphate (TPP) (**58**) is the biologically active form of vitamin B_1 and functions as the coenzyme of several enzymes, including pyruvate decarboxylase, pyruvate dehydrogenase and transketolase[86]. Its structure was elucidated and synthesis was reported in the 1930's and it was found to contain two distinct structural subunits; a pyrimidine (4-amino-5-hydroxymethyl-2-methyl pyrimidine) and thiazole (4-methyl-5-(β-hydroxyethyl) thiazole) (Figure 1.11). Thiamine is readily biosynthesised[87, 88] by many micro-organisms and higher plants, but mammals require thiamine as an essential part of their diet, the recommended daily dose for the average adult male being about 1.5 mg[89]. Its deficiency can lead to beriberi, a disorder that seriously affects the heart, cardiovascular and nervous systems. It is therefore readily available as a supplement and frequently added to food products, such as bread and the annual world production of this vitamin is in excess of 4000 tonnes.

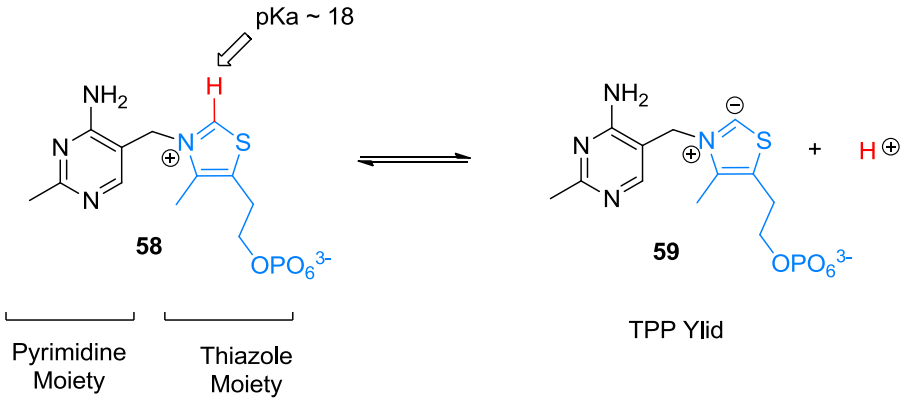

Figure 1.11 Structure of thiamine pyrophosphate (TPP), the biologically active form of the vitamin.

The chemistry of the thiamine pyrophosphate co-factor relies on the weakly acidic proton adjacent to the C2 carbon of the thiazole moiety. This proton has a pKa of about 18 due to the stabilisation of the resulting anion by the adjacent positive charge. Deprotonation of TPP yields the active ylid (**59**), which functions either as a nucleophile or as a leaving group[90, 91]. This feature of the TPP ylid is the key to its biological activity and enables the catalytic cleavage of C—C bonds, in particular the decarboxylation of α-keto acids and the formation of activated aldehydes. An example which demonstrates this is the biosynthesis of 1-deoxy-D-xylulose-5-phosphate (DXP) (**67**) from pyruvate (**60**) and glyceraldehyde-3-phosphate (**63**) (see Scheme 1.11). This reaction is catalysed by DXP synthase (Dxs), an enzyme which utilises TPP as a co-factor. The TPP ylid nucleophilically attacks the ketone of pyruvate (**60**) and the adduct then undergoes a decarboxylation. A resonance form of the resulting intermediate (**64**) has a negative charge on the carbonyl carbon meaning the polarity of this atom has been reversed. This anion reacts with the aldehyde functional group of glyceraldehyde-3-phosphate (**63**) forming a new carbon-carbon bond. The final step of the mechanism of is release of the DXP product (**67**) and the catalytic TPP ylid (**59**)[88, 92-94].

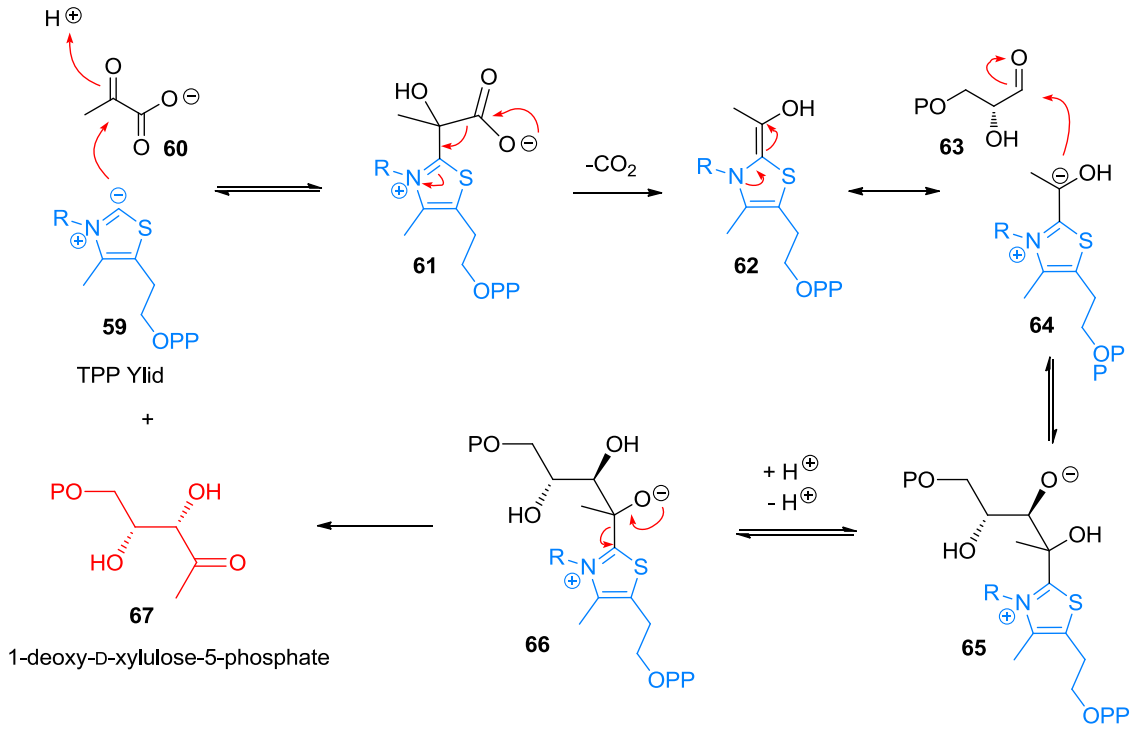

Scheme 1.11 Mechanism for the biosynthesis of DXP.

1.3.2 *Thiamine Biosynthesis in Bacteria*

The biosynthesis of TPP (**58**) involves the coupling of the independently formed thiazole and HMP moieties in the final steps. In bacteria, the HMP moiety is formed in a single step by an extremely complicated rearrangement of 5-aminoimidazole ribotide (AIR). Paradoxically, one of three precursors to the thiazole moiety is DXP (**67**). The other two precursors are a sulphur atom, derived from cysteine (**71**) and transferred via a sulphur carrier protein, ThiS (see Scheme 1.12) and dehydroglycine (**11**).

These three precursors act as substrates for thiazole synthase (ThiG), an enzyme responsible for formation of the 5-membered thiazole ring (**86**) (see Scheme 1.13). Thiazole synthase has a highly conserved lysine residue (K96 in *Bacilus subtilis*) which is positioned in the active site and forms an imine (**78**) with the carbonyl of DXP[95]. Formation of an iminium species is a common process in enzyme reactions and results in a 10^8 fold increase in the acidity of the proton at the α–carbon. The next step in the mechanism of thiazole synthase is indeed the deprotonation at the α–carbon, a step which is facilitated by the basic glutamate residue (E98 in *B. subtilis*) present in the active site. This catalyses an Amadori type rearrangement with a ketone group now at the C3 position (**80**) (rather than C2, as in DXP).

The next step in the mechanism involves incorporation of the sulfur atom, which is facilitated by nucleophilic attack by a thio-carboxylate group (**76**). This thio-carboxylate group is positioned at the C-terminus of the sulphur carrier protein (ThiS). ThiS can form a tight complex with thiazole synthase[96] and another protein involved in bacterial thiazole biosynthesis called ThiF. ThiF along with IscS and ThiI catalyses the transfer of a sulphur atom from cysteine to form the C-terminal thio-carboxylate on ThiS (see Scheme 1.12). The C-

terminus of ThiS has two conserved glycine residues providing a protruding appendage which can infiltrate the active site of thiazole synthase (see Figure 1.12), placing the thiocarboxylate in close proximity to the DXP derived intermediate (**80**). Formation of the new carbon-sulfur bond is followed by an S/O acyl shift and elimination of a water molecule and the ThiS-carboxylate (**68**)[96-99].

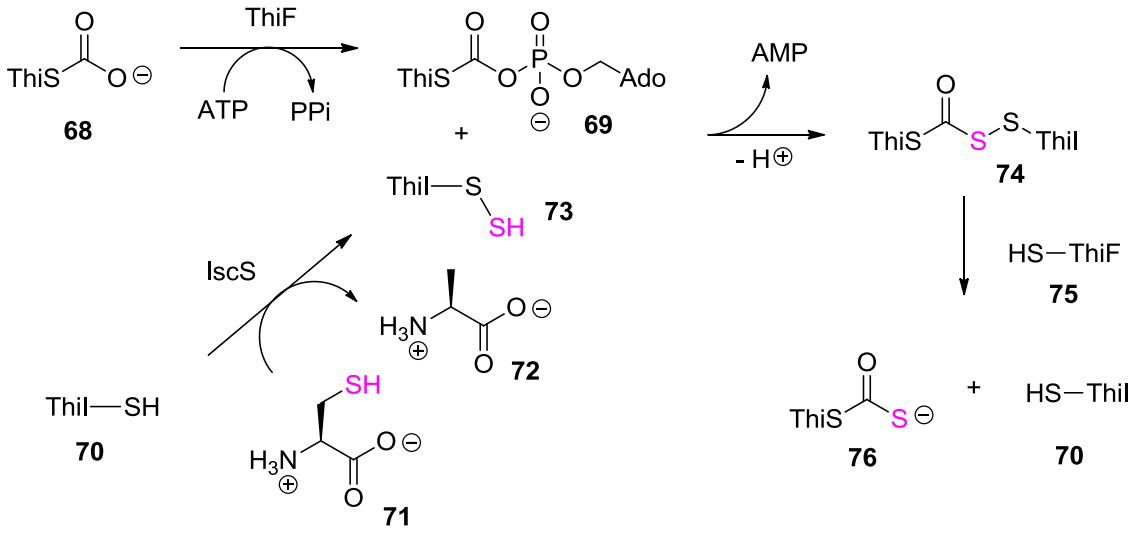

Scheme 1.12 Mechanism of sulfur transfer generating ThiS-thiocarboxylate.

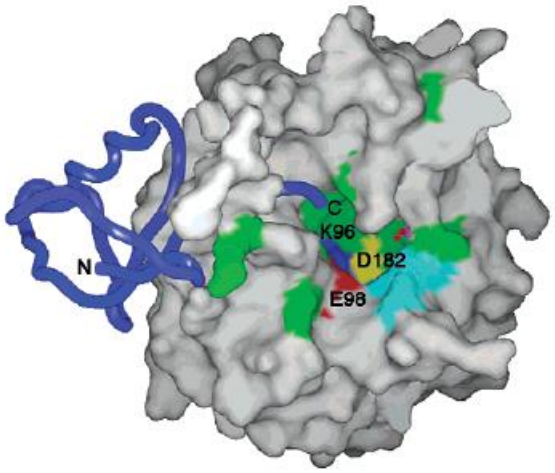

Figure 1.12 X-ray structure derived image of ThiS docking to the active site of thiazole synthase. (Adapted from[96])

The final steps of the mechanism of thiazole formation involve the insertion of the C2—N3 fragment and closing of the 5-membered ring. The third precursor, dehydroglycine (**11**), serves an an electrophile and reacts with the deprotonated thiol group (**82**). A subsequent 5-exo-trig cyclisation forms the thiazole ring[100]. Finally the lysine side chain is released and made available for another catalytic cycle. In *Bacilus subtilis*, the product of thiazole synthase was recently characterised as the non-aromatic thiazole carboxylate (**86**)[101]. Another enzyme, called TenI, is responsible for aromatisation of the thiazole ring. Decarboxylation occurs during the coupling of thiazole phosphate to HMP[88].

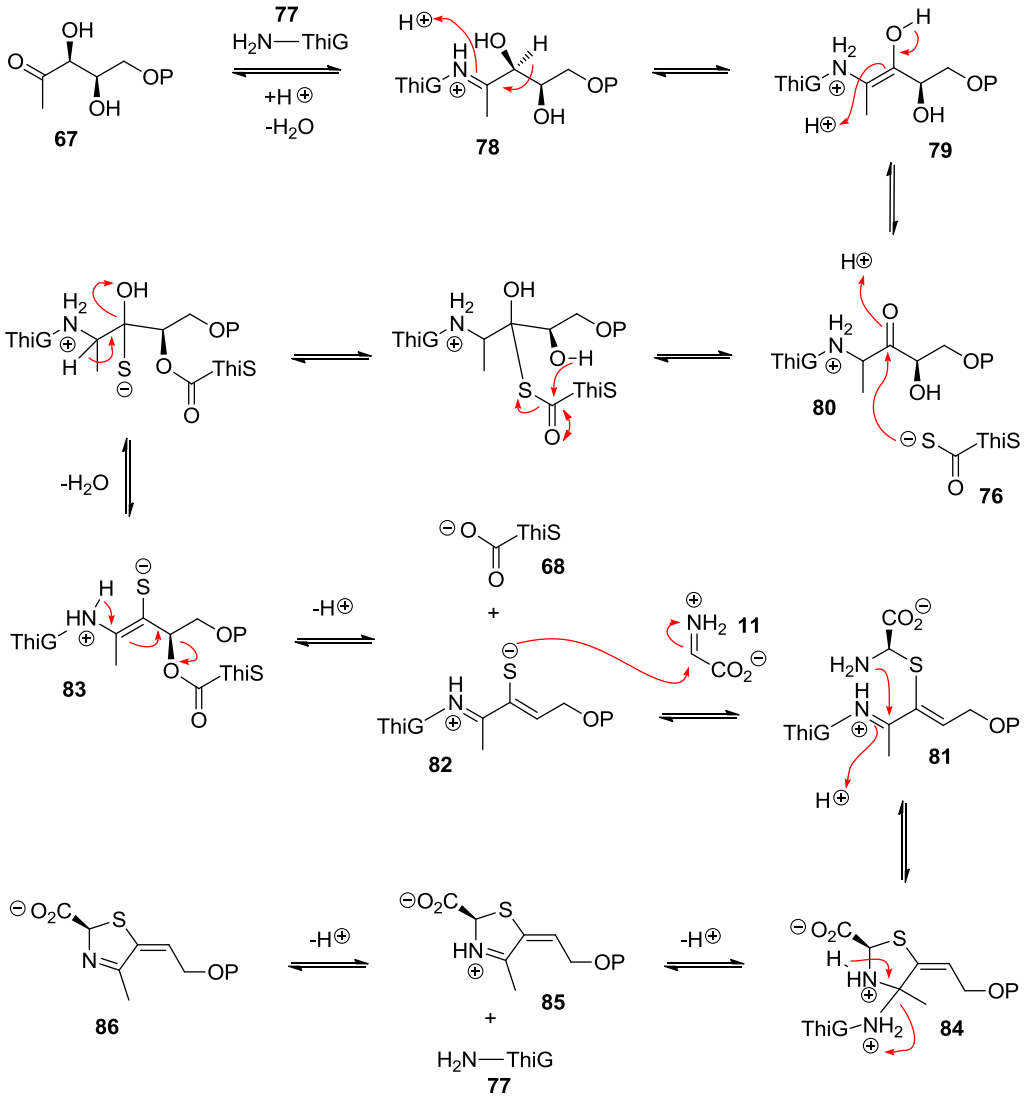

Scheme 1.13 Mechanism of thiazole biosynthesis catalysed by ThiG, proposed by Settembre *et al.*.[96]

The formation of dehydroglycine (**11**) represents the primary difference in aerobic and anaerobic prokaryotic thiazole biosynthesis. The model organism for studying the mechanism described above was *Bacilis subtilis* (*B. subtilis*), which is an aerobe. This organism sources dehydroglycine by oxidising glycine (**87**) in a reaction mediated by glycine oxidase (ThiO), which is dependent on flavin adenine dinucleotide (FAD)[102]. The catalytic cycle of ThiO involved the reduction of an oxygen molecule to hydrogen peroxide. Organisms that exist in an anaerobic environment, such as *Escherichia coli* (*E. coli*), require a different mechanism for arriving at this electron deficient intermediate as oxygen will not always be available. The pathway employed by these organisms utilises tyrosine (**10**) and requires cleavage of the Cα—Cβ bond, with the Cα—N fragment ending up incorporated into the thiazole ring[103, 104]. The enzyme which catalysis this cleavage reaction is tyrosine lyase (ThiH) which is a member of the radical SAM family[105] and as such, requires SAM and a reductant for activity[106, 107].

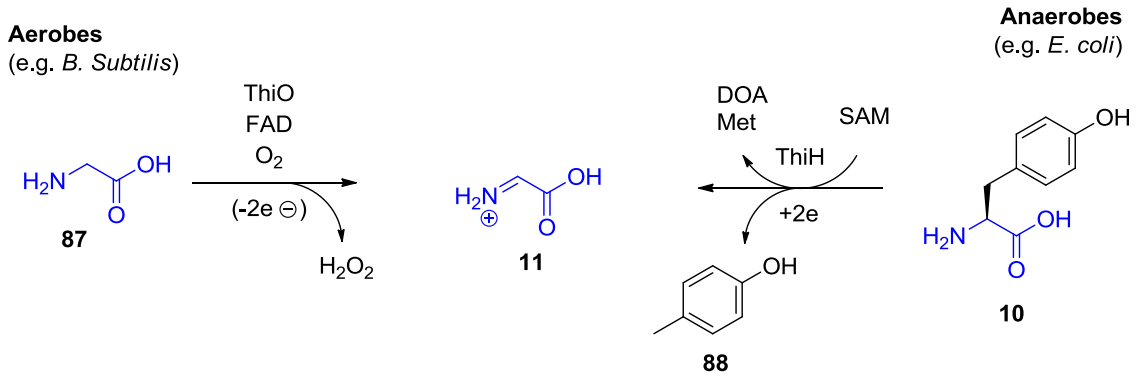

Scheme 1.14 Formation of dehydroglycine in aerobic and anaerobic bacteria.

The biosynthesis of the 4-amino-5-hydroxymethyl-2-methyl pyrimidine (HMP) moiety involves a complicated rearrangement of 5-aminoimidozole ribotide (AIR)[108, 109] (**89**) yielding HMP monophosphate (**90**), which is then phosphorylated to HMP diphosphate (**94**). The rearrangement is mediated by HMP synthase (ThiC) and the phosphorylation is dependent on HMP kinase (ThiD)[110]. AIR (**89**) is an intermediate on the purine biosynthetic pathway and it was previously noted that formation of HMP *in vivo* was dependent on methionine. ThiC has

recently been rigorously characterised and has expanded the radical SAM family[81, 82], which explains this observation (SAM is biosynthesised from ATP and methionine). Labelling studies have shown that all the atoms in HMP originate from AIR[111], and alluded to an extremely complex rearrangement mechanism. Very recently a more detailed study has begun to elucidate the mechanism and showed that two by-products derived from AIR are formate and carbon monoxide[112]. One equivalent of DOA was formed in the reaction, however, AIR bearing deuterium labels at C4' and C5' showed that both are transferred to DOA (see Figure 1.13 B). This result indicates that the 5'deoxyadenosyl radical initiates the reaction by generating a radical at one of these positions (despite the observation of a backbone free radical on ThiC in a different study). Rearrangement of this substrate radical yields a second intermediate radical, which is quenched by hydrogen atom abstraction from DOA, reforming the 5'-deoxyadenosyl radical. A second hydrogen atom abstraction then yields another intermediate radical which undergoes further rearrangement. This radical would appear to be quenched by a different mechanism to account for the equivalent of DOA which forms in the reaction. The observation of two different hydrogen atom abstractions from the same substrate by the same 5'-deoxyadenosyl radical was unprecedented prior to the studies on ThiC. As was discussed in Section 1.2.5, ThiC ligates its 4Fe-4S cofactor through three conserved cysteines which form part of a motif not originally classified as a radical SAM enzyme. It will be interesting to note from future studies (either on ThiC or other radical SAM enzymes that may emerge with the same 4Fe-4S binding motif) whether this difference in reactivity is linked to the different binding motif?

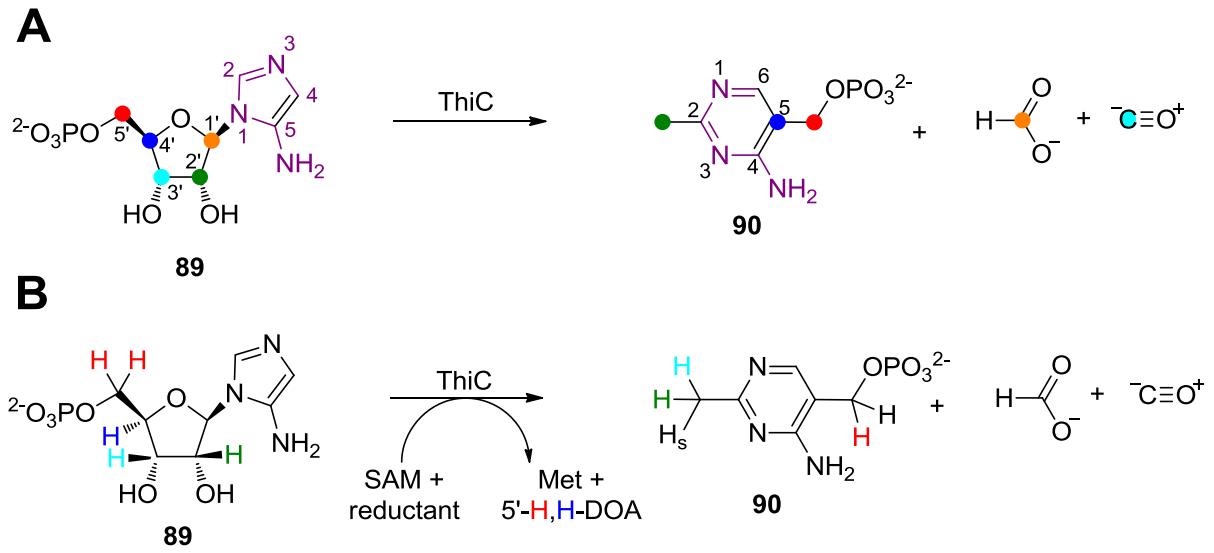

Figure 1.13 A summary of the labelling studies reported on ThiC[111, 112].

The biosynthesis of TPP in *B. subtlilis* is completed by coupling the independently formed thiazole and HMP moieties, a step accomplished by thiamine phosphate synthase (ThiE)[113]. Phosphorylation to the biologically active form of the co-factor, thiamine pyrophosphate by thiamine phosphate kinase (ThiL) completes the biosynthetic pathway. The mechanism of ThiE begins with loss of a phosphate from HMP pyrophosphate (**91**) and generation of a carbocation (**92**) (see Scheme 1.15). This charged species is stabilised by the adjacent aromatic ring. Nucleophilic attack of thiazole phosphate (**94**) forms thiamine monophosphate (**95**) which is the product of ThiE. ThiE can accept both thiazole and the carboxylated form of the thiazole, which is formed by ThiG, as substrates. A fact which initially led to the mis-assignment of the ThiG product, as ThiG activity was analysed by its ability to form thiamine monophosphate by the addition of ThiE and HMP pyrophosphate[100]. There is no available information in the literature as to where or how the decarboxylation of thiazole or thiamine occurs. It is likely that decarboxylation of thiamine would be more favourable than decarboxylation of thiazole as the resultant anion would be stabilised by the neighbouring positive charge on the nitrogen.

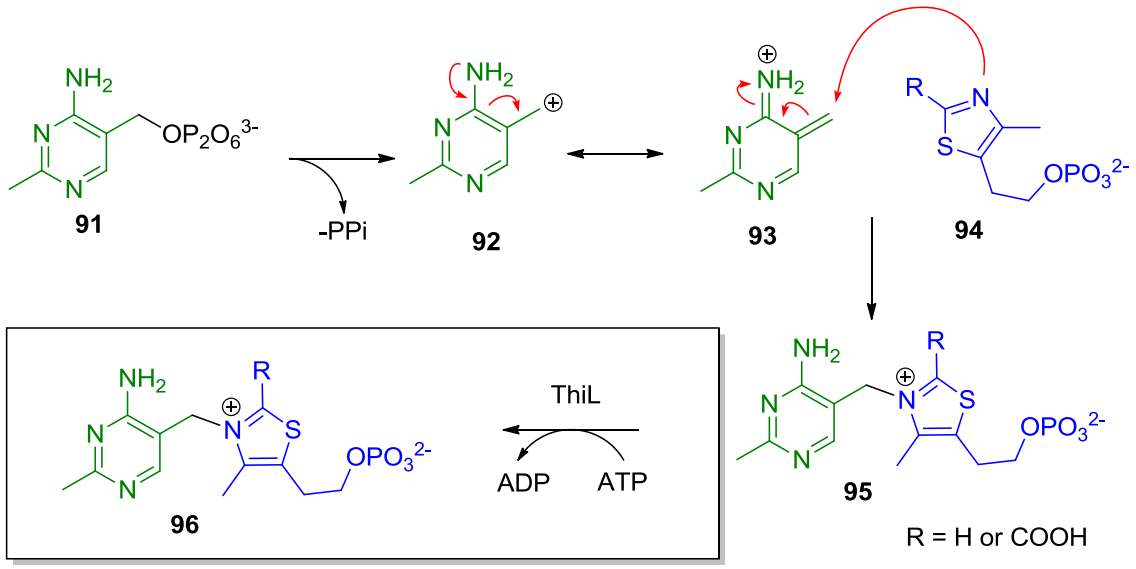

Scheme 1.15 Mechanism of ThiE generating thiamine phosphate, which is phosphorylated to thiamine pyrophosphate by ThiL (shown in the box).

1.3.3 *Tyrosine Lyase*

The aerobe: *Bacilus subtilis* has been used as the model organism for elucidating the bacterial thiamine biosynthetic pathway. A mechanistic understanding exists for each step towards the biosynthesis of thiazole phosphate in this organism[88]. However, there is only a limited understanding of the mechanism from which the intermediate, dehydroglycine, is derived from tyrosine in anaerobic bacteria. This step is seemingly wasteful as it requires cleavage of the tyrosine Cα—Cβ bond, which is an energetically demanding step, and dispenses with the aromatic portion of tyrosine as a byproduct. The mechanism by which aerobes generate this electrophilic intermediate is dependent on dioxygen[102]. Organisms that exist in anaerobic environments, such as *E. coli*, cannot depend on oxygen as an electron acceptor and as such require an alternative mechanism to arrive at electron deficient (or more oxidised) molecules.

Tyrosine lyase (ThiH) has been isolated as a complex with thiazole synthase (ThiG) and has been identified as a member of the radical SAM superfamily[106]. The protein sequence includes the characteristic "CXXXCXXC" 4Fe-4S binding motif and after careful chemical reconstitution the presence of the 4Fe-4S cluster was inferred by EPR (see Figure 1.14) and UV-vis spectroscopy[114]. The 4Fe-4S cluster was far more labile towards reduction in the presence of SAM which is consistent with observations on other members of the radical SAM family[75]. Mutation of some of the residues conserved among other radical SAM enzymes thought to be responsible of SAM or 4Fe-4S cluster binding suppressed thiazole biosynthesis *in vivo*, further supporting the notion that ThiH is a radical SAM enzyme[105].

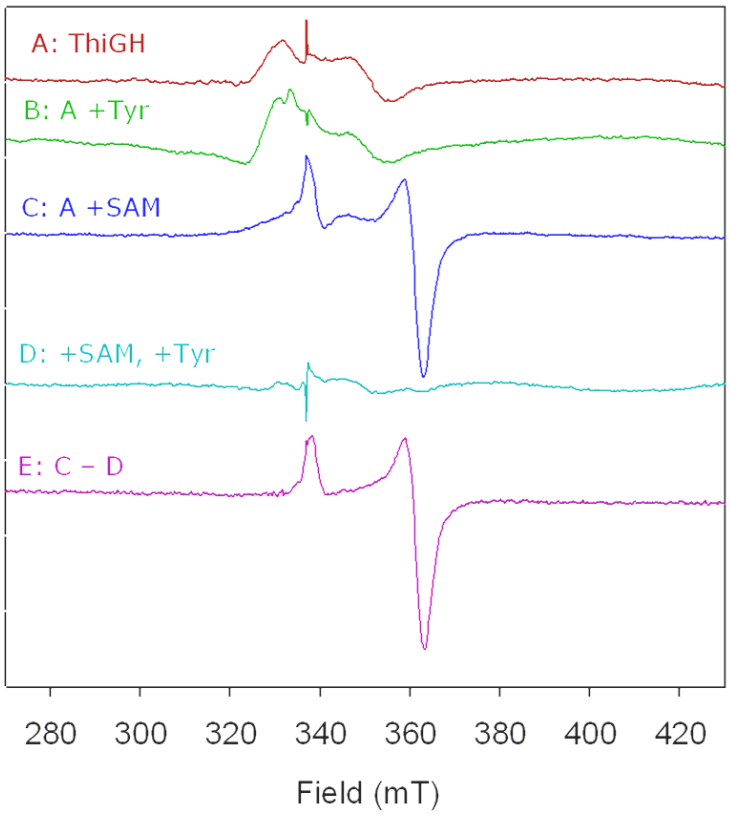

Figure 1.14. EPR spectra of ThiGH A) reconstituted ThiGH; B) A plus tyrosine; C) A plus SAM; D) A plus tyrosine and SAM; E) subtraction of C from D. The sharp spike at 338 milliteslas (*mT*) in each spectrum is a background signal. (Adapted from[114])

The *E. coli* thiazole biosynthetic pathway was reconstituted *in vitro* and was found to have an absolute requirement for L-tyrosine, SAM and a reductant. The EPR studies shown in Figure 1.14 used sodium dithionite as a chemical reductant. Reconstitution of the thiazole biosynthetic pathway utilised flavodoxin (FldA), flavoprotein NADPH oxidoreductase (Fpr) and NADPH as a source of electrons. Flavodoxin is thought to be the physiological reductant for radical SAM 4Fe-4S clusters in *E. coli*. Use of the assumed physiological reductant is important as it has more relevance to *in vivo* function of the enzyme. In particular as radical SAM enzymes use redox potential as a method of controlling radical generation (see Section 1.2.4) and reduction with dithionite can increase the amount of uncoupled reductive SAM cleavage. This is reflected

in the fact that in the absence of SAM ~20% of the cluster is reduced (Figure 1.14, spectra A), compared to >90% in the presence of SAM (Figure 1.14, spectra C).

Improvements in the isolation and chemical reconstitution enabled *in vitro* assays to be scaled up allowing for NMR characterisation of the reaction mixture[115]. Uniformly labelled ^{13}C-tyrosine was incubated with the ThiGH complex along with SAM and the FldA / Fpr / NADP reducing system. After removal of the protein a ^{13}C NMR spectra was the recorded of the reaction mixture and the signal of any tyrosine derived molecules was enhanced due to the ^{13}C label. In addition the labelling gave unique coupling of each carbon derived from tyrosine as it would be adjacent to a spin active ^{13}C isotope. ^{13}C NMR experiments identified glyoxylate (**98**) as one of the products of tyrosine cleavage *in vitro*. Glyoxylate was proposed to result from the rapid hydrolysis of dehydroglycine (see Scheme 1.16). An organic extract of the reaction mixture was prepared to characterise the aromatic by-product of tyrosine cleavage. A characteristic doublet with a chemical shift of 20 ppm was found to correspond to a benzylic methyl group, which suggested that the aromatic byproduct was *p*-cresol (**88**)[115]. This was an unexpected observation as a previously reported by product of thiamine biosynthesis in *E. coli* was 4-hydroxybenzyl alcohol (**97**)[116]. This observation was made from *in vivo* experiments and it was considered that the *in vitro* observations might be an artefact of the experiment. This observation raised an important question about the potential for variation in the products of ThiH *in vitro* and *in vivo* and is addressed in Chapter 2 of this thesis. It is essential that the *in vitro* experiments are relevant to *in vivo* metabolism before a valid mechanistic hypothesis for tyrosine cleavage by ThiH can be constructed.

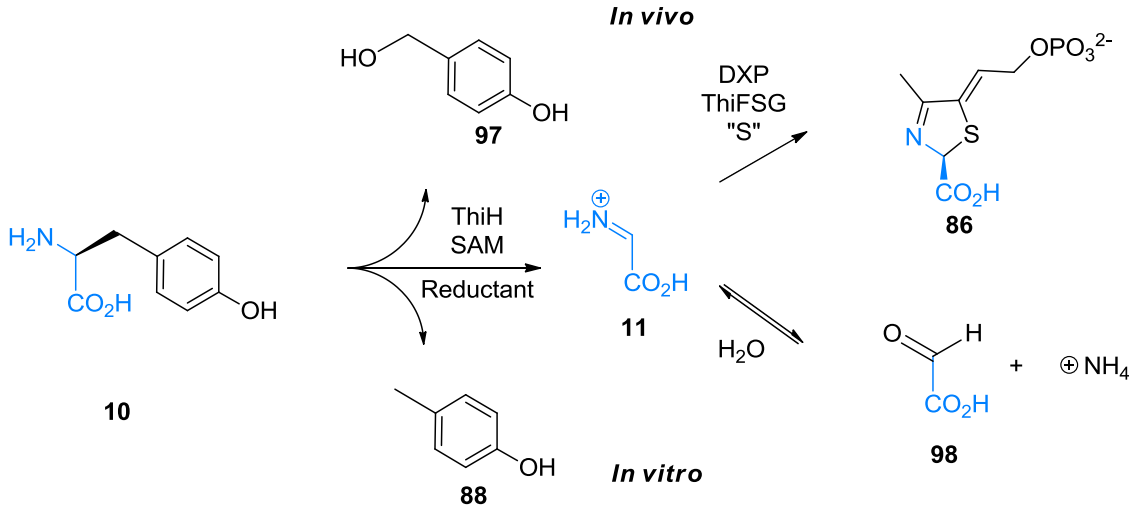

Scheme 1.16 Variation in the products of ThiH mediated tyrosine cleavage *in vivo* and *in vitro*.

1.4 *Aims of this Thesis*

The primary objective of this thesis is to build a mechanistic model for ThiH mediated tyrosine Cα-Cβ bond cleavage.

This will be achieved by:

- Confirming that *in vitro* experiments are relevant to *in vivo* metabolism
- Developing a robust assay for measuring ThiH activity
- Elucidating the mechanism using kinetic measurements, isotopic labelling and experiments with structural analogues of L-tyrsosine

2 Studies on Thiamine Biosynthesis *in vivo*

2.1 *Introduction*

The nature of the aromatic by product derived from tyrosine during thiamine biosynthesis was first investigated by White, who used GCMS to identify the accumulation of 4-hydroxybenzyl alcohol (4-HBA) (**97**) in cultures of *E. coli* actively biosynthesising thiamine[116]. Experiments in which cultures of an *E. coli* B strain were fed with ^{13}C labelled tyrosine were shown to produce ^{13}C 4-HBA. The characterisation of 4-HBA required extraction of the cell culture into DCM and analysis of the organic phase by GC-MS. Our recent results, discussed in chapter 1 (Section 1.3.3), demonstrated that the products of tyrosine cleavage in *vitro* were *p*-cresol (**88**) and glyoxylic acid (**98**), which is the hydrolysis product of dehydroglycine (**11**) (see Scheme 1.16), a result clearly in disagreement with the observations of White[116]. It is important to consider that the observations made *in vitro* might well be an artefact of the experiment (e.g. 4-HBA was reduced to *p*-cresol by a chemical reductant).

The observation of *p*-cresol *in vitro* has raised important questions about the fate of the aromatic by-product in the formation of dehydroglycine from tyrosine, in particular the potential for variations in the by-products formed *in vitro* and *in vivo*. In order to validate the observations made from *in vitro* experiments and subsequently build a mechanistic model relevant to *in vivo* thiamine biosynthesis, measurement of the formation of *p*-cresol *in vivo* was required. These experiments were based on the experimental methods developed by White, but included several refinements. In particular it was necessary to also define the requirement of ThiH in this metabolic process. Therefore, a prerequisite for these studies was an experiment to determine whether ThiH is functional *in vivo*.

2.2 *In vivo assay for ThiH function*

E. coli has several mechanisms to regulate the thiamine biosynthetic pathway, including the thi-box riboswitch to inactivate the expression of ThiCEFSGH[117-119]. The biosynthesis of TPP involves some metabolically inefficient steps and the riboswitch provides a regulation mechanism to avoid the cell producing an excess of TPP. However, this regulation is a disadvantage for studying the chemistry of TPP biosynthesis *in vivo* as it would restrict the formation of any metabolites which could make their characterisation difficult. To overcome this potential problem, a strain of *E. coli* from the Keio collection, which had had the genomic copy of ThiH deleted[120] was utilised. As such, this strain was auxotrophic for the thiazole moiety of TPP. Two derivatives of this strain were produced: one transformed with pRL1020 which would enable ThiH expression and the other with pBAD-His as a negative control (see Table 2.1). Under minimal growth conditions these two derivative strains would be dependent on biosynthesized TPP in order to grow. The control of the expression of genes harboured on a pBAD derived plasmid (including ThiH) is dependent on the arabinose concentration and is independent of thiamine concentration. Thus in the presence of arabinose, ThiH would be overproduced and any ThiH dependent reactions, including tyrosine cleavage reactions may readily occur, potentially providing a sufficient quantity of the aromatic by product for unequivocal characterization.

For these experiments, an important negative control is a culture of cells lacking a copy of ThiH. This would allow for the detection of any tyrosine metabolite derived from a non-thiamine biosynthetic pathway. The principle of the biological *in vivo* assay is that only cells actively biosynthesising thiamine should grow. Therefore, cultures of these strains would need to be supplemented with thiamine. To monitor the growth of these cultures over long time periods a method was developed which made use of a plate reader (see Method 20). 200 µL were prepared in a 96 well, transparent microplate and incubated in the plate reader. The

absorbance at 600 nm was monitored over a period of up to 24h. It was found that cultures in the plate reader could not be incubated at 37 ºC, as evaporation and condensation interfered with absorbance reading. Therfore, cultures in the plate reader were incubated at 30 ºC.

Strain	Plasmid	Genes present	Ability to biosynthesise TPP
BW25113 (*-thiH*)	pRL1020	ThiFSGH	Yes
	pBAD-His	None	No

Table 2.1 *E. coli* derivatives used to study thiamine biosynthesis *in vivo*

The derivative strains were initially cultured overnight, from a glycerol freeze stock, in nutrient rich media. The cells were then isolated, washed and cultured in Davis Mingioli minimal media (DM media)[121]. To allow any bacterial growth at all, it was necessary to supplement DM media with glucose to provide a readily available carbon source. However, it was soon discovered that while growing in rich media, cells could accumulate and store enough TPP to grow for some time when they were subsequently transferred to a minimal medium. To combat this, a period of 'starvation' was introduced where the cells were harvested from rich media, then re-suspended and cultured in 100 mL of DM media for 24 h, during which time, the previously accumulated store of thiamine was depleted (see Method 19). After the starvation phase, the culture was used to inoculate fresh 200 µL aliquots of DM media on a 96 well micro-plate and cultured in the plate reader at 30 ºC. As a result of this period of starvation a significant difference was observed in the growth of pBAD-His and pRL1020 transformed mutants in DM media that lacked thiamine supplement (see Figure 2.1). This demonstrates that the *thiH* gene on the pRL1020 plasmid is complementing the role of the deleted chromosomal copy of *thiH.*

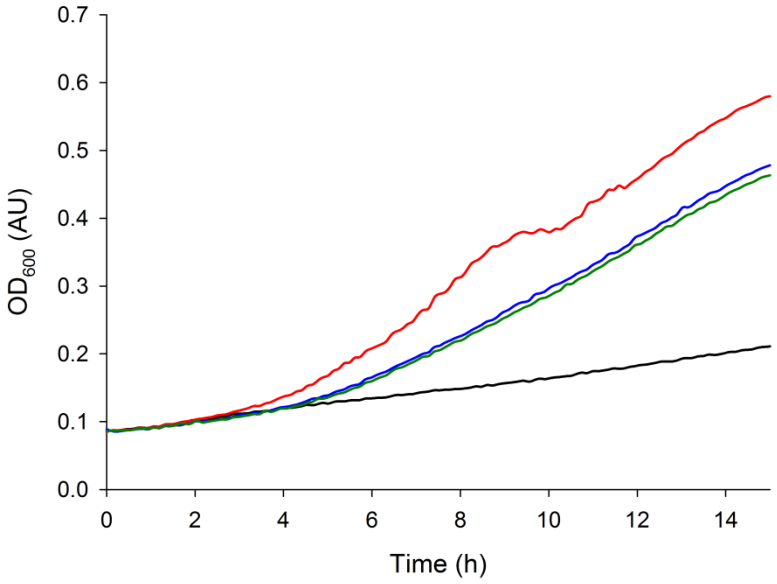

Figure 2.1 Growth of starved derivatives of *–thiH* mutant strains in 200 µL cultures of minimal media incubated at 30 ºC in a plate reader. (—) = *–thiH* (pBAD-His), no supplement; (—) = *-thiH* (pBAD-His) + thiamine supplement; (—) = *-thiH* (pRL1020), no supplement; (—) = *-thiH* (pRL1020) + thiamine supplement. Data is the average of a triplicate data set.

2.3 *Organic Extraction of E. coli Cell Cultures*

It was anticipated that an organic extraction would permit the isolation of some of the organic metabolites which the bacteria may excrete into solution during growth. Diethyl ether was considered to be a suitable solvent as it had been employed in detecting *in vivo* formation of *p*-cresol previously[122]. Dichloromethane (DCM) was also tested as this was the solvent previously employed by White in the detection of 4-HBA[116]. The volatility of both these solvents is an advantage as the organic extract needed to be concentrated *in vacuo* prior to analysis. The efficiency of the extraction was measured in a positive control experiment in which 10 µM of both *p*-cresol and 4-HBA were added to 100 mL of DM media. After extraction of the media, the concentration of *p*-cresol and 4-HBA in the extract was estimated by HPLC analysis (see Method 22b) and the efficiency of organic extraction is shown in Table 2.2. Diethyl ether was chosen as it was shown to extract both *p*-cresol and 4-HBA.

Extraction Solvent	**Compound**	**Efficiency of Extraction (%)**
DCM	*p*-cresol	71
	4-HBA	6
Diethyl ether	*p*-cresol	49
	4-HBA	64

Table 2.2 The estimated efficiency of the organic extraction of *p*-cresol and 4-HBA from DM media. Concentrations were estimated by HPLC analysis.

Cell cultures of derivatised –*thiH* mutant strains were used to inoculate 100 mL of fresh DM media, after 24h of 'starvation', and then cultured for 24h. After this time the culture was cleared by centrifugation and the supernatant extracted into diethyl ether and the organic extract dried and concentrated *in vacuo.* Initial analysis of this organic extract by normal phase TLC (see Method 22a) made use of the elution conditions developed by Kriek in the characterization of *p*-cresol *in vitro*[115] (see Figure 2.2). The extract from the ThiH complimented culture showed several clearly resolved spots, which were visible under UV light and after staining with potassium permanganate. Comparison with standards of several potential aromatic by-products inferred the presence of *p*-cresol. The sensitivity and resolution in these initial experiments did not allow any definite conclusions to be drawn. However the potential for this strategy was demonstrated and prompted further studies employing analytical methods with much greater resolution and sensitivity.

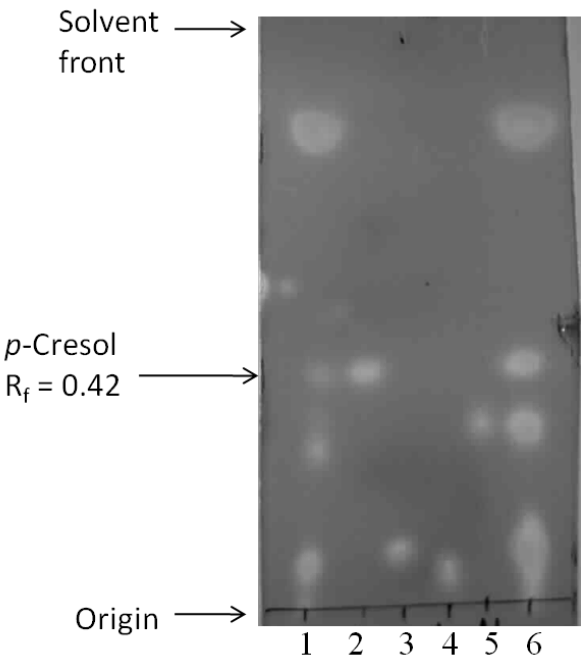

Figure 2.2 Normal phase TLC of organic extract from –*thiH* (pRL1020) (lane 1), developed in 15:1 chloroform:^{t}butanol and visualized by staining with $KMnO_4$. lane 2 = *p*-cresol; lane 3 = 4-HBA; lane 4 = 4-hydroxybenzoic acid; lane 5 = 4-hydroxybenzyl aldehyde; lane 6 = mixed spot.

To improve the resolution of the analysis, the mixture of compounds extracted from the cell culture were analysed by HPLC (see Method 22b). Comparison with synthetic standards further implied the presence of *p*-cresol and also suggested the presence of 4-HBA (see Figure 2.3). However, under the chromatographic conditions employed several compounds with similar retention times to *p*-cresol (~21 min) and 4-HBA (~7 min) were observed in both cultures. This problem was partially resolved by optimizing the separation slightly. Careful comparison of the region of the chromatogram between 19 – 22 minutes showed a slight difference in the *thiH* containing strain (-*thiH*(pRL1020)) to the negative control (-*thiH*(pBAD-His)). Compounds observed in the *thiH* containing strain but not in the negative could potentially result from reactions catalyzed by ThiH and the inference is that one compound formed is *p*-cresol.

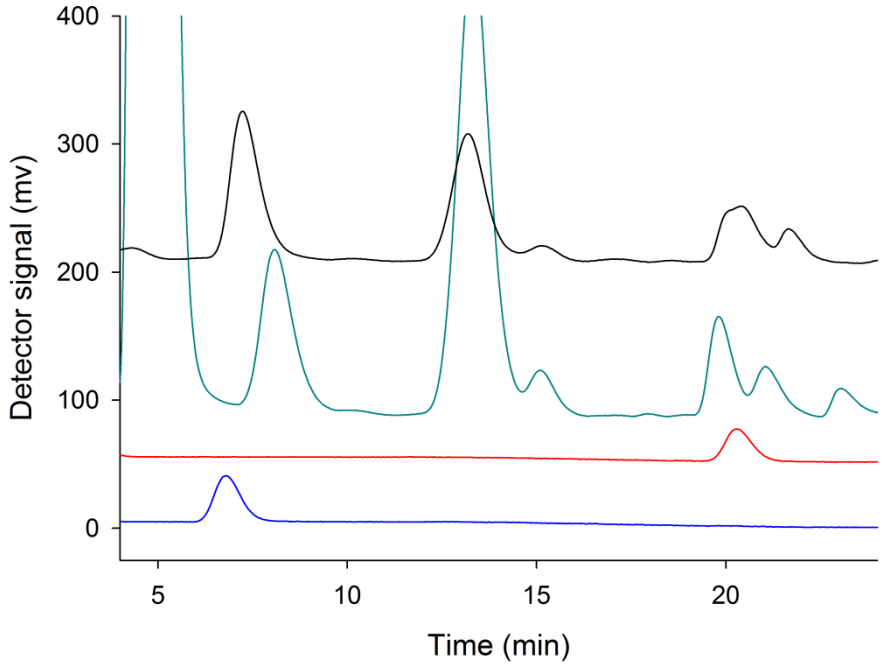

Figure 2.3 HPLC analysis of organic extracts from -*thiH*(pRL1020) (—), -*thiH*(pBAD-His) (—), compared to standards of *p*-cresol (—) and 4-HBA (—). Traces are displaced upwards for clarity.

To confirm this observation organic extracts were co-injected with synthetic standards of *p*-cresol and 4-HBA. The co-injected sample of pRL1020 appeared to have enhancement of the peaks in the *p*-cresol and HBA regions of the chromatograms. This suggested the presence of both these compounds in this extract. The region of the chromatogram at 7-8 min, where 4-HBA elutes was puzzling. The pBAD-His negative control appeared to contain compounds with a very similar retention time to 4-HBA, but the peak was not enhanced when co-injected. Additionally this peak was apparently not observable in the pRL1020 extract. Figure 2.4 shows the region of the chromatogram where *p*-cresol elutes and demonstrates an enhancement to the suspected *p*-cresol peak in the pRL1020 extract (the shoulder at 20.5 mins in Figure 2.4B), but no peak enhancement in the same region from the pBAD-His extract (see Figure 2.4A).

HPLC analysis had suggested the accumulation of *p*-cresol in cell cultures expressing ThiH, however, the results were by no means unequivocal. Reverse phase chromatography of metabolites isolated from an organic extraction was made difficult by the requirement to re-dissolve the mixture in a suitable solvent for injection onto a reverse phase HPLC column. A mixture of methanol / water was used to prepare the samples and this led to variations in the retention time of up to 0.5 minutes. The HPLC chromatograms show multiple peaks derived a series of unknown metabolites, some of which overlap. As such, HPLC lacked the required resolution to analyse such a complicated mixture with confidence. To improve the time resolution of the chromatography and the confidence with which peaks could be assigned, it was advantageous to use GCMS.

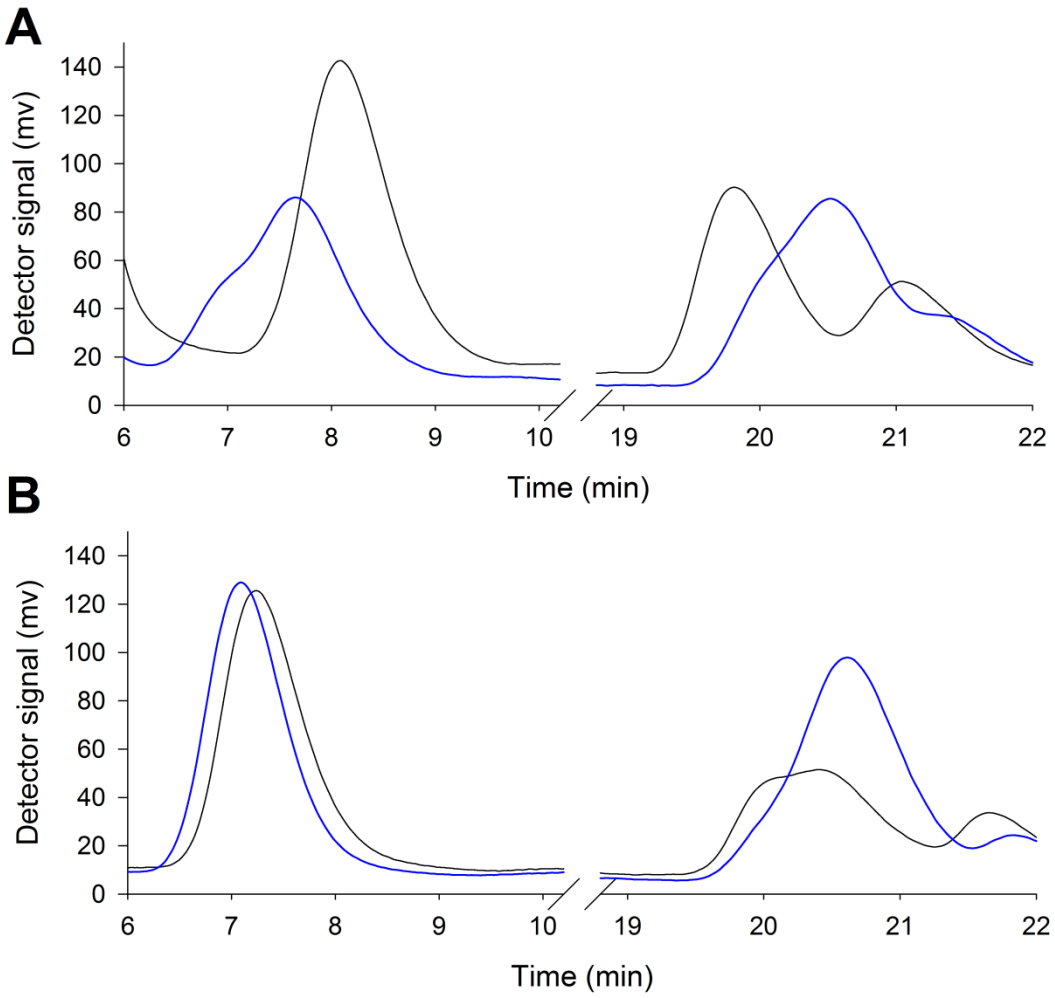

Figure 2.4 Samples of organic extracts of A) –*thiH*(pBAD-His) and B) −*thiH*(pRL1020) co-injected with standards of 4-HBA and *p*-cresol (—), compared to the original sample (—).

2.4 *Characterisation of p-Cresol as the in vivo By-product of ThiH Reactions*

Organic extracts of cell cultures were prepared as described in Method 21. Prior to GCMS analysis the organic extracts concentrated *in vacuo* to 1 mL and this sample directly analysed, thus negating the problem of re-dissolving the sample. Comparisons between organic extracts from cultures of the two derivative strains and synthetic standards of *p*-cresol could be made. For clarity the design of the experiment is shown in Figure 2.5.

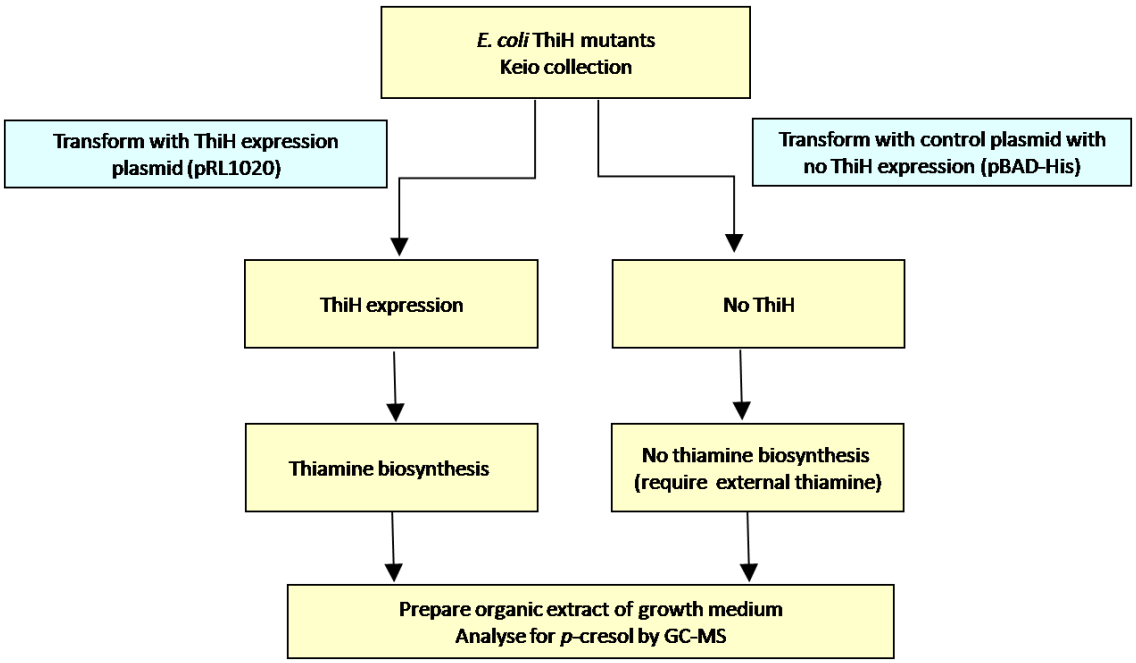

Figure 2.5 Flow chart showing the strategy for confirming *p*-cresol as the aromatic byproduct of tyrosine cleavage by ThiH *in vivo*

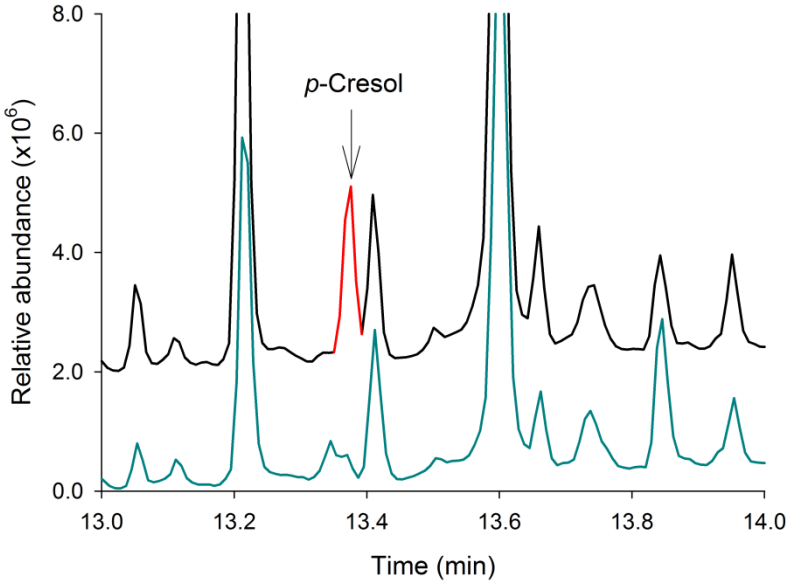

Figure 2.6 Section of the GCMS chromatogram of an extract of medium from *E. coli* cultures that express ThiH ((—), displaced upwards for clarity) and the negative control sample (—).

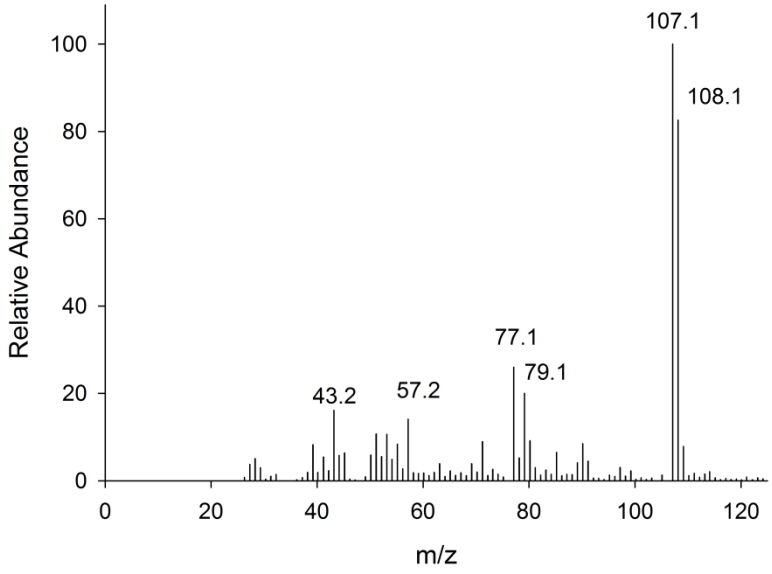

Figure 2.7 Mass spectrum of the peak at 13.38 min (displayed in red in figure 2.6) in the GC of an organic extract of –*thiH*(pRL1020).

A synthetic standard of *p*-cresol was shown to elute with a retention time of 13.38 minutes under the conditions used (see Method 22c). Figure 2.6 shows this region of the chromatogram when analyzing organic extracts of –*thiH*(pBAD-His) and –*thiH*(pRL1020). The pattern of peaks observed in both these samples was very similar however; the strain with the requirement for functional ThiH in order to biosynthesise TPP in order to grow had a new peak with a retention time of 13.38 min (shown in red). The EI mass spectrum of this peak corresponded to the observed spectrum of a standard sample of *p*-cresol. The extremely consistent pattern of non *p*-cresol (background) peaks between the two samples gave increased confidence in the reproducibility of the GCMS analysis. The fact that it is not observed in the strain not biosynthesizing TPP suggests that it is generated as a result of thiamine biosynthesis and almost certainly as a result of tyrosine cleavage by ThiH. The small peak (relative abundance $< 1.0 \times 10^{-6}$) observed in the negative control sample, with a similar retention time of 13.38 minutes does not show a mass spectrum consistent with *p*-cresol. Interestingly, thiamine biosynthesis appears to be the only pathway in *E. coli* that leads to the generation of *p*-cresol.

It was not possible to resolve 4-HBA using the GC-MS conditions described (see Method 22c). A procedure for derivatising a synthetic standard of 4-HBA with trfluoroacetic anhydride was developed. However, analysis of derivatised organic extracts proved unsuccessful. The evidence obtained that *p*-cresol accumulated *in vivo* in cultures of cells actively biosynthesising thiamine, combined with *in vitro* results gave enough confidence that the correct assignment of the aromatic by-product from tyrosine cleavage by ThiH was *p*-cresol. The correct assignment of the products allows for a more accurate and detailed mechanistic model to be constructed.

2.5 *Implications for the Mechanism of ThiH*

The observation of *p*-cresol (**88**) and glyoxylate (**98**) (the hydrolysis product of dehydroglycine (**11**)) as the products of ThiH reactions *in vitro* was a significant advancement in understanding the role of ThiH. In particular, the fact that dehydroglycine is formed as a discrete intermediate in the biosynthetic pathway. Additionally the aromatic byproduct of the reaction was characterized as *p*-cresol. This result disagreed with previous observations of White[116] which reported that 4-HBA (**97**) was the by-product. This difference may arise because the measurements made by White were *in vivo*. The results presented in this chapter clearly demonstrate that *p*-cresol does accumulate *in vivo* as a result of thiamine biosynthesis. This result supports and validates *in vitro* experiments on ThiH[115], eliminating the possibility that *in vitro* observations were an artefact of the experiment.

The apparent contradiction in observations reported here to those reported by White can be explained by the nature of the cell strain used. One consideration is that *p*-cresol may be toxic for the cell and as a result, the bacterium may have a mechanism for removal of this toxin, possibly via oxidation to the more water soluble 4-HBA. The organism: *Pseudomonas putida* has been shown to express an enzyme called *p*-cresol methyl hydroxylase (PCMH), which converts *p*-cresol to 4-HBA[123] yet sequence similarity searching failed to yield any similar enzymes present in *E. coli*. However, certain strains of *E. coli* have been shown to possess a gene which expresses an enzyme characterized as an aromatic hydoxylase, which has been demonstrated to accept *p*-cresol as a substrate[124]. White's study, which demonstrated 4-HBA as a thiamine biosynthetic by-product utilized a B strain of *E. coli*, which possesses this gene. However, the strain employed in our study is a K-12 strain and does not contain a chromosomal copy of this gene. It is, therefore, probable that *p*-cresol is formed *in vivo* but is converted to HBA in strains that contain a suitable oxidase.

In vitro studies have shown ThiH to possess a 4Fe-4S cluster and can bind a molecule of SAM and as such it is proposed that ThiH can reductively cleave SAM, generating methionine and a 5'deoxyadenosyl radical intermediate (Scheme 1.4)[106]. This reactive, primary radical is proposed to generate a substrate radical. This could occur through abstraction of the phenolic hydrogen atom, generating a phenolic tyrosine radical (**99**) (Scheme 2.1, A and B), or by a by abstraction of a hydrogen atom from the amine, generating the ammonium radical cation (**104**) (Scheme 2.1, C) The initial hypothesis was that generation of a phenolic radical would result in homolysis of the Cα—Cβ bond yielding a glycine radical (**100**)[114] (Scheme 2.1, A). This hypothesis was attractive as the byproduct of this cleavage mechanism is quinone methide (**101**), which could react with water to yield 4-HBA (**97**). The observation of *p*-cresol (**88**) as the by-product has provided a precedent for a second potential cleavage mechanism of the phenolic tyrosine radical (Scheme 2.1, B). Abstraction of the phenolic hydrogen atom results in an electron deficient π-system, thus facilitating attack from the lone pair located on nitrogen followed by heterolytic cleavage of the Cα—Cβ bond. This mechanism directly forms dehydroglycine (**11**) along with a resonance stabilized radical anion (**102**), which can be reduced to form *p*-cresol (**88**). As depicted in structure **102a** the radical anion has an electron poor oxygen and an electron rich carbanion. The resonance stabilisation of the radical anion can be explained by a single electron being delocalised throughout the π-orbitals of the benzene ring.

The detection of *p*-cresol does not rule out the hypothesis of a homolytic cleavage mechanism. Modelling the thermodynamics of the reaction[1] has shown that the homolytic cleavage, towards the glycine radical (**100**) and quinone methide (**101**), (see Scheme 2.1) is more favourable by 33 $kJmol^{-1}$ (± 5 $kJmol^{-1}$)[115]. The modelling studies fail to take account of any interactions within

[1] Modelling was conducted by Dr. Anna Croft at the University of Bangor and is described in reference 115

the active site, such as hydrogen bonds that may preferentially stabilize certain intermediates or transition states. Reduction of the quinone methide (**101**) could occur *in situ* negating the possibility of it being released to solution and reacting with water to form 4-HBA (**97**). Indeed the glycine radical (**100**) needs to be oxidised and it could be that electron transfer to the quinine methide (**101**) facilitates this step and thus reduces the quinone methide to the resonance stabilised radical anion (**102**), which is subsequently reduced to *p*-cresol (**88**). Generation of the ammonium radical cation by abstraction of an ammonium hydrogen atom could also facilitate homolytic cleavage of the Cα—Cβ bond (Scheme 2.1, C). This would also lead directly to dehydroglycine (**11**) and the resonance stabilised radical anion (**102**), which is reduced to form *p*-cresol (**88**). The thermodynamics for this potential pathway were not modelled.

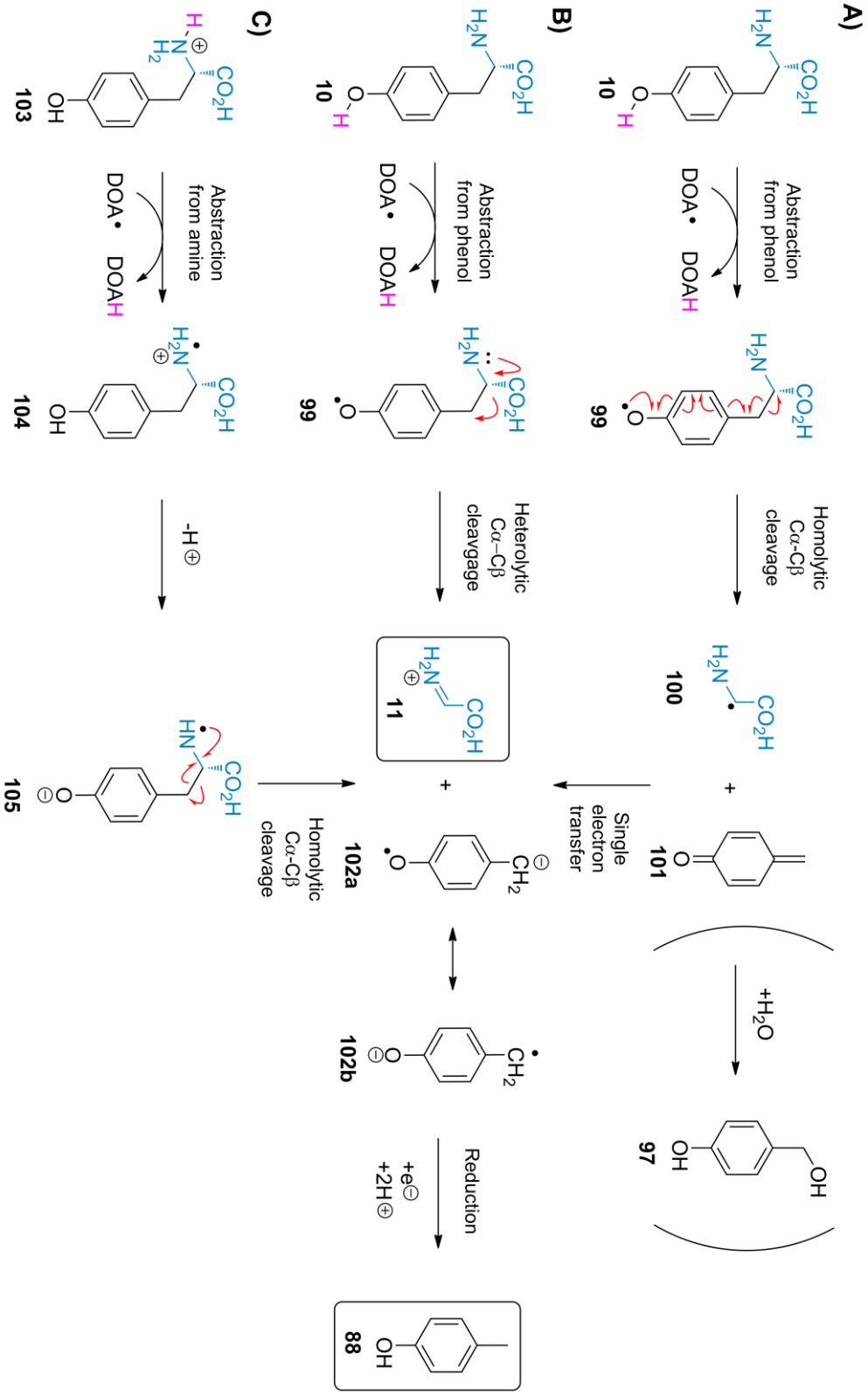

Scheme 2.1 Three potential mechanisms for ThiH leading to the products dehydroglycine (**11**) and *p*-cresol (**88**). The 5'-deoxyadenosyl radical (DOA•) is generated by reductive cleavage of SAM, mediated by the 4Fe-4S cluster.

The proposed heterolytic mechanism (Scheme 2.1, B) involving an umpolung has some features that are analogous to those in the mechanism of *p*-hydroxyphenylacetate decarboxylase (HPAD) proposed by Selmer and Andrei[42]. The function of the HPAD enzyme in *Clostridium difficile* is to form *p*-cresol (88), which acts as a toxin to other competing bacteria in the human intestine [122, 125]. *p*-Cresol is formed by decarboxylation of *p*-hydroxyphenylacetate (106), which is derived from tyrosine. The enzyme expressed in *C. difficile* that catalyses this reaction is *p*-hydroxyphenylacetate decarboxylase (Hpc) this organism *p*-hydroxyphenylacetate (106) undergoes decarboxylation and is catalysed by the hydroxyphenylacetate decarboxylase (Hpd) group of enzymes, one of which (HpcB) has an iron sulfur cluster and is dependent on SAM for activity[12, 126]. HPAD is a glycyl radical enzyme[21, 42, 127] and as such the activase sub-unit contains the enzymatic machinery to reductively cleave SAM and eventually generate a catalytic thiyl radical. This is proposed to form a substrate radical (107) by abstraction of the phenolic hydrogen atom of *p*-hydroxyphenylacetate (see Scheme 2.2). This initiates decarboxylation, which forms the same resonance stabilised radical anion (102), proposed for heterolytic cleavage of tyrosine by ThiH. Although ThiH and HPAD utilise different radical centres to initiate the reaction, it seems likely that there are similarities in subsequent steps of the mechanism. In HPAD cresol is proposed to be formed by re-abstracting a hydrogen atom from the cysteine residue, thus reforming the catalytic thiyl radical. ThiH has been shown to use SAM as a substrate, so it is unlikely that a hydrogen atom is re-abstracted from DOA. Therefore, ThiH must source the electron from a different source (potentially the 4Fe-4S cluster) to reduce the radical anion to *p*-cresol.

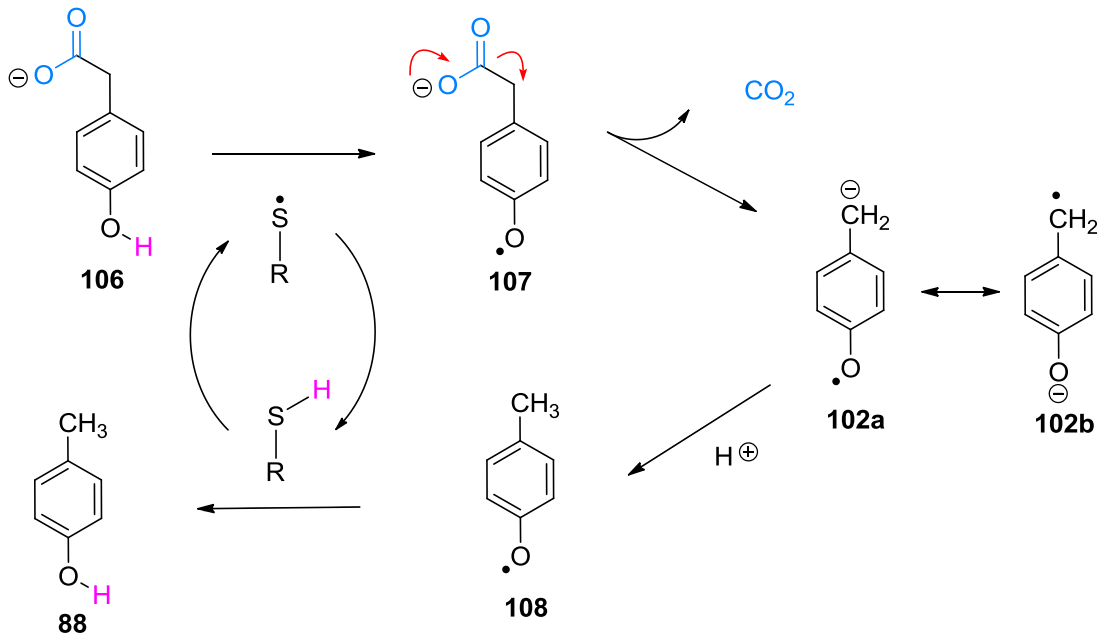

Scheme 2.2 Mechanism of the catalytic subunit of HPAD, proposed by Selmer[42].

2.6 ***Summary and Conclusions***

In vivo experiments were designed to support the observation made from *in vitro* experiments that the by-product of ThiH mediated tyrosine cleavage was *p*-cresol. ThiH forms part of the thiamine biosynthesis gene cluster in anaerobic bacteria and as such these *in vivo* experiments were designed to show a relationship between the accumulation of *p*-cresol and the cell's ability to actively biosynthesise thiamine. It was found that deletion of the *thiH* gene prevented growth in media deficient in thiamine. GC-MS analysis of organic extracts of cell cultures confirmed the presence of *p*-cresol, only in strains that were expressing ThiH. The increased confidence that *p*-cresol is the by-product of tyrosine cleavage has allowed for the proposal of a more accurate mechanistic model Cα—Cβ bond cleavage. Some of the key questions to address are: what is the site of hydrogen atom abstraction from tyrosine? And what is the source of the electron that reduces the aromatic intermediate to p-cresol? (see Scheme 2.1). Subsequent chapters in this thesis seek to design an *in vitro* activity assay to seek the answers to these questions.

3 Development of a Catalytic Activity Assay for Tyrosine Lyase

3.1 *Introduction*

The products of tyrosine cleavage by ThiH have been characterised as dehydroglycine (**11**) and *p*-cresol (**88**) (angew). *In vivo*, dehydroglycine is proposed to be transferred to ThiG, where it reacts with a DXP derived intermediate (**82**) to form the thiazole moiety of thiamine. *In vitro* experiments on the purified ThiGH complex defined the product of the ThiH catalysed reaction as glyoxylate (**98**), presumably as a result of rapid hydrolysis of dehydroglycine after it is released from the enzyme.

An overview of the chemistry involved in the ThiGH activity assay is shown in Figure 3.1. At selected timepoints, ThiH turnover is stopped by the addition of a strong acid, which causes the proteins to precipitate. Precipitated material can then be removed by centrifugation. HPLC analysis of the resulting solution gives a quantitative detection of *p*-cresol and DOA (shown in boxes in Figure 3.1). Glyoxylate can be quantified by pre column derivitization with *o*-phenylenediamine, under acidic conditions, to the fluorescent 2-quinoxalinol[115, 128] (see Figure 3.1 D). This *in vitro* study analysis (Figure 3.2) showed that glyoxylate (**98**) and *p*-cresol (**88**) form in a 1:1 ratio with the first order rate constants and maximum product concentrations shown in Table 3.6. In a separate experiment it was demonstrated that DOA was formed in an approximate 1.3:1 ratio with respect to *p*-cresol, indicating some uncoupled SAM cleavage had occurred. These time course experiments had been designed as single turnover experiments, by limiting the amount of substrates and reducing equivalents present in the assay[115, 129]. The assay utilises the assumed natural reducing system for *E. coli* proteins, Flavodoxin (FldA), Flavoprotein:NADPH oxidoreductase (Fpr) and NADPH. This has the advantage of being more selective for reduction of the 4Fe-4S cluster of ThiH and could restrict uncoupled SAM cleavage due to the carefully controlled redox potential of the 4Fe-4S cluster (see Section

1.2.4)[75]. The alternative reagent employed in studies of radical SAM enzymes is dithionite[23, 130], a powerful reductant that is more likely to react with other molecules in the assay, including enzyme derived products. The mechanistic hypothesis discussed in Chapter 2 (see Scheme 2.1 – p65) requires input of 2 electrons in order to arrive at the products (1 for reductive cleavage of SAM and 1 for reduction of the aromatic radical anion by-product to *p*-cresol). NADPH provides 2eq of electrons (Figure 3.1A) and thus 1 equivalent of NADPH is required per turnover of ThiH.

The stability of the protein, in particular the oxygen sensitive 4Fe-4S cluster, meant that a small proportion of ThiH precipitated during time course experiments. It was also anticipated that ThiH, like some other members of the radical SAM family', such as BioB[31] and LipA[32] may not be able to function catalytically *in vitro*. BioB and LipA function to insert sulphur atoms to their respective substrates and are constrained to a single turnover *in vitro* due to the depletion of the holo-protein derived sulphur source. This makes studying these reactions challenging as obtaining sufficient quantities of enzymatically derived products / intermediates to characterise can require relatively large amounts of protein. This constraint is negated by many of the radical SAM enzymes, which although they require stoichiometric quantites of SAM, the 4Fe-4S cluster can repeatedly access the reduced +1 oxidation state, providing a molar excess of SAM and reducing agents are available. The vulnerability of 4Fe-4S clusters to oxygen makes preparations of large quantities of the active form of these proteins difficult. Therefore, it is desirable to achieve multiple turnovers to make studying the enzyme catalysed reaction easier.

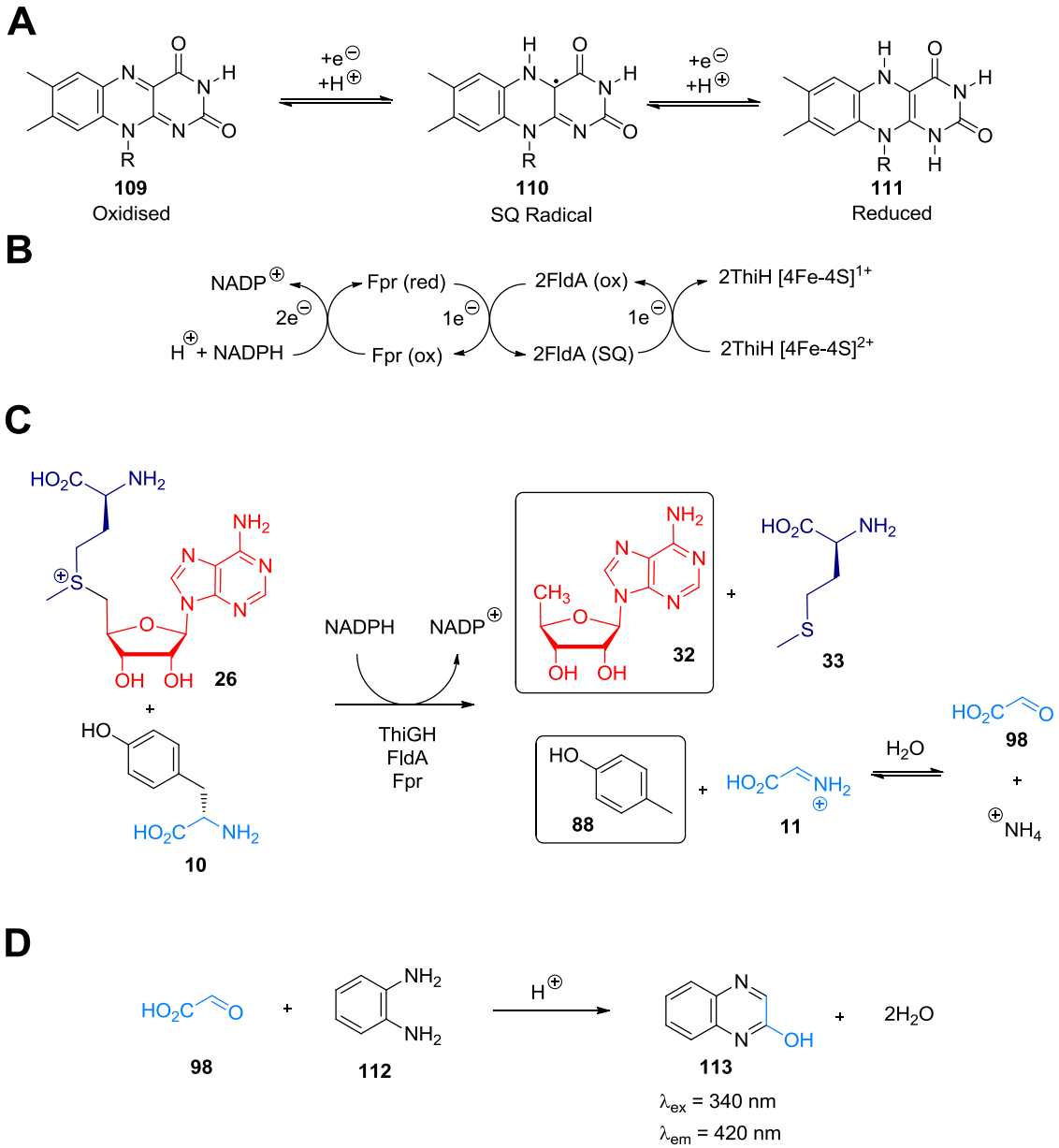

Figure 3.1 A) The flavin moiety of flavin mononucleotide (the co-factor of FldA) and flavin adenine dinucleotide (the cofactor of Fpr) in the oxidised form, when partially reduced to the semiquinone and fully reduced. B) Electron transfer involved in the reuduction of the 4Fe-4S cluster of ThiH bu NADPH. C) Scheme showing the substrates, reagents and products in ThiH activity assays. The boxes highlight that these two compounds can be analysed by HPLC, without the need for derivitisation. D) Derivitisation of glyoxylate to the fluorescent 2-quinoxalinol.

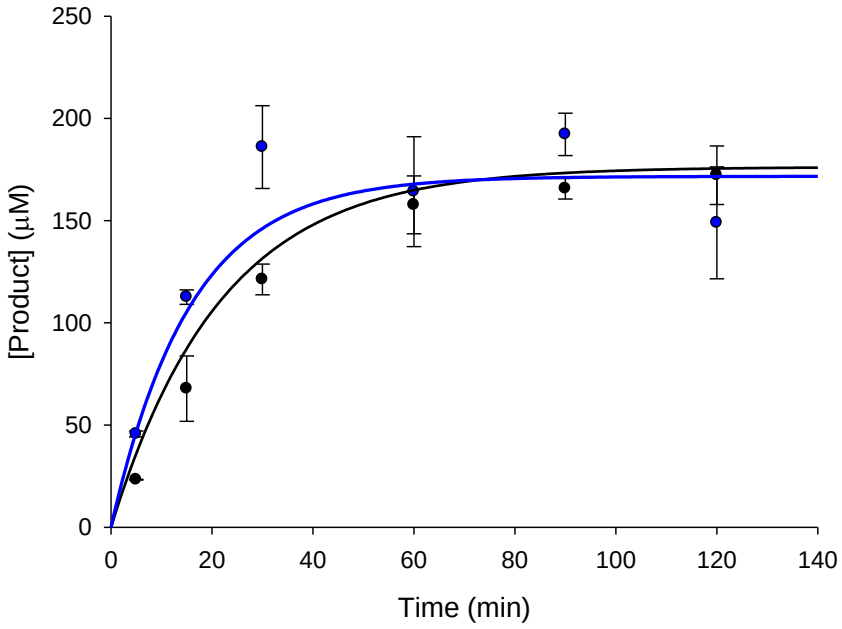

Figure 3.2 Time course of glyoxylate (●) and *p*-cresol (●) formation in ThiGH activity assays restricted to a single turnover. Assays contained ThiGH (444 μM), tyrosine (350 μM), SAM (655μ M), FldA (50 μM), Fpr (9 μM) and NADPH (540 μM). (Adapted from[115])

Product	**Rate constant ($\times 10^{-2}$ min $^{-1}$)**	**Final concentration (μM)**
Glyoxylate	6.3 ± 1.1	171.6 ± 7.9
p-Cresol	4.6 ± 0.7	176.2 ± 7.8

Table 3.1 Kinetic parameters of product formation by ThiGH, obtained by fitting data in figure 3.1 to a first order process. (Adapted from[115])

These results represented significant progress on understanding ThiH, but for further development, two areas needed improvement. Firstly the experiments reported by Kriek and Martins were designed assuming single turnover and it important to test whether ThiH can

function catalytically. Secondly, the ThiH used in these studies was substantially purified, but was known to exist in two forms: a large, hexadiameric complex of ThiG and ThiH (i.e. $(ThiGH)_6$) and a monomeric form[106]. Isolation of these two forms of the protein may also be beneficial in developing an understanding of the chemistry catalysed by ThiH in the context of thiazole biosynthesis.

In *E. coli* the *thiH* gene forms part of the *thiCEFSGH* operon. Extensive expression studies have demonstrated that a soluble form of ThiH can be obtained during aerobic growth of *E. coli* BL21(DE3) by co-expressing ThiH with ThiF, ThiS and ThiG. The plasmid, pRL1020 (Figure 3.5), which is used to express ThiH contains the *thiFSGH* part of the natural operon with a hexahistidine (His_6) tag at the C-terminus of ThiH, allowing for purification by Ni-affinity chromatography. Despite the fact that ThiH could be expressed aerobically, purification required strictly anaerobic conditions due to the oxygen sensitive nature of the 4Fe-4S cluster and upon oxidation the protein tended to precipitate[131]. The experiments described above were known to contain a mixture of $(ThiGH)_6$ and ThiH, obtained from the pRL1020 expression plasmid and purified by Ni-affinity chromatography. The characterisation of $(ThiGH)_6$ and monomeric ThiH was achieved by analytical gel filtration chromatography[106].

The work presented in this chapter sets out to optimise a robust and routine assay for ThiH activity. This involves:

- Investigating different expression systems for ThiH
- Optimising the purification
- Optimising the HPLC analysis of ThiH activity assays
- Investigating potential for catalytic activity by adding an excess of substrates and reductant

3.2 *HPLC Detection of Reaction Products*

As shown in Figure 3.1, quantitative detection of DOA (**32**) and *p*-cresol (**88**) can be achieved by HPLC as they both have relatively strong absorbance's. DOA can be detected by monitoring absorbance a 254 nm and *p*-cresol can be detected by monitoring absorbance at 280 nm. The primary reason to optimise the HPLC analysis of ThiH activity assays is to accurately quantify these two products. As *p*-cresol is a product of tyrosine cleavage and DOA is a product of SAM cleavage, quantification of these two products enables the monitoring of two distinct steps in the mechanism. This provides scope to probe the kinetics of the ThiH catalysed reaction in detail and is of particular relevance to understanding uncoupled SAM cleavage[26]. Other potentially interesting compounds were included in the optimisation of the HPLC method including adenine, which results from hydrolysis of SAM or DOA, MTA, an impurity present in SAM stocks and two structural analogues of tyrosine (4-hydroxyphenypropionic acid (4-HPPA) (**119**) and 4-hydroxycinamic acid (4-HPCA)). These tyrosine structural analogues are discussed in Chapter 4 (Section 4.5).

SAM (**26**) can degrade by various pH dependant routes[132] (see Scheme 3.1). Hydrolysis results in formation of the adenine base (**116**) and S-ribosylmethionine (**117**). A second pathway, which occurs under basic conditions, is nucleophilic addition by the α-carboxylate onto the γ-C of methionine, resulting in homoserine lactone (**115**) and methylthioadenosine (MTA) (**114**). To allow for these side reactions in subsequent experiments, the retention times of adenine and MTA was also an important consideration to avoid co-elution of any of these SAM derived impurities with assay substrates and products. MTA was routinely observed as the major impurity in commercial SAM stocks, with varying levels (up to ~20%) depending on the age and batch of the SAM. This proved problematic when trying to quantify the amount of SAM

utilised in assays as obtaining accurate calibrations was difficult. The work up procedure for assays with ThiGH involves precipitating the protein with perchloric acid and there was a concern that any SAM or DOA in the assays might potentially hydrolyse, releasing adenine. This problem was circumvented by storing assay samples at -80 ºC and analysing them as soon as possible.

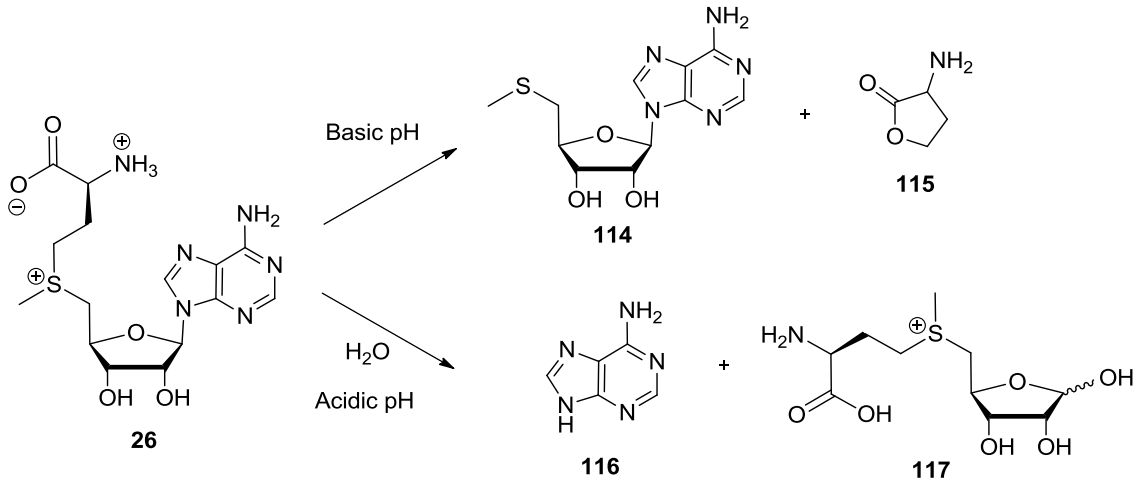

Scheme 3.1 Two potential degradation pathways of SAM which occur at different pH.

A summary of different HPLC methods is shown in Table 3.2. Previous efforts to optimise the HPLC separation were successful in achieving quantification of tyrosine, DOA and *p*-cresol[129]. This provided a good method to accurately quantify *p*-cresol, but it was difficult to achieve reproducible data for DOA due to noise in the baseline. To study the kinetics of ThiH in detail it was deemed important to find a highly reproducible method to quantify *p*-cresol and DOA from the same sample. The highly polar nature of the substrates in comparison with the relative hydropobicity of the products make finding a universal method for separating all the compounds by reverse phase chromatography difficult. The initial variation was to increase the length of the HPLC column from 150 mm to 250 mm. Several mobile phase conditions were investigated,

including the use of sodium octane sulfonate. This surfactant is useful in reverse phase HPLC as it ion pairs to polar compounds, greatly increasing their retention times. The disadvantage of using this method was that it was difficult to separate all the compounds from each other. The use of phosphate buffer improved the retention time for SAM; however, it was found that this method was not very reproducible. Eventually method 2 in Table 3.2 was selected as it gave the best all round separation and was highly reproducible. An example chromatogram is shown in Figure 3.3 and the full protocol described in the experimental section (Method 17).

Method No.	Column	Aqueous solvent	Organic solvent	Comments
1	Gemini 5u, C18 (250 x 4.6mm)	20mM NH_4OAc, pH 6	20mM NH_4OAc, pH 6 in 50:50 H_2O:MeCN	Good separation for Adenine, DOA and MTA. Poor separation for tyrosine, SAM, 4-HPPA, 4-HPCAand *p*-cresol
2	Gemini 5u, C18 (250 x 4.6mm)	0.1% AcOH / H_2O	0.1% AcOH / MeCN	Good separation for tyrosine DOA, MTA, 4-HPPA, 4-HPCA, *p*-cresol. Adenine and SAM have short retention times
3	Gemini 5u, C18 (250 x 4.6mm)	25 mM AcOH, 8 mM sodium octane sulfonate / H_2O	25 mM AcOH, 8 mM sodium octane sulfonate / 50:50 MeCN:H_2O	Good retention time for SAM, but very difficult to separate all the compounds
4	HICHROM, S5, C18 (250 x 4.6 mm)	50 mM Na_2HPO_4 / 0.5% TFA, pH 3.0	Methanol	Good separation and retention time for tyrosine, SAM, Adenine, DOA, MTA. 4-HPPA and 4-HPCA co-elute with *p*-cresol. Not very reproducible

Table 3.2 Summary of HPLC conditions for analysing ThiH activity assays.

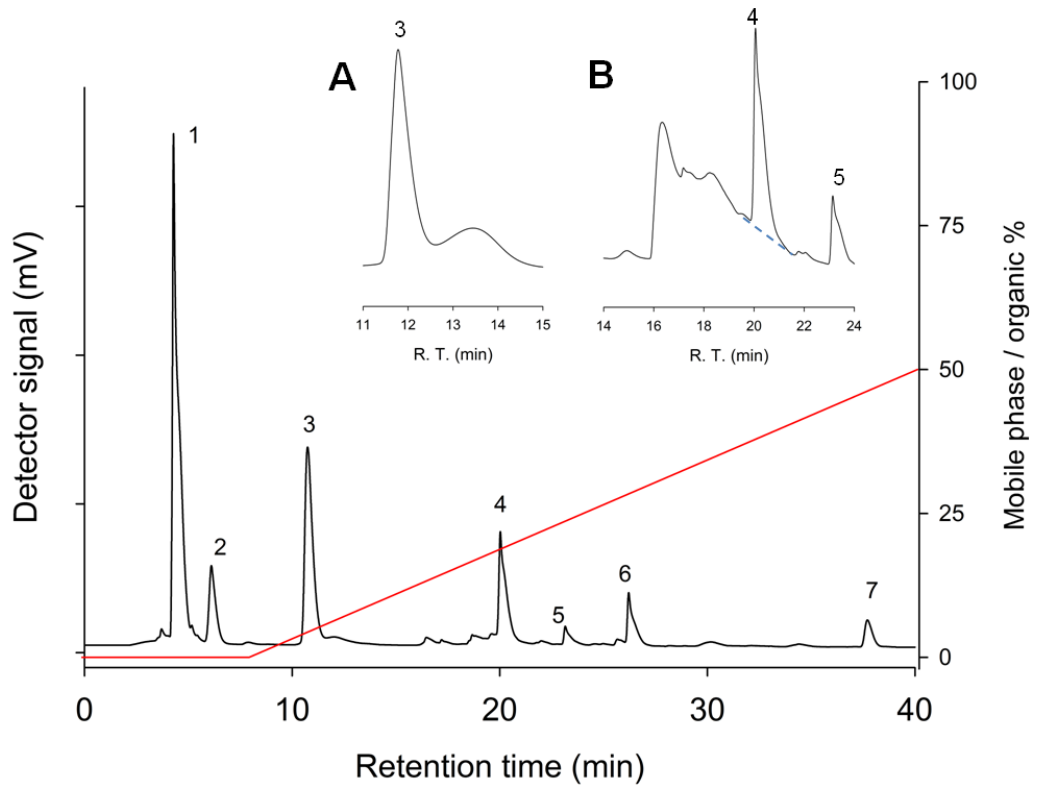

Figure 3.3 HPLC chromatogram, monitoring the absorbance at 280 nm (—) of a ThiH activity assay using method 2 in table 3.2. Also shown is the proportion of organic solvent in the mobile phase (—). Peaks were identified as: 1) SAM; 2) adenine; 3) tyrosine; 4) DOA; 5) MTA; 6) riboflavin (derived from the reducing system); 7) *p*-cresol. Inset A is an example of poor peak shape for tyrosine elution and inset B shows the baseline noise that can sometimes occur in the region of the chromatogram where DOA elutes. In these cases integration of the peak area was achieved by adjusting the baseline, shown by the dashed line.

The disadvantage is that to separate SAM and tyrosine the initial mobile phase consisted of 100% aqueous buffer. At low amounts (<5%) of organic buffer the mixing of the aqueous and organic buffers is inaccurate and can lead to strange peak shapes in compounds eluting at the start of the gradient. Unfortunately this affects the analysis of tyrosine in this case (see inset A in Figure 3.3).

3.3 *Modifying the ThiH Assay Buffer*

In vitro experiments on ThiGH, including the time course shown in Figure 3.2, used phosphate buffer at pH 7.5. This was selected as data from ^{13}C NMR experiments could be more easily interpreted as there was no background signal from the assay buffer. The disadvantage is that the ThiGH protein used in these experiments is unstable and some precipitation was often observed during *in vitro* experiments[129]. This is particularly a problem when trying to monitor the kinetics of the reaction as protein inactivation due to precipitation could be a limiting factor. Therefore, it was considered necessary to optimise the assay buffer to increase the stability of the enzyme and ensure that it remained in solution during turnover experiments. During the extensive development of the ThiH purification protocol[106, 114, 129, 131], it was found that ThiH was stable and able to be stored, frozen at -80 °C, in Buffer D (50 mM MOPS, pH 7.7, 100 mM NaCl, 12.5% (w/v) glycerol, 5 mM DTT) (see Method 10). This buffer was used as a template for a new assay buffer and an experiment was designed to test the four buffers shown in Table 3.6 for their suitability for ThiH activity assays. Protein isolated by Ni-affinity chromatography was reconstituted (Method 14a) and split into four fractions and exchanged into one of buffers 1-4. Protein precipitation was visually observed and activity assays were prepared (method 16) to measure how the turnover was affected by each buffer.

The presence of glycerol and sodium chloride was required to maintain the solubility of the protein. However, regardless of this fact it was surprisingly found that the amount of DOA and *p*-cresol formed was similar in all assay buffers. One explanation of this observation is that the precipitated protein was inactive, possibly due to inefficient reconstitution. All subsequent activity measurements were conducted in Buffer 1 (see Table 3.6) as the protein remained soluble, allowing for increased confidence in any observations.

Buffer	Buffer contents	Precipitation observed?	[DOA] formed after 1h	[*p*-Cresol] formed after 1h
1	50 mM MOPS pH 7.5 100 mM NaCl 5% (w/v) glycerol	No	192 µM	178 µM
2	50 mM MOPS pH 7.5 100 mM NaCl	Yes	205 µM	177 µM
3	50 mM MOPS pH 7.5 5% (w/v) glycerol	Yes	198 µM	179 µM
4	50 mM MOPS pH 7.5	Yes	181 µM	169 µM

Table 3.3 Variations in the buffer used for ThiH activity assays.

Unfortunately, the presence of glycerol in assay samples presented a problem in the HPLC analysis. The baseline in the region between 15 – 25 minutes (see inset B in Figure 3.3) became variable and noisy. This was attributed to the presence of glycerol and could largely be overcome by washing the HPLC column, by injecting a water (blank) sample between the injections of each assay sample. When integrating any peaks that were affected by the baseline variation, the baseline was adjusted to provide the best possible estimate of the peak area (see inset B in Figure 3.3).

3.4 *Increasing the Amount of Substrate and Reductant in Tyrosine Lyase assays*

As noted in Section 3.1, previous time course experiments were limited by the amount of substrate and reductant added. The reducing agent in tyrosine lyase activity assays is NADPH, however for efficient reduction of the iron sulphur cluster flavodoxin (FldA) and flavoprotein:NADPH oxidoreductase (Fpr) are also required. The electron transfer chain to reduce the cluster (Figure 3.1 B) first involves a two electron reduction of the Fpr co-factor: flavin adenine dinucleotide (FAD). This then reduces the FldA cofactor: flavin mononucleotide (FMN) to the semiquinone in a one electron reduction. The FMN semiquinone is then responsible for the 1 electron reduction of the iron sulfur cluster (Equation 3.1).

$$[4\mathrm{Fe}-4S]^{2+} + \mathrm{FMN.SQ} \leftrightarrow [4\mathrm{Fe}-4S]^{+} + \mathrm{FMN.Ox} \qquad \text{(Eq 3.1)}$$

The mid-point redox potential of FMN.SQ ↔ FMN.Ox has been reported to be -260 mV[133]. The midpoint potential for reduction of $[4Fe\text{-}4S]^{2+} \leftrightarrow [4Fe\text{-}4S]^{+}$ is significantly lower and is also dependent on the environment of the cluster. In LAM, when SAM is ligated to the 4Fe-4S cluster the midpoint potential has been estimated as -450 mV[75].

The large discrepancy in these two values may explain why it is necessary to incubate a mixture of NADPH, Fpr and FldA prior to addition to ThiGH to ensure a high proportion of FMN.SQ (observable by its blue colour). The Nernst equation[134] (Equation 3.2) describes the relationship between the ratios of oxidised or reduced species to the actual redox potential of the system.

$$E_{red} = E^{\emptyset}{}_{red} - \frac{RT}{zF} ln \frac{[Red]}{[Ox]} \quad \text{(Eq. 3.2)}$$

Where E_{red} is the potential of the system, $E^{\Phi}{}_{red}$ is the mid-point potential, *R* is the ideal gas contant, *T* is temperature, *z* is the number of electrons and *F* is the Faraday constant. >99% of FMN needs to be in the semiquinone (reduced) form in order for the potential to reach the mid-point potential typical of a 4Fe-4S cluster. This suggests that the position of equilibrium in Equation 3.1 is quite far to the left.

The stoichiometry of single turnover of tyrosine lyase requires the input of two electrons (one to reduce the iron sulphur cluster and one to reduce the aromatic portion to *p*-cresol after Cα—Cβ bond cleavage – see Scheme 2.1) and hence requires one equivalent of NADPH. In order to achieve multiple turnovers an excess of NADPH needs to be added to assays. Table 3.4 shows the amounts of the components of the reducing mixture added in assays reported by Kriek *et al.*[115] and the design of a modified reducing mixture with the potential to stimulate catalytic activity of tyrosine lyase.

Thus, assays were prepared with the modified reducing mixture which also contained >10 equivalents of tyrosine and SAM. After 1 h incubation at 37 ºC the proteins were acid precipitated and pelleted by centrifugation (see Method 16). The resulting supernatant was analysed by HPLC (see Method 17) to estimate the amount of DOA and *p*-cresol formed. It was found that after one hour, ThiH had achieved nearly four turnovers. Unfortunately there were some rather irreproducible variations in time dependent product formation (see Figure 3.4 and Figure 3.7). This is discussed in the remainder of this chapter. Subsequent experiments in which catalytic activity was measured routinely contained 1 mM of tyrosine and SAM, which corresponded to at least 10 molar equivalents of these substrates, relative to the concentration of

ThiH. The variable in each experiment was the ThiH concentration, due to variability in the isolation and reconstitution and this is reported in the figure legends for any activity measurements.

A

Component	Stock concentration / mM	Volume added to reducing mix / µL	Concentration in reducing mix / mM	Concentration in assay[1] /µM
FldA	0.61	60	0.41	25
Fpr	0.46	21	0.11	6.5
NADPH	100	9	10	**600**

[1] From 15 µL addition to a 200 µL assay

B

Component	Stock concentration / mM	Volume added to reducing mix / µL	Concentration in reducing mix / mM	Concentration in assay[1] /µM
FldA	0.61	90	0.37	37
Fpr	0.46	30	0.09	9.
NADPH	100	30	20	**2000**

[1] From 15 µL addition to a 150 µL assay

Table 3.4 Concentration of the components of the reducing mixture in A) Single turnover experiments reported by Kriek *et al.*[114, 115] and B) Catalytic turnover experiments reported in this thesis.

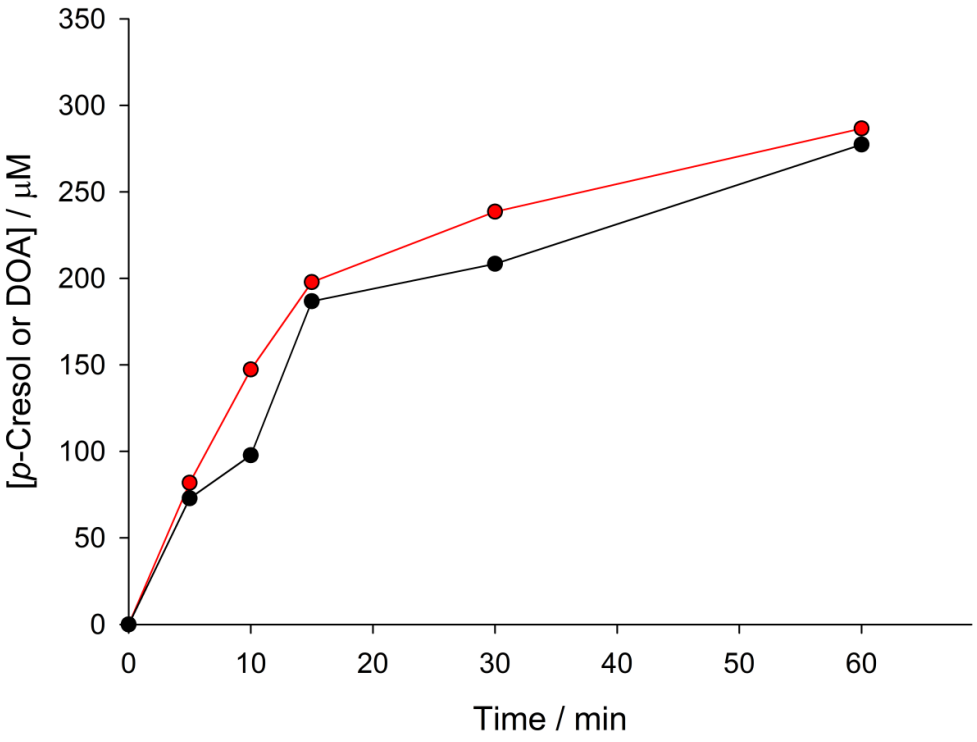

Figure 3.4 Catalytic activity of chemically reconstituted ThiGH, isolated by Ni-affinity chromatography. Formation of DOA (●—) and *p*-cresol (●—) in a ThiGH activity assay was monitored by HPLC. The assays contained: ThiGH (83 µM); SAM (830 µM); tyrosine (830 µM); FldA (36 µM); Fpr (9 µM) and NADPH (2 mM) and were stopped at selected time points by protein precipitation with perchloric acid.

3.5 *Expression and Purification of Tyrosine Lyase*

3.5.1 *Investigating Different Expression Systems for ThiGH*

A typical sample of ThiGH, expressed from pRL1020 (Method 9) and purified by Ni-affinity chromatography, then desalted on a S-75 column (Method 10) contained ~1 equivalent of iron, compared to the expected 4 equivalents from the 4Fe-4S cluster[106]. Therefore, careful chemical reconstitution is necessary in order to achieve active protein (see Method 14a). In an attempt to improve the iron content of isolated ThiGH or ThiH, the ThiFSGH operon was co-expressed with IscS, IscU, IscA, IscB and HscA. These proteins are responsible for the assembly of iron sulphur clusters in bacteria and it was anticipated that they might promote *in vivo* assembly of the 4Fe-4S cluster of ThiH[135]. The plasmid pRL1021 (see Figure 3.5) contains the same *thiFSGH* insert as pRL1020 with the addition of the *iscS, iscU, iscA, iscB, hscA* and *fdx* genes. Previous attempts to purify ThiH / ThiGH from this expression system in BL21 were unsuccessful, due to the expression of YqjI, which co-purified with ThiGH on a Ni-affinity column. To avoid this problem a mutant strain with deletion of the *yqjI* gene was investigated as a potential strain for expression of ThiH from pRL1021.

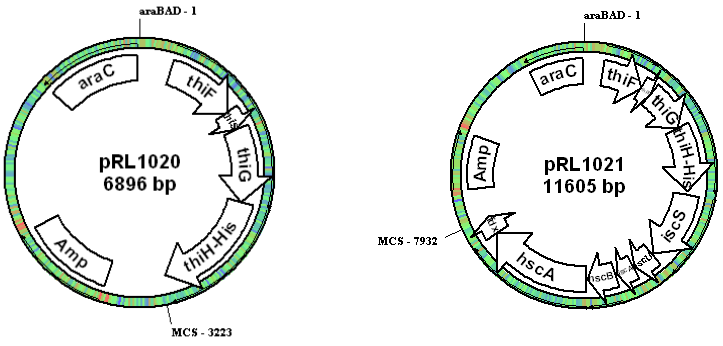

Figure 3.5 Plasmid maps of pRL1020 and pRL1021, which are used to express ThiH.

Unfortunately, growing this strain on a large scale gave very low yields of cell paste (typically 12-15 g per 5 L media, see Table 3.5). This is probably due to the adverse effect of overexpressing the Isc proteins in this strain. It is feasible that the expression of YqjI in normal BL21(DE3) was induced by a part of a feedback mechanism to mitigate the harmful effects these enzymes have on the cell's metabolism. It was also found that there was no significant improvement in yield or iron content of purified ThiH expressed from pRL1021 (see Table 3.5) and it also appeared as if there was a slight increase in the amount of monomeric ThiH isolated (see Figure 3.6). This observation was investigated by further purifying the protein (isolated by Ni-affinity chromatography) by S200 gel filtration chromatography. In addition the activity of ThiGH isolated from the two expression systems was investigated.

Plasmid	**Proteins expressed**	**Cell Strain**	**Yield of cell paste[1]**	**Yield of ThiGH[1]**	**Equivalents of Fe**
pRL1020	ThiFSGH-His	Bl21(DE3)	38 - 42 g	150 - 250 mg	1.8 ± 0.1
pRL1021	ThiFSGH-His, IscS, IscU, IscA, IscB, HscA	*-yqjI*	12 - 15 g	20 – 40 mg	2.0 ± 0.1

[1] values obtained from a typical 5L cell culture (see Methods 9 and 10)

Table 3.5 Yields of cell paste and ThiGH obtained from different expression systems.

The activity of ThiGH from pRL1020 (BL21) and pRL1021 (*yqjI*-) is shown in Table 3.6. ThiGH expressed from pRL1021 shows an apparent slight improvement in activity. This was further investigated by monitoring the time dependent formation of products (Figure 3.7) The time course data showed some variations in the rates of product formation which at this stage of the investigation were difficult to interpret. One possible source of variation was the presence of both ThiGH complex and monomeric ThiH in the assay. As these can be readily separated by gel filtration chromatography, the further purification of these two forms may simplify the

kinetic profile. Therefore, an additional preparative gel filtration step in the purification protocol of ThiH was developed.

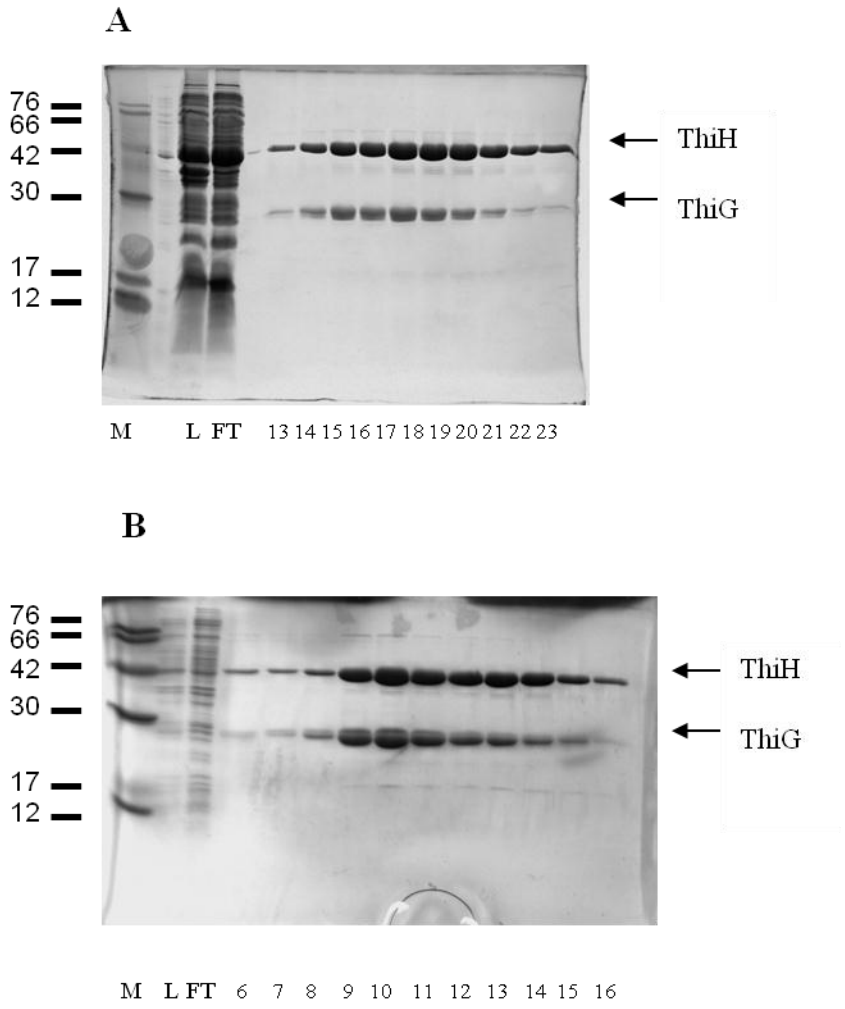

Figure 3.6 SDS-PAGE analysis of ThiH purification by Ni-affinity chromatography from **A)** pRL1021 (-*yqjI*) and **B)** pRL1020 (BL21). M = molecular weight marker; L = lysate; FT = flow through; number = fraction number.

	Number of Turnovers w.r.t.	
	5'-DOA	*p*-Cresol
pRL1020 (BL21)	3.7 ± 0.4	2.1 ± 0.2
pRL1021 (*yqjI*-)	4.0 ± 0.1	2.8 ± 0.0

Table 3.6: Comparison of the number of turnovers in 1 h by ThiGH from the different expression systems, pRL1020 (BL21) and pRL1021 (*yqjI*-)

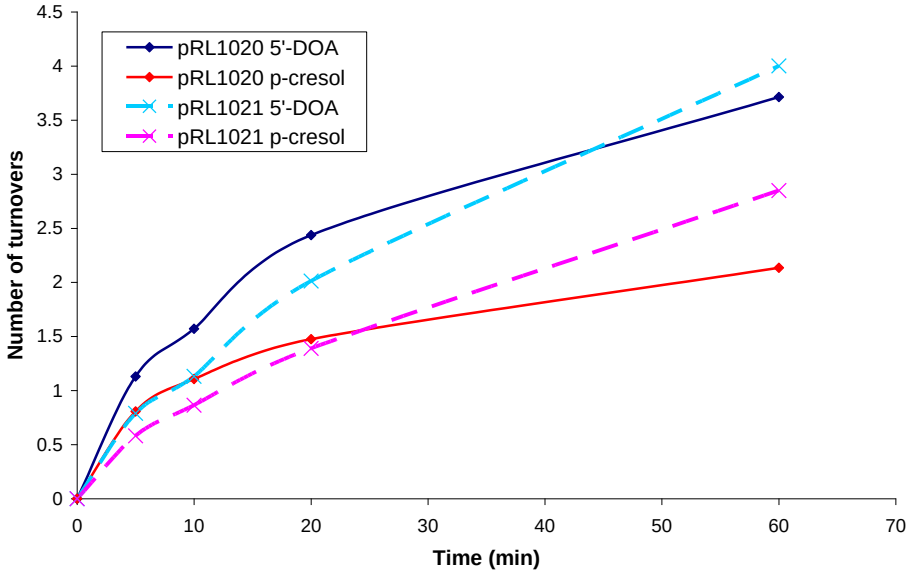

Figure 3.7 Comparison of the activity of ThiGH isolated from the different expression systems, pRL1020 (BL21) and pRL1021 (*yqjI*-).

3.5.2 *Isolation of Monomeric ThiH and ThiGH complex*

Analytical gel filtration chromatography[106] has shown that the protein isolated from the initial nickel-charged chelating Sepharose column contained a mixture of two forms of ThiH: as part of a large multimeric complex with at least 6 ThiGH heterodimers (apparent MW ~440 kDa); or as a monomer (apparent MW ~42 kDa). Resolution of these two species was achieved by preparative gel filtration chromatography using Sephadex 200 resin. The protein isolated after nickel-charged chelating Sepharose chromatography (ThiGH / ThiH mixture) (see Method 10) was chemically reconstituted (see Method 14a) to improve the stability of ThiH[129], allowing it to be concentrated to ~25 mg / mL for application to the preparative gel filtration column (see Method 13). Typically a 1:1 molar ratio of ThiGH:ThiH was isolated from the Ni-affinity column and successfully separated, with approximately 1 μmol of each being successfully isolated, by gel filtration (see Figure 3.8 and Table 3.7). Despite working under anaerobic conditions (less than 1 ppm O_2), the labile 4Fe-4S cluster did not remain intact during this purification step and the iron content (see Method 15) of purified protein fractions was reduced to 3.1 ± 0.2 mol equivalents of Fe per ThiGH and 2.5 ± 0.3 mol equivalents of Fe per ThiH (see Table 3.7). UV-visible spectroscopy also showed that the 4Fe-4S cluster had degraded during this purification step (Figure 3.9 C). The cluster was reconstituted again (see Method 14b) before activity measurements and the effectiveness of this reconstitution assessed by UV-visible spectroscopy (Figure 3.9 D).

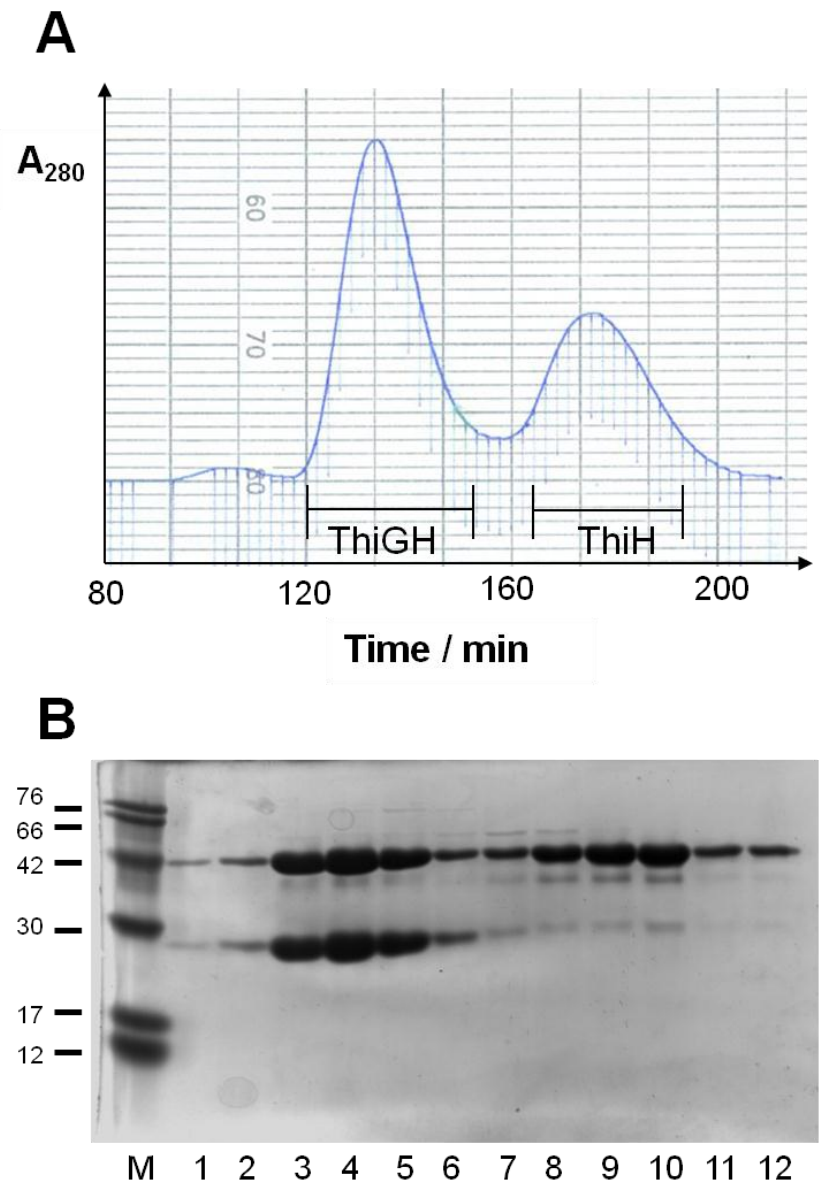

Figure 3.8 Gel filtration chromatography of ThiGH / ThiH. A) Elution of hexadiameric ThiGH and monomeric ThiH from a sephadex 200 gel filtration column. B) SDS-PAGE analysis of protein containing fractions. M, low molecular weight marker; numbers correspond to protein containing fractions.

Fraction	Contents	Moles of Protein ($\times 10^{-9}$)	Equivalents of Iron
2	$(ThiGH)_6$	23 ± 5	2.4 ± 0.1
3	$(ThiGH)_6$	250 ± 50	3.3 ± 0.2
4	$(ThiGH)_6$	430 ± 100	3.2 ± 0.2
5	$(ThiGH)_6$	280 ± 70	2.9 ± 0.3
6	$(ThiGH)_6$	50 ± 15	3.6 ± 0.3
7	ThiH	54 ± 10	3.2 ± 0.2
8	ThiH	160 ± 50	3.4 ± 0.2
9	ThiH	390 ± 60	2.1 ± 0.2
10	ThiH	280 ± 50	1.6 ± 0.02
11	ThiH	85 ± 9	2.4 ± 0.01

Table 3.7 Moles of protein and relative iron content in ThiH containing fractions from S200 gel filtration column. Moles of protein was estimated by the Bradford assay (Method 6)[136] and iron content was assayed by the method of Fish (Method 15)[137].

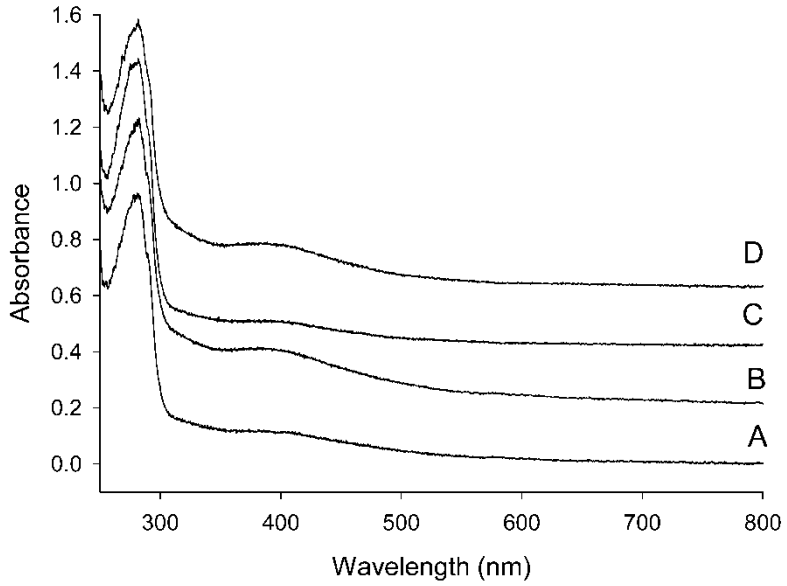

Figure 3.9 UV-vis spectroscopy of ThiH samples. A) Protein isolated by Ni affinity chromatography; B) Protein isolated by Ni affinity chromatography after chemical reconstitution; C) ThiGH fractions isolated by Sephadex 200 gel filtration chromatogrpathy; D) ThiGH fractions isolated by Sephadex 200 gel filtration chromatogrpathy after chemical reconstitution. The broad absorbance at 400 nm is due to the 4Fe-4S cluster (ref. 17). The spectra are displaced upwards for clarity.

3.6 ***Kinetic Studies on ThiH***

3.6.1 *Activity of the ThiGH Complex*

The time dependence of product formation was studied with ThiGH complex isolated by gel filtration chromatography. In previous experiments, tyrosine lyase activity had been limited to less than one turnover (angew) but this may have resulted from insufficient reductant or substrate in the assay. ThiGH assays were therefore prepared with greater than 10 mol. equivalents of tyrosine and SAM and a large excess of reductant (2 mM NADPH) to ensure the [4Fe-4S] cluster could repeatedly access the +1 oxidation state during catalytic turnover. Analytical HPLC was used to quantify the formation of the products DOA and *p*-cresol. Reactions were stopped at a range of selected time points up to 1 hour. The data from the time course showed a pre-steady state burst phase and could be fitted to a function which contains a single exponential and a linear, steady state component (see Figure 3.10)[138]:

$$[\mathrm{P}] = [\mathrm{E}](1 - e^{(1-k_{\mathrm{burst}}t)}) + Lt \qquad \text{(Eq. 3.3)}$$

where [P] is the observed concentration of product; [E] is the amplitude of the burst phase and is equal to the concentration of enzyme active sites in the reaction; k_{burst} is the observed single exponential rate constant for the burst phase; L is the observed linear rate and t is time. The rate constant for the steady state phase (k_{ss}) was derived by dividing the observed linear rate by the burst amplitude. This analysis gave the rate constant for *p*-cresol formation in the pre-steady state, exponential phase of 53 ± 5.9 x 10^{-4} s^{-1} and during steady state phase k_{cat} was calculated as 1.6 ± 0.2 x 10^{-4} s^{-1}. The rate constant for formation of 5'-deoxyadenosine was 63 ± 10 x 10^{-4} s^{-1} during the burst phase phase, but this slowed to 2.9 ± 0.2 x 10^{-4} s^{-1} during the steady state phase. The fitting of the data gave values of 89 ± 3.5 and 90 ± 4.4 µM for burst phase amplitude, which corresponds to the concentration of ThiH active sites and is in good agreement with the ThiGH

concentration estimated by the Bradford assay[136] (see Method 6) of 80 µM. This data is summarised in Table 3.8 (p99).

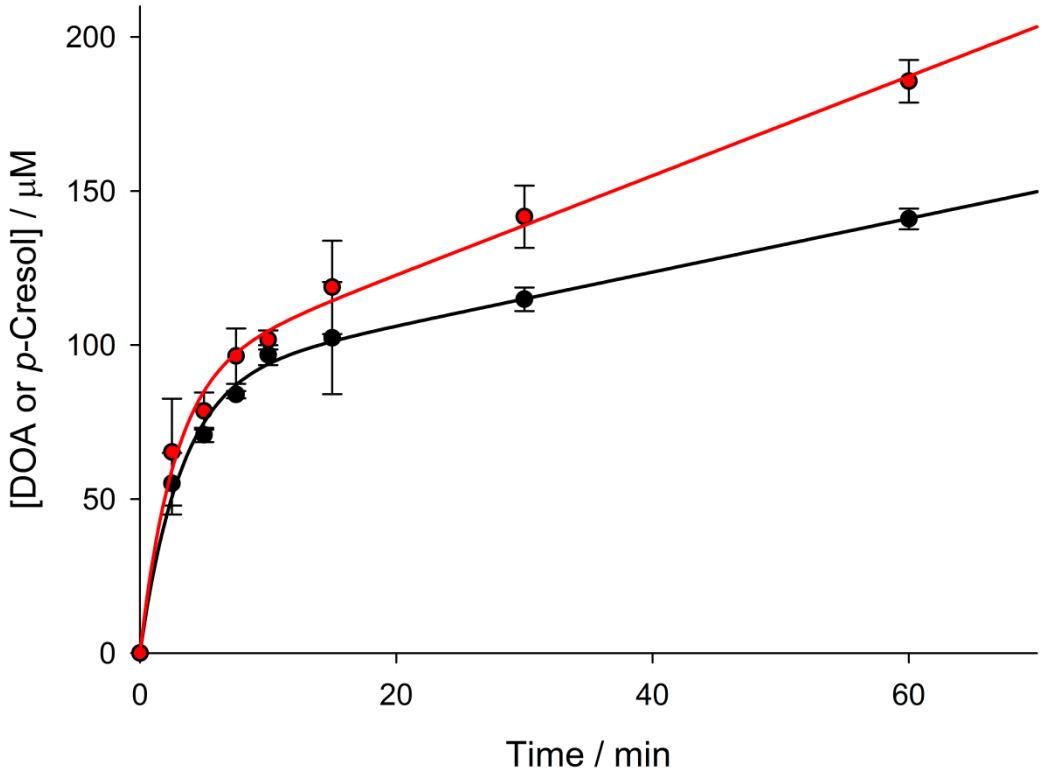

Figure 3.10 *In vitro* time course of tyrosine lyase activity by ThiGH. Formation of DOA (●—) and *p*-cresol (●—) in a ThiGH activity assay (containing 80 µM of ThiGH) was monitored by HPLC. Data are the average of experiments carried out in duplicate, shown with the standard error and were fitted to a pre steady state burst phase function (equation 3.3) to give the results shown in Table 3.8 (p99).

The pre-steady state burst phase (up to approximately 10 min, Figure 3.10) reflects the catalytic rate for the chemical reaction. The observation of burst phase kinetics indicates a rate limiting step that occurs after chemical catalysis, which can be a conformational change or the release of

products from the active site (see Scheme 3.2). ThiH yields four reaction products providing potential for a complex pattern of product inhibition. The hydrolytic instability of dehydroglycine implies that a tight interaction with ThiGH would be advantageous, helping to sequester the imine away from the aqueous environment. Dehydroglycine needs to be transferred to the ThiG active site where it is a substrate for thiazole formation and it seems likely that the transfer of dehydroglycine from ThiH to ThiG is tightly controlled and may explain the functional role of complex formation between ThiH and ThiG. It is essential to avoid its release from ThiGH and subsequent rapid hydrolysis to glyoxylate and ammonium, as this would not only result in formation of compounds potentially damaging to the cells metabolism, but also a wasted turnover of ThiH, which is a metabolically expensive step.

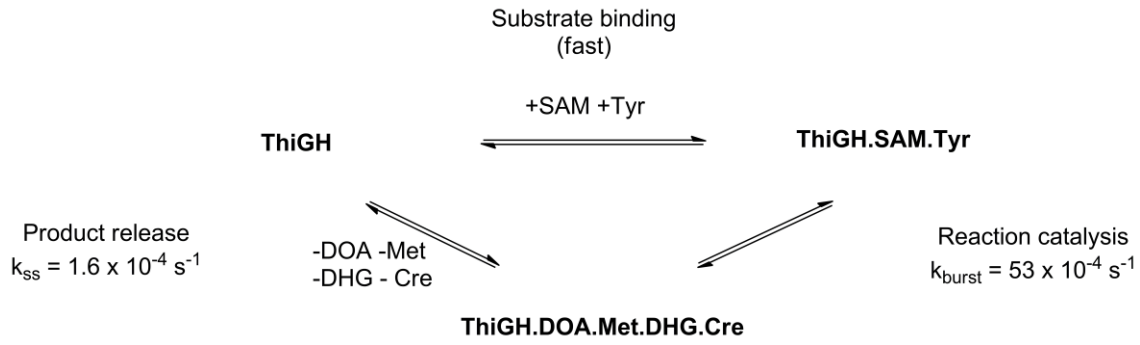

Scheme 3.2 Catalytic cycle of ThiGH. The first turnover results in saturation of the enzyme active site with products. To allow for subsequent turnovers, the products need to be released making the active site available for a new substrate molecule to bind. The rate of substrate binding is assumed to be very fast relative to the observed rates of reaction catalysis and product release.

In a typical experiment, after 1 h, ThiGH had generated 1.8 mole equivalents of *p*-cresol and 2.3 mol equivalents of DOA, with an overall DOA:*p*-cresol ratio of 1.3:1, indicating that there was some uncoupled turnover of SAM to DOA. During the burst phase, when reaction catalysis is

rate limiting, there is efficient coupling of DOA formation to tyrosine cleavage: for example, after 5 minutes, the concentration of DOA was 79 ± 6.0 μM and the concentration of *p*-cresol was 71 ± 2.3 μM, giving a DOA to *p*-cresol ratio of 1.1:1. However, after the first turnover, when the release of products becomes rate limiting, the reaction slows down and uncoupled turnover of SAM become more significant. In the steady state phase (after about 15 mins, Figure 3.10) the ratio of the rate of formation of DOA to the rate of *p*-cresol formation increases to 1.7:1. Experiments on inhibition of ThiH activity by the products are reported in Chapter 4. Discussion on the implications for the mechanism of tyrosine cleavage and uncoupled SAM cleavage is developed in Chapter 4 in light of these observations.

3.6.2 *Activity of Monomeric ThiH*

Size exclusion chromatography allowed the purification of ThiGH complex and monomeric ThiH. The natural pathway for thiazole biosynthesis includes efficient transfer of dehydroglycine from ThiH to ThiG and it was therefore of interest to determine the kinetic properties of ThiH in the absence of ThiG. The time course obtained using HPLC analysis of activity assays with monomeric ThiH is shown in Figure 3.11. The kinetics of product formation from ThiH showed burst phase similar to that observed with ThiGH and the data could be fitted to equation 3.3. Fitting of the data to equation 3.3 gave a burst phase rate constant ($32 \pm 7.8 \times 10^{-4}$ s^{-1} for *p*-cresol) that is marginally slower than for ThiGH, but a substantially faster steady state rate ($5.9 \pm 0.2 \times 10^{-4}$ s^{-1} for *p*-cresol) which is consistent with a faster (but still rate limiting) product release step. Therefore, the rate of product release is different depending on whether ThiH is in a complex with ThiG and this may indicate the importance of the transfer of dehydroglycine. However, without any structural data it is extremely difficult to rationalise this and no firm conclusions can yet be drawn from this experiment.

The observation of a higher steady state rate constant for monomeric ThiH helped to explain the observations presented in Figure 3.7. Protein purified by Ni-affinity chromatography from the pRL1021 expression system appears to have a slightly higher proportion of monomeric ThiH, relative to ThiGH complex (Figure 3.6). Therefore, time course experiments on protein expressed form pRL1021 that had not been purified by gel filtration showed a kinetic profile more characteristic of monomeric ThiH. Protein expressed from pRL1020 contained relatively more of the ThiGH complex and this is reflected in the kinetic profile, where the steady state rate appears slightly slower. These results highlight the importance of fully optimising the purification of a protein to permit interpretation of the kinetics.

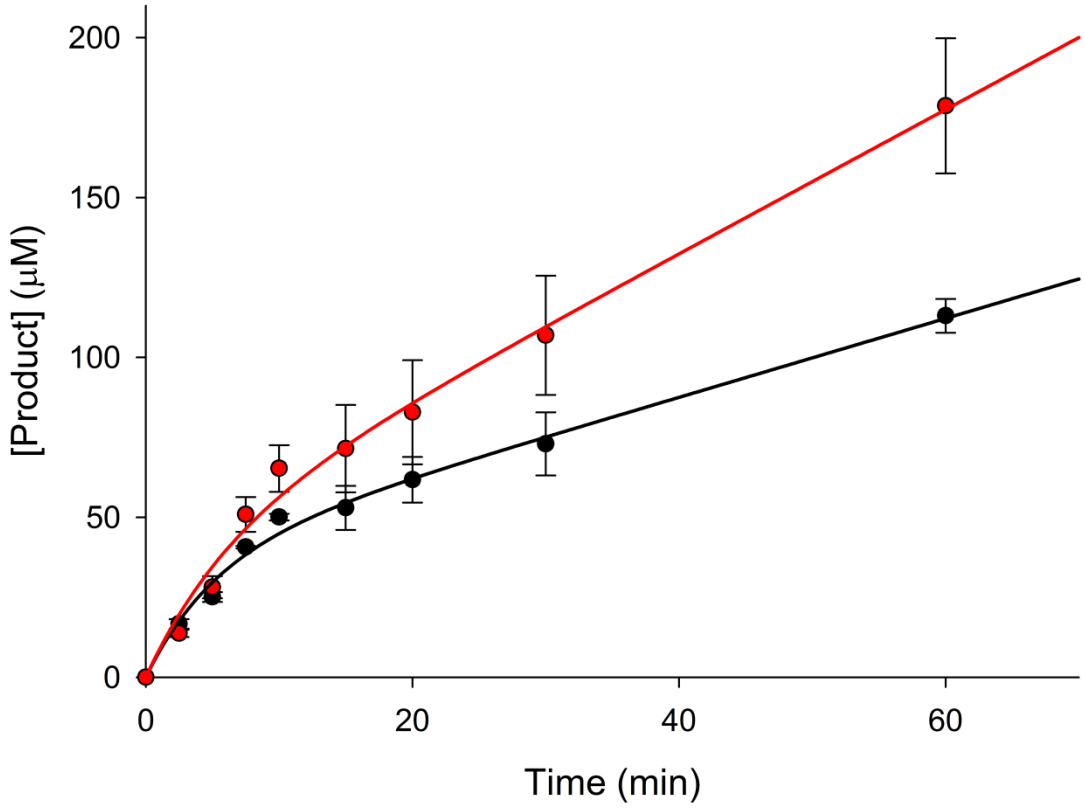

Figure 3.11 *In vitro* time course of tyrosine lyase activity by ThiH. Formation of DOA (●—) and *p*-cresol (●—) in a ThiH activity assay (containing 35 μM of ThiH) was monitored by HPLC. Data are the average of experiments carried out in duplicate, shown with the standard error and were fitted to a pre steady state burst phase function (equation 3.3) to give the results shown in Table 3.8.

Form of ThiH	Product	[E]/μM	k_{burst} ($\times 10^{-4}$ s^{-1})	k_{ss} ($\times 10^{-4}$ s^{-1})	R^2
ThiGH complex	*p*-Cresol	89 ± 3.5	53 ± 5.9	1.6 ± 0.2	0.99
	DOA	90 ± 4.4	63 ± 10	2.9 ± 0.2	0.99
Monomeric ThiH	*p*-Cresol	38 ± 4.4	32 ± 7.8	5.9 ± 0.2	0.99
	DOA	42 ± 8.9	27 ± 11	10.7 ± 1.0	0.99

Table 3.8 Kinetic analysis of tyrosine lyase activity. These results were obtained by fitting data to equation 3.3. [P] is the observed concentration of product; [E] is the observed burst amplitude; k_{burst} is the observed single exponential rate constant for the burst phase and k_{ss} is the steady state rate constant, derived by dividing the observed linear rate by the burst amplitude. Data are presented with standard errors and R^2 is a measure of the goodness of fit.

3.7 *Summary and Conclusions*

An assay that utilised reverse phase HPLC was developed to routinely quantify the amount of DOA and *p*-cresol in ThiH activity assays. Modification of the assay buffer to contain both sodium chloride and glycerol was necessary to avoid protein precipitation during assay experiments. Using the developed assay it was possible to achieve multiple turnovers of ThiH when an excess of substrates and reductant were present. The kinetics of ThiH was investigated and product formation was shown to follow a pre-steady state burst phase profile. It was preferential to perform kinetic experiments on purified monomeric ThiH or ThiGH complex to simplify the interpretation of the data. Purification of the ThiGH complex and monomeric ThiH (isolated in a mixture by Ni-affinity chromatography) was achieved by preparative gel filtration using Sephadex 200 gel filtration resin. A slight improvement in the ratio of monomeric ThiH could be achieved by using an expression system that included the Isc operon. However, protein expression from this system required the use of an *E. coli* strain with deletion of the *yqjI* gene, to avoid the co-purification of this gene product. This gave a much lower yield of cells with no improvement to the yield of protein.

The development of the assay has allowed for resolution of the kinetics of ThiGH and ThiH. Additionally, in developing these experiments a great deal of experience, which built on the understanding developed by Leonardi[106, 107, 131], Kriek[114, 115] and Martins[129], of handling the ThiH protein was achieved. In particular, the importance of maintain strictly anaerobic conditions at all times, but especially during chemical reconstitution of the 4Fe-4S. This understanding, combined with the robust assay for ThiH activity allowed for a diverse range of *in vitro* experiments to further elucidate the mechanism of ThiH to be undertaken, which are reported in the next chapter.

4 Mechanistic Studies on Tyrosine Lyase

4.1 *Introduction*

The lack of any structural data for ThiH or ThiGH makes elucidation of the enzymatic mechanism of tyrosine cleavage difficult. However, several clues to the mechanism have been gleaned from studies on other members of the radical SAM family. The mechanism of SAM cleavage, generating the 5'-deoxyadenosyl radical in ThiH, is extremely likely to be similar to what is suggested from structural and spectroscopic observations on other members of the radical SAM family[10, 63] (see Section 1.2). One possible hypothesis is that direct hydrogen atom abstraction form tyrosine by the 5'-deoxyadenosyl radical (**9**) mediates Cα—Cβ bond cleavage, possibly by one of the mechanisms shown in Scheme 2.1 (p64). However, developing an understanding of the mechanism of tyrosine cleavage in the context of thiazole formation presents a far greater challenge. Dehydroglycine (**11**) is an electrophilic intermediate required for the ThiG mediated formation of the 5-membered thiazole ring (see Scheme 1.13, p40). As such it can be thought of as an "electron deficient" species and its formation from an amino acid moiety (tyrosine (**10**) or glycine (**87**)) involves a loss of electrons from the amine. Compared to the direct oxidation of glycine in *B. subtilis* (and other aerobic bacteria), the use of tyrosine as the source of this intermediate in *E. coli* (and other anaerobic bacteria) is puzzling, especially as the aromatic by-product, characterised as *p*-cresol (**88**), is toxic to the cell. Additionally, the tyrosine cleavage reaction uses SAM stoichiometrically (generating methionine and DOA as products) and requires the input of two electrons, which adds a further metabolic cost to the reaction. This raises the important question of why anaerobes choose to use this ThiH mediated pathway and highlights the importance of its regulation to avoid unproductive reactions.

In Chapter 3 it was shown that tyrosine lyase could function catalytically *in vitro*, providing there was ample reductant present allowing the 4Fe-4S cluster to repeatedly access the overall +1 oxidation state. Analysis of the kinetic data suggested that the enzyme was prone to inhibition by accumulation of the products. This product inhibition could result from the hydrolytic sensitivity of one of the products, dehydroglycine and may serve a useful function, preventing further turnovers of ThiH in the absence of ThiG or one of its substrates. The generation of four reaction products provides a potentially complex pattern of product inhibition and in this chapter the inhibitory effects of some of the products, either individually or cooperatively, are examined. In addition studies with structural analogues of tyrosine which could undergo partial reactions were used to provide evidence for the site of hydrogen atom abstraction from tyrosine and the importance of certain functional groups on Cα—Cβ bond cleavage. The results of product inhibition experiments and substrate analogue experiments could be integrated into a broader mechanistic hypothesis. A more detailed model of the mechanism is presented towards the end of the chapter which provides an explanation for observed uncoupled turnover and is rationalised with the functional requirement of ThiH in the biosynthesis of thiazole.

4.2 *Inhibition by DOA and Methionine*

Product inhibition by the SAM cleavage products, DOA and Methionine, have been studied previously on biotin synthase[139] and lipoyl synthase[23]. Biotin synthase (BioB) and lipoyl synthase (LipA) are radical SAM proteins which insert sulfur atoms during the final step of the biosynthesis of biotin[22, 24] and lipoyl groups[23, 25]. *In vitro* activity assays have shown that biotin or lipoyl groups are produced in a stoichiometric ratio with the BioB or LipA proteins[32, 54] as a result of single enzyme turnover, probably due to depletion of the sulfur donor. (A recent report[140] has actually suggested BioB can behave catalytically *in vitro* providing an excess of sulfide is present. The activity also showed burst phase kinetics). The potential for product inhibition by DOA and methionine *in vitro* had only been reported in the literature for a single example protein from the radical SAM family, biotin synthase (BioB). These experiments have yielded conflicting results: data from Ollagnier-de-Choudens *et al.* [141] indicated almost complete inhibition of BioB at a molar ratio of 1.5 DOA per BioB, corresponding to a DOA concentration of ~ 55 μM. However, this was not observed by Tse Sum Bui *et al.* [55] who reported that BioB was not inhibited by DOA. However, Ziegert observed co-operative inhibition of BioB *in vitro* by DOA and methionine[139, 142]. In his studies he reported that the individual compounds had a weak inhibitory effect, which was greatly increased when they were present in equimolar amounts. This is relevant as DOA and methionine are generated in a 1:1 ratio as products of radical SAM enzymes that use SAM stoichiometrically. Ziegert also reported that addition of 5'-methylthioadenosine / *S*-adenosylhomocysteine nucleosidase (MTAN) alleviated any inhibition by DOA. These results were consistent with the observations of Choi-Rhee and Cronan[143] who demonstrated that BioB could function catalytically *in vivo* (20 – 60 molecules of biotin formed per BioB), but the catalytic activity was dependent on MTAN. It was found that MTAN could hydrolyse the glycosidic bond of DOA (**32**) to yield adenine (**116**) and 5'-deoxyribose (**118**)[144, 145] (see Scheme 4.1), thus extending the substrate specificity of this enzyme which had previously been reported to utilise *S*-adenosylhomocysteine (SAH) and 5'-methylthioadenosine (MTA)[146]. Choi-Rhee and Cronan

suggested that variable amounts of MTAN in BioB preparations could account for variations in ability of DOA to inhibit BioB and provides an explanation for the previously reported contradictory observations.

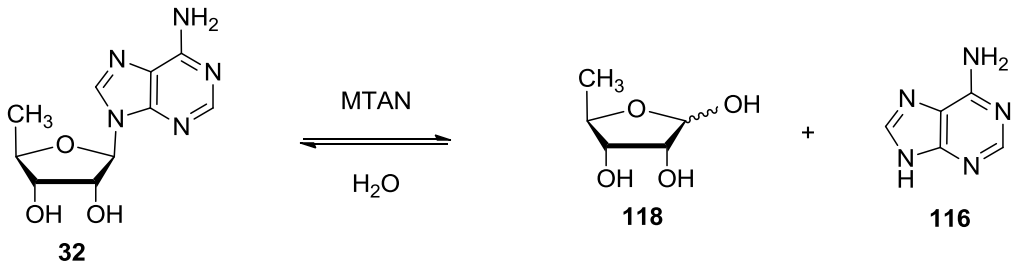

Scheme 4.1 MTAN mediated hydrolysis of DOA to adenine and 5'-deoxyribose.

Analogous studies by Douglas[142, 147], demonstrated a similar pattern of product inhibition by DOA and methionine on lipoyl synthase. Taken together these observations on LipA and BioB suggest a trend of product inhibition of radical SAM enzymes by DOA and methionine which use SAM stoichiometrically (see Section 1.2.2). Tyrosine lyase falls into this category of radical SAM enzyme but is also capable of multiple turnovers as the protein does not act as a substrate, which is the case for BioB and LipA. These observations on BioB and LipA combined with the observed pre-steady state burst phase kinetics on tyrosine lyase inspired studies of the potential inhibition of ThiGH by DOA and methionine.

4.2.1 *The Effect of DOA and Methionine on ThiH Activity*

To investigate the possibility that the SAM cleavage products inhibit tyrosine lyase activity, increasing amounts of each product was added to activity assays (see Method 25). Relative activity was calculated by comparison with a standard assay to which no products had been added and was assessed by the amount of *p*-cresol formed. This strategy negated the variations in the kinetics of ThiGH and ThiH and the experiments reported in this section were conducted on the ThiH / ThiGH mixture isolated by Ni-affinity chromatography which was not further purified by gel filtration chromatography. Methionine had no observable effect on the activity, even at a concentration of 1 mM, which is far greater than might accumulate in a typical *in vitro* assay (Figure 4.1 – blue dots). DOA was found to be a weak inhibitor (Figure 4.1 – red dots) and 1 mM of DOA only resulted in 50 – 60% inhibition. As DOA and methionine are produced in equimolar amounts, their potential to inhibit in a cooperative manner was investigated. The addition of a combination of DOA and methionine to assays resulted in a greater degree of inhibition than the individual compounds (Figure 4.1 – purple dots). The inhibition could be fitted to a 3 parameter logistic sigmoid to give the apparent IC_{50} for ThiGH under the assay conditions of 445.6 ± 35 μM.

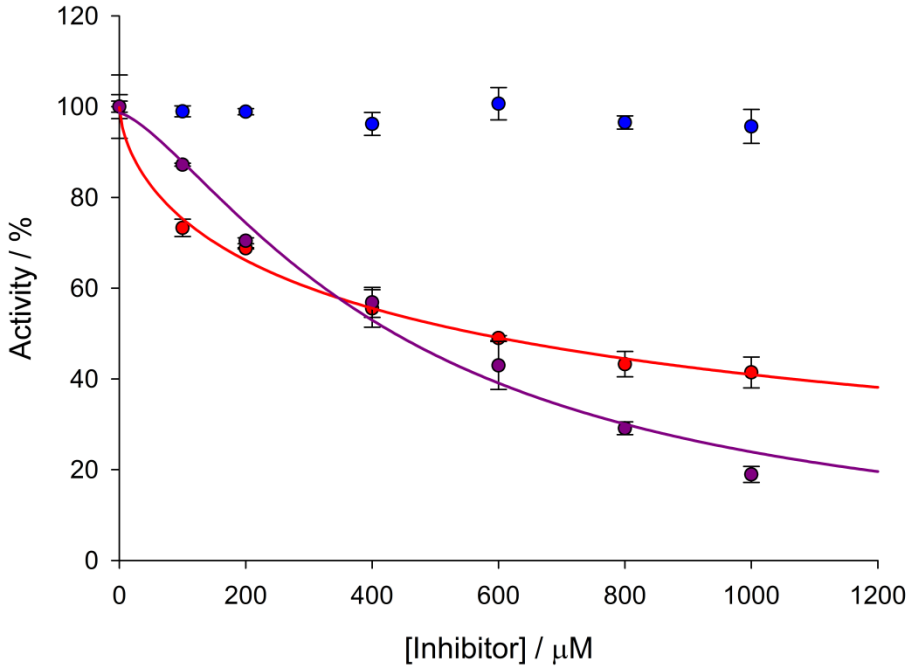

Figure 4.1 The effect of methionine (●), DOA (●) and equimolar amounts of DOA and methionine (●) on tyrosine lyase activity. Data were fitted to a 3 parameter logistic sigmoid. The data for the effect of methionine could not be fitted.

4.2.2 *Kinetic Analysis of MTAN with DOA as the Substrate*

Choi-Ree *et al*. have demonstrated that DOA is a substrate for MTAN[144]. To further understand the substrate diversity, the kinetic parameters of this enzyme with DOA as the substrate were investigated. MTAN activity assays were prepared at seven different substrate concentrations and the disappearance of DOA and formation of adenine monitored by HPLC (Figure 4.2 – see Method 27). The initial rate of reaction was estimated by fitting the formation of adenine to a linear function. The initial rates of reaction at the seven substrate concentrations were then fitted to the Michaelis-Menten equation[148] (see Figure 4.3) giving the kinetic parameters which are reported in Table 4.1. Although the disappearance of DOA could be monitored by HPLC, it could not be fitted with such confidence, especially at high DOA concentrations.

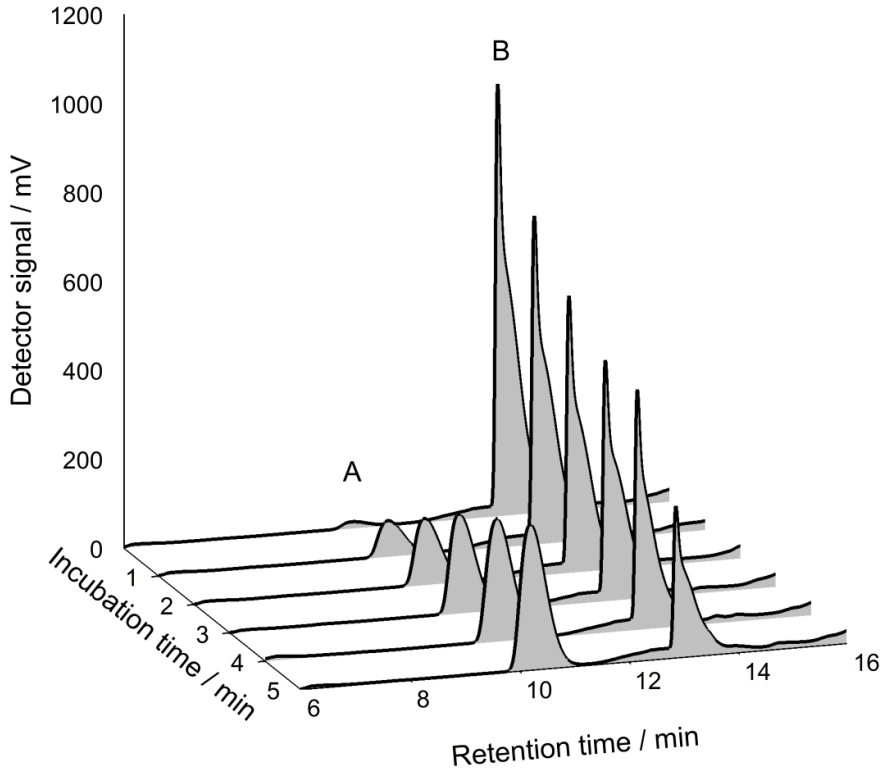

Figure 4.2 HPLC analysis of MTAN activity. Adenine (peak A) and DOA (peak B) were detected by monitoring the absorbance at 254 nm.

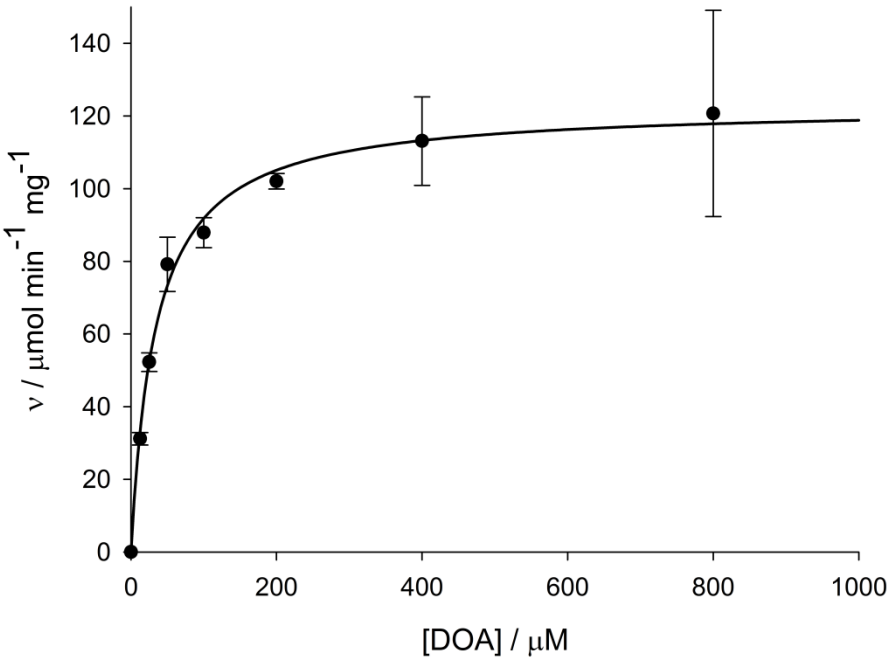

Figure 4.3 Michaelis-Menten plot for MTAN with 5'-DOA as the substrate.

Substrate	**V_{max} / µmol min^{-1}mg^{-1}**	**K_M / µM**	**k_{cat} / s^{-1}**	**Catalytic Efficiency / M^{-1} s^{-1}**
DOA	120 ± 3	33 ± 3	49	1.5 x 10^6
MTA	370	0.40	150	370 x 10^6
SAH	No Data	4.3	No Data	No Data

Table 4.1 Kinetic constants of MTAN. Data for MTA and SAH were derived from Della Ragione *et. al.*[149]

4.2.3 *Removal of DOA from ThiH Activity Assays*

Having demonstrated that MTAN can rapidly hydrolyse DOA, we sought to test it as a solution to potentially problematic inhibition by methionine and DOA. Therefore, the effect of adding MTAN to *in vitro* activity assays that had been doped with inhibitory concentrations of DOA and methionine was investigated. After incubation at 37 °C, the comparison of activity assays with and without MTAN shows that MTAN restored the activity (Figure 4.4, sample 2). The activity in the MTAN containing samples exceeds the observed activity of the positive control (Figure 4.4, samples 1 and 3), due to the hydrolysis of the DOA formed during the reaction. This conclusion is supported by the observation that the addition of MTAN to an activity assay from the beginning of the reaction resulted in a reproducible enhancement of activity (Figure 4.4, samples 4).

Radical SAM proteins can be divided into two groups, based on whether they use the deoxyadenosyl radical catalytically or stoichiometrically[27]. The enzymes that utilize the DOA radical catalytically (e.g. lysine amino mutase and DNA spore photoproduct lyase) are unlikely to accumulate enough DOA or methionine to reach inhibitory concentrations. However, ThiH is like the majority of family members characterised thus far, and forms DOA as a product that is released from the active site at the end of each catalytic cycle. The apparent IC_{50} value for co-operative inhibition by DOA and methionine suggests that inhibition by these two products has a significant effect during *in vitro* assays. The addition of the nucleosidase MTAN relieves the cooperative inhibition of tyrosine lyase and furthermore, results in a significant increase in the amount of product formed (Figure 4.4). This is likely to be due to any potentially inhibitory DOA formed during the reaction being hydrolysed by MTAN *in situ*.

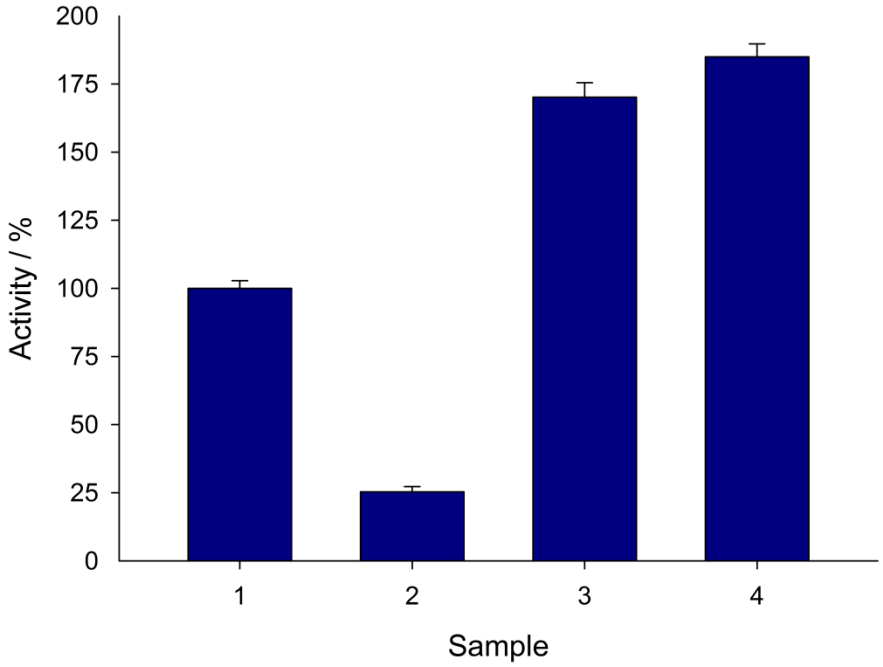

Figure 4.4 Effect of adding MTAN to tyrosine lyase activity assays. Assays were supplemented with the following additional reagents: sample 1, no further additions; sample 2, DOA and methionine (1 mM of each); sample 3, MTAN (10 μM), DOA and methionine (1 mM of each); sample 4, MTAN (10 μM).

These observations of product inhibition by DOA and methionine are consistent with observations made on BioB and LipA[142]. It was also found that the inhibition could be relieved by addition of MTAN. Thus, the addition of MTAN to radical SAM activity assays may represent a useful general approach that is applicable to the large number of radical SAM proteins currently subject of mechanistic investigation. The absence of product inhibition may simplify kinetic analysis as well as increase the observed rates of reactions.

4.3 *Kinetics of Tyrosine Lyase in the Presence of MTAN*

The observation of burst phase kinetics in time course experiments on tyrosine lyase had implied a potentially complex mechanism of product inhibition. As MTAN was shown to relieve product inhibition by DOA and methionine it was considered that addition of MTAN to tyrosine lyase activity assay might simplify the interpretation of subsequent kinetic experiments. Therefore, a time course was conducted with 10 µM MTAN present in the assay. The results are shown in Figure 4.5. Adenine could be readily quantified using the same analytical HPLC protocol developed in chapter 2 (R_t = 6.0 min – peak 2 in Figure 3.3). During the quantification of adenine produced in these time course experiments, particular care was required with negative control samples (lacking reductant), as commercial supplies of SAM contain a small proportion of 5'-methylthioadenonine (MTA) (**114**), which also yields adenine upon hydrolysis by MTAN[150]. Care was then taken to ensure that this background was subtracted from activity assays, giving the data shown in Figure 4.5.

The addition of MTAN changed the profile of the ThiGH activity time course. *In situ* hydrolysis of the DOA eliminated the burst phase and extended the period of relatively rapid turnover (where k_{cat} for the formation of cresol was in the range 30-50 x 10^{-4} s^{-1}) beyond a single turnover. The rate of product formation slowly declined and could be fitted as a first order process:

$$[P] = 1 - ([P]_{max} e^{-kt}) \qquad \text{(Eq. 4.1)}$$

where [P] is the observed concentration of product; $[P]_{max}$ is the maximum observed product concentration and *k* is the observed first order rate constant.

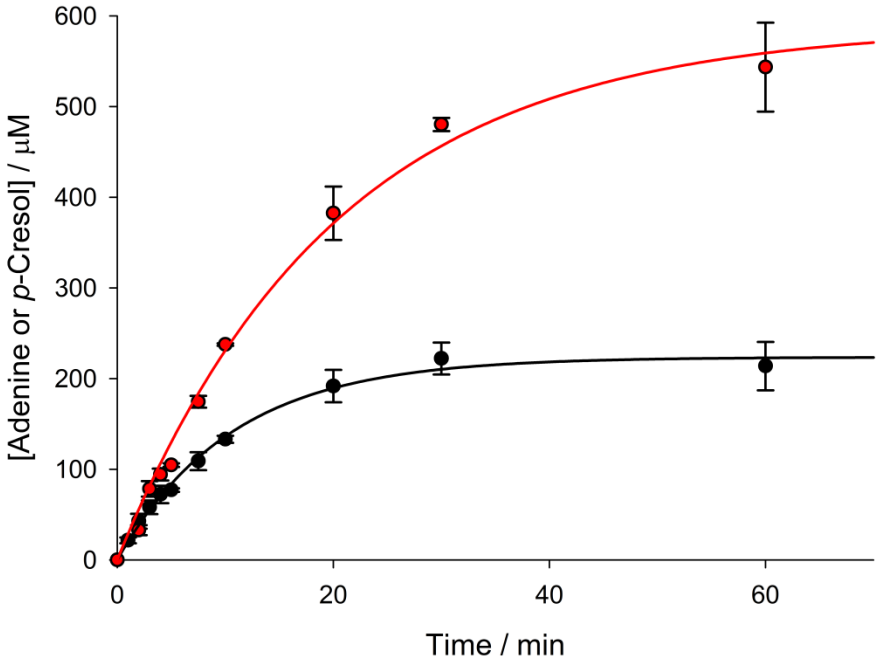

Figure 4.5 *In vitro* time course of tyrosine lyase activity by ThiGH coupled with MTAN mediated hydrolysis of DOA. Formation of adenine (●) and *p*-cresol (●) in a ThiGH activity assay (containing 95 µM of ThiGH), coupled with MTAN mediated hydrolysis of DOA, were monitored by HPLC. Data are the average of experiments carried out in duplicate, shown with standard errors and were fitted to a first order exponential function (equation 4.1).

To derive the initial turnover number (k_{cat}^{0}) the following equation was used:

$$k_{cat}^{o} = \frac{k[P]_{max}}{[E]} \qquad \text{(Eq. 4.2)}$$

where [E] is the ThiGH concentration as estimated by the Bradford assay[136].

The final *p*-cresol from the fit of equation 4.1 to the data ($[P]_{max}$) concentration was 220 ± 5.2 µM (~2.3 turnovers). Subsequent experiments with lower ThiGH concentrations demonstrated that after 1 h, ThiGH could produce up to seven equivalents of *p*-cresol (see Table 4.2). However the maximum concentration of *p*-cresol measured in any ThiGH assay did not exceed 250 µM. The initial turnover numbers (k_{cat}^{0}) for ThiGH calculated from the initial rates are 37 ± 3.0 x 10^{-4} s^{-1} and 51 ± 6.4 x 10^{-4} s^{-1} for the formation of *p*-cresol and adenine respectively. These initial rates are similar to those observed in the absence of MTAN. At time points beyond five minutes, a further increase in uncoupled turnover of SAM was observed and the final concentration of adenine reached 590 ± 24 µM, corresponding to a ratio of adenine:*p*-cresol of 2.7:1. The addition of MTAN to monomeric ThiH assays did not abolish the burst phase; however, it did increase the degree of uncoupled turnover (see Figure 4.6). This suggests that for monomeric ThiH, a step other than release of DOA is rate limiting.

[ThiGH] / µM	**[*p*-Cresol] / µM**	**Number of turnovers**
95	214 ± 26	2.3
64	227 ± 2.0	3.6
51	207 ± 1.5	4.1
38	175 ± 1.6	4.6
26	129 ± 1.0	5.1
13	77.9 ± 1.6	6.1
6.5	46.0 ± 2.5	7.2

Table 4.2 Number of turnovers of tyrosine cleavage achieved by ThiGH. The assays contained ThiGH (as shown), SAM (1 mM), tyrosine (1 mM), flavodoxin (36 µM), flavodoxin NADPH reductase (9 µM) and NADPH (1.9 mM) and were incubated at 37 °C for 1h. The concentration of *p*-cresol was estimated by HPLC (Method 17).

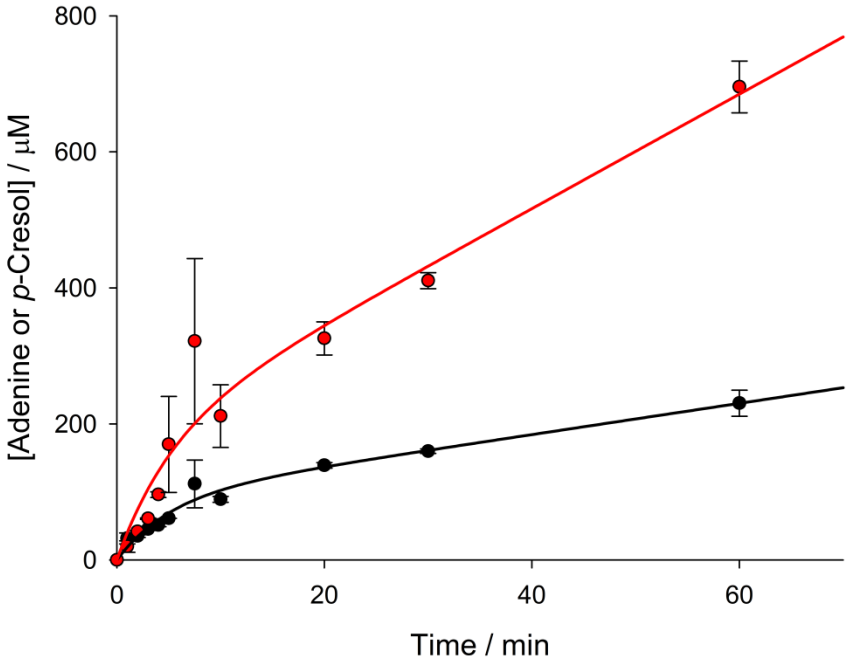

Figure 4.6 *In vitro* time course of tyrosine lyase activity by monomeric ThiH, coupled with MTAN mediated hydrolysis of DOA. Formation of adenine (●) and *p*-cresol (●) in a ThiH activity assay (containing 90 µM of ThiH), coupled with MTAN mediated hydrolysis of DOA, were monitored by HPLC. Data are the average of experiments carried out in duplicate, shown with standard errors and were fitted to equation 3.3.

4.4 *Inhibition of Tyrosine Lyase by Glyoxylate and Ammonium Ions*

The addition of MTAN to tyrosine cleavage assays with the ThiGH complex altered the kinetics, giving a prolonged period where reaction catalysis was assumed to be rate limiting. However, despite there being an excess of SAM, tyrosine and NADPH the maximum concentration of *p*-cresol observed remained at about 220 µM. In assays on monomeric ThiH the steady state rate of tyrosine cleavage was not altered by the addition of MTAN, also implying inhibition by a different product. Therefore, the potential of dehydroglycine to inhibit the reaction was tested. A different strategy was required for investigating the potential of dehydroglycine to inhibit tyrosine lyase. The hydrolysis of dehydroglycine is a rapidly reversible equilibrium and the addition of relatively high concentrations of glyoxylate and ammonium ions yields a low concentration of dehydroglycine in the solution. This method was used advantageously by Begley and co-workers[100] during studies in which they demonstrated that the addition of glyoxylate and ammonium ions provided sufficient dehydroglycine to reconstitute the ThiG dependent cyclisation reaction.

Using this approach to examine the effect of dehydroglycine on tyrosine lyase activity, increasing concentrations of glyoxylate and ammonium ions were added to activity assays. To ensure product inhibition by DOA did not disguise any effects of glyoxylate and ammonium ions, these assays also contained sufficient MTAN to hydrolyse the DOA produced in the assay to adenine (**116**) and 5'-deoxyribose (**118**) (see Scheme 4.1). The effects of glyoxylate and ammonium ions on ThiH activity were measured using HPLC analysis, measuring tyrosine cleavage by detecting the production of *p*-cresol and reductive cleavage of SAM by detecting the production of adenine. The data for *p*-cresol was fitted to a 4 parameter logistic sigmoid:

$$A = A_0 + \frac{\Delta A}{1 + \left(\frac{[\mathrm{I}]}{IC_{50}} \right)^h} \qquad \text{(Eq. 4.3)}$$

where A is the observed activity; A_0 is the minimum activity, ΔA is the difference between the maximum and minimum observed activity; [I] is the concentration of inhibitor (glyoxylate and ammonium ions) and h is the Hill co-efficient. This fit showed that the combination of ammonium ions and glyoxylate inhibited the cleavage of tyrosine with an apparent IC_{50} of 440 ± 55 µM and a Hill co-efficient of 1.1 ± 0.1, suggesting a 1:1 complex of the inhibitor and the enzyme, although it is not possible to determine from this experiment whether glyoxylate or dehydroglycine is binding to the enzyme. In contrast, no inhibition of SAM cleavage was observed over the whole range of glyoxylate and ammonium concentrations. At high glyoxylate and ammonium concentrations (2 mM), greater than 90% of the reductive cleavage is uncoupled, resulting in the accumulation of up to 600 µM of adenine but only 40 µM of *p*-cresol. Similar results were obtained in experiments using either ThiGH complex or monomeric ThiH, suggesting the presence of ThiG alone does not influence this inhibition. Subsequent experiments in which 1 mM of the individual species was added to activity assays (Figure 4.8) showed this inhibition was also observed when only glyoxylate was added and that there was no effect by adding only ammonia. Therefore, it cannot be differentiated whether glyoxylate or dehydroglycine is interacting with the protein.

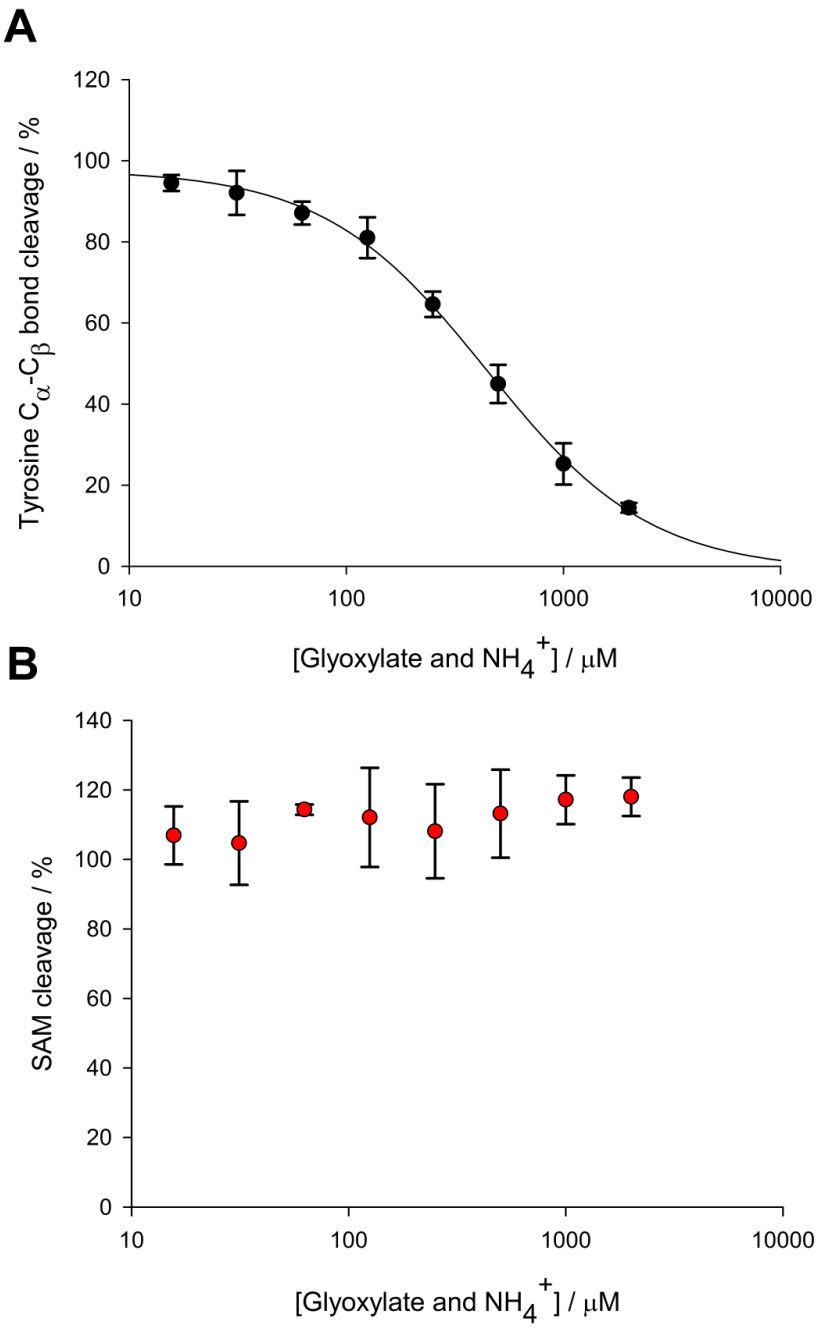

Figure 4.7 Inhibition of tyrosine lyase activity by glyoxylate and ammonium ions. Assays were coupled with MTAN mediated hydrolysis of DOA to preclude the possibility of inhibition by DOA and methionine. A) Tyrosine Cα—Cβ bond cleavage was measured by the formation of *p*-cresol and was fitted to equation 4.3. B) SAM cleavage was measured by the formation of adenine. Assays were incubated for one hour and analyzed by HPLC and values are relative to standard assays with no additions. Data are the average of experiments carried out in duplicate and shown with standard error.

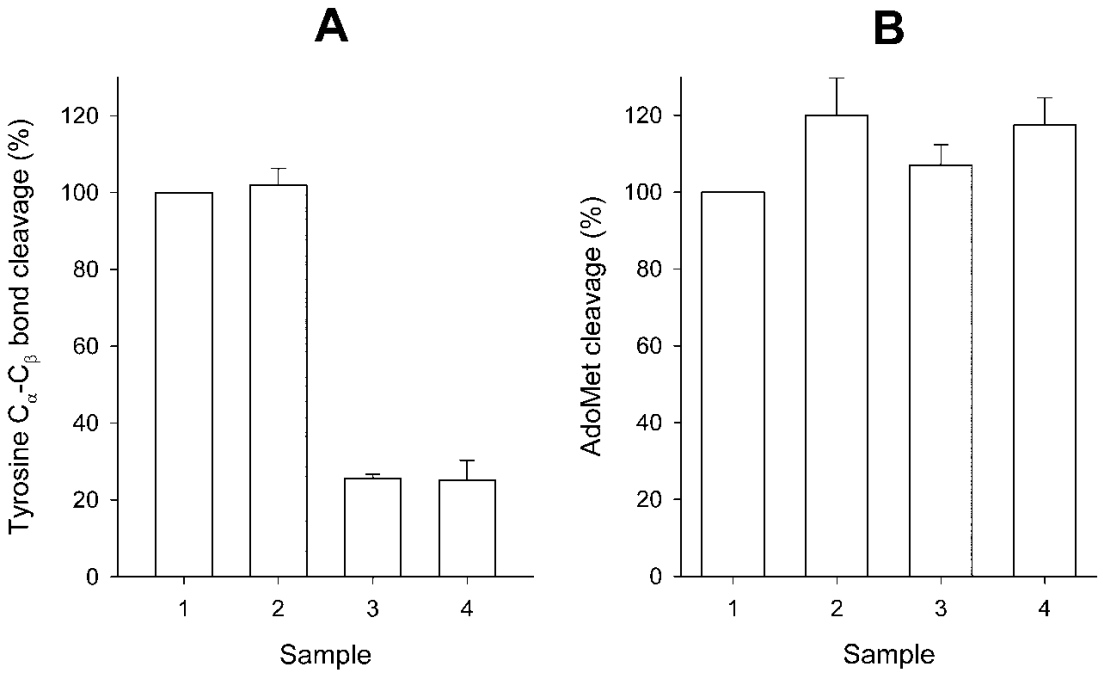

Figure 4.8 Inhibition of tyrosine lyase activity by glyoxylate and ammonium ions. Assays were coupled with MTAN mediated hydrolysis of DOA to preclude the possibility of inhibition by DOA and methionine. A) Tyrosine Cα—Cβ bond cleavage was measured by the formation of *p*-cresol. B) SAM cleavage was measured by the formation of adenine. Assays were incubated for one hour and analyzed by HPLC. Assays were supplemented with the following additions: sample 1, no additions; sample 2, ammonium ions (1 mM); sample 3; glyoxylate (1 mM); sample 4, glyoxylate and ammonium ions (1 mM of each). Data are the average of experiments carried out in duplicate, shown with the standard errors.

4.5 *Activity Assays with Tyrosine Analogues*

To obtain further insight into the mechanism of tyrosine cleavage, the reactivity of structural analogues of tyrosine in ThiGH activity assays was investigated. These studies had two main objectives: to define which functional groups were required for tyrosine cleavage and what factors promoted uncoupled turnover. The analogue assays were incubated at 37 ºC for one hour and analysed by HPLC. This allowed two steps in the mechanism to be monitored: the formation of DOA indicated the extent of the reductive cleavage of SAM and the formation of *p*-cresol or other aromatic products allowed the measurement of the Cα—Cβ bond cleavage step. As the assays were not designed to monitor the kinetics, they were performed on the ThiH / ThiGH mixture, isolated by Ni-affinity chromatography which was not further purified by gel filtration chromatography. An initial investigation of several tyrosine analogues (see Figure 4.9) was undertaken using this strategy. The negative control for these experiments (which contained chemically reconstituted ThiGH, SAM and a reductant, but no tyrosine) was particularly important as very little uncoupled SAM cleavage occurred in the absence of tyrosine. It was found that tyramine (**122**) and L-phenylalanine (**120**) were not substrates and did not show an increase in the cleavage of SAM relative to the negative control. However, it was found that 4-hydroxyphenylpropionic acid (4-HPPA) (**119**) and 4-hydroxyphenyl-α-hydroxypropionic acid (4-HPHPA) (**121**) led to the formation of ~50% of the amount of DOA compared to the positive control (with tyrosine as the substrate). Careful examination of the HPLC trace (Figure 4.10) confirmed that little or no *p*-cresol was formed in assays containing 4-HPPA (less than 5% relative to positive control samples). This result suggests that this analogue was not undergoing Cα—Cβ bond cleavage but can support uncoupled SAM cleavage.

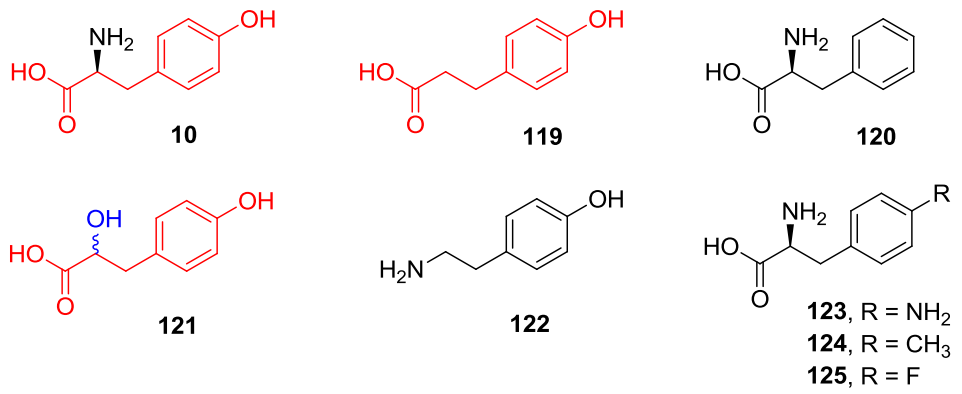

Figure 4.9 Structures of tyrosine analogues. Only analogues that contained a 4-hydroxyphenylpropionic acid motif (shown in red) were able to support any reaction

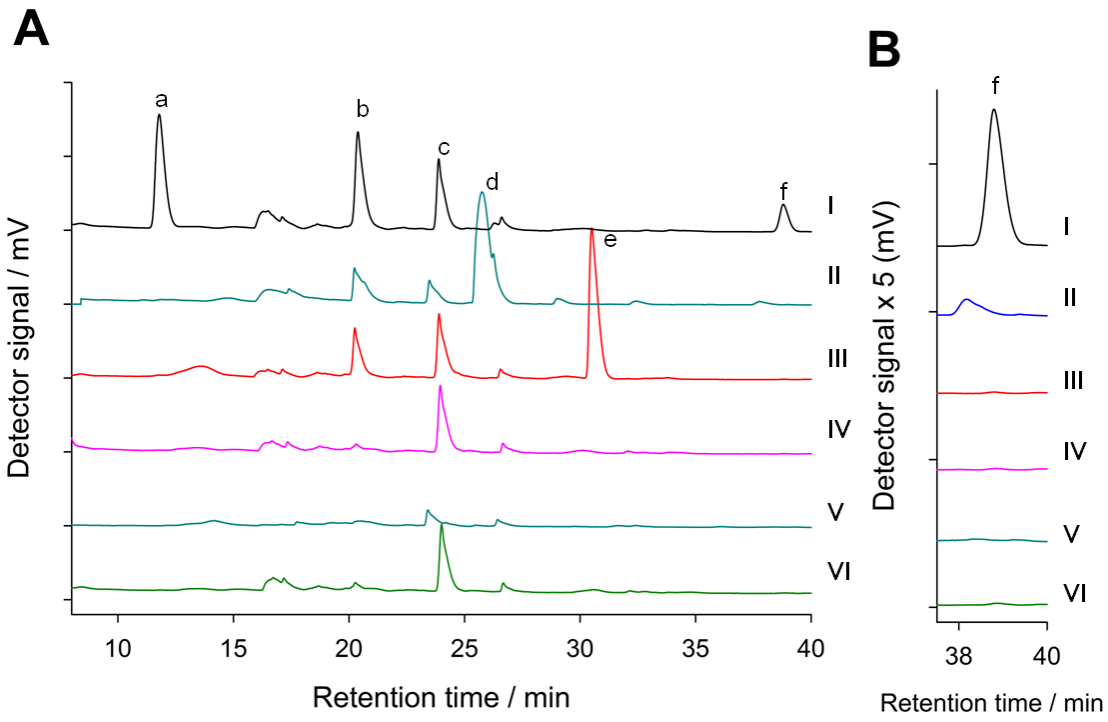

Figure 4.10 A) Analytical HPLC traces of tyrosine lyase activity assays with tyrosine analogues. B) Section of the HPLC chromatogram showing the *p*-cresol elution at ×5 magnification. The detector measures the absorbance at 280 nm. The traces are for assays with (from top to bottom): I) L-tyrosine (**10**), II) 4-HPHPA (**121**), III) 4-HPPA (**119**), IV) tyramine (**122**), V) L-phenylalanine (**120**), VI) no substrate (negative control). Comparison with authentic samples identified the following peaks: a, tyrosine; b, DOA; c, MTA; d, 4-HPHPA; e, 4-HPPA; f, *p*-cresol.

In assays containing 4-HPHPA (**121**), a small amount of *p*-cresol was observed to form relative to positive control assays. The amount of *p*-cresol formed was variable, ranging between 5 – 40% (see Table 4.3) and the average of four experiments implied that 20 ± 8% of Cα—Cβ bond cleavage of 4-HPHPA (**121**) occurred, relative to the amount of Cα—Cβ bond cleavage observed for tyrosine (**10**). This result suggests that this analogue also increases the amount of uncoupled turnover.

Experiment	SAM Cleavage / %	Cα—Cβ Cleavage / %
1	47	12
2	62	41
3	47	4.5
4	66	21
Average	**56 ± 5**	**20 ±8**

Table 4.3 Activity measurements of assays with 4-HPHPA (**121**). SAM cleavage and Cα—Cβ cleavage was measured as the relative amounts of DOA and *p*-cresol formed compared to a positive control assay (with tyrosine (**10**) as the substrate) conducted in parallel. The average value is shown with the standard error.

This strategy of analysing for DOA formation was used to screen further tyrosine analogues (see Table 4.4). Analogues with different functional groups at the phenol position were investigated, specifically 4-amino- (**123**), 4-methyl- (**124**) and 4-fluoro-L-phenylalanine (**125**). None of these tyrosine analogues increased SAM cleavage or yielded detectable aromatic products. Assays with D-tyrosine showed relatively slow uncoupled SAM cleavage, but no *p*-cresol formation was observed. Further experiments in which reaction products or potential substrate mimics were

added to activity assays are shown in Table 4.5. They show that combinations of reaction products do not increase uncoupled SAM cleavage unless L-tyrosine is present in the mixture.

Compound	SAM cleavage (%)
L-Tyrosine (**10**)	100
4-Hydroxyphenylpropionic acid (**119**)	50.9 ± 3.0
4-Hydroxyphenyl-α-hydroxypropionic acid (**121**)	55.5 ± 5.0
D-Tyrosine	14.3
4-Hydroxyphenylcinnamic acid	7.2 ± 2.2
Tyramine (**122**)	5.9 ± 3.0
L-Phenylalanine (**120**)	5.4 ± 1.3
4-Amino-L-phenylalanine (**123**)	4.8 ± 0.6
4-Methyl-L-phenylalanine (**124**)	3.0
4-Fluoro-L-phenylalanine (**125**)	2.6
No Substrate (negative control)	6.6 ± 1.7

Table 4.4 Amount of turnover from substrate analogues. SAM cleavage was assessed by monitoring the amount of DOA produced. Values are given as a percentage with respect to the amount of activity observed in a standard assay (including tyrosine as the substrate) that was measured in parallel. Standard errors are given where the results have been replicated.

Compound(s)	SAM cleavage (%)	C_α—C_β bond cleavage (%)
L-Tyrosine	100	100
NH_4^+ + glyoxylate + L-tyrosine	117 ± 7.0	25.2 ± 5.1
Glycine + *p*-cresol	8.4	N/A
p-Cresol	7.8	N/A
NH_4^+ + glyoxylate + *p*-cresol	6.9	N/A
Glycine	6.8	N/A
NH_4^+ + glyoxylate	4.8	N/A

Table 4.5 Amount of turnover measured from combinations of in vitro products or potential substrate mimics. SAM cleavage was assessed by monitoring the amount of DOA generated and Cα—Cβ bond cleavage was assessed by monitoring the amount of *p*-cresol formed. Values are given as a percentage with respect to the amount of activity observed in a standard assay (including tyrosine as the substrate) that was measured in parallel. Standard errors are given where the results have been replicated.

4.6 *Discussion of the Mechanism of Tyrosine Lyase*

All of the tyrosine structural analogues that replaced the phenol functional group were inactive and it appears that ThiH is very sensitive to modifications at this position. Fluorine has 97% of the van der Waals radius of oxygen, but 4-fluoro-L-phenylalanine (**125**) was not sufficiently similar to L-tyrosine to increase SAM cleavage above the background level. Although the ArO—H bond is weak in phenols such as tyrosine, a comparison of the bond dissociation energy (BDE) of phenol (ArO—H, 360 $kJmol^{-1}$), aniline (ArNH—H, 388 $kJmol^{-1}$) and toluene ($ArCH_2$—H, 355 $kJmol^{-1}$) (see Table 1.1, p3)[3] indicate that 4-amino- (**123**) and 4-methyl-L-phenylalanine (**124**) ought to be susceptible to hydrogen atom abstraction by the 5'deoxyadenosyl radical. As neither of these analogues resulted in SAM cleavage, the subtle substrate selectivity of tyrosine lyase cannot be based purely on the bond strength. The substrates that permitted SAM cleavage, L- and D-tyrosine, 4-HPPA (**119**) and 4-HPHPA (**121**) (Figure 4.10 and Table 4.4) share a common structural motif of being 4-hydroxyphenylpropionic acids and the phenol appears to be required for SAM cleavage.

The problem of uncoupled SAM cleavage in radical SAM proteins is well documented[26]. The reactivity of the primary 5'-deoxyadenosyl radical makes its uncontrolled formation potentially hazardous for the cell. There are several mechanisms by which this family of enzymes regulate uncoupled SAM cleavage, including modifying the redox potential of the 4Fe-4S cluster in response to substrate binding[74, 75] or by cooperative substrate binding[51]. The nature of the reductant has been proposed to have a role in the degree of uncoupled SAM cleavage with less uncoupling being observed when using the natural electron donor systems. The ThiH activity assay uses the NADPH, flavodoxin and flavodoxin reductase system, which is assumed to be the natural intracellular reductant for *E. coli* ThiGH and therefore, limits uncoupled turnover. The fact that when ThiGH is incubated with SAM and the reducing system, but no substrate (negative control in the substrate analogue experiments) results in very little DOA formation

implies that formation of the 5'-deoxyadenolsyl radical is controlled by the presence of a substrate. This also suggests that only a very small proportion of uncoupled turnover occurs as a result of the 5'deoxyadenosyl radical becoming quenched by reacting with a compound other than the intended substrate.

The strong preference shown by tyrosine lyase for a phenolic substrate does not rule out the potential for Cα—Cβ bond cleavage to be initiated by abstraction of a hydrogen atom other than from the phenol functional group; for example formation of the ammonium radical-cation intermediate by hydrogen atom abstraction from the amino functional group (see Scheme 2.1 C, p65). However, the fact that no reaction was observed when ThiH was incubated with tyramine (**122**), phenylalanine (**120**) or any of the 4-substituted phenylalanine analogues (**123**, **124** and **125**) makes it difficult to find a precedent for this mechanism from the data currently available. Unequivocal assignment of the site of hydrogen atom abstraction from tyrosine requires structural determination of tyrosine and SAM bound to the active site of ThiH. The results presented here strongly indicate that hydrogen atom abstraction occurs at the phenolic position and this is what will be discussed hereafter.

The selectivity of ThiH for phenolic substrates highlights the importance of a phenolic O—H bond in the active site as a prerequisite for SAM cleavage. However it does not provide evidence for concerted SAM cleavage and phenolic hydrogen atom abstraction. The formation of a tyrosine radical is thermodynamically favourable as a result of the reactivity of the primary deoxyadenosyl radical, the strength of the C—H bond formed in 5'-deoxyadenosine and relative weakness of the phenolic O—H bond (see Table 1.1, p3). The strong dependence of DOA formation upon a phenolic substrate suggests that reductive cleavage of SAM (detectable as the formation of DOA) is coupled to the generation of a phenolic tyrosine radical. However, the fact that the aniline analogue (**123**) was not a substrate may suggest an interaction of the lone pairs

on the phenol with juxtaposed protein residues may help to facilitate hydrogen atom abstraction by orientating the phenolic O—H bond to ensure appropriate overlap of the O—H σ* orbital with the radical on the 5' carbon of DOA.

The observed product inhibition, uncoupled turnover and studies with tyrosine analogues can be integrated into an improved mechanistic model, shown in Scheme 4.2. The model proposes two possible fates for the phenolic radical (**126**): either turnover leading to product formation; or completion of a futile cycle leading back to tyrosine. Turnover leading to product formation is facilitated by the electron deficient nature of the phenolic radical, which can undergo Cα—Cβ bond cleavage with the assistance of the lone pair of electrons on the α-amine of tyrosine. Such a mechanism provides a direct route to dehydroglycine (**11**) and the resonance stabilized radical anion **102a↔102b** that requires reduction and protonation to form the observed product, *p*-cresol (**88**). A reduction step in addition to reductive cleavage of SAM is unusual for a radical SAM protein[10]. The immediate source of the additional reducing equivalent is unknown, but the [4Fe-4S] cluster that is used to accelerate the reductive cleavage of SAM is a possible candidate.

To achieve uncoupled turnover, the phenolic tyrosine radical (**126**) is proposed to undergo immediate reduction to the phenoxide (**127**) followed by protonation, giving a direct route back to tyrosine. In this model, the difference between the uncoupled and product forming pathways depends on the timing of the reduction of either phenolic radical (**126**) or (**102**) relative to the Cα—Cβ bond cleavage step. It may be that that the observed uncoupled turnover is accelerated in the *in vitro* assay by the presence of a large excess of reducing equivalents.

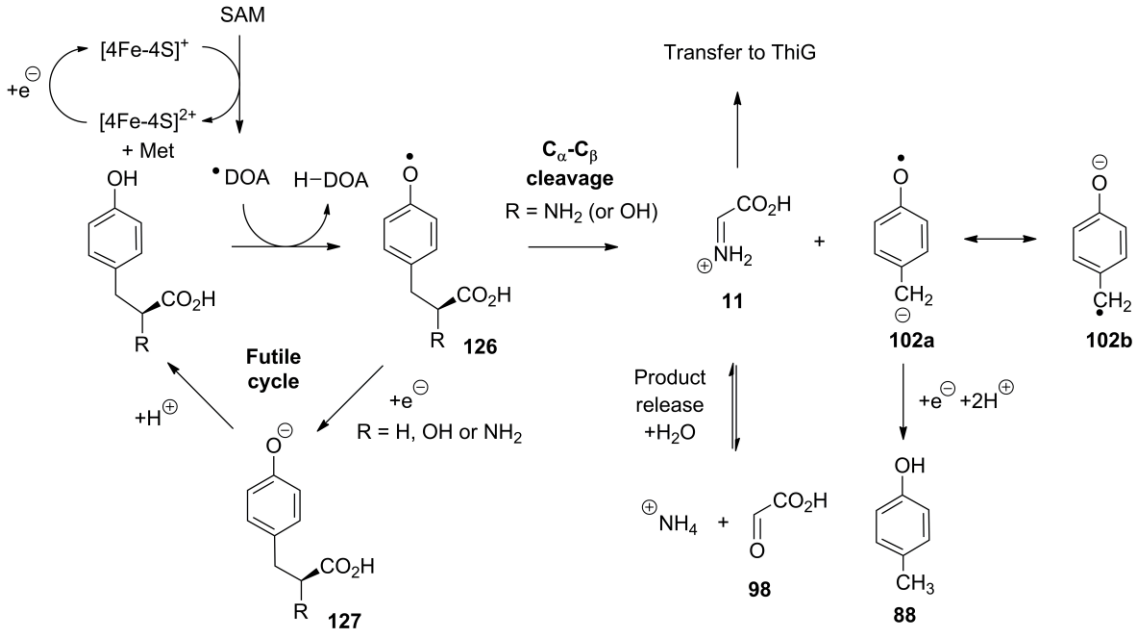

Scheme 4.2 Proposed mechanism of tyrosine lyase including uncoupled turnover by completion of a futile cycle. The reductive cleavage of SAM yields the 5'-deoxyadenosyl radical which can abstract a hydrogen atom from the phenolic O—H bond. The resultant phenolic radical (**126**) can follow two possible reaction pathways and the nature of the group R can effect which of these two pathways is favoured. Immediate reduction, followed by protonation completes an unproductive futile cycle back to the substrate. For L-tyrosine ($R=NH_2$) (**10**), cleavage of the Cα—Cβ bond yields dehydroglycine (**11**) and the resonance stabilized radical anion **102a↔102b** which requires the addition of two protons and an electron to give *p*-cresol (**88**).

In a scenario where the Cα—Cβ is dramatically slowed down, such as in the case of the analogues 4-HPPA (**119**) which lacks the α-nitrogen lone pair, then reduction of the tyrosine radical becomes kinetically more favourable. This reduction step, leading to a futile cycle, quenches any potentially reactive radical species and has the net result of generating methionine and DOA from reductive cleavage of SAM with no overall change to the tyrosine substrate. Hence this futile cycle is a source of uncoupled SAM cleavage in ThiH. In the case of D-tyrosine and the analogue 4-HPHPA (**121**), little or no Cα—Cβ bond cleavage was observed

despite the presence of a α-lone pair and these substrates appear to be restricted mainly to futile cycling. Again, a precise stereoelectronic explanation for the observed substrate selectivity will require a structural model of the ThiH active site. However, it can be implied from these observations that the orientation of the α-lone pair may be crucial to driving Cα—Cβ bond cleavage.

The effects of a phenolic radical on tyrosine have been investigated using computational methods. It was found that there was a small conformationally driven structural change in line with potential cleavage. The Cα—Cβ bond becomes longer when the lone pair on the nitrogen was aligned antiperiplanar to the electron deficient π cloud of the phenolic radical (see Figure 4.11 B). Also, when the nitrogen- Cα—Cβ bond-phenol was fixed in an antiperiplanar orientation the singly occupied molecular orbital (SOMO) is shown to have some spin density on the nitrogen (see Figure 4.11 A). Therefore this orientation of tyrosine provides good orbital overlap to allow delocalisation of the spin. One interpretation of this data is that if the tyrosine was held in a fixed orientation by the enzyme active site, then this may provide substantial catalysis for Cα—Cβ bond cleavage. This could include fixing the Cα—Cβ bond σ* orbital in a position that would allow for donation of electrons from the nitrogen lone pair, the result of which would be the resonance stabilised radical anion (**102**) (see Scheme 4.2 and Figure 4.12). Appropriately positioned residues could also help to improve the stability of this radical anion. Computational attempts to break the Cα—Cβ bond of the phenolic tyrosine radical in the gas phase were unsuccessful. Therefore, it is suggested that a substantial enzyme component is required to drive this cleavage (Dr. A. Croft (University of Bangor), personal communication).

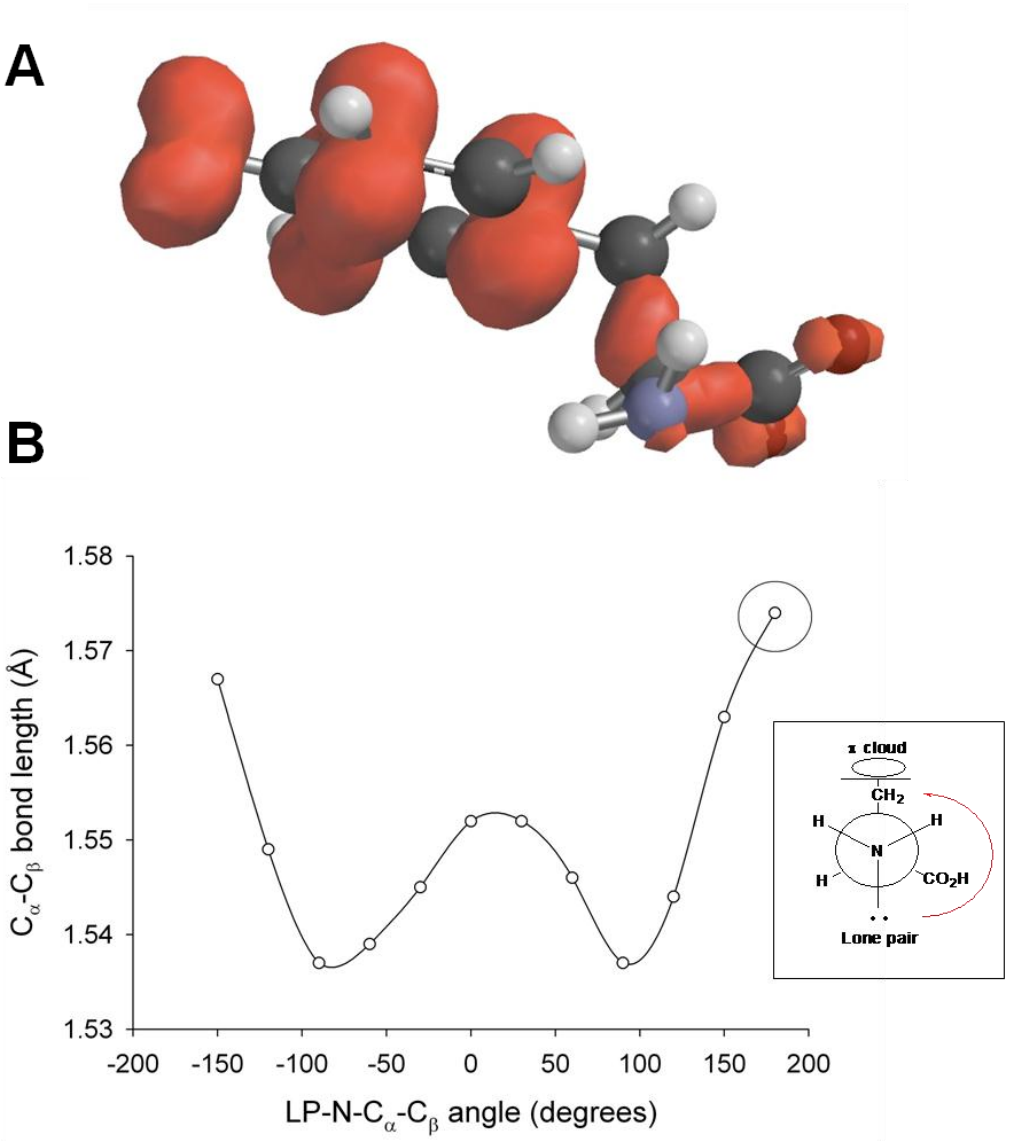

Figure 4.11 A) Spin density of the SOMO of the tyrosine radical in the gas phase when the nitrogen lone pair is aligned antiperiplanar to the pi-cloud. (Image was constructed by Dr. A. Croft (University of Bangor) and shared in a personal communication). B) The effect of rotating the Cα—N bond (see inset) on the length of the Cα—Cβ bond length.

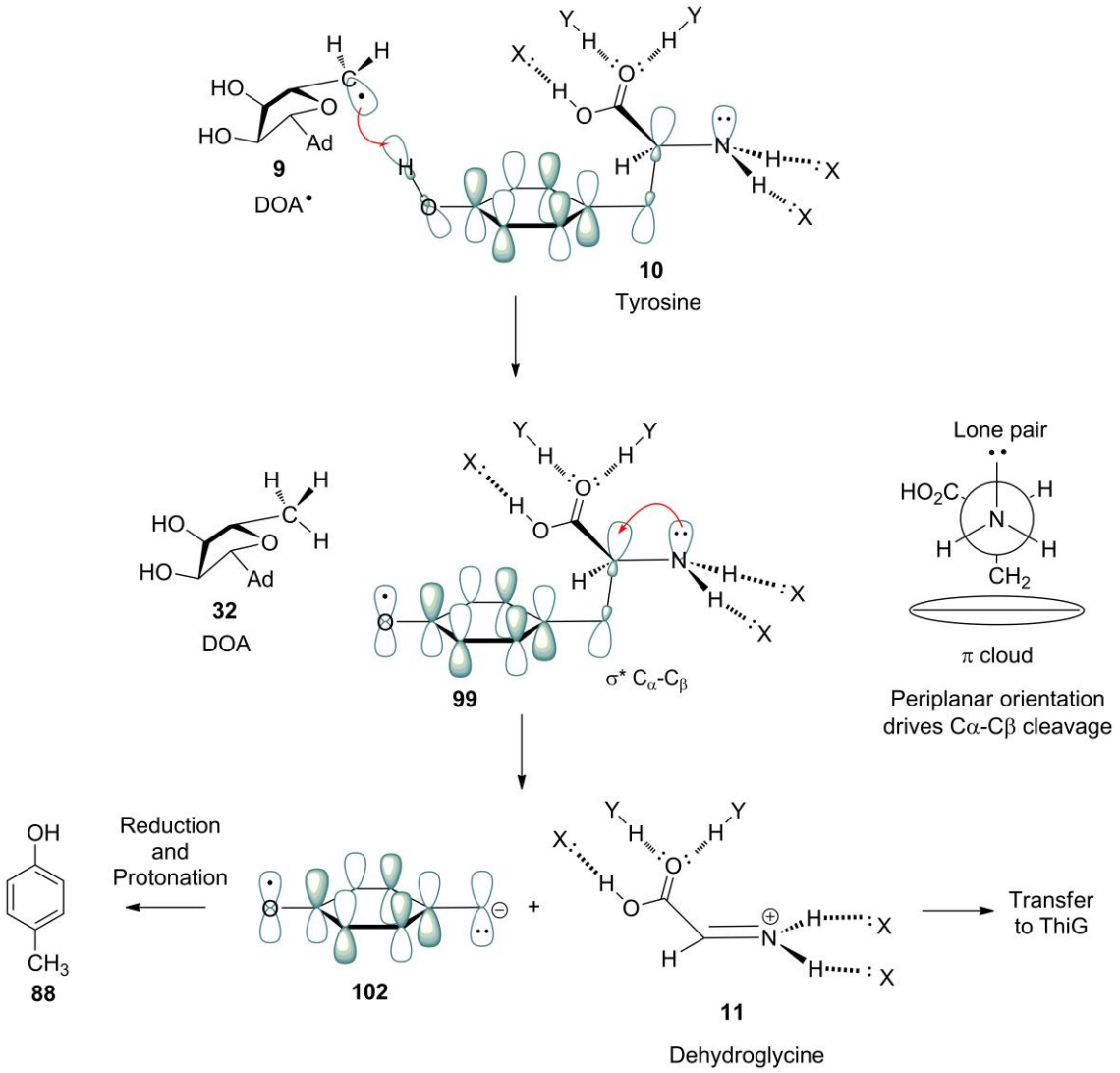

Figure 4.12 Proposed mechanism for tyrosine Cα—Cβ bond cleavage. The cleavage is proposed to be driven by the enzyme fixing the orientation of tyrosine, possibly by hydrogen bonds to the amino acid moiety.

The hydrolytic instability of electrophilic dehydroglycine (**11**) implies that a tight interaction with ThiGH would be advantageous, helping to sequester the sensitive imine away from the aqueous medium. This concept was introduced in Chapter 3 and used to explain the observed burst phase kinetics. The observed product inhibition by a combination of glyoxylate and ammonium ions (which are in rapid equilibrium with a low concentration of dehydroglycine) may reflect such a tight binding constant. A more surprising observation was the almost

complete (>90%) uncoupling of SAM turnover from the tyrosine cleavage reaction in the presence of relatively high concentrations of glyoxylate and ammonium ions (2 mM of each). This apparently wasteful process is unlikely to occur in a cellular context and the effect was maximized under specific *in vitro* conditions with the addition of MTAN plus high concentrations of glyoxylate and ammonium. However, the experiment does indicate that in cells where ThiGH is not actively synthesizing the thiazole carboxylate, one of the functions of product inhibition by DOA may be to reduce the uncoupled turnover of SAM. The release of dehydroglycine observed *in vitro* is unlikely to occur during cellular thiamine biosynthesis, when transfer of the dehydroglycine probably occurs directly between ThiH and ThiG.

As was alluded to earlier, turnover of ThiH is a metabolically costly process and in addition to the consumption of tyrosine, also uses up an equivalent of NADPH and an equivalent of SAM, which is biosynthesised from ATP and methionine. The generation of dehydroglycine needs to be synchronised with the generation of its cyclisation partner on ThiG (**82**) (see Figure 4.13). The formation of this nucleophilic thiol intermediate (**82**) is by no means trivial and involves the interaction of at least two proteins. The transfer of dehydroglycine from ThiH to ThiG may explain the functional reason behind ThiGH complex formation. Additionally the regulation and transfer of dehydroglycine is crucial to avoid wasted turnover of ThiH. Where the tight binding of dehydroglycine to ThiGH will help in its transfer, the product inhibition by DOA and methionine may help to minimise uncoupled SAM cleavage. Although evidence has been found in these studies for product inhibition of tyrosine lyase by both DOA and dehydroglycine, the complexity of the reaction catalysed by ThiGH does not allow the description of a definitive kinetic model for product release or transfer at this stage.

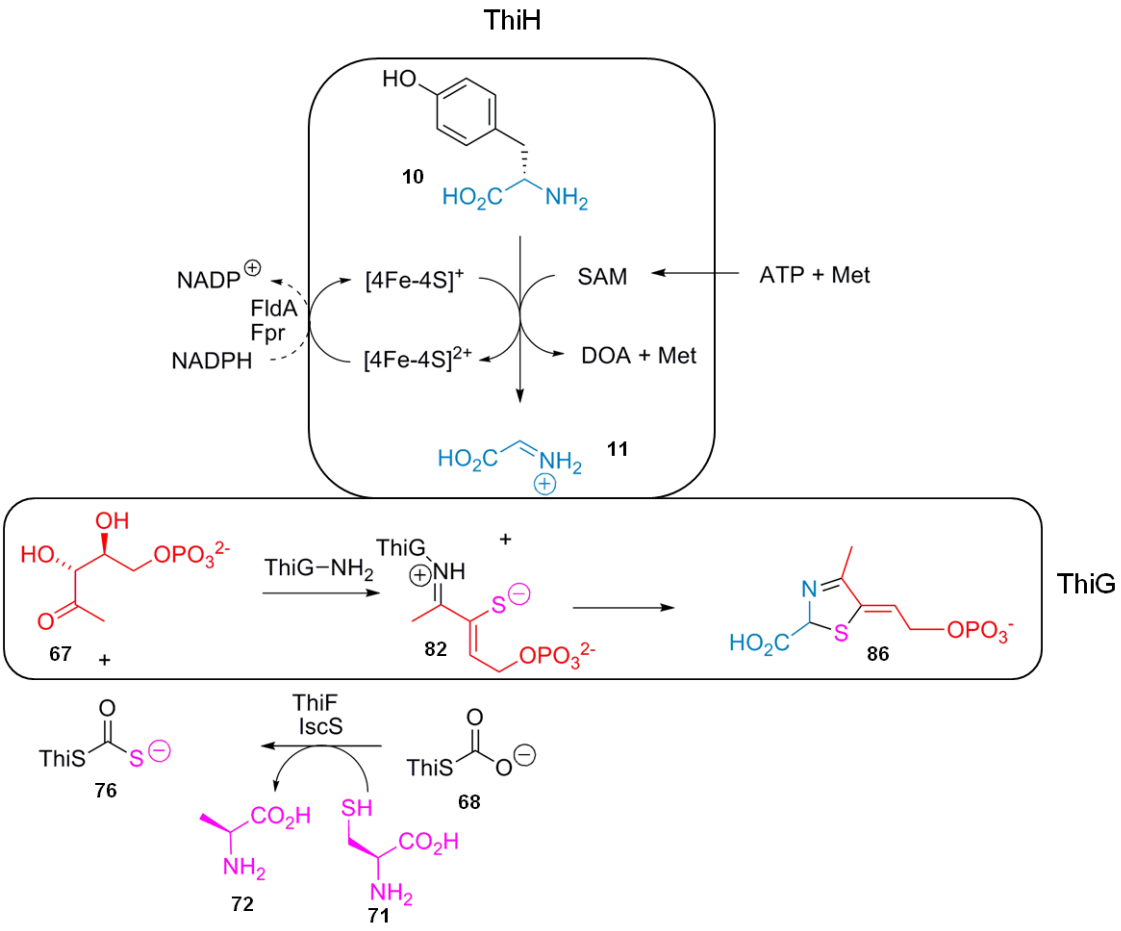

Figure 4.13 Scheme depicting the need for synchronisation of the activity of ThiH and ThiG. A turnover of ThiH results in consumption of one equivalent of tyrosine, ATP and NADPH.

In the context of the substrate analogue experiments however, the observation of almost complete uncoupled turnover at high glyoxylate and ammonium concentrations may help to further elucidate the Cα—Cβ bond cleavage mechanism. It has already been inferred that the observation of SAM cleavage (by monitoring the formation of adenine in this experiment) is coupled to generation of a phenolic tyrosine radical. It may be the case that the binding interaction between tyrosine and ThiH which orientates the substrate and drive Cα—Cβ bond cleavage may also function to bind dehydroglycine and help to sequester it away from the aqueous media and aid its transfer to ThiG. If glyoxylate or dehydroglycine were interacting with some of the ThiH residues that drive the cleavage reaction then this may explain the

observed uncoupled turnover at high glyoxylate and ammonium concentrations. This analysis is further supported by the observation that uncoupled turnover is found to be more prevalent during steady state, when it is proposed that release of dehydroglycine from the active site is rate limiting. Additionally, the amount of SAM cleavage observed in assays containing glyoxylate and ammonium ions was observed to be slightly greater than in assays that didn't contain any of these inhibitors (~110% relative to positive controls). This again may suggest that, even at low concentrations, dehydroglycine or glyoxylate is interacting with ThiGH in a manner that increases uncoupled turnover.

4.7 *Summary and Conclusions*

The rate of ThiH mediated tyrosine cleavage is strictly controlled by the accumulation of the products. The function of this product inhibition in cells actively synthesising thiamine may be to coordinate the rate of formation of dehydroglycine by ThiH with its' utilization by ThiG for thiazole formation. Structural analogues of tyrosine have been used to define the substrate requirements of the enzyme and in particular the need for a phenolic O—H bond. Furthermore, phenolic tyrosine analogues which lacked a correctly positioned amine functional group were able to undergo a partial reaction leading to uncoupled SAM cleavage, but the rate of Cα—Cβ bond cleavage was dramatically reduced in the absence of a correctly positioned amine functional group. A precise mechanistic interpretation of these observations will require structural information on the ThiH active site, but an improved mechanistic model was constructed from the data on product inhibition and substrate analogues. This model was particularly useful for explaining uncoupled turnover of ThiH, which is postulated to proceed through a futile cycle of the tyrosine radical.

5 Deuterium Labelling and a Kinetic Isotope Effect on Tyrosine Lyase Activity

5.1 *Introduction*

Deuterium labelling of substrates is a common technique in elucidating enzyme mechanisms[151]. It is a convenient way of monitoring hydrogen transfer steps, either by detection of deuterated products, or in some cases a kinetic isotope effect can be observed, which provides information on the kinetics and can reveal the rate limiting step of catalysis. The mechanistic proposal discussed in Chapters 2 and 4 suggests (Scheme 2.1, p65, Scheme 4.2, p127 and Figure 4.12, p130) that the exchangeable, phenolic hydrogen atom is abstracted from tyrosine. Abstraction of an exchangeable hydrogen atom is unusual for a radical SAM enzyme and in the majority of examples studied to date the substrate radical is generated by cleavage of a non-exchangeable C—H bond[10, 27]. In order to clarify the site of hydrogen atom abstraction from tyrosine by the 5'-deoxyadenosyl radical, the substrate was labelled with deuterium atoms. As a negative control, tyrosine that was uniformly deuterated at all the non-exchangeable positions was incubated with ThiGH. To obtain tyrosine that was deuterated at all the exchangeable positions, it was necessary to prepare ThiGH assays in D_2O.

DOA can be detected by LCMS (with positive ion electrospray detection), using the liquid chromatography conditions that were routinely used for activity assays. Abstraction of a deuterium atom would result in the formation of 5'-deutero-DOA (D-DOA) with an increased mass of one unit with respect to proteo-DOA (H-DOA), which forms normally (see Scheme 5.1). The initial objective was to monitor the formation of D-DOA to clarify the site of hydrogen atom abstraction. However, an apparent kinetic isotope effect was observed which provoked some more detailed, kinetic experiments.

5.2 *Initial Deuterium Labelling Studies*

N.B. The ThiH activity measurements reported in this section were conducted on the ThiH / ThiGH mixture isolated by Ni-affinity chromatography which was not further purified by gel filtration chromatography.

Initial experiments were designed simply to monitor any formation of D-DOA by LCMS from ThiGH activity assays incubated with tyrosine deuterated at the non-exchangeable positions (**128**), or from an assay incubated in 50% D_2O, in which 50% of the tyrosine will be deuterated at the exchangeable positions (**129**) (see scheme 5.1). Compound **128** did not cause any D-DOA to form (data not shown). However the mass spectra of the DOA peak from the LCMS chromatogram from a series of assays prepared in either 100% H_2O, or 50% D_2O (as described in Method 32) is shown in Figure 5.1. From the assay incubated in 50% D_2O, there is a clear increase in the relative abundance of the m/z = 253 mass ion. In the positive control assay (incubated in 100% H_2O), this ion is due to the natural abundance of ^{13}C in the DOA. It can be assumed that the increase in relative abundance of this mass ion is due to the presence of D-DOA in this sample.

It would be expected, however, that as the assays were prepared in 50% D_2O and if no other factors perturb the reaction, the relative abundance of D-DOA and H-DOA should be equal. The results shown in Figure 5.1 shows that this is not the case. One possible interpretation of these observations is that relatively less D-DOA was being formed, consistent with a kinetic isotope effect on the hydrogen atom abstraction. This is supported by the smaller amounts of products forming in assays incubated in 50% D_2O relative to 100% H_2O (see Table 5.1), implying a slower rate of reaction.

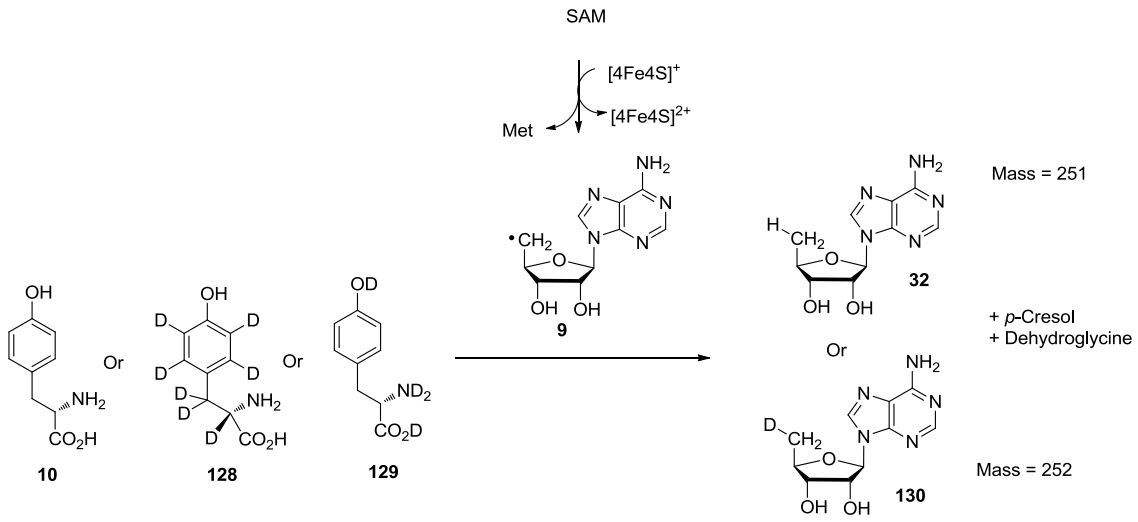

Scheme 5.1 Deuterium labelling of tyrosine resulting in the formation of D-DOA.

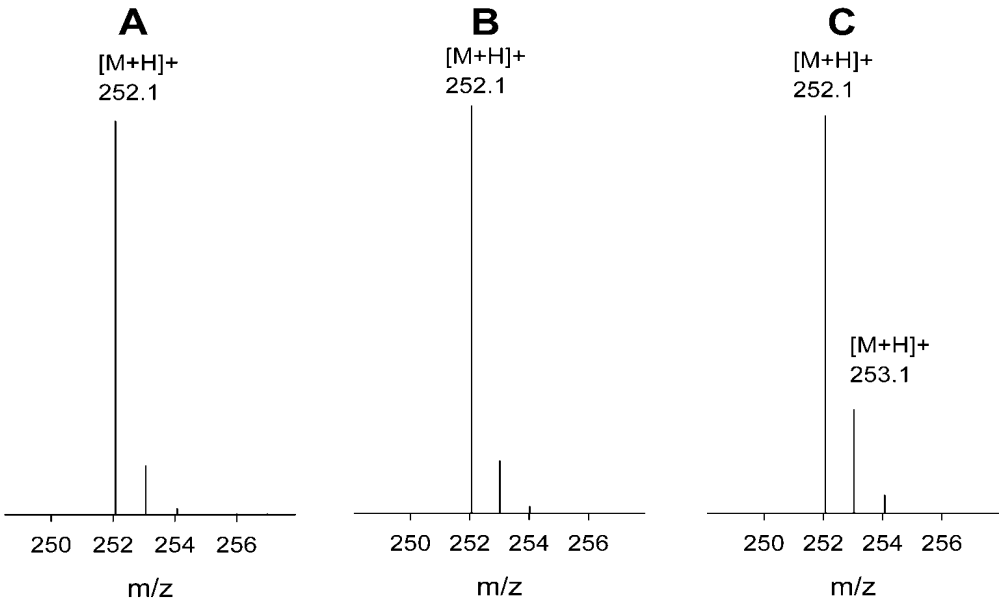

Figure 5.1 Mass spectra of DOA obtained from A) a synthetic standard of DOA; B) a positive control ThiGH activity assay incubated in 100% H_2O; C) a ThiGH activity assay incubated in 50% D_2O / H_2O.

Conditions	1h in H_2O	1h in 50% D_2O	2h in 50% D_2O
DOA formed / μM	126	83 (66%)	103
p-Cresol formed / μM	87	52 (60%)	56

Table 5.1 Amount of product formed in ThiGH assays monitored by HPLC. The numbers in brackets is the relative amount of product relative to the positive control.

5.3 *Measurement of a Kinetic Isotope Effect in 50% D_2O*

N.B. The ThiH activity measurements reported in this section were conducted on the ThiGH complex which had been purified by gel filtration chromatography (Method 13).

5.3.1 *Initial Data Collection*

To follow up on the observations shown in Table 5.1 a time course experiment of tyrosine lyase activity in 50% D_2O was carried out. In order to draw direct comparisons, a positive control time course in 100% H_2O was performed in parallel (see Method 32). As discussed later in this chapter, experiments with very high percentages of D_2O (approaching 100%) were unsuccessful. Unfortunately, derivation of an estimate for the kinetic isotope effect from substrates that are not isotopically pure is slightly more complicated as a direct measurement of the rate of reaction from pure deuterated (V_D) substrate is not obtainable.

The data obtained from time course experiments is shown on Figure 5.2 and was fitted to equation 3.1 (as described in Section 3.6). The experiment in 50% D_2O / H_2O caused an observable change on the initial rate and the burst phase amplitude. In 50% D_2O / H_2O the majority of products formed in the assays are as a result of the rate of turnover in H_2O (the 50% of the assay that is abstracting a hydrogen atom from tyrosine and thus turning over at the normal rate). Information about the small amount of product formed as a result of deuterium atom abstraction (V_D) requires a subtraction of the observed rate (V_{obs}) in 50% D_2O. The level of complexity is compounded by the fact that ThiGH displays burst-phase kinetics. Therefore, the rate of the tyrosine cleavage reaction is reflected in the burst phase rate only. It is apparent from these experiments that the presence of D_2O may also be affecting the rate at steady state, but further experiments are required to clarify this observation.

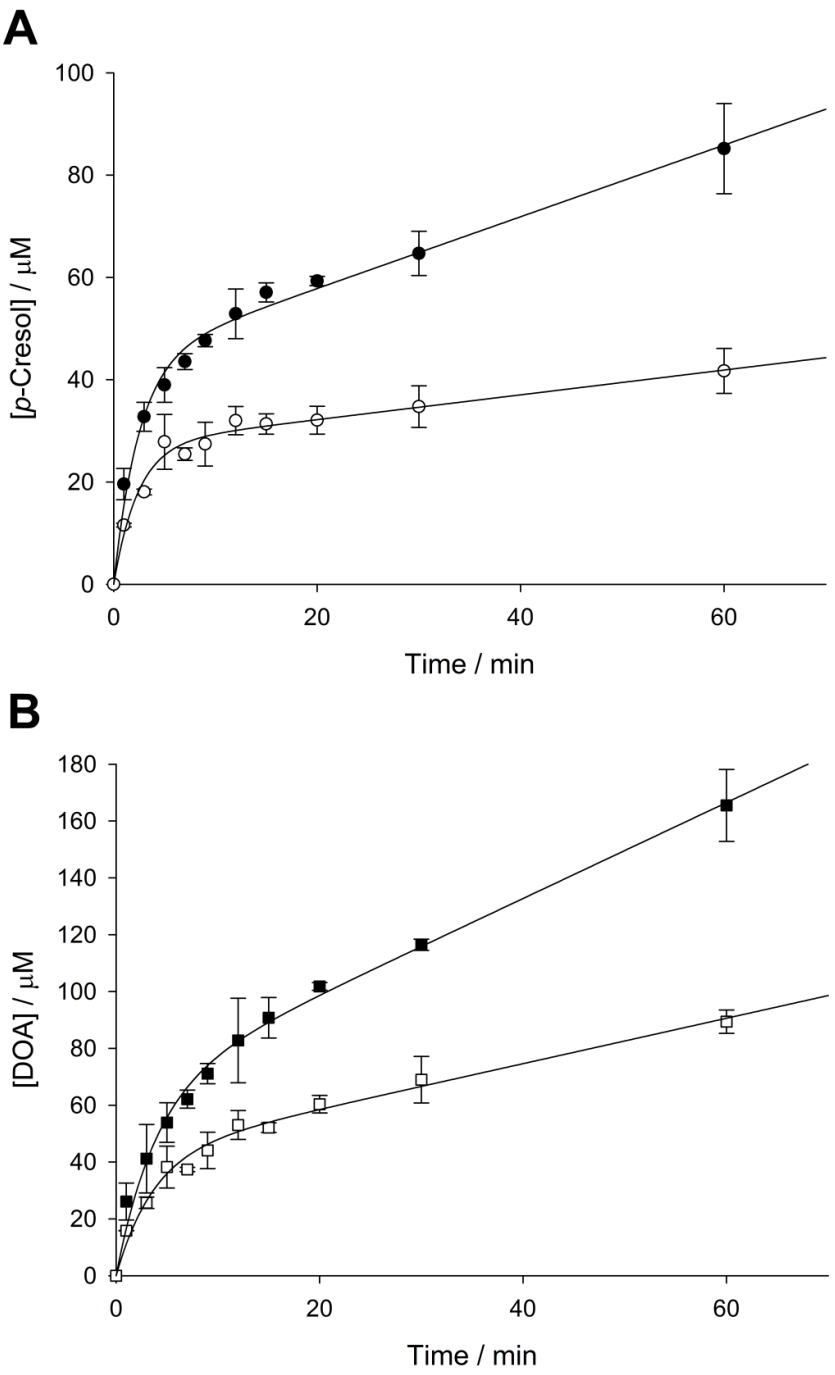

Figure 5.2 Time course data comparing the observed rates of product formation in 100% H_2O and 50% D_2O / H_2O A) *p*-cresol formation in 100% H_2O (●) and 50% D_2O / H_2O (○); B) DOA formation in 100% H_2O (■) and 50% D_2O / H_2O (□). Data is the average of a duplicate data set shown with standard errors.

5.3.2 *Data Analysis*

A deuterium kinetic isotope effect is the ratio of the rates of reaction with proteo substrate against the rate of reaction with deutero substrate (equation 5.1).

$$\text{KIE} = \frac{V_H}{V_D} \qquad \text{(Eq. 5.1)}$$

Therefore, in order to estimate the KIE an estimate of V_H and V_D is required. The data from both time courses (in 100% H_2O and 50% D_2O / H_2O) was fitted to equation 3.1, as for previous time course experiments discussed in chapters 3 and 4. Fitting of the data to equation 3.1 gave values of [E], k_{burst} and L with their associated errors (see Table 5.2).

$$[\text{P}] = [\text{E}](1 - e^{(1-k_{\text{burst}}t)}) + Lt \qquad \text{(Eq. 3.1)}$$

In order to calculate the initial rate of reaction (V_{obs}), equation 3.1 was differentiated, giving equation 5.1. The initial rate of reaction in 100% H_2O (V_H) and in 50% D_2O / H_2O, was derived by substituting t = 0 into equation 5.1, (note that at $t = 0$, $e^{k_{\text{burst}}.t} = 1$).

$$V_{obs} = \frac{d[\text{P}]}{dt} = [\text{E}].k_{\text{burst}}.e^{-k_{\text{burst}}.t} + L \qquad \text{(Eq. 5.2)}$$

Product	Conditions	[E] / µM	k_{burst} / min^{-1}	L / µMmin^{-1}	$V_{t=0}$ / µMmin^{-1}	R^2
p-Cresol	100% H_2O	43.8 ± 1.8	0.40 ± 0.05	0.70 ± 0.06	18.2 ± 2.3	0.99
	50% D_2O	27.3 ± 1.3	0.42 ± 0.07	0.24 ± 0.04	11.7 ± 2.0	0.98
DOA	100% H_2O	65.2 ± 4.1	0.26 ± 0.04	1.7 ± 0.1	17.9 ± 2.7	0.99
	50% D_2O	42.6 ± 2.9	0.28 ± 0.05	0.80 ± 0.08	12.7 ± 2.3	0.99

Table 5.2 Values of [E], k_{burst} and L derived from fitting data to equation 3.1 and shown with their standard error. $V_{t=0}$ was calculated by substituting these values into equation 5.3. Details of the estimate of the error associated with $V_{t=0}$, are described at the end of this chapter.

For substrates that are not isotopically pure it is necessary to correct the observed rate (V_{obs}) to calculate the rate of reaction for pure deutero substrate (V_D). This is achieved by equation 5.3, which can be rearranged to equation 5.4 in order to directly calculate V_D from V_{obs}, measured form a reaction with an isotopically impure substrate and V_H.

$$V_{obs} = V_H X + V_D(1 - X) \quad \text{(Eq. 5.3)}$$

$$V_D = \frac{V_{obs} - V_H X}{(1 - X)} \quad \text{(Eq. 5.4)}$$

X is the fraction of isotopic impurity to the total substrate concentration and described by equation 5.5. For experiments in 50% D_2O, X = 0.5

$$X = \frac{[S_H]}{[S_H]+[S_D]} \qquad \text{(Eq 5.5)}$$

Calculated values of V_H, V_D and the KIE with respect to *p*-cresol formation and DOA formation are shown in Table 5.3. There was an observable KIE on the rate of formation of both these products. The experimental errors associated with both observe KIE's is very large (for derivation of the errors see Section 5.6). These large errors are due to the fact that several calculations are required to derive the KIE's from the data collected. This is despite the relatively good fit ($R^2 = 0.99$) of equation 3.1 to the data.

Product	V_H **/ µMmin^{-1}**	V_D **/ µMmin^{-1}**	V_H **/** V_D
p-Cresol	18.2 ± 2.3	5.2 ± 4.6	**3.5 ± 3.1**
DOA	17.9 ± 2.7	7.5 ± 5.3	**2.4 ± 1.7**

Table 5.3 Estimate of the deuterium KIE derived from the estimated rates of reaction, at t = 0, with proteo tyrosine and deutero tyrosine derived from the formation of two products, *p*-cresol and DOA. The derivation of the errors associated with these values of V_D and V_H / V_D are described at the end of the chapter.

5.3.3 *Potential Improvements to the Experiment*

The most obvious adjustment to the experimental design that would increase the accuracy of the observed KIE would be to obtain a direct measurement of V_D. In the case of ThiH, this requires incubating ThiGH, along with substrates and reductants, in a buffer containing 100% D_2O. The practical considerations of preparing multiple ThiGH assays, suitable for a time course experiment, in 100% D_2O are very serious. The ThiGH activity assay requires strictly anaerobic conditions and contains four proteins (ThiGH, FldA and Fpr) and three organic compounds (SAM tyrosine and NADPH). Additionally, as was shown in Chapter 3, the stability of ThiGH is dependent on the presence of sodium chloride and glycerol in the buffer. Several attempts were made to optimise the assay to permit the use of 100% D_2O, without success. Initially, each compound required for the assay (tyrosine, SAM and NADPH) was dissolved in D_2O buffer. The proteins (ThiGH, FldA and Fpr) were exchanged into D_2O buffer using NAP-10 columns. In order to maximise the degree of buffer exchange, this step was repeated three times. However, during this time the co-factors (4Fe-4S cluster, FMN or FAD) became dissociated from the protein. Attempts were made to overcome this by adding fresh aliquots of FMN and FAD (prepared in D_2O) to FldA or Fpr. However this gave very little observed activity, even in positive control assays in 100% H_2O. (NB. Positive control experiments involve identical protein manipulations. For example, the number of buffer exchange steps are the same, but carried out in H_2O buffer).

The lack of success of the trial experiments to achieve activity in 100% D_2O was attributed to the instability of ThiGH and the fact that multiple buffer exchange steps were irreversibly degrading the 4Fe-4S cluster. One possible solution to this problem would be to chemically reconstitute the 4Fe-4S cluster after ThiGH had been exchanged into D_2O buffer. The experiments described in this chapter divide chemically reconstituted ThiGH into two, to directly compare the activity in D_2O to the activity in H_2O. Chemical reconstitution of the 4Fe-

4S cluster can lead to small batch to batch variations in the amount of active ThiH. One potential source of variability in ThiH activity measurements can be eliminated by dividing the protein after chemical reconstitution. Chemically reconstituting ThiGH in D_2O may help overcome the loss of activity due to repeated buffer exchange steps, but this will reduce the confidence in making direct comparisons between activity measurements made in H_2O and D_2O.

Addition of MTAN to ThiGH activity assays altered the kinetic profile and *p*-cresol formation could be fitted to a first order process. This gave an increased period where the rate of reaction catalysis was rate limiting. In contrast, in the absence of MTAN, ThiGH shows a burst phase profile where product release becomes rate limiting after an initial turnover. Simplification of the kinetics by the addition of MTAN may help improve the accuracy of estimating the KIE. However, the observation that the rate of SAM cleavage (by monitoring the formation of DOA) and the rate of tyrosine cleavage (by monitoring the formation of *p*-cresol) were affected by changing the rate limiting step is potentially highly significant in understanding the mechanism of ThiH. The relative rate of uncoupled turnover was significantly higher in assays containing MTAN reported in chapter 4. Therefore, it must be considered that although the addition of MTAN may help to derive a value for the KIE in terms of productivity of the enzyme, it may be less useful in fully understanding the connection between SAM cleavage and tyrosine cleavage.

In the interests of balancing the level of understanding gleaned from the experiment with the practical difficulties, it may be the case that simply performing the experiment in higher amounts of D_2O is the best option. This could be achieved by adding small volumes of highly concentrated ThiGH stocks to assays prepared purely in D_2O. It is estimated that an assay containing >85% D_2O / H_2O could be prepared in this way.

5.4 *Discussion of the Kinetic Isotope Effect*

The observation of a kinetic isotope effect suggests that hydrogen atom abstraction is the rate limiting step of catalysis. This has been observed for other members of the radical SAM family, including LipA[32, 147] and anaerobic Sulfatase Maturating Enzyme (anSME)[152]. The KIE of 3.5 observed on the rate of tyrosine cleavage is within the expected range of between 1 and 7 for a deuterium isotope effect[153]. The KIE observed for the rate of anSME catalysis (see Scheme 5.2) was 5.6. Interestingly, although a KIE of 5.6 was observed on the rate of anSME catalysed oxidation of the substrate, no KIE was observed on DOA formation. In the experiment with the deuterated substrate anSME produced 4.5 times more DOA than peptide derived product. This would imply that uncoupled turnover observed for anSME occurs via an abortive pathway. In reactions with deuterated cysteinyl peptide, the rate of hydrogen atom abstraction is dramatically slowed down causing the abortive pathway to become more favourable.

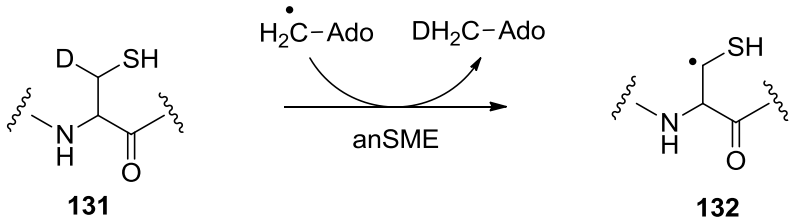

Scheme 5.2 Hydrogen atom abstraction from cysteinyl peptide by the 5'-deoxyadenosyl radical produced by anSME.

The experiments on ThiGH showed an apparent KIE on both tyrosine cleavage and SAM cleavage. It was inferred from previous experiments on substrate analogues (see Section 4.5) that SAM cleavage is directly coupled to formation of a substrate radical, particularly as incubation of ThiGH with SAM and a reductant, but no substrate gave only a very small amount of detectable SAM cleavage. This implies that the observed uncoupled turnover occurs via a

futile cycle with quenching of the tyrosine radical (see Scheme 4.2, p127), rather than by quenching of the 5'deoxyadenosyl radical. Assuming the phenolic hydrogen atom is abstracted, the relative BDE's would suggest that formation of the 5'deoxyadenosyl radical in the presence of tyrosine would result in rapid hydrogen atom abstraction, generating the more stable phenolic radical. The KIE observed on DOA formation may reflect a concerted mechanism for SAM cleavage and hydrogen atom abstraction in ThiH. However there is no precedent for this interpretation from studies on other members of the radical SAM family and it is widely accepted that the 5'deoxyadenosyl radical is an intermediate.

However, one consideration is that the relative stability of the phenolic radical may provide a thermodynamic driving force for ThiH catalysis. Therefore, the SAM cleavage step and hydrogen atom step are not necessarily concerted, but are dependent on one another to drive the reaction. This interpretation of a thermodynamic driving force would also suggest that reductive cleavage of SAM and hydrogen atom abstraction are both reversible steps and that the ability of ThiH to generate a relatively stable intermediate shifts the equilibrium of reductive SAM cleavage. Reversible SAM cleavage and hydrogen atom abstraction would be consistent with data emerging for other members of the radical SAM family that use SAM as a substrate, including BioB and BtrN. (see Section 1.2.4)[31, 35]. Careful observation of the mass spectra of DOA formed in assays incubated in 50% D_2O shows an enhancement of the m/z = 253.1 ion. This is consistent with the formation of some D-DOA in these assays. The m/z ion at 254.1 is consistent with the natural abundance of ^{13}C in the D-DOA formed in the assay. There is no evidence in these experiments, on ThiH, for the formation of di-deutero or tri-deutero DOA. Studies on BtrN[35] have demonstrated that both these species are formed when the enzyme is incubated with a deuterated substrate. These results have been used to support a mechanism in which the hydrogen atom abstraction step is reversible. For BioB and BtrN the substrate radical is generated by cleavage of a C—H bond, generating a carbon centred radical. At least for that case of BioB, this can be a primary radical (by abstraction of a hydrogen atom from C9 of

dethiobiotin), which will be similar in reactivity to the 5'-deoxyadenosyl radical as the C—H BDE's will be similar. It is perfectly feasible, therefore, that this radical intermediate could react with DOA to re-abstract a hydrogen atom which would re-form the 5'deoxyadenosyl radical. In the case of ThiH, the substrate derived radical is far less reactive, so re-abstraction of a hydrogen atom from DOA by the tyrosinyl radical would be unfavourable. If the formation of the phenolic radical is very favourable and the reverse reaction is slow, insofar that it is not measurable, then the forward reaction becomes, for practical purposes, irreversible and this may explain why no di-dutero or tri-deutero DOA is observed in these experiments on ThiH.

This interpretation is explained by Figure 5.3. Reductive cleavage of SAM generates the reactive 5'-deoxyadenosyl radical intermediate (**9**) and is an energetically uphill process. In the absence of tyrosine, the position of equilibrium of this step is far to the left (e.g. $k_{-1} > k_1$). If tyrosine is present, then the reactive 5'-deoxyadenosyl radical intermediate abstracts a hydrogen atom from tyrosine (**10**), generating a stabilised radical intermediate (**99**). This is an energetically downhill step, so the position of equilibrium is far to the right (i.e. $k_2 > k_{-2}$). Therefore, the reverse reaction for this step is unfavourable.

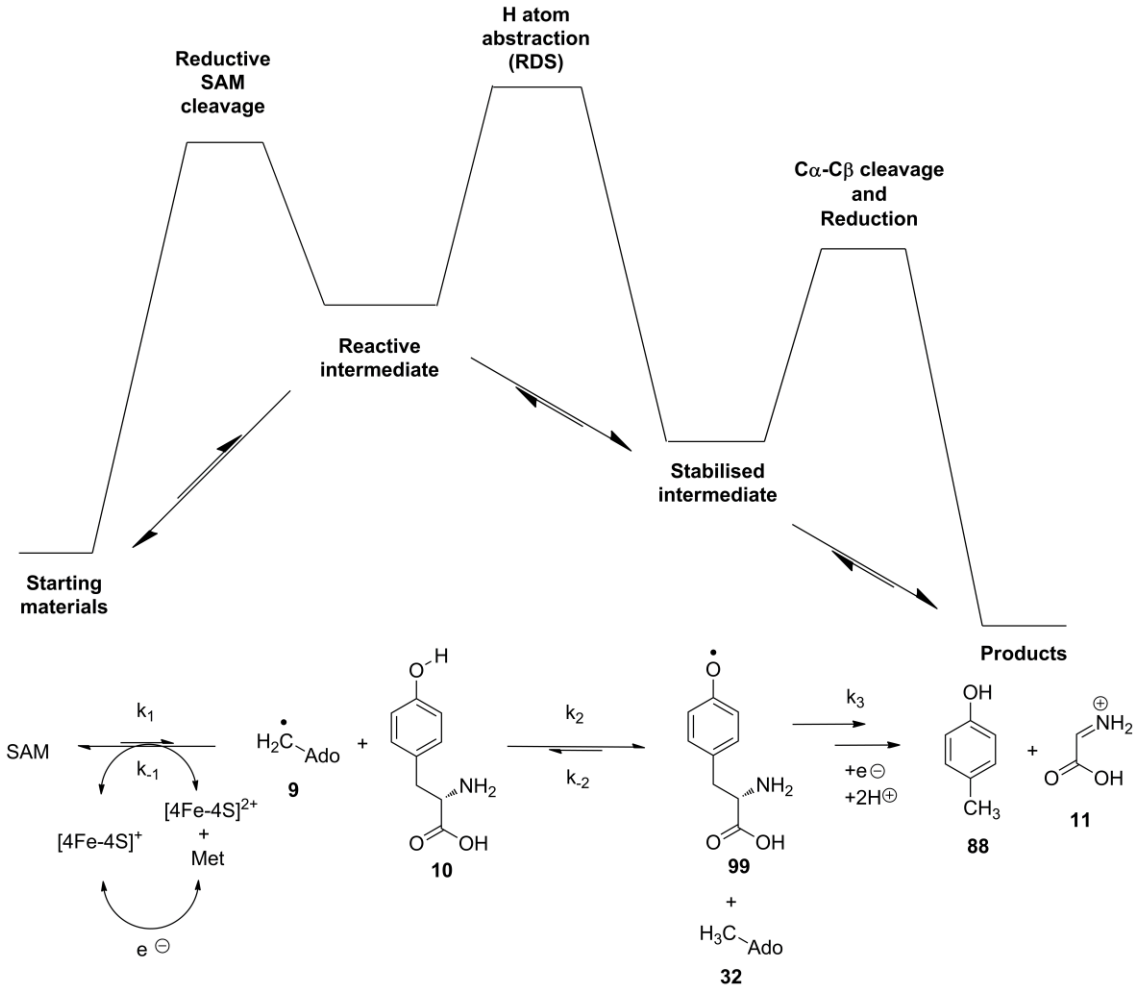

Figure 5.3 Energy diagram representing the early steps of ThiH catalysis.

5.5 *Summary and Conclusions*

Incubation of ThiGH activity assays in 50% D_2O / H_2O gave an observable kinetic isotope effect of 3.5 on the rate of catalysis. This was estimated from the rates of formation of *p*-cresol, which is a product of tyrosine cleavage. Additionally, a kinetic isotope effect of 2.4 could be estimated from the rates of formation of DOA, which is a product of SAM cleavage. The errors associated with these values were very large and this was attributed to methods of calculation and significant improvement in the experimental design is required to increase the confidence of these estimates. Improvements would initially be incubating the assay in higher concentrations of D_2O with the ultimate objective being the use of 100% D_2O which would give a direct measurement of the rate of catalysis with deuterated substrate.

5.6 *Derivation of Error in the Kinetic Isotope Effect*

5.6.1 *Derivation of Error in V_{obs}*

Values of V_{obs} were derived from differentiating equation 3.1, giving:

$$V_{obs} = \frac{d[\mathrm{P}]}{dt} = [\mathrm{E}].k_{\mathrm{burst}}.e^{-k_{\mathrm{burst}}.t} + L \qquad \text{(Eq. 5.1)}$$

To calculate the error on V_{obs} the following equation was used:

$$\Delta V^2 = \left[\frac{\delta V}{\delta[\mathrm{E}]}\right]^2.\Delta[\mathrm{E}]^2 + \left[\frac{\delta V}{\delta(k_{\mathrm{burst}})}\right]^2.\Delta(k_{\mathrm{burst}})^2 + \left[\frac{\delta V}{\delta L}\right]^2.\Delta L^2 \qquad \text{(Eq 5.6)}$$

Which is derived to give the following equation:

$$\Delta V^2 = [k_{\mathrm{burst}}.e^{-k_{\mathrm{burst}}.t}]^2.\Delta[\mathrm{E}]^2 + \left[[\mathrm{E}].k_{\mathrm{burst}}(t.e^{-k_{\mathrm{burst}}.t}) + A(e^{-k_{\mathrm{burst}}.t})\right]^2.(\Delta k_{\mathrm{burst}})^2 + \Delta L^2$$

(Eq. 5.7)

When $t = 0$, this equation can be simplified to:

$$\Delta V^2 = [k_{\mathrm{burst}}]^2.\Delta[\mathrm{E}]^2 + [[\mathrm{E}]]^2.\Delta(k_{\mathrm{burst}})^2 + \Delta L^2 \qquad \text{(Eq. 5.8)}$$

The values and standard errors for k_{burst}, [E] and L shown in Table 5.2 were substituted into this equation to give the calculated variation on V_{obs}, also shown in Table 5.2.

5.6.2 *Derivation of Error in V_D*

To calculate V_D equation 5.3 was used:

$$V_{D=}\frac{V_{obs}-V_H 0.5}{(1-0.5)} \quad \text{(Eq. 5.3)}$$

To calculate the error in V_D, Equation 5.3 was first rearranged:

$$V_D = 2V_{obs} - V_H \quad \text{(Eq 5.9)}$$

The error in V_D is calculated by the following equation:

$$\Delta {V_D}^2 = 2^2 . \Delta {V_{obs}}^2 + \Delta {V_H}^2 \quad \text{(Eq. 5.10)}$$

Error in V_D for *p*-cresol:

$$\Delta {V_D}^2 = 2^2 . 2.0^2 + 2.3^2$$

$$\Delta {V_D}^2 = 21.29$$

$$\boldsymbol{\Delta V_D = 4.6}$$

Error in V_D for DOA:

$$\Delta V_D{}^2 = 2^2.2.3^2 + 2.7^2$$

$$\Delta V_D{}^2 = 28.45$$

$$\boldsymbol{\Delta V_D = 5.3}$$

Product	$\boldsymbol{V_H}$ **/ µMmin^{-1}**	$\boldsymbol{\Delta V_H}$	$\boldsymbol{V_D}$ **/ µMmin^{-1}**	$\boldsymbol{\Delta V_D}$
p-Cresol	18.2	2.3	5.2	4.6
DOA	17.9	2.7	7.5	5.3

Table 5.4 Values of V_H and V_D shown with the variance calculated as described above.

5.6.3 *Derivation of Error in V_H / V_D*

To calculate the error in V_H / V_D, the following equation was used:

$$\left[\frac{\Delta\left(V_H/V_D\right)}{\left(V_H/V_D\right)}\right]^2 = \left[\frac{\Delta V_H}{V_H}\right]^2 + \left[\frac{\Delta V_D}{V_D}\right]^2 \qquad \text{(Eq. 5.11)}$$

Substituting with the values shown in Table 5.4 gives:

Error in V_H / V_D for *p*-cresol (V_H / V_D = 3.5):

$$\left[\frac{\Delta\left(V_H/V_D\right)}{\left(V_H/V_D\right)}\right]^2 = \left[\frac{2.3}{18.2}\right]^2 + \left[\frac{4.6}{5.2}\right]^2$$

$$\left[\frac{\Delta\left(V_H/V_D\right)}{\left(V_H/V_D\right)}\right]^2 = 0.799$$

$$\frac{\Delta\left(V_H/V_D\right)}{\left(V_H/V_D\right)} = 0.894$$

$$\Delta\left(\boldsymbol{V_H/V_D}\right) = \mathbf{3.1}$$

Therefore V_H / V_D for *p*-cresol = **3.5 ± 3.1**

Error in V_H / V_D for DOA (V_H / V_D = 2.4):

$$\left[\frac{\Delta\left(V_H/V_D\right)}{\left(V_H/V_D\right)}\right]^2 = \left[\frac{2.7}{17.9}\right]^2 + \left[\frac{5.3}{7.5}\right]^2$$

$$\left[\frac{\Delta\left(V_H/V_D\right)}{\left(V_H/V_D\right)}\right]^2 = 0.522$$

$$\frac{\Delta\left(V_H/V_D\right)}{\left(V_H/V_D\right)} = 0.723$$

$$\Delta\left(\boldsymbol{V_H/V_D}\right) = \mathbf{1.7}$$

Therefore V_H / V_D for DOA = **2.4 ± 1.7**

6 Conclusions and Future Outlook

6.1 *Conclusions*

6.1.1 *Improved Mechanistic Model for ThiH*

The aromatic by-product of radical mediated Cα—Cβ of tyrosine by ThiH was unequivocally characterised as *p*-cresol from *in vivo* experiments. Development of an *in vitro* activity assay showed that ThiH could function catalytically when an excess of substrates and reductant was present. The kinetics of ThiH turnover was investigated using either purified ThiGH complex or monomeric ThiH and product formation could be fitted to a pre-steady state burst phase profile. The interpretation of the kinetic profile was that product release was rate limiting when the enzyme was undergoing multiple turnovers. The products DOA and methionine were found to co-operatively inhibit ThiH activity. This inhibition could be removed by the addition of the nucleosidase, MTAN which catalysed rapid hydrolysis of DOA to adenine and 5'deoxyribose. Addition of MTAN to time course experiments on the ThiGH complex altered the kinetic profile and product formation could be fitted to a first order process. In addition the amount of uncoupled SAM cleavage was observed to greatly increase. Additional product inhibition studies showed that addition of glyoxylate inhibited the tyrosine cleavage reaction and greatly increased uncoupled turnover. Structural analogues of tyrosine were used to define the substrate requirements of the enzyme and in particular the need for a phenolic O–H group. Furthermore, phenolic tyrosine analogues that lacked a correctly positioned amine functional group were able to undergo a partial reaction leading to uncoupled SAM cleavage but with no evidence for Cα—Cβ bond cleavage. Experiments in D_2O confirmed that an exchangeable hydrogen atom was abstracted by the 5'deoxyadenosyl radical and this step appeared to be rate limiting.

These observations were integrated into an improved model for the mechanism of tyrosine cleavage by ThiH, which is shown in Scheme 6.1. The information on each step of the mechanism which has been gleaned from the studies presented in this thesis is summarised below.

Step 1: Reductive cleavage of SAM generating the 5'-deoxyadenosyl radical

- This step is likely to be reversible
- SAM cleavage is not observed to occur in the absence of tyrosine (or a 4-hydroxyphenylpropionic acid analogue)

Step 2: Abstraction of the phenolic hydrogen atom

- This is suggested to be the rate determining step (RDS) of reaction catalysis
- The tyrosine radical can be reduced and protonated to reform tyrosine, resulting in a futile cycle and uncoupled SAM cleavage
- Very little uncoupled SAM cleavage appears to occur as a result of an abortive pathway

Step 3: Cα—Cβ bond cleavage

- This step can be inhibited by glyoxylate (**98**), or by accumulation of dehydroglycine (**11**)
- This step appears to be sensitive to the orientation of the substrate
- This step also shows a requirement for an α-amino group
- Inhibition of this step results in a much greater amount observed uncoupled turnover and would suggest a far greater amount of futile cycling

Step 4: Reduction of the radical anion (**102**) to *p*-cresol (**88**)

- The rate of this step is likely to be similar to the rate of futile cycle (2c)
- The source of the electron for this step is unknown

Step 5: Release of products

- This is the RDS at steady state.
- Under physiological conditions dehydroglycine is transferred to ThiG where it reacts to form thiazole

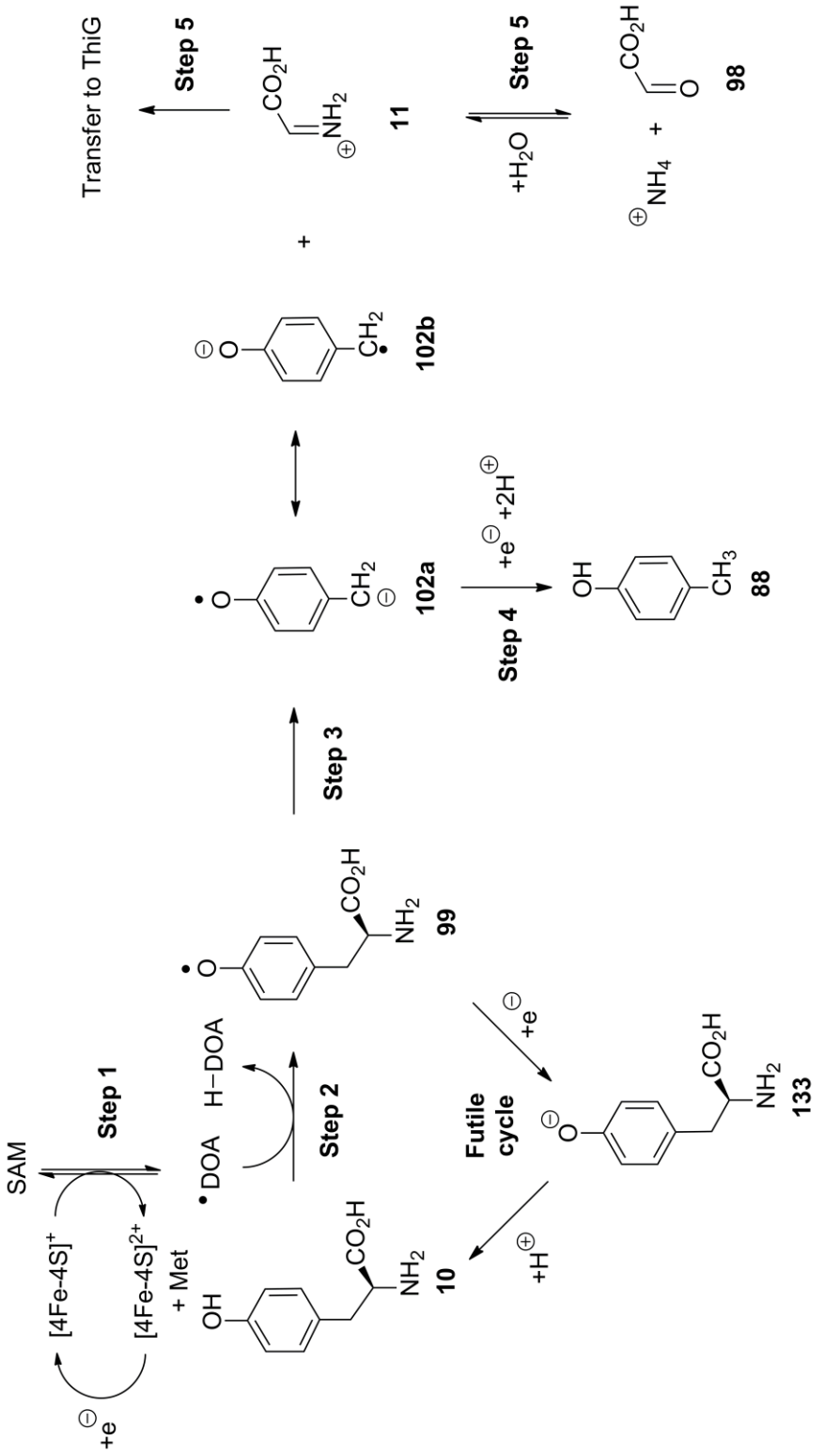

Scheme 6.1 Current mechanistic model for radical mediated tyrosine cleavage, catalysed by ThiH.

6.1.2 *Implications of the Mechanistic Model*

Tyrosine was identified as the source of the C2-N3 fragment of the thiazole moiety of thiamine in anaerobic bacteria in 1978[103, 104]. However, an understanding of why this seemingly wasteful step in thiamine biosynthesis was necessary in these organisms required elucidation of the mechanism of thiazole biosynthesis[96, 100, 115, 154]. Thiazole biosynthesis, catalysed by ThiG, requires the electrophile, dehydroglycine (**11**) as an intermediate. Where aerobic bacteria can derive this intermediate by oxidation of glycine, anaerobic bacteria require an alternative pathway to this intermediate that can function under anaerobic conditions, where oxidising equivalents are not readily available. ThiH functions in anaerobic bacteria to cleave the Cα—Cβ bond of tyrosine to generate this intermediate. ThiH is a member of the radical SAM family and like all members of this family; catalysis is initiated by the reductive cleavage of SAM by a reduced 4Fe-4S cluster generating the reactive 5'-deoxyadenosyl radical intermediate. This radical intermediate initiates the tyrosine cleavage reaction by abstraction of a hydrogen atom from tyrosine. Thus, the 5'-deoxyadenosyl radical is acting as an oxidant as this step involves loss of an electron form the substrate[27]. Cleavage of the Cα—Cβ and formation of dehydroglycine involves a further loss of electrons from the amine, into the aromatic ring of tyrosine. Therefore, the use of tyrosine as the precursor to dehydroglycine and the formation of *p*-cresol as the byproduct can be explained by the overriding need to form the electron poor dehydroglycine intermediate under anaerobic conditions.

The necessity for this chemically wasteful pathway means that the biosynthesis of thiamine needs to be strictly controlled. This is achieved at the level of gene expression by the Thi-Box riboswitch[117-119]. The implications from this mechanistic model are that control of thiamine biosynthesis extends to the regulation of some of the individual biochemical steps, thus avoiding wasteful turnovers. It is apparent that ThiH mediated tyrosine cleavage is strictly controlled by the accumulation of the products, which results in a burst phase kinetic profile.

The function of this product inhibition in cells actively synthesizing thiamine may be to coordinate the rate of formation of dehydroglycine by ThiH with its utilization by ThiG for thiazole formation.

ThiH is not unique in its ability to cleave the Cα—Cβ bond of an aromatic amino acid. Recently, HydG has been shown to perform an extremely similar tyrosine cleavage reaction, which formed *p*-cresol as a product. The other products of HydG mediated tyrosine cleavage were characterised as cyanide (**134**)[130] and carbon monoxide (**135**)[155] which ultimately function as ligands in the complex active site cofactor of [FeFe]-hydrogenases[156]. Evidence was found that dehydroglycine was formed as an intermediate in the biosynthesis of cyanide and carbon monoxide, implying that the early steps in the mechanism are identical to ThiH. HydG shows extremely high homology to ThiH, but has an additional ~70 amino acids at its C-terminus, thought to be responsible for the decarbonylation of dehydroglycine to cyanide and carbon monoxide. Sequence analysis of several radical SAM proteins showed that ThiH and HydG formed a small subfamilyalong with another enzyme, NosL (Figure 6.1)[157]. NosL is a radical SAM enzyme required for the rearrangement of tryptophan to provide the 3-methylindolyl moiety during the biosynthesis of the antibiotic Nosiheptide. This rearrangement requires a Cα—Cβ bond cleavage and the extrusion of the Cα—N fragment of tryptophan (Figure 6.2). ThiH, HydG and NosL share the common feature of cleaving the Cα—Cβ bond of aromatic amino acids and it is likely these transformations proceed by related mechanisms, potentially forming aromatic radicals and resulting in a benzylic radical intermediate.

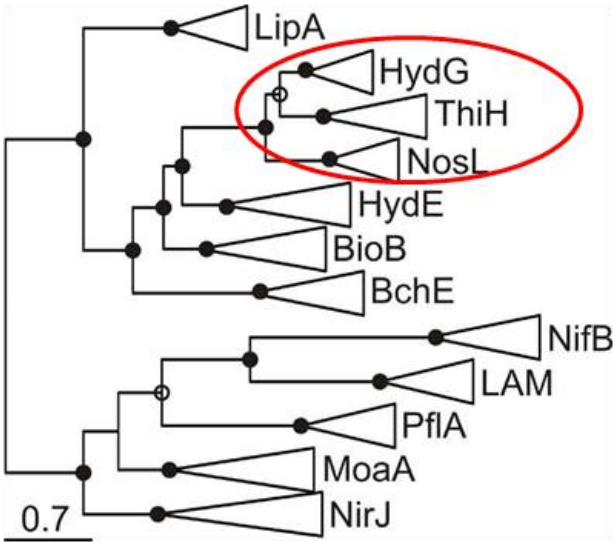

Figure 6.1 Phylogenetic reconstruction of representative radical SAM proteins. The grouping of the Cα-Cβ lyase subfamily is shown with a red circle. (Adapted from[130])

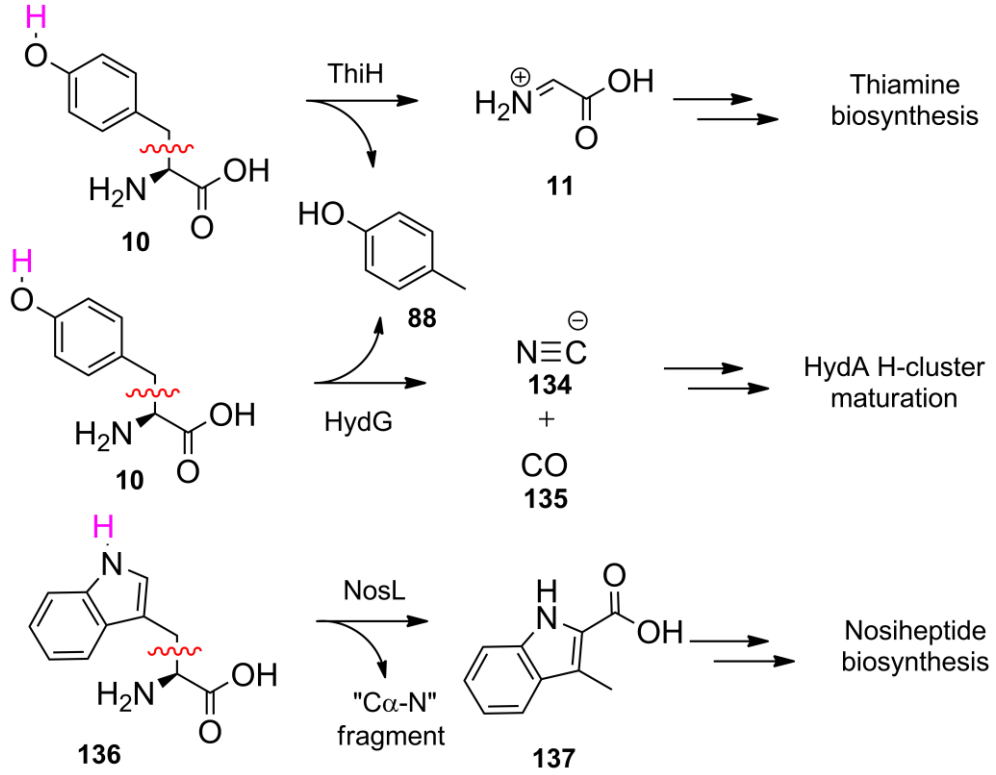

Figure 6.2 The Cα-Cβ lyase subfamily with currently characterised biochemical functions.

6.2 *Further Experiments*

The mechanistic model presented for tyrosine lyase is consistent with the currently available data. However, to resolve some of the outstanding questions, such as to unequivocally assign the site of hydrogen atom abstraction from tyrosine reuires further experimentation. An X-ray crystal structure of tyrosine lyase would assist in providing a stereoelectronic explaination for the mechanism of tyrosine cleavage and may highlight key residues in the enzyme active site that assist in reaction catalysis. The improved purification protocol is likely to be useful in obtaining any crystals of the enzyme and it would be worthwhile attempting to crystalise both the monomeric form of ThiH and the ThiGH complex. Structural data on the ThiGH complex may prove essential in fully interpreting the complex issue of product transfer from ThiH to ThiG.

EPR spectroscopic characterisation of the tyrosine radical may also provide vital data on understanding the subtle control of the tyrosine Cα—Cβ cleavage reaction. The proposed mechanism provides two possible fates of the tyrosine radical; either Cα—Cβ cleavage, or reduction and protonation back to tyrosine in a futile cycle. Despite the anticipated stability of the tyrosine radical the potential for reduction may mean that this intermediate does not pesist long enough to obtain an EPR spectrum unless rapid freeze quench techniques are used. Or one alternative is to use a photoreductant, such as deazaflavin, which could stoichiometrically reduce to 4Fe-4S cluster, allowing for reductive SAM cleavage, but not providing the necessary electron to reduce either tyrosine of the resultant radical anion, allowing for characterisation of any substrate radicals by EPR.

The 4-hydroxyphenylpropionic acid analogues described in Chapter 4 were initially chosen for their potential to trap any tyrosine radical intermediates. No EPR data was obtained during the

course of the research presented in this thesis, however a further sub-set of tyrosine analogues with modifications at the 3-position (see Figure 6.3) may also prove useful in stabilising any tyrosine derived radical intermediates.

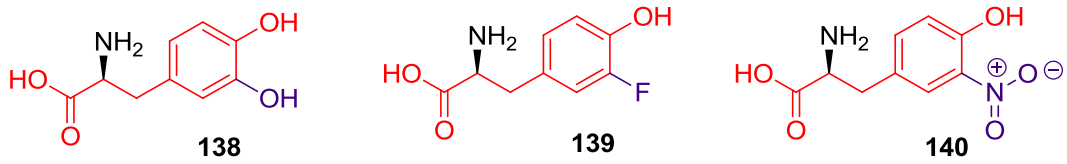

Figure 6.3 3-substituted tyrosine analogues.

The compounds shown in Figure 6.3 were analysed by the same method described in Chapter 4 (Method 31). 3-hydroxy-L-tyrosine (L-DOPA) (**138**) and 3-fluoro-L-tyrosine (**139**) were observed to turn over apparently with greater activity that the positive control, with tyrosine as the substrate. Modifications of the 3-position of a phenol will affect the BDE of the phenolic O—H bond[158], by stabilisation of the resultant phenolic radical. Stabilisation of a phenolic radical may result in an observed change in the rate of hydrogen atom abstraction due to the weakening of this bond. The observation that hydrogen atom abstraction by the 5'-deoxyadenosyl radical was the rate limiting step of ThiH catalysis made these experiments potentially significant. However, information on the relative binding affinities of these compounds relative to tyrosine is required to make these observations relevant. Data on the binding affinity could be obtained from spectroscopic experiments analogous to Ugulava *et al.*[51] or by performing detailed kinetic measurements and estimating values for K_M and V_{max}.

7 Experimental

7.1 *General Experimental Methods*

7.1.1 *Materials*

Wizard® *Plus* Minipreps were purchased from Promega (Southampton). Bacto Tryptone, Yeast Extract and Bacto Agar, for culture media, were purchase from Oxoid and Difco.

DTT, NADPH, IPTG and antibiotics were obtained from Melford Laboratories Ltd. Polyacrylamide-bis polyacrylamide (30% w/v, 37:5:1) was purchased from Amresco, Protein chromatograpy media (Superdex 75 (S-75), Superdex 200 (S200), and Chelating Fast Flow resins) were purchased from Pharmacia. All other chemicals used were purchased from Aldrich, Sigma or Fluka.

7.1.2 *Equipment*

FPLC. All aerobic enzyme purifications were performed using a Pharmacia FPLC System in a cold room, maintained at 4 °C. Anaerobic enzymes were purified using an AKTA Prime FPLC from Amersham biosciences in the glove box maintained at 20 ºC.

pH determination. pH measurements were performed using a Mettler Delta 340 pH meter connected to a Mettler Toledo Inlab 413 Combination Electrode. This was calibrated at pH 4.0 to 7.0 or pH 7.0 to 10.0 before use and stored in 3 M potassium chloride.

UV-Vis Spectroscopy. Absorbance readings and UV-vis spectra were recorded on a Lamba 2 spectrophotometer (Perkin-Elmer), or on a USB2000 spectrophotometer using a light source Mini-D2-GS (Ocean Optics (Duiven, The Netherlands)).

Centrifugation. Samples were centrifuged at 4 ºC using a Sorval centrifuge fitted with a SLC6000 or a JA-14 rotor. For small volumes (< 1.5 ml) a bench top microcentrifuge was used at room temperature.

HPLC Analysis. A Gilson System Workcenter including 321 pumps and 234 Gilson Autoinjector was connected to a Shimadzu RF-10Axl fluorimeter and/or to a Gilson UV/Vis-155 detector, and used for high performance liquid chromatography (HPLC) analysis at room temperature.

LCMS. LCMS analysis data was obtained using a Gilson HPLC coupled to a Thermo Finnigan Surveyor MSQ single quadrupole mass spectrometer with electrospray ionization. The data were collected and processed using the XCalibur software system.

GCMS. GCMS analysis data was obtained on a Thermo TraceMS equipped with an AS800 autosampler and a PE-Wax (30 m x 0.25 mm x 0.25 μm) column.

7.1.3 *Anaerobic Techniques*

All anaerobic experiments (protein purification, reconstitution and activity assays) were carried out in an anaerobic glove box (Belle Technology, Weymouth, UK) maintained at less than 1 ppm O_2. All containers (bottles, jars, tubes, beakers etc.) and equipment required during the experiments were degassed overnight inside the glove box. Buffers and solutions were bubbled with N_2 for 10 minutes before being introduced into the glovebox and were allowed to deoxygenate overnight before use.

UV-vis spectra of anaerobic proteins were recorded on an Ocean Optics (Duiven, The Netherlands) USB2000 spectrophotometer using a light source Mini-D2-GS connected by optical fibers P-400-2-UV/SR to a cuvette holder inside the glove box.

For anaerobic protein purification, columns were placed outside the box but the buffer lines were introduced in a sealed gastight fashion into the box so that the anaerobic buffers could be pumped through the system and used to equilibrate the column, wash and elute the proteins; the column flow through was fed back into the box to permit anaerobic fraction collection. Protein elution was monitored by absorption at 280 nm.

7.1.4 *General Microbiological Methods*

Standard sterile techniques were applied throughout microbiological experiments. Growth media and heat stable solutions were sterilised in a PriorClave autoclave (Priorclave Ltd) at 121 °C for 25 min., whilst heat labile solutions were filter sterilised through 0.22 µm filters (Millipore). Growth media were supplemented with the appropriate antibiotic (see Table 7.1 and Table 7.12, p177). Liquid bacterial cultures were incubated in an Innova 4400 Incubator Shaker (New Brunswick Scientific) or in an Innova 4230 Refrigerated Incubator Shaker (New Brunswick Scientific) at 180 rpm. Bacterial plate cultures were grown at 37 °C overnight in an Economy Incubator Size 2 (Gallenkamp).

Antibiotic	**Final Concentration**	**Stock Concentration**
Ampicillin	100 µg / mL	100 mg / mL in H_2O
Kanymycin	30 µg / mL	30 mg / mL in H_2O
Streptomycin	10 µg / mL	10 mg / mL in H_2O

Table 7.1 Stock solutions and amount of antibiotics added to growth media.

Method 1: Prparation of competent cells. Competent cells were prepared by the rubidium chloride method (ref Sambrook). A smear of selected strain was incubated overnight at 37 ºC in 2-YT [159] media (10 mL), which did not contain any antibiotic. The culture was then used as a 1% inocula into fresh 2-YT media (100 mL), again with no antibiotic, and the culture grown at 37 ºC to an OD_{600} of 0.6 (c.a. 2 h). All further manipulations were conducted in a cold room at 4 ºC. Cells were harvested by centrifugation (4000 rpm, 10 min 4 ºC) and the supernatant removed, before being re-suspended in ice cold TBF I buffer (10 mL) (Table 7.2). Suspension was maintained on ice for 10 min before further centrifugation (4000 rpm, 10 min 4 ºC) and

removal of the supernatant. The cells were then re-suspended in TBF II buffer (1.5 mL) (Table 7.3) and 200 μL aliquots were immediately frozen on dry ice.

Reagent	Quantity
Potassium acetate	0.588 g
Rubidium chloride	2.42 g
Calcium chloride	0.294 g
Manganese chloride	2.0 g
Glycerol	30 mL
Deionised water	Adjust volume to 200 mL
pH adjusted to 5.8 with 1% acetic acid	

Table 7.2 TBF I buffer

Reagent	Quantity
MOPS	0.21 g
Rubidium chloride	0.121 g
Calcium chloride	1.10 g
Glycerol	30 mL
Deionised water	Adjust volume to 100 mL
pH adjusted to 6.5 with dilute NaOH	

Table 7.3 TBF II buffer

Method 2: Transformations. Aliquots of competent cells (150 - 200 μL) contained in 1.5 mL tubes were defrosted on ice for 10 min before the addition of purified plasmid DNA (1-2 μL).

The tubes were maintained on ice for 30 min and then heat-shocked for 45 sec at 42°C. The cell suspensions were returned to ice for 2 min and mixed with room temperature SOC medium (250µL) (Table 7.4). Cell suspensions were incubated in an orbital shaker at 37 °C (230 rpm) for 1 h before being plated onto 2-YT agar plates and incubated at 37 °C overnight. Plates were then stored in a cold room at 4 °C. Positive colonies (those containing the correct construct), were identified as well isolated single colonies. These were picked from plates with a 10 µL sterile tip and incubated overnight in 2-YT medium (10 mL), supplemented with ampicillin (100µg/mL) for further investigation or storage.

Reagent	**Concentration**	**Volume**
$MgCl_2$	1 M	1 mL
$MgSO_4$	2 M	1 mL
Glucose	20% (w/v)	1 mL
2-YT medium	-	Make up to 100 mL

Table 7.4 SOC Medium

Method 3: Glycerol Freeze Preparation. Well isolated single colonies were picked from plates with a 10 µL sterile tip and incubated overnight at 37 ºC in 2-YT medium (10 mL), supplemented with the appropriate antibiotic. Glycerol (125 µL) was added to the cell culture (500 µL), mixed vigorously, before storage at –80 °C.

Method 4: Minipreps. Plasmid DNA was isolated using Wizard® *Plus* Minipreps DNA Purification System, used as stated in manufacturer's instructions. Sterile water was used to elute the isolated plasmid DNA.

Method 5: Analytical Restriction enzyme digestion. Analytical digestion of plasmid DNA (45 μL, 50-75 ng / μL) isolated from bacterial culture (5 - 10 mL) was carried out using the conditions shown inTable 7.5.

	Volume	Concentration	Total Quantity
Plasmid	5 μL	50 - 75 ng / μL	250 - 375 ng
Buffer	1 μL	10X	1X
BSA	1 μL	1 mg / mL	1 μg
Restriction Enzyme (each)	0.5 μL	10 U / μL	5 U
Sterile Water	2 μL		

Table 7.5 Analytical digestion reaction mixture

Reactions were incubated at 37 °C for 1.5 hours before loading onto a 1% agarose gel.

Method 6: Protein concentration determination. Protein concentration was assayed using the method of Bradford[136]. Bradford reagent (1 mL) was added to a protein sample (20 μL) and incubated at room temperature for 5 min, then A_{595} was measured using pure Bradford reagent as a control. The sample was diluted if A_{595} exceeded 1.0. Appropriate correction factors for proteins of unknown concentration were obtained from calibration curves constructed with BSA standards.

Method 7: 15 % SDS-PAGE denaturing gel. For 10 mL of resolving gel solution (5 mL per plate) the following components were mixed in the order as shown inTable 7.6. 4 mL of this solution was then poured into each plate, the surface covered with a thin layer of water and

allowed to set for 45 minutes. The water was then removed carefully and the stacking gel was prepared as in Table 7.7.

Reagent	Quantity
H_2O	2.2 mL
30 % Acrylamide / bis acrylamide	5.0 mL
1.5 M Tris/HCl (pH 8.8)	2.6 mL
10 % SDS	0.1 mL
10 % Ammonium Persulphate	0.1 mL
TEMED	4 μL

Table 7.6 Resolving gel mixture

Reagent	Quantity
H_2O	3.4 mL
30 % Acrylamide / bis acrylamide	0.83 mL
1.5 M Tris/HCl (pH 8.8)	0.63 mL
10 % SDS	0.05 mL
10 % Ammonium Persulphate	0.05 mL
TEMED	5 mL

Table 7.7 Stacking gel mixture

This mixture was then directly poured onto the top of the resolving gel and a Teflon comb inserted into the gel solution. Teflon combs were removed after one hour and gels immediately used or stored at 4 ºC.

Samples were prepared by mixing 20 μL protein sample with 20 μL sample loading buffer (Table 7.8) and denaturing at 95 °C for 5 minutes. Samples (20 μL)were then applied to the gel.

Reagent	**Quantity**
0.2 M Tris/HCl (pH 6.8)	2.5 mL
DTT	154 mg
SDS	200 mg
Bromophenol Blue	10 mg
Glycerol	1 mL
Deionised water	Adjust volume to 10 mL

Table 7.8 Sample loading buffer stock solution

Reagent	**Quantity**
Tris Base	15.1 g
Glycine	94 g
10% SDS solution	50 mL
Deionised water	Adjust volume to 1000 mL

Table 7.9 SDS-PAGE running buffer (×5 stock solution)

Reagent	Quantity
Coomassie brilliant blue	2.5 g
Methanol : water (1 : 1)	90 mL
Glacial acetic acid	10 mL

Table 7.10 Coomassie brilliant blue protein stain

Reagent	Quantity
Deionised water	4375 mL
Methanol : water (1 : 1)	375 mL
Glacial acetic acid	250 mL

Table 7.11 Destain solution

Electrophoretic separation was at 200 V (~15 V / cm) in SDS-PAGE running buffer (Table 7.9) and analysed. Gels were stained using Coomassie brilliant blue stain (Table 7.10) and destained (Table 7.11).

Method 8: Small scale expression experiments. An overnight starter culture (10 mL) (inoculated from glycerol freeze stock) was used to inoculate 2-YT medium (100 mL) containing appropriate antibiotics (Table 7.13). Culture was incubated in a shaker (37 ºC, 180 rpm), and growth monitored by OD_{600}. Cells were induced at OD_{600} = 0.6 by the addition of arabinose for pBAD expression vectors (final concentration 0.2 %). The incubation temperature was reduced to 27 °C and cells grown for a further 4 h before harvesting by centrifugation

(10 min, 5,000 rpm, 4 ºC). Cell pellets were resuspended in lysis buffer (750 μL) and lysed by sonication (6 × 3 s on / off). Cell debris was separated by centrifugation (13,000 rpm, 10 min) and the supernatant decanted. Cell debris was resuspended in lysis buffer (100 × pellet volume). Protein concentration was then estimated by Bradford assay (Method 6). The protein content of both supernatant and pellet were analysed by SDS-PAGE (Method 7).

Method 9: Large scale protein expression. An overnight starter culture was used as a 1 % innocula for 4 × 1.25 L 2-YT medium (containing appropriate antibiotic). Cultures were incubated in an orbital shaker (37 ºC, 180 rpm) and cell growth monitored by OD_{600}. At OD_{600} 0.6 cells were induced by the addition of arabinose for pBAD expression vectors (final concentration 0.2 %), or IPTG for pET expression vectors (final concentration 1 mM) and the incubation temperature lowered to 27 ºC for four hours. Cells were harvested by centrifugation (SLC6000, 6,000 rpm, 30 min, 4 ºC) and stored at -80 ºC.

7.1.5 *Protein Purification*

Protein	Plasmid	Antibiotic	Inducer	Technique	Reference
ThiGH	pRL1020	Ampicillin	Arabinose	Ni affinity	[106]
FldA	LPETGGHis$_6$(2) (pFlav)	Kanamycin	IPTG	Cation exchange	[160]
Fpr	pLLC155 (pFdr-His)	Ampicillin	Arabinose	Ni affinity	unpublished
MTAN	pProExHTApfs (pPfs)	Ampicillin	IPTG	Ni affinity	[150]

Table 7.12 Summary of expression and purification techniques for proteins used in this study.

Method 10: Expression and purification of ThiGH. Cells were cultured and protein expressed by method 9. A typical yield of wet cell paste was 40 g.

For purification, the frozen cell pellet (~40 g) was transferred to the glove box and suspended in anaerobic buffer A (50 mM MOPS pH 7.7, 200 mM NaCl, 12.5% (w/v) glycerol, 50 mM imidazole) (~100 mL). Lysozyme (0.1 mg / mL) was added and the suspension stirred for 1 h before the cells were lysed, on ice, by sonication (30 min, amplitude: 20, 1 sec pulse). Benzonase (10 μL) was added and the lysate cleared by centrifugation (Beckmann JA14, 125000 rpm, 25 min, 4 °C). The supernatant was loaded onto a Chelating Sepharose column (50 ml) previously charged with $NiSO_4$ and equilibrated with anaerobic buffer A (250 mL). The column was washed with buffer B (50 mM MOPS pH 7.7, 500 mM NaCl, 12.5% (w/v) glycerol, 50 mM imidazole) (300 mL), and then buffer A (50 mL). The protein was eluted with buffer C (50 mM MOPS pH 7.7, 200 mM NaCl, 12.5% (w/v) glycerol, 500 mM imidazole) at

an increasing gradient of 0 – 50% of buffer C over 50 mL, followed by an isocratic wash at 50 % buffer C . 5 mL fractions were collected and the six fractions (30 mL) containing the most concentrated ThiGH complex (typically 15 – 20) were pooled and immediately loaded onto a S-75 gel filtration column, previously equilibrated with anaerobic buffer D (50 mM MOPS pH 7.7, 200 mM NaCl, 12.5% (w/v) glycerol, 5 mM DTT) (150 mL). The column was eluted with buffer D yielding 5 x 10 mL fractions which were stored at -80 °C. SDS-PAGE was used to determine the composition of each fraction.

N.B. The instability of ThiH in buffers containing high imidazole concentrations meant that it was preferable to avoid time consuming SDS-PAGE analysis after the Ni-affinity step.

Method 11: Flavodoxin Expression purification. Cells were cultured and protein expressed by method 9. The media was supplemented with flavin mononucleotide (2 mg / L) and a further addition was affected when protein expression was induced. A typical yield of wet cell paste was 15g which was blue-grey in colour.

For purification, the frozen blue-grey cell pellet (50 g) was suspended in buffer E (10% (w/v) glycerol / 50 mM Tris, pH 8.1) (150 mL) and lysozyme (15 mg) added. The suspension was stirred for a further 15 min before cell lysis by sonication (12 x 30 s on / 30 s off). Benzonase (10 μL) was added and the suspension stirred for a further 10 min before removal of the cell debris by centrifugation (SLC15000, 12000 r.p.m., 30 min, 4 ˚C). The supernatant was then loaded onto a Q-Sepharose ion exchange column (180 mL), which had been pre-equilibrated with Buffer F (50 mM Tris, pH 8.1) (300 mL), Buffer G (1 M NaCl, 50 mM Tris, pH 8.1) (300 mL) and again with Buffer F (300 mL). The column was washed with Buffer F (500 mL), during which time the protein underwent a colour change from blue – yellow, before elution

with a gradient of 0% – 20 % Buffer G over 100 mL followed by 20% – 70% over the next 900 mL. When the yellow colour was observed to begin to elute (~32 % of Buffer G), 10 mL fractions were collected and every third fraction analysed for protein concentration and by SDS-PAGE. Fractions that were observed to contain > 95% (fractions 26 – 34) of flavodoxin by SDS-PAGE were pooled and stored at 4 ˚C overnight.

The protein was reconstituted by the addition of 5 equivalents of flavin mononucleotide and stirred at 4 ˚C for 45 min, before concentrating to a volume of 50 mL on a 10 KDa NMCO membrane. The excess flavin mononucleotide was removed by desalting the protein, in two batches of 25 mL each, into Buffer H (200 mM NaCl, 50 mM Tris, pH 8.1) via a S-75 gel filtration column (50 mL), equilibrated with Buffer H (150 mL). Protein containing fractions (3 mL) from both batches were pooled and the final protein concentration determined as 12.1 mg / mL. UV-vis spectroscopy confirmed the presence of the bound co-factor. Flavodoxin was stored in 1mL aliquots at -80 °C.

Method 12: Flavoprotein: NADPH oxidoreductase (Fpr) expression and purification. Cells were cultured and protein expressed by method 9. The media was supplemented with flavin adenine dinucleotide (2 mg / L) when protein expression was induced. A typical yield of wet cell paste was 40g.

For purification, the frozen blue grey cell pellet (40 g) was suspended in buffer E (10% (w/v) glycerol / 50 mM Tris, pH 8.1) (120 mL) and lysozyme (0.1 mg / mL) added. The suspension was stirred for 15 min before cell lysis by sonication (12 x 30 s on / 30 s off). Benzonase (10 μL) was added and the suspension stirred for a further 10 min before removal of the cell debris by centrifugation (SLC15000, 12000 r.p.m., 30 min, 4 ˚C). The supernatant was then

loaded onto chelating sepharose fast flow column, charged with $NiSO_4$ and equilibrated with Buffer J (50 mM Tris, pH 8.1, 200 mM NaCl, 25 mM Imidazole). The column was washed with 300 mL of Buffer J before a gradient to 500 mM Imidazole over 100 mL using Buffer K (50 mM Tris, pH 8.1, 200 mM NaCl, 500 mM Imidazole). Fractions (5 mL) were analysed by SDS-PAGE and those containing >95% Fpr were pooled and concentrated to ~20 mL on a 10 KDa NMCO membrane.

Fpr was reconstituted by stirring with 5 eq. FAD for 45 min, dialysed into buffer H (50 mM Tris, pH 8.1, 200 mM NaCl) and the final protein concentration estimated to be 12.5 mg / mL. Flavodoxin reductase was stored in 150 µL aliquots at -80 °C.

Method 13: Purification of ThiGH and ThiH by Sephadex 200 gel filtration chromatography. The protein was chemically reconstituted (method 14) and concentrated to a volume of less than 5 mL using a 10 kDa molecular weight cut off filter (Millipore). The concentrated protein was then applied to a Sephadex 200 gel filtration column (2.6 x 60 cm) pre-equilibrated in anaerobic buffer D (50 mM MOPS pH 7.7, 100 mM NaCl, 12.5% (w/v) glycerol, 5 mM DTT). The column was eluted with buffer D (~100 mL) until the A_{280} was observed to rise, at which point 7.5 mL fractions were collected. The ThiGH complex typically eluted in the first six fractions and the ThiH-monomer in the following six fractions (see figure 3.x). An aliquot of each fraction (150 µL) was retained for SDS-PAGE (method 7) and iron analysis (method 15) and the remainder stored at -80 ˚C in sealed 15 mL Falcon tubes for further investigation.

7.1.6 *ThiGH Reconstitution and activity assays*

All protein manipulations were carried out in the anaerobic glove box. The following are optimised methods that were developed throughout the course of experiments reported in Chapter 3.

Method 14a: ThiGH reconstitution. The ThiGH / ThiH mixture isolated by Ni affinity chromatography (method 10) was thawed inside the anaerobic glove box (maintained at less than 1 p.p.m. O_2). DTT (5 mM) was added and the solution gently mixed. After 15 min, 5 mol eq of $FeCl_3$ (10 mM solution in anaerobic water) were added dropwise. After a further 15 min gentle mixing 5 mol eq of Na_2S (10 mM solution in anaerobic water) were added likewise. The protein solution was gently mixed at room temperature for a further 2 h. Precipitated iron sulfide was removed by centrifugation and the protein was concentrated using a 10 kDa molecular weight cut off filter. The protein was then applied to a NAP-10 gel filtration column equilibrated in anaerobic buffer L (50 mM MOPS pH7.5, 100 mM NaCl and 5% (w/v) glycerol). Successful chemical reconstitution was assessed by UV-vis spectroscopy. Reconstituted ThiGH was used immediately for further investigation. However it is possible to store reconstituted ThiGH (maximum concentration of 6 mg / mL, in buffer D) at -80 ºC overnight.

Method 14b: Reconstitution of ThiH or ThiGH that had been purified by Sephadex 200 gel filtration chromatography. The same protocol (method 14a) was followed except that only 2.5 molar equivalents of $FeCl_3$ or Na_2S were added.

Method 15: Iron analysis. The amount of iron present in purified ThiGH was analysed by the methods of Fish[137] and was determined either in duplicate or triplicate. For the iron analysis, the following solutions were prepared: reagent A, 0.142 M $KMnO_4$ in 0.6 M HCl, obtained by mixing equal volumes of 1.2 M HCl and 0.284 M $KMnO_4$ in H_2O (445 mg in 10 mL), and reagent B, 6.5 mM ferrozine, 13.1 mM neocuproine, 2 M ascorbic acid, 5 M ammonium acetate in H_2O, prepared by first dissolving the ammonium acetate (4.85 g) and ascorbate (4.4 g) in H_2O (12.5 mL) followed by ferrozine and neocuproine (40 mg each). Reagent A was freshly prepared every time, whilst reagent B was stored in the dark for no longer than 3 weeks. Standards were prepared from a stock solution of $FeSO_4 \cdot 7\ H_2O$ in water (500 µg in 10 ml, 180 µM) as indicated in Table 7.13.

180 µM Fe^{2+} Stock Solution / µl	H_2O / µl	nmoles of Fe^{2+}
400	600	72
350	650	63
300	700	54
250	750	45
200	800	36
150	850	27
100	900	18
50	950	9
30	970	5
10	990	2
0	1000	0

Table 7.13 Summary of prepared stock concentrations of Fe^{2+} solutions

ThiGH-His samples were diluted to 1 mL with water and incubated, together with the standards, for 2 h at 60 °C after the addition of reagent A (500 µL). At the end of the 2 hour incubation, samples were allowed to cool down to room temperature before adding reagent B (100 µL). When the purple colour was completely developed (15-20 min) the A_{562} of the samples was measured. If necessary, protein precipitate was removed by centrifugation before reading the absorbance. The amount of iron present in the ThiGH-His samples was estimated from standard calibration curves constructed in parallel.

Method 16: ThiH activity assays. Stock solutions of SAM and NADPH were prepared by dissolving pre-weighed aliquots in anaerobic water. Tyrosine stock solutions were prepared by addition of a 33 mM solution of tyrosine, prepared by dissolving in 200 mM HCl (350 µL) to 1 M NaOH (120 µL) to give a tyrosine stock at a pH suitable for adding to buffered protein solutions without causing precipitation. Assays (150 µl) were prepared in 1.6 ml microcentrifuge tubes by addition of components to the following final concentrations (see Table 7.14: ThiH protein (either ThiGH / ThiH mixture isolated by Ni-affinity chromatograph or Sephadex 200 purified ThiGH complex or monomeric ThiH) (35–100 µM), SAM (1 mM), and tyrosine (1 mM). The assay solutions were equilibrated at 37 °C by incubating in a water bath contained within an anaerobic glove box for 5 min. A stock solution of the reductant system was prepared containing flavodoxin 1 (280 µM), flavoprotein:NADPH oxidoreductase (70 µM), and NADPH(15 mM) and incubated at room temperature for 15 min to permit the formation of the blue-coloured semiquinone. The assays were initiated by the addition (20 µl) of the reductant system (final concentrations of flavodoxin 1 (37 µM), flavoprotein:NADPH oxidoreductase (9 µM), and NADPH (2 mM)). Each time point (1–60 min) was stopped by protein precipitation with 20% perchloric acid (10 µl) and then cleared by centrifugation (Eppendorf 5415D microcentrifuge, maximum speed). Supernatants were stored at -80 ºC until analysis by HPLC.

Component	Stock concentration	Volume added / µl	Final concentration
ThiGH / ThiH	Variable	119.9	Variable[1]
SAM	33 mM	4.5	1 mM
Tyrosine	26 mM	5.6	1 mM
Reducing mixture	FldA: 280 µM Fpr: 70 µM NADPH 15 mM	20	FldA: 37 µM Fpr: 9 µM NADPH 2 mM

[1] Greater than 35 µM is desirable to improve the accuracy of the product concentration in the burst phase.

Table 7.14 Summary of ThiH activity assay preparation.

Method 17: HPLC analysis of ThiH activity assay supernatant. Supernatants were analysed by HPLC using a Gemini C_{18}, 5 µm, 110 Å reverse phase column (Phenomenex). The mobile phase solvents were 0.1% AcOH in water (Solvent A) or 0.1% AcOH in acetonitrile (Solvent B) and the flow rate was 0.8 mL/min. An initial isocratic phase of 100% solvent A for 8 minutes was followed by a linear gradient to 50% solvent B over 32 min, followed by an increase to 100% solvent B over 3 min, which was held for 5 min before returning to 100% solvent A over 2 min and re-equilibration for 10 min (total time of 60 min). A typical assay chromatogram is shown in Figure 7.1. The dual wavelength detector monitored the absorbance at 254nm for detection of DOA and related compounds and 280 nm for detection of *p*-cresol and tyrosine. Concentrations of DOA and *p*-cresol in assays were estimated by comparing to a calibration curve derived from synthetic standards (see Figure 7.2).

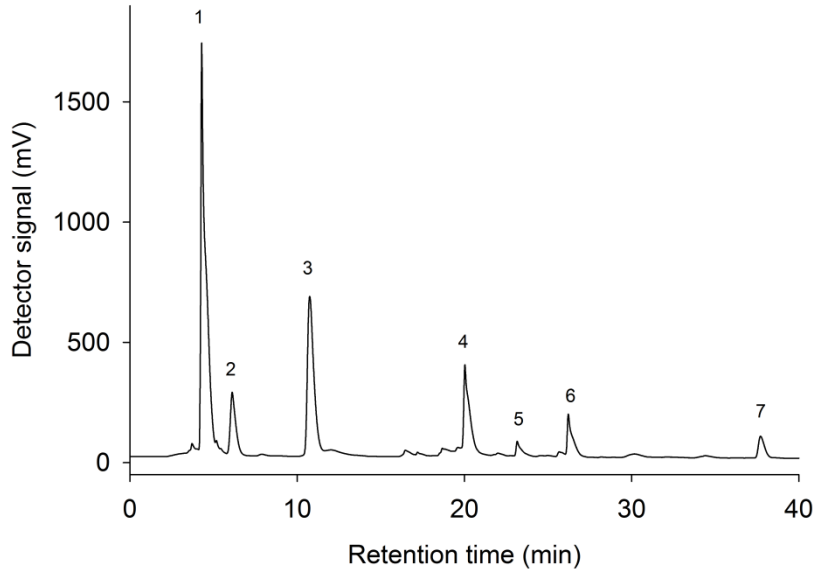

Figure 7.1 Example chromatogram from a ThiH activity assay incubated for 1h. The UV-detector records the absorbance at 280 nm and peaks were identified as follows: 1) SAM; 2) adenine; 3) tyrosine; 4) DOA; 5) MTA (from SAM stock); 6) riboflavin (from reductant); 7) *p*-cresol.

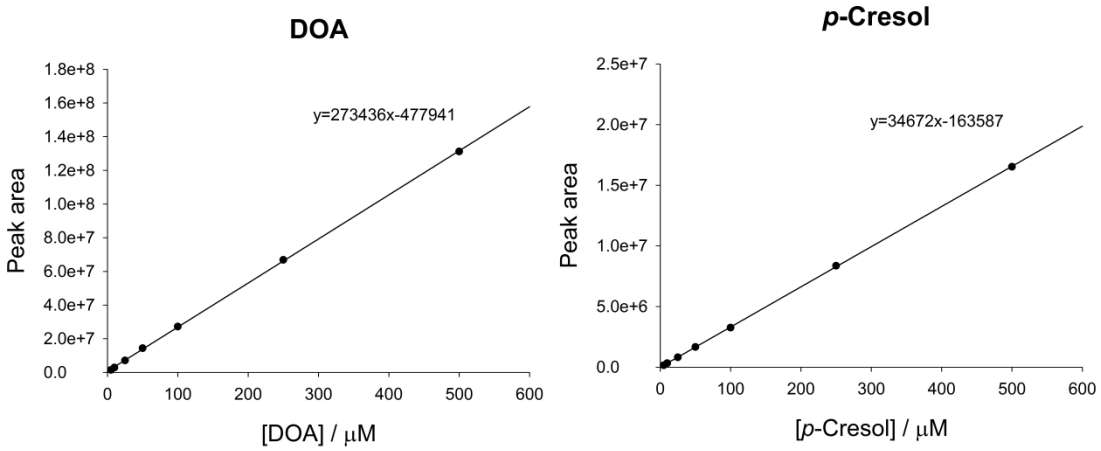

Figure 7.2 Typical calibration plots for determining the concentration of DOA and *p*-cresol in ThiH activity assays

7.2 *Experimental for Chapter 2*

Method 18: Preparation of derivatised –*thiH* mutant cell strains. An *E. coli* K-12 strain, BW25113, with specific deletion of the *thiH* gene (baba) were made competent (Method 1) and transformed with either pRL1020 (RL FBS) (positive sample) or pBAD-His (negative control sample) (Method 2). Single colonies were picked, grown overnight in 2-YT medium (10 ml) and the culture used to prepare glycerol freeze stocks (Method 3).

Method 19: Starvation of derivatised –*thiH* mutant cell strains. Glycerol freeze stocks were used to inoculate overnight starter cultures in 2-YT medium (10 ml), which were harvested by centrifugation (4000 rpm, 10 min, 4 °C). The cell pellet was washed twice by re-suspension in medium A [Davis Mingioli medium[121] (Table 7.15) modified with the addition of ampicillin (100 µg / ml), arabinose (0.2 %) and glucose (0.4%)] (5 ml) followed by centrifugation (4000 rpm, 10 min, 4 °C). The pellet was re-suspended in medium A (10 ml) and this was used as a 1% innocula into fresh medium A (100 ml). The culture was incubated at 37 °C for 24 h before being used as 1% innocula fresh medium for further experiments.

Method 20: Monitoring growth of derivatised –*thiH* mutant cell strains. Either medium B [medium A plus tyrosine (0.2 mM)] or medium C [medium A plus tyrosine (0.2 mM) and thiamine (50 µM)] (190 µL) was added to a well of a 96 well microplate. Cell cultures prepared by method 19 were diluted to an OD_{600} of 0.8. 10 µl of the culture was used to inoculate each well of the microplate. The plate was then incubated at 30 °C on the plate reader, monitoring the OD_{600} every 400 seconds.

Reagent	Quantity
K_2HPO_4	7.0 g
KH_2PO_4	3.0 g
Na_3-citrate.$3H_2O$	0.5 g
$MgSO_4.7H_2O$	0.1 g
$(NH_4)_2SO_4$	1.0 g
Deionised water	Adjust volume to 1,000 mL

Table 7.15 Davis Mingioli medium[121]

Method 21: Organic extraction of cell cultures. Cell cultures prepared by method 19 were used as a 1% innocula into medium B [medium A plus tyrosine (0.2 mM)] for pRL1020 (-*thiH*) (positive sample) or medium C [medium A plus tyrosine (0.2 mM) and thiamine (50 µM)] for pBAD-His (-*thiH*) (negative sample), conditions which ensure growth of these strains. The cultures were incubated at 37 °C for 24 h and after this time the cells were removed by centrifugation (4000 rpm, 10 min, 4 °C). The cleared supernatant was stirred vigorously with diethyl ether (50 ml) for 30 min and the phases separated. The aqueous phase was then re-extracted with diethyl ether (3 x 40 ml) and the combined organic phases dried over anhydrous $MgSO_4$ and concentrated *in vacuo* to a volume of 1 ml.

Method 22a: Analysis of the Organic Extract by TLC. The concentrated organic extract was used to spot a normal phase TLC plate, which was developed in 15 : 1 chloroform : ^{t}butanol. Visualisation was achieved by UV light or staining with $KMnO_4$.

Method 22b: Analysis of the organic extract by HPLC. The concentrated organic extract was reduced to dryness under a stream of N_2. The sample was then re-dissolved in 50 μL of methanol and 250 μL of 20 mM ammonium formate. This was centrifuged (13,000 rpm, 5 min, r.t.) and the soluble and insoluble phases separated. The insoluble layer was washed (2 x 100 μL 20 mM ammonium formate) and the soluble phases combined, giving a sample volume of 500 μL. 40 μL was injected onto a Phenomenex, Hypersil, 5 μ, C18 column (150 x 4.60 mm). The mobile phase (0.8 mL / min) began at 5% MeOH (0.1% AcOH) (solvent B); 95% H_2O (0.1% AcOH) (solvent A) for 7 min, followed by an increase in solvent B to 50% over 22 min, where it was held for 5 min. The column was then washed by increasing solvent B to 70% (over 0.5 min) followed by 4 min isocratic wash. The mobile phase was then returned to original 5% solvent B over 5 min. Detection of compounds was achieved by UV at 280 nm and standards of HBA were observed to elute after c.a. 7 min and *p*-cresol after c.a. 20.5 mins.

Method 22c: Analysis of the organic extract by GCMS. The concentrated organic extract was reduced to dryness under a stream of N_2 and weighed. It was then redisolved in diethyl ether (1 mL) and analysed by GC-MS, employing a PE-Wax (30 x 0.25 mm). Helium was used as a carrier gas (flow 1 ml/min) and samples (1.0 μl) were injected with a speed of 10 (μl/s). The temperature was held at 40 °C for 4 mins followed by an increase, at 20 °C / min, to 240 °C where the temperature was held for a further 6 mins. The detector was set at 70 eV EI-MS, the source temperature at 200 ºC with a trap current 150 μA and using the full scan acquisition mode (2 scans/s from 20-500 amu).

7.3 *Experimental for Chapter 3*

Method 23: Expression and purification of ThiGH from pRL1021(-*yqjI*). An *E. coli* strain with specific deletion of the *yqjI* gene was made competent (method 1) and transformed with pRL1021 (method 2). Single colonies were picked, grown overnight in 2-YT medium (10 ml) and the culture used to prepare glycerol freeze stocks (method 3). Protein was expressed and purified on a large scale by method 10.

Method 24: Investigating different assay buffers. ThiGH was reconstituted (method 14a), concentrated and split into 4 batches and loaded onto a NAP-10 column pre-equilibrated in either buffer 1 – 4 (see Table 7.16). The protein was maintained at ambient temperature for 30 minutes and any observed precipitation noted. The activity of each protein sample was then assessed by monitoring the amount of products formed after 1h at 37 ºC using Methods 16 and 17.

Buffer	Buffer contents
1	50 mM MOPS pH 7.5 100 mM NaCl 5% (w/v) glycerol
2	50 mM MOPS pH 7.5 100 mM NaCl
3	50 mM MOPS pH 7.5 5% (w/v) glycerol
4	50 mM MOPS pH 7.5

Table 7.16 Composition of buffers used to test ThiGH stability.

7.4 *Experimental for Chapter 4*

Many experiments described in this section utilise the ThiH activity assay described in Method 16 and Table 7.14 (p 187). For any experiments requiring extra additions (e.g. reaction products to measure product inhibition or MTAN) the volume of ThiGH / ThiH was reduced to accommodate these additions and maintaining a consistant assay volume of 150 µl.

Method 25: Investigating product inhibition by DOA and methionine. ThiGH isolated by Ni-affinity chromatography (Method 10) was chemically reconstituted (Method 14a). To investigate product inhibition, the reaction products (DOA, methionine or DOA plus methionine) were added to activity assays (prepared as described in Method 16) at selected concentrations between 0 – 1 mM. The activity of each protein sample was then assessed by monitoring the amount of *p*-cresol formed after 1h at 37 ºC by HPLC (Method 17).

Method 26: Expression and purification of MTAN. Cells were cultured and protein expressed by Method 9. A typical yield of wet cell paste was 40 g.

The cell pellet (40 g) was suspended in lysis buffer (10% (w/v) glycerol / 50 mM Tris, pH 8.1) (120 mL) and lysozyme (0.1 mg / mL) added. The suspension was stirred for 15 min before cell lysis by sonication (12 x 30 s on / 30 s off). Benzonase (10 µL) was added and the suspension stirred for a further 10 min before removal of the cell debris by centrifugation (SLC15000, 12000 r.p.m., 30 min, 4 ˚C). The supernatant was then loaded onto chelating sepharose fast flow column, charged with $NiSO_4$ and equilibrated with Buffer A (50 mM Tris, pH 8.1, 25 mM Imidazole). The column was washed with 300 mL of Buffer A before a gradient to 250 mM Imidazole over 50 mL using Buffer B (50 mM Tris, pH 8.1, 200 mM NaCl, 500 mM Imidazole), followed by an isocratic wash at 250 mM Imidazole. Fractions (5 mL) were analysed by SDS-PAGE and those containing >95% MTAN were pooled and concentrated to

~20 mL on a 10 KDa NMCO membrane. MTAN was dialysed into 50 mM Tris, pH 8 and the protein concentration estimated as 40 mg / mL. MTAN was stored in 1 mL aliquots at – 80 C. A 1 mL aliquot was slit into further aliquots of 50 L, which were diluted up to 0.5 mL (4 mg / mL) with anaerobic assay buffer prior to addition to ThiH activity assays.

Method 27: MTAN activity assay. The MTAN activity assay contained MTAN (5 nM), DOA (12.5-800 μM), ammonium acetate (20 mM, pH 7.5) and BSA (0.1 mg mL^{-1}). To estimate the K_M for DOA, assays were initiated in parallel in a 96 well PCR plate incubated at 37 ˚C. Assays were initiated by the addition of MTAN and stopped at time points (0 -5 min) by the addition of perchloric acid (1% v/v). The precipitated protein was removed by centrifugation, supernatants (100 μL) neutralised with ammonium hydroxide and analysed by RP-HPLC using a Gemini C_{18} (4.6 x 250 mm, 5 μm, 100 Å) reverse phase HPLC column (Phenomenex). The mobile phase (0.7 mL / min) was an initial 5 min isocratic phase of 5% acetonitrile in 20 mM ammonium acetate, pH 6.0, followed by a 10 min linear gradient to 50 % acetonitrile. Standards of adenine and DOA had retention times of 10 min and 13 min respectively and were used to construct a calibration curve to quantify the concentration of DOA and adenine in activity assays.

Method 28: Investigating alleviation of product inhibition with MTAN. ThiGH isolated by Ni-affinity chromatography (Method 10) was chemically reconstituted (Method 14a). Activity assays were prepared as described in Method 16 and reaction products (DOA, methionine or DOA plus methionine) (1 mM) and / or MTAN (10 μM) were added. Before addition MTAN applied to a NAP-10 gel filtration column equilibrated in anaerobic buffer L to exchenge the protein into anaerobic assay buffer. The activity of each protein sample was then assessed by monitoring the amount of *p*-cresol formed after 1h at 37 ºC by HPLC (Method 17) and comparing to a positive control assay with no additions.

Method 29: ThiH activity assays with the addition of MTAN. ThiGH / ThiH isolated by Sephadex 200 gel filtration chromatography (Method 13) was chemically reconstituted (Method 14b). Activity assays were prepared as described in Method 16. To investigate the effect of removing DOA formed *in situ* during the experiment, the reaction assays were supplemented with MTAN (10 μM) which had been previously exchanged into anaerobic buffer L.

Method 30: Investigating inhibition by glyoxylate and ammonium. ThiGH / ThiH isolated by Sephadex 200 gel filtration chromatography (Method 13) was chemically reconstituted (Method 14b). Activity assays were prepared as described in Method 16. To investigate inhibition by glyoxylate and ammonia these compounds (10 – 2000 μM) were added to the assay.

Method 31. Experiments with substrate analogues. Stock solutions (33 mM) of substrate analogues were prepared in 100 mM ammonium bicarbonate and deoxygenated in an anaerobic glove box overnight. ThiGH / ThiH isolated by Ni affinity chromatography (Method 10) was chemically reconstituted (Method 14a). Assays were prepared with chemically reconstituted ThiGH / ThiH mixture (60 – 90 μM), SAM (1 mM), substrate (1 mM). The amount of products formed after 1h at 37 ºC were estimated by HPLC (Method 17).

7.5 *Experimental for Chapter 5*

Method 32: Preparation of ThiH activity assays in 50% D_2O / H_2O. Stock solutions of SAM and NADPH were prepared by dissolving pre-weighed aliquots in anaerobic water. Tyrosine stock solutions were prepared by addition of a 33 mM solution of tyrosine, prepared by dissolving in 200 mM HCl (350 µL) to 1 M NaOH (120 µL) to give a tyrosine stock at a pH suitable for adding to buffered protein solutions without causing precipitation. Chemically reconstituted ThiGH was concentrated, using a 10kDa MWCO ultrafiltration membrane and The protein was then applied to a NAP-10 gel filtration column equilibrated in anaerobic buffer M (100 mM MOPS pH7.5, 200 mM NaCl and 10% (w/v) glycerol). Assays (250 µl) were prepared in 1.6 ml microcentrifuge tubes by addition of the amounts of stock solutions shown in Table 7.17 as follows: ThiH protein (either ThiGH / ThiH mixture isolated by Ni-affinity chromatograph or Sephadex 200 purified ThiGH), SAM, tyrosine and D_2O (125 µl) were incubated at room temperature for 30 minutes to allow for proton / deuteron exchange. In all cases a positive control, in which H_2O (125 µl) was added instead of D_2O was prepared in parallel in order to draw direct comparisons. The assay solutions were then equilibrated at 37 °C by incubating in a water bath contained within an anaerobic glove box for 5 min. A stock solution of the reductant system was prepared containing flavodoxin 1 (280 µM), flavoprotein:NADPH oxidoreductase (70 µM), and NADPH (15 mM) and incubated at room temperature for 15 min to permit the formation of the blue-coloured semiquinone. The assays were initiated by the addition (33.3 µl) of the reductant system (final concentrations of flavodoxin 1 (37 µM), flavoprotein:NADPH oxidoreductase (9 µM), and NADPH (2 mM)). Each time point (1–60 min) was stopped by protein precipitation with 20% perchloric acid (10 µl) and then cleared by centrifugation (Eppendorf 5415D microcentrifuge, maximum speed). Supernatants were stored at -80 ºC until analysis by HPLC (Method 17) or LCMS (Method 33).

Component	Stock concentration	Volume added / µl	Final concentration
ThiGH / ThiH	> 140 µM (~10 mg/ml)	74.5	> 40 µM
SAM	33 mM	7.6	1 mM
Tyrosine	26 mM	9.6	1 mM
D_2O (or H_2O)[1]	-	125	-
Reducing mixture	FldA: 280 µM Fpr: 70 µM NADPH 15 mM	33.3	FldA: 37 µM Fpr: 9 µM NADPH 2 mM

[1] For preparation of positive control assays in 100% H2O, the addition of D_2O was replaced with H_2O

Table 7.17 Summary of ThiH activity assay preparation for assays that contained 50% D_2O.

Method 33: LCMS analysis of ThiH assays. Supernatants (100 µl injection volume) were anlaysed by LCMS using identical chromatography conditions (column, mobile phase and UV detection) as described in method 17. A 1:4 split, followed by dilution with 3% formic acid in 50% methanol / water was used to achieve MS analysis. Data processing was achieved using the XCaliber software. DOA eluted with a retention time of ~20 min and was identified by comparison with a synthetic standard. The peak width was typically 0.8 minutes. To achieve the spectra shown in Figure 5.1 (p137) the mass ions in the chromatogram from 0.4 minutes before and 0.4 minutes after the DOA peak elution were subtracted from the mass ions present in the peak corresponding to DOA.

8 Bibliography

[1] B. Halliwell, J. M. C. Gutteridge, *Free Radicals in Biology and Medicine*, 3rd ed., Oxford University Press, New York, **1999**.

[2] P. Sykes, *A Guidebook to Mechanism in Organic Chamistry*, 5th ed., Longman, London and New York, **1981**.

[3] J. Fossey, D. Lefort, J. Sorba, *Free Radicals in Organic Chemistry*, John Wiley and Sons Ltd., Chichester, UK, **1995**.

[4] M. Fontecave, *Cell Mol Life Sci* **1998**, *54*, 684.

[5] J. Stubbe, W. A. van der Donk, *Chem Biol* **1995**, *2*, 793.

[6] P. L. Roach, I. J. Clifton, C. M. Hensgens, N. Shibata, C. J. Schofield, J. Hajdu, J. E. Baldwin, *Nature* **1997**, *387*, 827.

[7] J. T. Jarrett, *Arch Biochem Biophys* **2005**, *433*, 312.

[8] J. C. Sheehan, K. R. Henery-Logan, *Journal of the American Chemical Society* **1959**, *81*, 3089.

[9] T. P. Chirpich, V. Zappia, R. N. Costilow, H. A. Barker, *J Biol Chem* **1970**, *245*, 1778.

[10] P. A. Frey, A. D. Hegeman, F. J. Ruzicka, *Crit Rev Biochem Mol Biol* **2008**, *43*, 63.

[11] S. J. Booker, *Curr Opin Chem Biol* **2009**, *13*, 58.

[12] W. Buckel, B. T. Golding, *Annu Rev Microbiol* **2006**, *60*, 27.

[13] E. L. Colichman, D. L. Love, *The Journal of Organic Chemistry* **1953**, *18*, 40.

[14] R. Lill, *Nature* **2009**, *460*, 831.

[15] K. S. Hewitson, J. E. Baldwin, N. M. Shaw, P. L. Roach, *FEBS Lett* **2000**, *466*, 372.

[16] J. Tamarit, C. Gerez, C. Meier, E. Mulliez, A. Trautwein, M. Fontecave, *J Biol Chem* **2000**, *275*, 15669.

[17] H. J. Sofia, G. Chen, B. G. Hetzler, J. F. Reyes-Spindola, N. E. Miller, *Nucleic Acids Res* **2001**, *29*, 1097.

[18] C. J. Walsby, D. Ortillo, W. E. Broderick, J. B. Broderick, B. M. Hoffman, *J Am Chem Soc* **2002**, *124*, 11270.

[19] J. Cheek, J. B. Broderick, *J Biol Inorg Chem* **2001**, *6*, 209.

[20] O. T. Magnusson, G. H. Reed, P. A. Frey, *Biochemistry* **2001**, *40*, 7773.

[21] T. Selmer, A. J. Pierik, J. Heider, *Biol Chem* **2005**, *386*, 981.

[22] O. M. Birch, M. Fuhrmann, N. M. Shaw, *J Biol Chem* **1995**, *270*, 19158.

[23] P. Douglas, M. Kriek, P. Bryant, P. L. Roach, *Angew Chem Int Ed Engl* **2006**, *45*, 5197.

[24] T. Ohshiro, M. Yamamoto, Y. Izumi, B. T. Bui, D. Florentin, A. Marquet, *Biosci Biotechnol Biochem* **1994**, *58*, 1738.

[25] X. Zhao, J. R. Miller, Y. Jiang, M. A. Marletta, J. E. Cronan, *Chem Biol* **2003**, *10*, 1293.

[26] K. S. Duschene, S. E. Veneziano, S. C. Silver, J. B. Broderick, *Curr Opin Chem Biol* **2009**, *13*, 74.

[27] S. C. Wang, P. A. Frey, *Trends Biochem Sci* **2007**, *32*, 101.

[28] J. Miller, V. Bandarian, G. H. Reed, P. A. Frey, *Arch Biochem Biophys* **2001**, *387*, 281.

[29] J. M. Buis, J. Cheek, E. Kalliri, J. B. Broderick, *J Biol Chem* **2006**, *281*, 25994.

[30] K. K. Wong, B. W. Murray, S. A. Lewisch, M. K. Baxter, T. W. Ridky, L. Ulissi-DeMario, J. W. Kozarich, *Biochemistry* **1993**, *32*, 14102.

[31] A. M. Taylor, C. E. Farrar, J. T. Jarrett, *Biochemistry* **2008**, *47*, 9309.

[32] R. M. Cicchillo, D. F. Iwig, A. D. Jones, N. M. Nesbitt, C. Baleanu-Gogonea, M. G. Souder, L. Tu, S. J. Booker, *Biochemistry* **2004**, *43*, 6378.

[33] H. L. Hernandez, F. Pierrel, E. Elleingand, R. Garcia-Serres, B. H. Huynh, M. K. Johnson, M. Fontecave, M. Atta, *Biochemistry* **2007**, *46*, 5140.

[34] T. L. Grove, K. H. Lee, J. St Clair, C. Krebs, S. J. Booker, *Biochemistry* **2008**, *47*, 7523.

[35] K. Yokoyama, M. Numakura, F. Kudo, D. Ohmori, T. Eguchi, *J Am Chem Soc* **2007**, *129*, 15147.

[36] D. Chen, F. J. Ruzicka, P. A. Frey, *Biochem J* **2000**, *348 Pt 3*, 539.

[37] F. J. Ruzicka, K. W. Lieder, P. A. Frey, *J Bacteriol* **2000**, *182*, 469.

[38] J. Cheek, J. B. Broderick, *J Am Chem Soc* **2002**, *124*, 2860.

[39] J. C. Pieck, U. Hennecke, A. J. Pierik, M. G. Friedel, T. Carell, *J Biol Chem* **2006**, *281*, 36317.

[40] J. Knappe, F. A. Neugebauer, H. P. Blaschkowski, M. Ganzler, *Proc Natl Acad Sci U S A* **1984**, *81*, 1332.

[41] D. Padovani, F. Thomas, A. X. Trautwein, E. Mulliez, M. Fontecave, *Biochemistry* **2001**, *40*, 6713.

[42] T. Selmer, P. I. Andrei, *Eur J Biochem* **2001**, *268*, 1363.

[43] G. Layer, J. Moser, D. W. Heinz, D. Jahn, W. D. Schubert, *EMBO J* **2003**, *22*, 6214.

[44] N. S. Lees, P. Hanzelmann, H. L. Hernandez, S. Subramanian, H. Schindelin, M. K. Johnson, B. M. Hoffman, *J Am Chem Soc* **2009**, *131*, 9184.

[45] P. Hanzelmann, H. Schindelin, *Proc Natl Acad Sci U S A* **2006**, *103*, 6829.

[46] T. L. Grove, J. H. Ahlum, P. Sharma, C. Krebs, S. J. Booker, *Biochemistry*, *49*, 3783.

[47] R. M. Cicchillo, M. A. Baker, E. J. Schnitzer, E. B. Newman, C. Krebs, S. J. Booker, *J Biol Chem* **2004**, *279*, 32418.

[48] R. M. Cicchillo, S. J. Booker, *J Am Chem Soc* **2005**, *127*, 2860.

[49] R. M. Cicchillo, K. H. Lee, C. Baleanu-Gogonea, N. M. Nesbitt, C. Krebs, S. J. Booker, *Biochemistry* **2004**, *43*, 11770.

[50] S. Ollagnier-De Choudens, Y. Sanakis, K. S. Hewitson, P. Roach, J. E. Baldwin, E. Munck, M. Fontecave, *Biochemistry* **2000**, *39*, 4165.

[51] N. B. Ugulava, K. K. Frederick, J. T. Jarrett, *Biochemistry* **2003**, *42*, 2708.

[52] N. B. Ugulava, B. R. Gibney, J. T. Jarrett, *Biochemistry* **2000**, *39*, 5206.

[53] N. B. Ugulava, B. R. Gibney, J. T. Jarrett, *Biochemistry* **2001**, *40*, 8343.

[54] N. B. Ugulava, C. J. Sacanell, J. T. Jarrett, *Biochemistry* **2001**, *40*, 8352.

[55] B. Tse Sum Bui, T. A. Mattioli, D. Florentin, G. Bolbach, A. Marquet, *Biochemistry* **2006**, *45*, 3824.

[56] B. Tse Sum Bui, M. Lotierzo, F. Escalettes, D. Florentin, A. Marquet, *Biochemistry* **2004**, *43*, 16432.

[57] B. Tse Sum Bui, R. Benda, V. Schunemann, D. Florentin, A. X. Trautwein, A. Marquet, *Biochemistry* **2003**, *42*, 8791.

[58] R. B. Broach, J. T. Jarrett, *Biochemistry* **2006**, *45*, 14166.

[59] M. R. Reyda, C. J. Fugate, J. T. Jarrett, *Biochemistry* **2009**, *48*, 10782.

[60] N. J. Cosper, S. J. Booker, F. Ruzicka, P. A. Frey, R. A. Scott, *Biochemistry* **2000**, *39*, 15668.

[61] B. W. Lepore, F. J. Ruzicka, P. A. Frey, D. Ringe, *Proc Natl Acad Sci U S A* **2005**, *102*, 13819.

[62] M. M. Cosper, N. J. Cosper, W. Hong, J. E. Shokes, W. E. Broderick, J. B. Broderick, M. K. Johnson, R. A. Scott, *Protein Sci* **2003**, *12*, 1573.

[63] Y. Nicolet, P. Amara, J. M. Mouesca, J. C. Fontecilla-Camps, *Proc Natl Acad Sci U S A* **2009**, *106*, 14867.

[64] F. Berkovitch, Y. Nicolet, J. T. Wan, J. T. Jarrett, C. L. Drennan, *Science* **2004**, *303*, 76.

[65] J. L. Vey, J. Yang, M. Li, W. E. Broderick, J. B. Broderick, C. L. Drennan, *Proc Natl Acad Sci U S A* **2008**, *105*, 16137.

[66] P. Hanzelmann, H. Schindelin, *Proc Natl Acad Sci U S A* **2004**, *101*, 12870.

[67] Y. Nicolet, J. K. Rubach, M. C. Posewitz, P. Amara, C. Mathevon, M. Atta, M. Fontecave, J. C. Fontecilla-Camps, *J Biol Chem* **2008**, *283*, 18861.

[68] Y. Nicolet, C. L. Drennan, *Nucleic Acids Res* **2004**, *32*, 4015.

[69] C. J. Daley, R. H. Holm, *Inorg Chem* **2001**, *40*, 2785.

[70] C. J. Daley, R. H. Holm, *J Inorg Biochem* **2003**, *97*, 287.

[71] G. Layer, K. Grage, T. Teschner, V. Schunemann, D. Breckau, A. Masoumi, M. Jahn, P. Heathcote, A. X. Trautwein, D. Jahn, *J Biol Chem* **2005**, *280*, 29038.

[72] E. Mulliez, D. Padovani, M. Atta, C. Alcouffe, M. Fontecave, *Biochemistry* **2001**, *40*, 3730.

[73] J. K. Rubach, X. Brazzolotto, J. Gaillard, M. Fontecave, *FEBS Lett* **2005**, *579*, 5055.

[74] S. C. Wang, P. A. Frey, *Biochemistry* **2007**, *46*, 12889.

[75] G. T. Hinckley, P. A. Frey, *Biochemistry* **2006**, *45*, 3219.

[76] X. Brazzolotto, J. K. Rubach, J. Gaillard, S. Gambarelli, M. Atta, M. Fontecave, *J Biol Chem* **2006**, *281*, 769.

[77] S. E. McGlynn, S. S. Ruebush, A. Naumov, L. E. Nagy, A. Dubini, P. W. King, J. B. Broderick, M. C. Posewitz, J. W. Peters, *J Biol Inorg Chem* **2007**, *12*, 443.

[78] S. E. McGlynn, E. M. Shepard, M. A. Winslow, A. V. Naumov, K. S. Duschene, M. C. Posewitz, W. E. Broderick, J. B. Broderick, J. W. Peters, *FEBS Lett* **2008**, *582*, 2183.

[79] D. W. Mulder, D. O. Ortillo, D. J. Gardenghi, A. V. Naumov, S. S. Ruebush, R. K. Szilagyi, B. Huynh, J. B. Broderick, J. W. Peters, *Biochemistry* **2009**, *48*, 6240.

[80] P. B. Vander Horn, A. D. Backstrom, V. Stewart, T. P. Begley, *J Bacteriol* **1993**, *175*, 982.

[81] A. Chatterjee, Y. Li, Y. Zhang, T. L. Grove, M. Lee, C. Krebs, S. J. Booker, T. P. Begley, S. E. Ealick, *Nat Chem Biol* **2008**, *4*, 758.

[82] N. C. Martinez-Gomez, D. M. Downs, *Biochemistry* **2008**, *47*, 9054.

[83] S. E. McGlynn, E. S. Boyd, E. M. Shepard, R. Lange, R. Gerlach, J. B. Broderick, J. W. Peters, *J Bacteriol* **2009**.

[84] J. B. Broderick, *Nature* **2010**, *465*, 877.

[85] Y. Zhang, X. Zhu, A. T. Torelli, M. Lee, B. Dzikovski, R. M. Koralewski, E. Wang, J. Freed, C. Krebs, S. E. Ealick, H. Lin, *Nature*, *465*, 891.

[86] M. Pohl, G. A. Sprenger, M. Muller, *Curr Opin Biotechnol* **2004**, *15*, 335.

[87] T. P. Begley, D. M. Downs, S. E. Ealick, F. W. McLafferty, A. P. Van Loon, S. Taylor, N. Campobasso, H. J. Chiu, C. Kinsland, J. J. Reddick, J. Xi, *Arch Microbiol* **1999**, *171*, 293.

[88] C. T. Jurgenson, T. P. Begley, S. E. Ealick, *Annu Rev Biochem* **2009**, *78*, 569.

[89] D. A. Bender, *Proc Nutr Soc* **1999**, *58*, 427.

[90] R. Breslow, *Journal of the American Chemical Society* **1958**, *80*, 3719.

[91] F. Jordan, *Nat Prod Rep* **2003**, *20*, 184.

[92] L. M. Lois, N. Campos, S. R. Putra, K. Danielsen, M. Rohmer, A. Boronat, *Proc Natl Acad Sci U S A* **1998**, *95*, 2105.

[93] G. A. Sprenger, U. Schorken, T. Wiegert, S. Grolle, A. A. de Graaf, S. V. Taylor, T. P. Begley, S. Bringer-Meyer, H. Sahm, *Proc Natl Acad Sci U S A* **1997**, *94*, 12857.

[94] S. Xiang, G. Usunow, G. Lange, M. Busch, L. Tong, *J Biol Chem* **2007**, *282*, 2676.

[95] P. C. Dorrestein, H. Huili Zhai, S. V. Taylor, F. W. McLafferty, T. P. Begley, *J Am Chem Soc* **2004**, *126*, 3091.

[96] E. C. Settembre, P. C. Dorrestein, H. Zhai, A. Chatterjee, F. W. McLafferty, T. P. Begley, S. E. Ealick, *Biochemistry* **2004**, *43*, 11647.

[97] P. C. Dorrestein, H. Zhai, F. W. McLafferty, T. P. Begley, *Chem Biol* **2004**, *11*, 1373.

[98] C. Lehmann, T. P. Begley, S. E. Ealick, *Biochemistry* **2006**, *45*, 11.

[99] C. M. Wright, P. M. Palenchar, E. G. Mueller, *Chem Commun (Camb)* **2002**, 2708.

[100] J. H. Park, P. C. Dorrestein, H. Zhai, C. Kinsland, F. W. McLafferty, T. P. Begley, *Biochemistry* **2003**, *42*, 12430.

[101] A. Hazra, A. Chatterjee, T. P. Begley, *J Am Chem Soc* **2009**, *131*, 3225.

[102] E. C. Settembre, P. C. Dorrestein, J. H. Park, A. M. Augustine, T. P. Begley, S. E. Ealick, *Biochemistry* **2003**, *42*, 2971.

[103] B. Estramareix, M. Therisod, *Biochim Biophys Acta* **1972**, *273*, 275.

[104] R. H. White, F. B. Rudolph, *Biochim Biophys Acta* **1978**, *542*, 340.

[105] N. C. Martinez-Gomez, M. Robers, D. M. Downs, *J Biol Chem* **2004**, *279*, 40505.

[106] R. Leonardi, S. A. Fairhurst, M. Kriek, D. J. Lowe, P. L. Roach, *FEBS Lett* **2003**, *539*, 95.

[107] R. Leonardi, P. L. Roach, *J Biol Chem* **2004**, *279*, 17054.

[108] B. Estramareix, S. David, *Biochim Biophys Acta* **1990**, *1035*, 154.

[109] P. C. Newell, R. G. Tucker, *Biochem J* **1968**, *106*, 279.

[110] G. Cheng, E. M. Bennett, T. P. Begley, S. E. Ealick, *Structure* **2002**, *10*, 225.

[111] B. G. Lawhorn, R. A. Mehl, T. P. Begley, *Org Biomol Chem* **2004**, *2*, 2538.

[112] A. Chatterjee, A. B. Hazra, S. Abdelwahed, D. G. Hilmey, T. P. Begley, *Angew Chem Int Ed Engl* **2010**, *49*, 8653.

[113] D. H. Peapus, H. J. Chiu, N. Campobasso, J. J. Reddick, T. P. Begley, S. E. Ealick, *Biochemistry* **2001**, *40*, 10103.

[114] M. Kriek, F. Martins, R. Leonardi, S. A. Fairhurst, D. J. Lowe, P. L. Roach, *J Biol Chem* **2007**, *282*, 17413.

[115] M. Kriek, F. Martins, M. R. Challand, A. Croft, P. L. Roach, *Angew Chem Int Ed Engl* **2007**, *46*, 9223.

[116] R. H. White, *Biochim Biophys Acta* **1979**, *583*, 55.

[117] N. Ontiveros-Palacios, A. M. Smith, F. J. Grundy, M. Soberon, T. M. Henkin, J. Miranda-Rios, *Mol Microbiol* **2008**, *67*, 793.

[118] A. Serganov, A. Polonskaia, A. T. Phan, R. R. Breaker, D. J. Patel, *Nature* **2006**, *441*, 1167.

[119] W. Winkler, A. Nahvi, R. R. Breaker, *Nature* **2002**, *419*, 952.

[120] T. Baba, T. Ara, M. Hasegawa, Y. Takai, Y. Okumura, M. Baba, K. A. Datsenko, M. Tomita, B. L. Wanner, H. Mori, *Mol Syst Biol* **2006**, *2*, 2006 0008.

[121] B. D. Davis, E. S. Mingioli, *J Bacteriol* **1950**, *60*, 17.

[122] S. R. Elsden, M. G. Hilton, J. M. Waller, *Arch Microbiol* **1976**, *107*, 283.

[123] S. Engst, V. Kuusk, I. Efimov, C. N. Cronin, W. S. McIntire, *Biochemistry* **1999**, *38*, 16620.

[124] M. A. Prieto, A. Perez-Aranda, J. L. Garcia, *J Bacteriol* **1993**, *175*, 2162.

[125] S. Hafiz, C. L. Oakley, *J Med Microbiol* **1976**, *9*, 129.

[126] L. Yu, M. Blaser, P. I. Andrei, A. J. Pierik, T. Selmer, *Biochemistry* **2006**, *45*, 9584.

[127] P. I. Andrei, A. J. Pierik, S. Zauner, L. C. Andrei-Selmer, T. Selmer, *Eur J Biochem* **2004**, *271*, 2225.

[128] L. A. McNeill, L. Bethge, K. S. Hewitson, C. J. Schofield, *Anal Biochem* **2005**, *336*, 125.

[129] F. Martins, University of Southampton **2010**.

[130] R. C. Driesener, M. R. Challand, S. E. McGlynn, E. M. Shepard, E. S. Boyd, J. B. Broderick, J. W. Peters, P. L. Roach, *Angew Chem Int Ed Engl* **2010**, *49*, 1687.

[131] R. Leonardi, University of Southampton **2003**.

[132] D. F. Iwig, S. J. Booker, *Biochemistry* **2004**, *43*, 13496.

[133] L. McIver, C. Leadbeater, D. J. Campopiano, R. L. Baxter, S. N. Daff, S. K. Chapman, A. W. Munro, *Eur J Biochem* **1998**, *257*, 577.

[134] P. Atkins, J. de Paula, *Physical Chemistry*, 7th ed., Oxford University Press, Oxford, UK, **2002**.

[135] M. Kriek, L. Peters, Y. Takahashi, P. L. Roach, *Protein Expr Purif* **2003**, *28*, 241.

[136] M. M. Bradford, *Anal Biochem* **1976**, *72*, 248.

[137] W. W. Fish, *Methods Enzymol* **1988**, *158*, 357.

[138] B. D. Grant, J. A. Adams, *Biochemistry* **1996**, *35*, 2022.

[139] T. Ziegert, University of Southampton **2003**.

[140] C. E. Farrar, K. K. Siu, P. L. Howell, J. T. Jarrett, *Biochemistry* **2010**, *49*, 9985.

[141] S. Ollagnier-de-Choudens, E. Mulliez, M. Fontecave, *FEBS Lett* **2002**, *532*, 465.

[142] M. R. Challand, T. Ziegert, P. Douglas, R. J. Wood, M. Kriek, N. M. Shaw, P. L. Roach, *FEBS Lett* **2009**, *583*, 1358.

[143] E. J. Choi-Rhee, J. E. Cronan, *Chemistry & Biology* **2005**, *12*, 589.

[144] E. Choi-Rhee, J. E. Cronan, *Chem Biol* **2005**, *12*, 589.

[145] E. Choi-Rhee, J. E. Cronan, *Chem Biol* **2005**, *12*, 461.

[146] J. A. Duerre, *J Biol Chem* **1962**, *237*, 3737.

[147] P. Douglas, Univesity of Southampton **2008**.

[148] I. H. Segel, *Enzyme Kinetics*, John Wiley and Sons Ltd., Chichester, UK, **1993**.

[149] F. Della Ragione, M. Porcelli, M. Carteni-Farina, V. Zappia, A. E. Pegg, *Biochem J* **1985**, *232*, 335.

[150] K. A. Cornell, M. K. Riscoe, *Biochim Biophys Acta* **1998**, *1396*, 8.

[151] A. Kohen, H. Limbach, *Isotope Effects in Chemistry and Biology*, Taylor & Francis, New York, London, **2006**.

[152] A. Benjdia, J. Leprince, C. Sandstrom, H. Vaudry, O. Berteau, *J Am Chem Soc* **2009**, *131*, 8348.

[153] M. B. Smith, J. March, *March's Organic Chemistry*, 5th ed., Wiley, Chichester, UK, **2001**.

[154] M. R. Challand, F. T. Martins, P. L. Roach, *J Biol Chem* **2009**.

[155] E. M. Shepard, B. R. Duffus, S. J. George, S. E. McGlynn, M. R. Challand, K. D. Swanson, P. L. Roach, S. P. Cramer, J. W. Peters, J. B. Broderick, *J Am Chem Soc* **2010**, *132*, 9247.

[156] J. W. Peters, W. N. Lanzilotta, B. J. Lemon, L. C. Seefeldt, *Science* **1998**, *282*, 1853.

[157] Y. Yu, L. Duan, Q. Zhang, R. Liao, Y. Ding, H. Pan, E. Wendt-Pienkowski, G. Tang, B. Shen, W. Liu, *ACS Chem Biol* **2009**, *4*, 855.

[158] M. Lucarini, P. Pedrielli, G. F. Pedulli, S. Cabiddu, C. Fattuoni, *The Journal of Organic Chemistry* **1996**, *61*, 9259.

[159] J. Sambrook, Fritsch, E. F., Maniatis, T., *Molecular Cloning: A Laboratory Manual* **1989**, *2nd Ed.*

[160] C. Osborne, L. M. Chen, R. G. Matthews, *J Bacteriol* **1991**, *173*, 1729.